nature reviews
rheumatology

April 2026

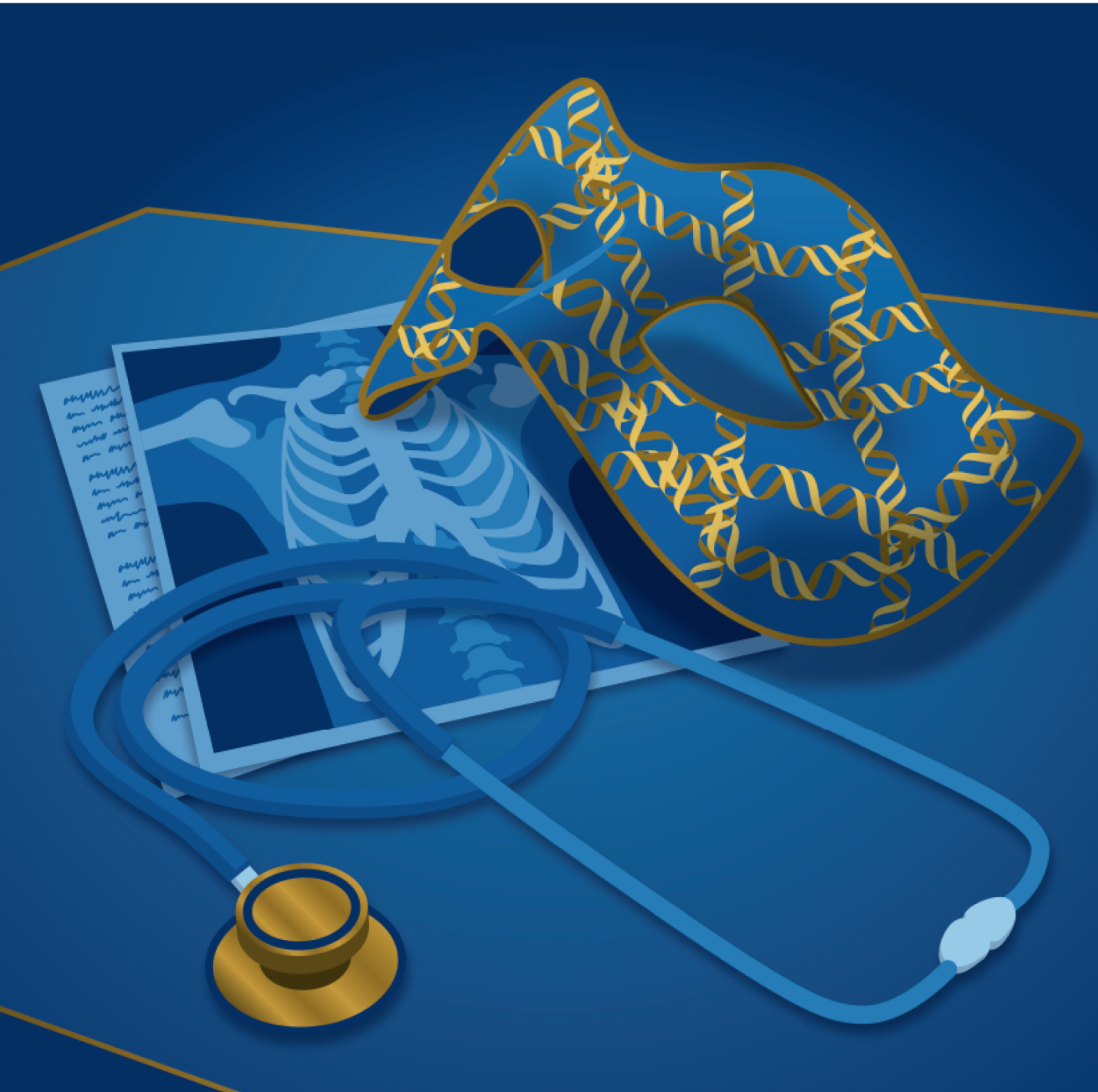

https://doi.org/10.1038/s41584-026-01357-7

Immune reset and immune retune: approaching cure?

John D. Isaacs

The emergence of potent depletion therapies for the treatment of refractory autoimmunity has led to the concept of immune reset. Understanding whether immune reset equates to cure, and whether cure is achievable through non-depleting approaches, depends on the identification of immune biomarkers for measuring healthy and pathological immunity.

Autoimmunity has traditionally been considered a 'one-way street' with no reversibility and, accordingly, treatment has comprised immunosuppressive and anti-inflammatory drugs, with the aim of suppressing symptoms and preventing damage. Although the possibility of cure through the use of immunomodulatory therapies first emerged from preclinical models four decades ago, clinical translation has been slow. Autologous and, in some instances, allogeneic stem cell transplantation has provided drug-free, long-term remission for a proportion of patients. In the past 5 years, however, encouraging early results of deep B cell depletion through the use of chimeric antigen receptor (CAR) T cell therapy and other modalities have led to increasing use of the term 'immune reset' (or 'B cell reset')[1]. However, in this context, what defines reset? Does it equate to cure, and are there alternative routes to resetting autoimmunity?

Whether B cell depletion achieves sustained, drug-free remission — the clinical manifestation of immune reset — and, potentially, cure is probably dependent on the eradication or neutralization of all autoreactive B cell clones. Even rituximab, which is now regarded as a relatively weak B cell-depleting therapy, can provide sustained benefit in some patients (T. Garcia and D. Isenberg, personal communication). This beneficial effect might reflect the stochastic and serendipitous eradication of autoreactive clones or an incomplete (particularly in the tissues) reduction beyond a crucial threshold[2,3]. A number of therapies now rank between rituximab and CAR T cells in terms of depth and breadth of depletion, including bi-specific and tri-specific T cell engagers and glycoengineered monoclonal antibodies. The breadth of depletion is determined by the B cell lineage target, broadening from CD20 (some B cells) and BCMA (predominantly plasmablasts and plasma cells) to CD19 (B cells and plasmablasts) and CD38 (B cells, plasmablasts and plasma cells).

An emerging dogma suggests that the deeper the depletion, particularly within tissues, the greater the likelihood of 'reset'[3]. This dogma is probably true as, statistically, deep depletion is the surest way to eradicate all autoreactive clones, which comprise a very small percentage of all B cells. An emerging challenge is managing relapse, particularly when less-potent depleting agents are used, and various potential strategies may be considered (Fig. 1). One consideration is that any rebound in BAFF secretion following B cell depletion could theoretically accelerate the maturation of residual autoreactive cells and exacerbate disease. The balance between B cell depletion and B cell regeneration also requires thought, with sustained depletion increasing infection risk.

The 'elephant in the room' of this discussion is the inability to identify and specifically eradicate disease-causing B cell clones. This gap has complicated the use of rituximab since its initial approval, which has led to numerous treatment schedules comprising distinct doses and dosing intervals, none of which are biomarker guided in terms of when to re-dose. It has become clear that monitoring total peripheral blood B cells is an inadequate measure in the standard clinical setting. Biomarker research performed in recipients of CAR T cell therapy has shown the emergence of naive B cell repertoires and even apparent resetting of metabolic and signalling pathways within diseased tissues[4]. These observations reinforce the concept of reset but do not bring the field any closer to targeted depletion of pathogenic B cell clones. Emerging technologies might make targeted approaches possible, such as chimeric autoantibody receptor (CAAR) T cell therapy[5]. Additionally, a few autoreactive B cell receptor sequences or families have been identified and could theoretically be targeted; however, the clinical application of specific autoreactive B cell depletion remains elusive. Conceptually, the equivalent of oncological 'minimal residual disease' is the goal, but with a focus on autoreactive B lineage cells rather than malignant cells. Additionally, without robust biomarkers of autoreactivity, 'cure' must remain a clinical concept that is impossible to diagnose with certainty.

Another important consideration is whether non-depleting therapies, which have fewer potential hazards than cell depletion, could achieve reset. Regulatory, as opposed to cytotoxic, CAR T cell therapy could be an option[6]. By contrast, many therapies are being developed to tolerize autoreactive T cells. These therapies are mostly non-depleting and might be considered to 'retune' rather than 'reset' the immune system; instead of eradicating autoreactivity, they retune it back towards the healthy state[7]. Most 'immune retune' T cell technologies are antigen specific and manipulate antigen presentation such that autoreactive T cells encounter autoantigen in a 'safe' context without co-stimulation. Other therapies target T cells more broadly, such as non-activating anti-CD3 antibodies or checkpoint agonists, some of which can, at least partially, deplete target cells. The concept of immune retune is gaining interest, in part because transient drug-free remission has been achieved for some patients with rheumatic disease (for example, rheumatoid arthritis) who have received conventional, non-depleting therapies[8]. As with immune reset, however, whether immune retune equates to cure remains unclear and, again, requires the development of relevant biomarkers. Rheumatologists measure inflammation and damage to monitor

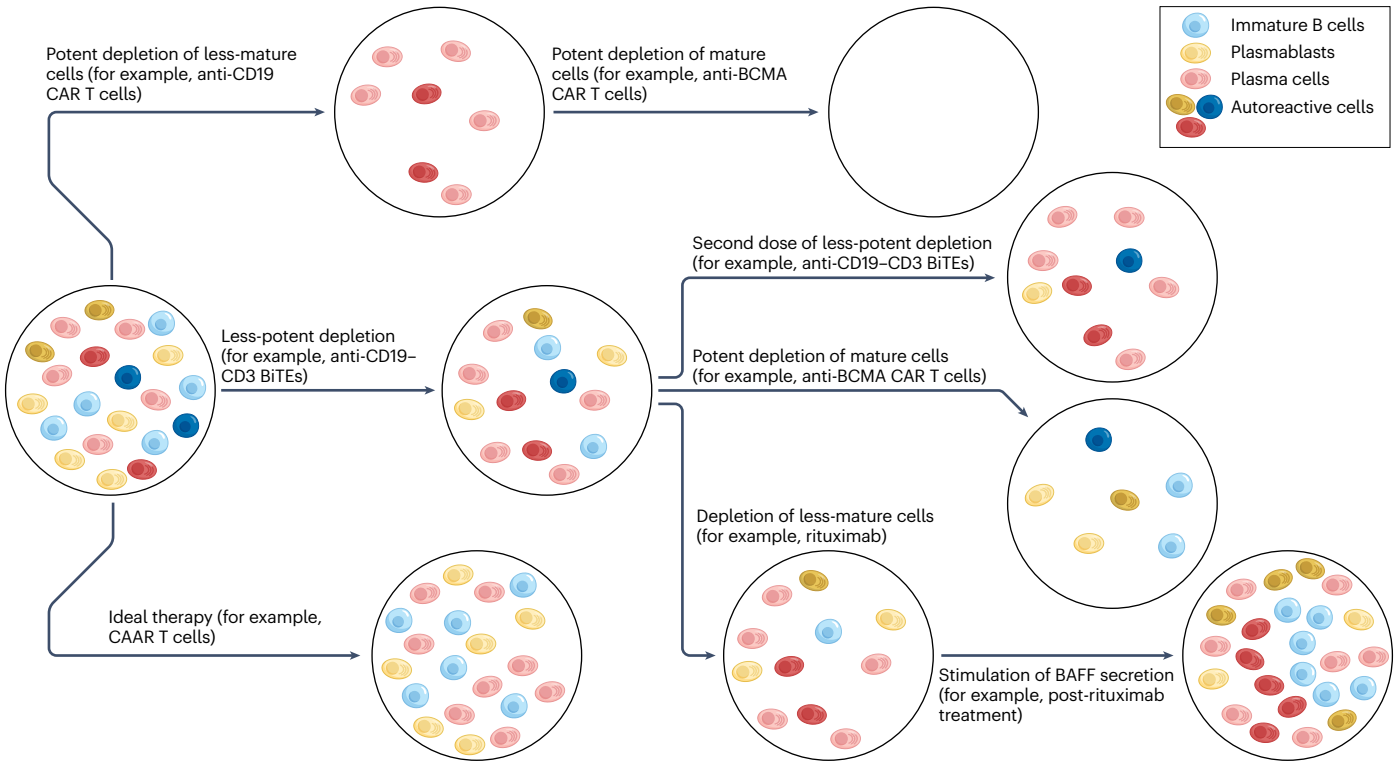

Fig. 1 | Strategies for tackling B cell autoreactivity. Each cell shown represents a cell of the B cell lineage. Immature B cells (light blue), such as CD20$^+$ B cells, can differentiate into plasmablasts (light red) that can, in turn, differentiate into plasma cells (light yellow). Autoreactive cells (dark blue, dark yellow and dark red) are shown within all B cell lineage subsets. Each large circle can represent any tissue. An example of each treatment approach is shown in parentheses. A potent depleting therapy that targets the two least mature subsets (such as CD19-targeted therapies) will eradicate these two subsets, including autoreactive cells contained within them. In many conditions (if autoreactivity resides only in these subsets), this treatment approach could lead to sustained, drug-free remission and 'B cell reset' as naive B cells return. A less-potent therapy that targets the same subsets will eradicate most but not all autoreactivity. This strategy might induce a temporary drug-free remission. A second course of the same therapy could be sufficient to eradicate, or further substantially reduce, the targeted subsets and autoreactive cells therein, leading to B cell reset and sustained, drug-free remission. This approach might increase the risk of adverse effects, such as infection, and any autoreactivity present in the most mature subset will remain. If, instead, the most mature subset is targeted with a potent therapy after relapse (such as anti-BCMA CAR T cells), this subset will be eradicated, but any residual autoreactivity within the less-mature subsets will not be eradicated. Residual (or potentially regenerated) autoreactivity among immature cells could be reduced with rituximab, although this would again delay immune reset, prolonging the risk of infection and delayed vaccine responses. Furthermore, any therapy that stimulates BAFF secretion could expand remaining cells, including autoreactive clones, and potentially accelerate relapse. The ideal therapy should target only autoreactive B cell lineage cells. BCMA, B cell maturation antigen; BiTE, bi-specific T cell engager; CAAR, chimeric autoantibody receptor; CAR, chimeric antigen receptor.

therapeutic success or failure. Reset therapies can provide rapid therapeutic benefit, whereas retune therapies might act more slowly, with benefits becoming evident only after several weeks or potentially months, as immune homeostasis is first re-established. As these therapies do not quickly reduce inflammation, objective immune biomarkers also will be essential for rational trial design, to guide decisions around administration route, dose, frequency and duration of therapy[9]. Fortunately, considerable effort is being invested in the identification and characterization of biomarkers that will inform immune retune[10].

The emergence of deep B cell depletion might signal a turning point in the management of at least some autoimmune diseases. As with all therapeutic revolutions, small-scale clinical trials must be accompanied by cutting-edge translational research and experimental medicine. This approach will enable iterative improvement of these revolutionary therapies and their optimal application. Ultimately, head-to-head trials of different therapies will be needed to demonstrate their relative efficacy and safety and the optimal management of relapse. The early success of deep B cell depletion also speaks to the important interactions between B cells and T cells and that sufficient B cell depletion can also control the activity of autoreactive T cells[3]. Improved understanding of autoreactivity and immune homeostasis, with the development of companion biomarkers, will hopefully be a consequence of this field. This understanding should facilitate the development of a range of therapies that can achieve immune reset or immune retune and, ultimately, provide an objective definition of cure.

John D. Isaacs [1,2,3]
[1]Translational and Clinical Research Institute, Newcastle University, Newcastle upon Tyne, UK. [2]Musculoskeletal Unit, Newcastle upon Tyne Hospitals NHS Foundation Trust, Newcastle upon Tyne, UK. [3]NIHR Newcastle Biomedical Research Centre, Newcastle upon Tyne, UK.
e-mail: john.isaacs@newcastle.ac.uk

Published online: 16 February 2026

References

1. Tobias, J. et al. Defining immune reset: achieving sustained remission in autoimmune diseases. *Nat. Rev. Immunol.* **25**, 528–541 (2025).
2. Anolik, J. B. et al. Delayed memory B cell recovery in peripheral blood and lymphoid tissue in systemic lupus erythematosus after B cell depletion therapy. *Arthritis Rheum* **56**, 3044–3056 (2007).
3. Tur, C. et al. Effects of different B-cell-depleting strategies on the lymphatic tissue. *Ann. Rheum. Dis.* **84**, 2065–2074 (2025).

4. Garantziotis, P. et al. Differential molecular signatures in response to CD19-CAR T cell therapy compared with conventional pharmacotherapy in systemic lupus erythematosus. *Ann. Rheum. Dis.* **85**, 153–163 (2026).
5. Oh, S. et al. Precision targeting of autoantigen-specific B cells in muscle-specific tyrosine kinase myasthenia gravis with chimeric autoantibody receptor T cells. *Nat. Biotechnol.* **41**, 1229–1238 (2023).
6. Mohseni, Y. R. et al. The future of regulatory T cell therapy: promises and challenges of implementing CAR technology. *Front. Immunol.* **11**, 1608 (2020).
7. Carballido, J. M. et al. The emerging jamboree of transformative therapies for autoimmune diseases. *Front. Immunol.* **11**, 472 (2020).
8. Rayner, F. et al. Clinical predictors of flare and drug-free remission in rheumatoid arthritis: preliminary results from the prospective BIO-FLARE experimental medicine study. *BMJ Open* **15**, e0924782025 (2025).
9. Long, E. L. et al. Autologous Tolerogenic Dendritic Cells for Rheumatoid Arthritis-2 (AuToDeCRA-2) study: protocol for a single-centre, experimental medicine study investigating the route of delivery and potential efficacy of autologous tolerogenic dendritic cell (TolDC) therapy for rheumatoid arthritis. *Trials* **26**, 278 (2025).
10. Arif, S. et al. Monitoring islet specific immune responses in type 1 diabetes clinical immunotherapy trials. *Front. Immunol.* **14**, 1183909 (2023).

Competing interests

J.D.I. has received research grants from Pfizer, Janssen and GSK, and has consulted for Abbvie, BMS, Astra Zeneca, Dragonfly Therapeutics, Eli Lilly, Istesso, Roche, AnaptysBio, Ono Pharma, Quell Therapeutics, Sanofi Aventis, Sonoma and UCB Bio.

Systemic sclerosis

SIX1 and PAI-1 emerge as therapeutic targets in systemic sclerosis

The findings of two studies published in *JCI Insight* suggest that the transcription factor SIX1 and its downstream mediator plasminogen activator inhibitor 1 (PAI-1) could be promising therapeutic targets for systemic sclerosis (SSc) and demonstrate the efficacy of the small-molecule PAI-1 inhibitor MDI-2517 in a preclinical model of the disease.

In one study, Wareing et al. sought to explore the mechanisms linking dermal white adipose tissue (DWAT) loss with fibrosis in SSc and the contribution of SIX1, which had previously been implicated as a driver of fibrosis, in this process. They showed that expression of SIX1 was increased in SSc-affected human skin samples, and that increased levels of SIX1 in adipocytes correlated with loss of DWAT in SSc skin.

Loss of DWAT was also evident in mice with bleomycin-induced dermal fibrosis, preceding fibrosis and accompanied by increased expression of *Six1*. In this mouse model, global or adipocyte-specific deletion of *Six1* attenuated DWAT atrophy and expression of pro-fibrotic genes.

In cultured mouse fibroblasts, upregulation of SIX1 directly promoted expression of *Serpine1*, the gene encoding PAI-1, thus linking SIX1 to a well-established profibrotic signalling pathway. "Rather than viewing adipocyte loss as secondary to fibrosis, our data suggest that SIX1 functions as a transcriptional switch connecting adipocyte identity loss to fibroblast-driven matrix deposition," notes co-corresponding author Harry Karmouty-Quintana. The study's findings also highlight the potential of inhibition of SIX1 or PAI-1 as a therapeutic strategy in SSc.

In a separate study, Su et al. explored the role of PAI-1 in the pathogenesis of SSc and the effectiveness of MDI-2517 to reduce skin and lung fibrosis in the bleomycin model of SSc. In mice with bleomycin-induced fibrosis, treatment with MDI-2517 reduced both skin and lung fibrosis with better efficacy than the anti-fibrotic agent pirfenidone, the immunosuppressant mycophenolate mofetil and tiplaxtinin, another PAI-1 inhibitor. MDI-2517 treatment also attenuated weight loss in the bleomycin model and seemed to preserve the intradermal adipose layer.

As well as finding increased PAI-1 expression in dermal fibroblasts from individuals with SSc-affected human skin, Su et al. demonstrated that treatment with MDI-2517 downregulated pro-fibrotic markers but did not directly inhibit expression of *SERPINE1* in cultured human SSc fibroblasts.

Further studies are needed to elucidate the precise mechanisms underlying the effects of PAI-1 inhibition and its potential in SSc and other fibrotic diseases. "Our data, and studies from others, suggest that PAI-1 can moderate multiple nodes driving fibrotic progression, including myofibroblast activation, inflammation and cell senescence," says Daniel Lawrence, corresponding author of the study by Su et al.

Sarah Onuora

Original articles: Wareing, N. et al. Adipocyte-specific deletion of sine oculis homeobox homolog 1 inhibits lipolysis and reduces skin fibrosis. *JCI Insight* https://doi.org/10.1172/jci.insight.181427 (2026); Su, E. J. et al. A potent inhibitor of PAI-1, MDI-2517, mitigates disease severity in a preclinical systemic sclerosis model. *JCI Insight* https://doi.org/10.1172/jci.insight.195005 (2026)

Rheumatoid arthritis

Fibroblast TGFβ drives treatment-refractory RA

Fibroblasts are associated with treatment resistance in rheumatoid arthritis (RA), but the underlying mechanisms remain unclear. A spatial transcriptomics study now provides insights into these mechanisms.

"We applied high-resolution spatial transcriptomics to synovial biopsies from patients with RA to identify the fibroblast-activation pathways that are responsible for treatment failure," explains corresponding author Kevin Wei. Synovial samples were obtained before treatment and 6 months after treatment.

The analysis of baseline synovial samples revealed that *COMP*$^{+}$ fibrogenic fibroblasts were expanded in TGFβ-rich vascular niches in those patients who did not achieve remission. This expansion was associated with persistent joint pain after treatment.

Notch signalling from endothelial cells controlled TGFβ responsiveness in the expanded fibroblasts, thus altering TGFβ-mediated fibrogenic signalling. In synovial tissue organoids, inhibiting Notch or TGFβ prevented this fibrogenic signalling cascade.

"A therapeutic strategy that prevents fibroblast activation represents an alternative strategy for patients who are resistant to conventional immunosuppressive therapies," notes Wei.

Holly Webster

Original article: Bhamidipati, K. et al. Spatial patterning of fibroblast TGFβ signaling underlies treatment resistance in rheumatoid arthritis. *Nat. Immunol.* https://doi.org/10.1038/s41590-025-02386-2 (2026)

Related article: Fibroblasts determine treatment outcome in rheumatoid arthritis. *Nat. Immunol.* https://doi.org/10.1038/s41590-026-02437-2 (2026)

Autoinflammatory diseases

https://doi.org/10.1038/s41584-025-01350-6

COPA syndrome spans multiple organs but is defined by STING in the lung

Anthony K. Shum

A large European cohort clarifies COPA syndrome as a multi-organ interferonopathy defined by STING-driven interstitial lung disease (ILD). These findings refine diagnosis and treatment and establish COPA syndrome as a model for systemic autoimmune rheumatic disease-associated ILD.

Refers to David, C. et al. Insights from a novel monogenic autoinflammatory disease: overview of a multicentric European cohort of 38 patients with COPA syndrome. *Ann. Rheum. Dis.* https://doi.org/10.1016/j.ard.2025.09.013 (2025).

COPA syndrome is an ultra-rare disorder of immune dysregulation caused by autosomal dominant missense mutations in the *COPA* gene. It was originally described in 2015 as an autoimmune disorder of interstitial lung disease (ILD) and arthritis, characterized by high-titre autoantibodies and elevated levels of activated, cytokine-secreting $CD4^+$ T cells[1]. A study by David et al.[2] now provides the largest comprehensive clinical analysis of COPA syndrome ever reported. Focusing on patients in Europe, the investigators reviewed data from over half of all patients with COPA syndrome in the published literature. This important work will help clinicians worldwide recognize which of their patients might have this rare disease and will provide valuable guidance on treating this challenging condition.

COPA is part of the COPI vesicle, which is responsible for transporting proteins between the Golgi apparatus and endoplasmic reticulum. In 2020, research by four teams found that patient-derived mutations impaired COPA function, resulting in failure to retrieve STING (stimulator of interferon genes) from the Golgi[3–6]. STING is dependent on trafficking for activation, with Golgi accumulation leading to aberrant activation of STING. A 2025 study confirmed that STING is necessary and sufficient to cause COPA syndrome in patients, firmly establishing the central role of this molecule in the pathogenesis of disease[7].

STING is an innate immune molecule that is part of the cGAS–STING signalling pathway that, under normal conditions, functions to provide protection against infection by sensing and responding to DNA, largely through type I interferons. COPA syndrome and the related monogenic disorder SAVI (STING-associated vasculopathy with onset in infancy) are classified as type I interferonopathies. Among these disorders, SAVI and COPA syndrome are uniquely defined by both abnormal STING activation and common and highly morbid ILD that can progress to respiratory failure[8].

The study by David et al. is a comprehensive and systematic retrospective analysis of a large European cohort of patients with genetically confirmed COPA syndrome, each of whom had a missense variant in the mutational hotspot of the *COPA* gene[2]. The study included patients with familial, de novo and somatic mosaic mutations, the last of which were first reported in 2025. The authors evaluated the clinical and immunological features of patients to gain better insight into the full spectrum of organ involvement and alterations to the immune profile. They confirm the core clinical features of COPA syndrome and provide further nuance on the specifics of organ involvement, including the patterns of ILD observed by chest imaging and the types of joint involvement that occur (that is, arthritis versus arthralgia). Rarely reported features such as hepatitis were also observed, and some less common potential manifestations of the disease were identified, including effects on the skin, heart and digestive system.

Nearly every patient in the study had lung disease[2], consistent with findings from another group, which reported that 100% of patients with COPA syndrome have ILD[7]. Importantly, the authors found that lung disease is often the earliest indicator of COPA syndrome and can be both the presenting manifestation and the principal manifestation of the disease[2]. Throughout life, ILD remains a dominant feature that often dictates management, as it causes the greatest degree of morbidity, is largely refractory to available therapies and can ultimately lead to lung transplantation or death[9]. The presence or absence of lung disease thus helps inform the likelihood of a diagnosis of COPA syndrome in a patient with undiagnosed inflammation; the persistent absence of lung disease prompts serious consideration of an alternative condition. This aspect of disease is particularly helpful when trying to prioritize *COPA* variants of unknown significance identified during genetic sequencing, particularly if they fall outside of the known mutational hotspot in the WD40 domain.

The analysis of treatments in the study is particularly informative[2]. The requirement for multiple immunomodulatory medications for many patients indicates how challenging it can be to control this disease. Janus kinase (JAK) inhibitors have been increasingly adopted by clinicians but are used mostly as an add-on therapy, probably because studies linking STING and type I interferons to COPA syndrome have emerged only in the past 5 years[3–6]. JAK inhibitors showed efficacy at controlling disease in about two thirds of patients in the study, but for many patients, disease became stable rather than improving, and some patients had progressive lung function decline[2]. Prospective studies are needed to understand whether earlier administration of JAK inhibitors and/or interferon receptor antagonists are effective and if streamlined drug regimens can be achieved. Comparisons between different JAK inhibitors could also be useful in determining if patients respond to some JAK inhibitors but not to others. Future research should also examine how antifibrotic drugs that target progressive pulmonary fibrosis fit into treatment algorithms.

The sheer number of patients included in the study by David et al. and its careful, systematic approach is highly valuable to the clinical and research communities[2]. This work will serve as an important framework for identifying the best treatments for patients and will help in the design of meaningful clinical endpoints for trials, particularly if novel therapeutics that more directly target the cGAS–STING

pathway are made available to patients with COPA syndrome. Moving forward, including patients from other registries in the analysis could be beneficial in determining whether some of the clinical manifestations described are indeed a part of COPA syndrome or are incidental findings that are not directly related to disease. Research from a 2025 study also shows that the *STING* genotype can have a considerable influence on disease penetrance. Thus, understanding whether the asymptomatic carriers in this cohort harbour the HAQ *STING1* allele, which has been shown to mediate disease protection, or whether other genetic modifiers exist will be important[7]. In addition, a comprehensive functional analysis (beyond simply an interferon score) of all reported variants, including those outside the known mutational hot spot and those of unknown significance, could be beneficial in defining potential genotype–phenotype correlations.

The pursuit of studies such as the one presented here should provide a degree of optimism for patients with COPA syndrome as researchers are striving to understand this very rare disorder so that new and better treatments can be identified. For the broader rheumatology and pulmonary communities, the breakthroughs being made in COPA syndrome, particularly in understanding of the pathogenic link between STING and ILD, have the potential to inform how clinicians manage other patients with systemic rheumatic diseases complicated by ILD, a devastating manifestation that afflicts far too many patients and remains challenging to treat[10].

Anthony K. Shum
Department of Medicine, University of California San Francisco, San Francisco, CA, USA.
e-mail: anthony.shum@ucsf.edu

Published online: 7 January 2026

References

1. Watkin, L. B. et al. *COPA* mutations impair ER-Golgi transport and cause hereditary autoimmune-mediated lung disease and arthritis. *Nat. Genet.* **47**, 654–660 (2015).
2. David, C. et al. Insights from a novel monogenic autoinflammatory disease: overview of a multicentric European cohort of 38 patients with COPA syndrome. *Ann. Rheum. Dis.* https://doi.org/10.1016/j.ard.2025.09.013 (2025).
3. Deng, Z. et al. A defect in COPI-mediated transport of STING causes immune dysregulation in COPA syndrome. *J. Exp. Med.* **217**, e20201045 (2020).
4. Lepelley, A. et al. Mutations in *COPA* lead to abnormal trafficking of STING to the Golgi and interferon signaling. *J. Exp. Med.* **217**, e20200600 (2020).
5. Mukai, K. et al. Homeostatic regulation of STING by retrograde membrane traffic to the ER. *Nat. Commun.* **12**, 61 (2021).
6. Steiner, A. et al. Deficiency in coatomer complex I causes aberrant activation of STING signalling. *Nat. Commun.* **13**, 2321 (2022).
7. Simchoni, N. et al. The common HAQ STING allele prevents clinical penetrance of COPA syndrome. *J. Exp. Med.* **222**, e20242179 (2025).
8. Goldbach-Mansky, R., Alehashemi, S. & de Jesus, A. A. Emerging concepts and treatments in autoinflammatory interferonopathies and monogenic systemic lupus erythematosus. *Nat. Rev. Rheumatol.* **21**, 22–45 (2025).
9. Simchoni, N., Vogel, T. P. & Shum, A. K. COPA syndrome from diagnosis to treatment a clinician's guide. *Rheum. Dis. Clin. North Am.* **49**, 789–804 (2023).
10. Johnson, S. R. et al. 2023 American College of Rheumatology (ACR)/American College of Chest Physicians (CHEST) guideline for the treatment of interstitial lung disease in people with systemic autoimmune rheumatic diseases. *Arthritis Care Res.* **76**, 1051–1069 (2024).

Acknowledgements

The author thanks N. Simchoni for useful edits.

Competing interests

A.K.S. has submitted a patent for HAQ *STING1* gene therapy for COPA syndrome.

nature reviews rheumatology

https://doi.org/10.1038/s41584-025-01349-z

Review article

Check for updates

Mechanisms of fibrotic tissue remodelling: insights from systemic sclerosis

Jörg H. W. Distler[1,2,3,10] ✉, David Launay[4,5,10], Carol Feghali-Bostwick[6,10], Alexandru-Emil Matei[1,2,3,10], Maria Trojanowska[7,10] & Johann E. Gudjonsson[8,9,10]

Abstract

Systemic sclerosis (SSc) is a prototypical systemic immune-mediated fibrosing disease that affects the skin, the lungs, the heart, the kidneys and the intestinal tract. Similar to many other fibrotic diseases, SSc is associated with high morbidity and mortality and therapeutic options are limited. Fibrosis arises from a complex interplay of vascular damage, inflammation and prolonged, misdirected repair responses. The progressive accumulation of extracellular matrix perturbs the physiological tissue architecture and commonly leads to failure of the affected organs. Understanding the mechanisms of fibrotic tissue remodelling can lead to the identification of preclinical targets. Novel fibrosis-promoting cell subpopulations, the interplay of fibroblasts with B cells and macrophages, the nerve–fibroblast axis, matrikines and matricryptins, senescence, profibrotic transcription factors, developmental pathways and epigenetic tissue memory are all important drivers of fibrotic tissue remodelling that might offer potential for novel therapies to improve outcomes for patients with SSc and possibly other fibrotic conditions.

Sections

Introduction

Fibroblasts in fibrotic tissue remodelling

Fibroblast heterogeneity in systemic sclerosis

Vasculature–fibroblast crosstalk in systemic sclerosis

Autoimmune and inflammation-mediated fibroblast activation in systemic sclerosis

Profibrotic transcription factors

Developmental pathways

Epigenetic changes and fibrotic tissue memory

Other self-maintaining activation loops

Conclusions

[1]Department of Rheumatology, University Hospital Düsseldorf, Heinrich-Heine University, Düsseldorf, Germany. [2]Hiller Research Center, University Hospital Düsseldorf, Heinrich-Heine University, Düsseldorf, Germany. [3]Fraunhofer Institute for Translational Medicine and Pharmacology ITMP, and Fraunhofer Cluster of Excellence for Immune Mediated Diseases CIMD, Frankfurt am Main, Germany. [4]Department of Internal Medicine and Clinical Immunology, CHU Lille, Lille, France. [5]University of Lille, Inserm, CHU Lille, U1286-INFINITE-Institute for Translational Research in Inflammation, Lille, France. [6]Division of Rheumatology, Department of Medicine, Medical University of South Carolina, Charleston, SC, USA. [7]Arthritis & Autoimmune Diseases Research Center, Department of Medicine, Boston University Chobanian & Avedisian School of Medicine, Boston, MA, USA. [8]Department of Dermatology, University of Michigan, Ann Arbor, MI, USA. [9]Department of Internal Medicine, Division of Rheumatology, University of Michigan, Ann Arbor, MI, USA. [10]These authors contributed equally: Jörg H. W. Distler, David Launay, Carol Feghali-Bostwick, Alexandru-Emil Matei, Maria Trojanowska, Johann E. Gudjonsson. ✉e-mail: joerg.distler@med.uni-duesseldorf.de

Key points

- The pathogenesis of systemic sclerosis (SSc) is characterized by an interplay of vascular damage, autoimmunity-induced inflammation and fibrotic tissue responses.
- These processes are highly interlinked and are active throughout all stages of the disease, although their relative contribution to disease progression can vary at different disease stages and in different patient populations.
- Advances in omics technologies have enabled identification and phenotyping of different cellular subpopulations with diverse functions in the pathogenesis of SSc.
- Interactions between leukocyte subpopulations, such as B cells and macrophages, and fibroblasts have an important role in disease progression.
- Molecular drivers of SSc include, but are not limited to, the nerve–fibroblast axis, matrikines, senescence, JAK–STAT signalling, nuclear receptors and other profibrotic transcription factors, developmental pathways and epigenetic tissue memory.

Introduction

Fibrosis describes the excessive deposition of collagen and other extracellular matrix (ECM) components in tissues. The accumulating ECM disrupts the normal tissue architecture and impairs organ function. Fibrotic tissue remodelling can affect almost every organ system. Moreover, fibrotic tissue responses are not limited to prototypical fibrotic disorders but are also highly prevalent in many chronic diseases, including cardiovascular diseases, chronic inflammatory diseases and cancer[1–3], in which these responses have a crucial impact on disease outcomes. Indeed, up to 45% of all deaths in developed countries might be attributed to fibrotic tissue responses[4]. Thus, fibrosis represents a substantial health care challenge, particularly as the incidence of fibrotic diseases is increasing further[1].

Fibrosis and normal wound healing share many commonalities and fibrotic diseases might be considered an exacerbated, prolonged repair response that is not appropriately terminated[5,6]. Fibrotic tissue remodelling can be divided into different, though overlapping phases: a triggering event in a genetically susceptible individual; an initiating phase, in which the trigger is converted into molecular responses and first histopathological changes; a phase of progression, in which type 2 inflammation and vascular damage promote fibroblast activation and fibrotic remodelling; and a late phase, which is highly variable and can range from mild-to-moderate regression of fibrosis. The latter phase occurs in every tissue; however, this phase is variable. In the skin, this phase can be associated with regression owing to ongoing inflammation-induced remodelling, persistent activation of profibrotic fibroblast subsets and progressive fibrosis driven by endogenous mechanisms independent of overt inflammation. This regression does not occur in the lungs[2,7,8].

Fibrosis can manifest in diverse ways depending on its localization within the tissue, the extent of remodelling[9] and the specific anatomical compartment or organ involved. In the skin, localized fibrotic disorders include lichen sclerosus, which primarily affects the anogenital region and is characterized by fibrosis in the upper layers of the dermis[10], morphea, which is associated with widespread fibrosis in the dermis[11] and types of scarring alopecia, such as discoid lupus erythematosus (fibrosis surrounds hair follicles and often leads to permanent hair loss and fibrosis), or hidradenitis suppurativa (scarring occurs at sites of prior inflammation[12]). By contrast, generalized and diffuse cutaneous fibrosis, often accompanied by internal organ involvement, is characteristic of systemic sclerosis (SSc).

In this Review, we discuss the molecular mechanisms that mediate fibrotic tissue remodelling in SSc as a prototypical immune-mediated systemic fibrotic disease. We focus on mechanisms that promote fibroblast activation at disease initiation and progression, and also on intrinsic mechanisms that can drive fibroblast activation and disease progression at later stages of disease. We highlight intracellular signalling cascades and molecular pathways that have not yet been translated into clinical trials; we do not explore core pathways of fibrosis such as canonical transforming growth factor-β (TGFβ), platelet-derived growth factor (PDGF), interferon or IL-6 signalling, for which molecular targets are currently under investigation in clinical trials and are reviewed elsewhere[2,6,13].

Fibroblasts in fibrotic tissue remodelling

Fibroblasts are key effector cells of fibrotic remodelling as they release the vast majority of ECM components that accumulate in fibrotic tissues[2,14,15]. The differentiation of disease-promoting fibroblast populations and/or different fibroblast states is thought to be initially driven by mediators released from infiltrating immune cells such as B cells, T cells and innate lymphoid cells, activated tissue-resident cells such as macrophages and plasma cells, and also from damaged endothelial cells. However, the role of fibroblasts extends beyond the synthesis of the ECM[16]. Fibroblasts also release mediators that modulate inflammatory responses, which might support the maintenance of chronic, low-grade inflammation in affected tissues. Moreover, fibroblasts can release pro-angiogenic and anti-angiogenic mediators that can modulate angiogenesis and thus alter the outcome of microvascular manifestations of SSc. Last, fibroblasts can release both profibrotic and antifibrotic mediators that can exert autocrine and paracrine effects. Fibroblasts in SSc and other fibrotic diseases are thus not passively converting stimuli from inflammatory cells and vascular cells into ECM production, but they themselves actively modulate the vascular, inflammatory and fibrotic pathogenesis of SSc[2].

Fibroblast heterogeneity in systemic sclerosis

Omics-based phenotyping data have revealed that fibroblasts are a heterogeneous population of phenotypically and functionally distinct subpopulations, even within a given patient and a given tissue[17] (Table 1 and Fig. 1). Certain fibroblast subpopulations are ubiquitous and can be found across all organs, whereas other fibroblast subpopulations and/or fibroblast states are restricted to certain tissues under homeostatic conditions[18]. In disease, the ratios of these individual fibroblast subpopulations can change dramatically, individual populations can show changes in phenotype and additional populations might emerge. Although omics studies have been highly informative and provided insights into fibroblasts biology, these findings are limited by the variations in fibroblast nomenclature used in each study[18–20]; however, efforts have been made to link and standardize nomenclature and definitions of specific fibroblast populations across human tissues[20]. Using skin as a reference tissue, the authors of this study defined six major fibroblast subsets in healthy skin along with three subsets in

Table 1 | Major fibroblast subsets

Subtype	Main markers or genes	Identification method	Localization in tissue	Function	Refs.
Superficial fibroblasts	*COL18A1*, *COL23A1*, *SFRP2*, *WIF1*, *APCDD1* and *NKD2*	scRNA-seq	Superficial papillary dermis	Possible role in epithelial homeostasis via interactions with the epithelium	20–24,104
Universal fibroblasts	*CD34*, *PI16* and *DPP4*	scRNA-seq	Deep in the skin (reticular dermis)	Found in many tissues and postulated to represent a precursor fibroblast state	17,22–26,28,47
Universal fascial fibroblasts	*CD34*, *PI16*, *DPP4*, *FGF18* and *CCN3*	scRNA-seq	Fascia	High expression of the myofibroblast gene signature and high ECM production	17,20,23, 25,26,28,47
Stroma^{+}*PPARG*$^{+}$ fibroblasts	*CD34*, *PI16*, *CXCL12*, *APOE*, *PLA2G2A*, *C7* and *SFRP2*	scRNA-seq	Deep perivascular immune infiltrate regions and interstitial stroma	The capability to differentiate into adipocytes	20,23,25,26,28, 47,124–126,152
Fibroblastic reticular cell-like fibroblasts	*CCL19*, *CH25H*, *IL33*, *CD74* and *HLA-DR*	scRNA-seq	Found in lymphoid organs and structures, enriched in superficial perivascular regions and adjacent to hair follicles in the skin	Maintenance of T cell populations and facilitation of T cell–dendritic cell interactions	20,26
Schwann-like fibroblasts					
Schwann-like *RAMP1*$^{+}$ fibroblasts	*RAMP1* and *PLEKHA6*	scRNA-seq	Enriched near eccrine (sweat) glands	Possibly form an interface with the nervous system	20
Schwann-like *NGFR*$^{+}$ fibroblasts	*NGFR* and *ITGA6*	scRNA-seq	Endoneurium and perineurium of nerve fibres	Nerve-associated fibroblast population	20,99
Myofibroblasts					
Classical myofibroblasts	*COL3A1*, *COL5A1*, *COL8A1*, *POSTN*, *TNC*, *ACTA2* and *SPARC*	scRNA-seq	Diffuse in the dermis	Excessive ECM production, typically enriched in skin diseases with high scarring risk and in established fibrosis	20,24
Inflammatory myofibroblasts	*CXCL5*, *CXCL6*, *CXCL8*, *CXCL13*, *IL11*, *IL24*, *MMP1* and *MMP3*	scRNA-seq	Diffuse in the dermis	Recruitment of neutrophils, monocytes and B cells, typically enriched in skin diseases with a high scarring risk, but not in established fibrosis	20,26, 51,63,64
Mechanosensing myofibroblasts	*SFRP4*, *LRRC17* and *PIEZO2*	scRNA-seq	Precise location remains to be determined	Excessive ECM production, mechanotransduction and associated with disease or wound healing	20
Fascia-like myofibroblasts	*ITGA10*, *THBS* and *PDLIM3*	scRNA-seq	Precise location remains to be determined	Excessive ECM production, present especially in Dupuytren contracture and associated with disease or wound healing	20
Lung fibroblasts					
Alveolar fibroblasts	*COL13A1*, *NDNF*, *TCF21*, *PDGFRA*, *FGF10* and *COL13A1*	scRNA-seq	Alveoli	Contribute to the maintenance of alveolar structure and function	35,37,50, 96–98
Hair follicle-associated fibroblasts					
DPEP1^{+} dermal sheath fibroblasts	*DPEP1* and *MYL4*	scRNA-seq	Dermal sheath	Precise function remains to be determined	12,20
TNN^{+}*COCH*$^{+}$ fibroblasts	*CRABP1*, *RSPO3*, *COL24A1*, *TNN*, *COCH*, *MKX* and *TNMD*	scRNA-seq	Isthmus (mid-hair shaft)	Precise function remains to be determined	12,20
HHIP^{+} dermal papilla fibroblasts	*CRABP1*, *RSPO3*, *COL24A1*, *HHIP* and *RSPO4*	scRNA-seq	Dermal papillae	Precise function remains to be determined	12,20–22
Fibroblasts described in SSc					
LGR5^{+} fibroblasts	*LGR5*, *MMP2* and *CD55*	scRNA-seq	Deep reticular dermis	Associated with several pathogenic features of SSc	28
PI16^{+} fibroblasts	*PI16*	scRNA-seq	Diffuse in the dermis	Homeostatic, precursors for other fibroblast subsets	18,26,27,29

Table 1 (continued) | Major Fibroblasts subsets

Subtype	Main markers or genes	Identification method	Localization in tissue	Function	Refs.
Fibroblasts described in SSc (continued)					
CCL19$^+$ fibroblasts	*CCL19*, *PTGDS*, *APOE*	scRNA-seq	Perivascular or diffuse in the dermis	Pro-inflammatory	25,27
COL11A1$^+$ fibroblasts	*COL11A1*, *TAGLN*, *POSTN*	scRNA-seq	Precise location remains to be determined	Profibrotic	27
SFRP4$^+$ *SFRP2*$^+$ fibroblasts	*SFRP4*, *MFAP5*, *C1QTNF3*	scRNA-seq	Precise location remains to be determined	Profibrotic	27
PRSS23$^+$*SFRP2*$^+$ fibroblasts	*PRSS23*, *DPP4*, *STC2* and *CTHRC1*	scRNA-seq	Precise location remains to be determined	Profibrotic	27
COL8A1$^+$ fibroblasts	*COL8A1* and *ACTA2*	scRNA-seq	Deep dermis	Profibrotic	25
SFRP2$^+$ PapD fibroblasts	*SFRP2*, *COL6A1* and *APCDD1*	scRNA-seq	Papillary dermis	Profibrotic	24–26
SFRP2$^+$ RetD fibroblasts	*SFRP2*, *SPAR* and *COL1A1*	cISH	Reticular dermis	Profibrotic	26
CCL19$^+$ PV fibroblasts	*CCL19*, *MALAT1* and *CD74*	cISH	Perivascular	Pro-inflammatory	26
CCL19$^+$ non-PV fibroblasts	*CCL19*, *PTGDS* and *APOE*	cISH	Diffuse localization in the dermis	Pro-inflammatory	26,27
S1PR$^+$ fibroblasts	S1PR	IMC	Diffuse localization in the dermis	Profibrotic	30
Thy1$^+$ADAM12^{high}PU.1^{high} fibroblasts	Thy1, ADAM12 and PU.1	IMC	Diffuse localization the dermis	Probably profibrotic	30,124
ADAM12$^+$ GLI1$^+$ fibroblasts	ADAM12 and GLI1	IMC	Papillary dermis	Probably profibrotic	30
Met^{hi} fibroblasts	Several key enzymes that are involved in glycolysis, the TCA cycle and OXPHOS	IMC	Diffuse localization in the dermis	Profibrotic	30,31

ADAM12, a disintegrin and metalloproteinase domain-containing protein 12; cISH, chromogenic in situ hybridization; ECM, extracellular matrix; GLI, glioma-associated oncogene homologue 1; IMC, imaging mass cytometry; Met, metabolism; OXPHOS, oxidative phosphorylation; PapD, papillary dermis; PV, perivascular; RetD, reticular dermis; S1PR, sphingosine-1-phosphate receptor; scRNA-seq, single-cell RNA sequencing; SSc, systemic sclerosis; TCA, tricarboxylic acid.

inflammatory states that often have distinct distribution in the skin (Table 1 and Fig. 1). These subsets included two major subsets of superficial fibroblasts (often referred to as papillary dermal fibroblasts[21–23]) and universal fibroblasts that are typically located deeper in the skin (often referred to as reticular fibroblasts[23,24]). Other subsets were more specialized and included fibroblastic reticular cells (FRCs), which are found in lymphoid organs, perivascular regions and adjacent to hair follicles. Stromal fibroblasts were found in deeper perivascular and interstitial regions, and hair follicle-associated fibroblasts and Schwann-like fibroblasts were enriched near sweat glands and nerves. The three fibroblast subsets identified in diseased tissues include inflammatory myofibroblasts (which express multiple chemokines, particularly those involved in neutrophil recruitment), myofibroblasts, and fascia-like myofibroblasts. In addition, these fibroblast subsets were used to derive a consensus nomenclature across human tissues, across diverse tissues such as the intestine, lungs, salivary glands, joints and skin[20].

Several subpopulations of fibroblasts have been described in SSc, which differ with regard to their location and function (Table 1). Myofibroblasts in SSc (which express high levels of *COL8A1*) seem to be derived from *SFRP2*$^+$ fibroblasts[25], which correspond to either the superficial or universal fibroblast subsets described previously. Two subpopulations of *SFRP2*$^+$ fibroblasts have been identified that can be separated based on both their gene expression and that of neighbouring cells using the spatial resolution provided by cyclic in situ hybridization (cISH)[26]. One *SFRP2*$^+$ fibroblast subpopulation is located in the papillary dermis, whereas the other is located in the reticular dermis. Although these subpopulations have distinct changes in frequency in SSc, both upregulate profibrotic signalling pathways[26]. Another population of *CCL19*$^+$ fibroblasts that have an inflammatory phenotype have been described in SSc and resemble the inflammatory fibroblasts described previously[27]. These *CCL19*$^+$ fibroblasts can be segregated by cISH according to their localization to either the perivascular region or diffusely in the dermis[26]. The number of *LGR5*$^+$ fibroblasts is lower in patients with diffuse cutaneous SSc (dcSSc) compared with patients who have limited cutaneous SSc (lcSSc) and healthy individuals[28]. In addition to changes in frequency, these fibroblasts also have altered signalling pathways related to fibrosis, vasculopathy and inflammation. Several studies show that *PI16*$^+$ fibroblasts are present across several organs, have stem-cell properties and can differentiate into specialized fibroblasts[18,29]. The frequency of *PI16*$^+$ fibroblasts is also lower in SSc skin than in healthy skin, as these cells can serve as a potential source of profibrotic fibroblasts, the lower number of these cells in SSc could indicate the differentiation of these cells into profibrotic fibroblasts[26,27].

The annotation of fibroblasts using single-cell RNA sequencing (scRNA-seq) or cISH in SSc has been refined by imaging mass cytometry (IMC), a spatial proteomics technique that has enabled the identification of 13 fibroblast subsets; the frequency of 8 of these subsets was altered in SSc[30]. Of these, a population of sphingosine-1-phosphate receptor (S1PR$^+$) fibroblasts had a higher frequency in both the papillary and the reticular dermis in SSc than in healthy individuals. This finding

correlated with the modified Rodnan skin score, particularly when not only the cellular frequency but also the interactions of S1PR$^+$ fibroblasts with other cell types, such as ADAM12$^+$ GLI1$^+$ fibroblasts, were taken into consideration.

In another study, thus far available only as a preprint, IMC enabled the identification of 8 metabolically defined subpopulations of fibroblasts in SSc that differ with regard to their metabolic regulome (composed of over 20 key enzymes across several metabolic pathways)[31]. One subpopulation of Met^{hi} (that is, metabolically active) fibroblasts had high glycolysis, hypoxia, reactive oxygen species signalling and tricarboxylic acid (TCA) and oxidative phosphorylation scores (indicative of the high level of activity of these pathways)[31]. Furthermore, these cells expressed high levels of α-smooth muscle actin (αSMA) and fibroblast activation protein (FAP), and thus had

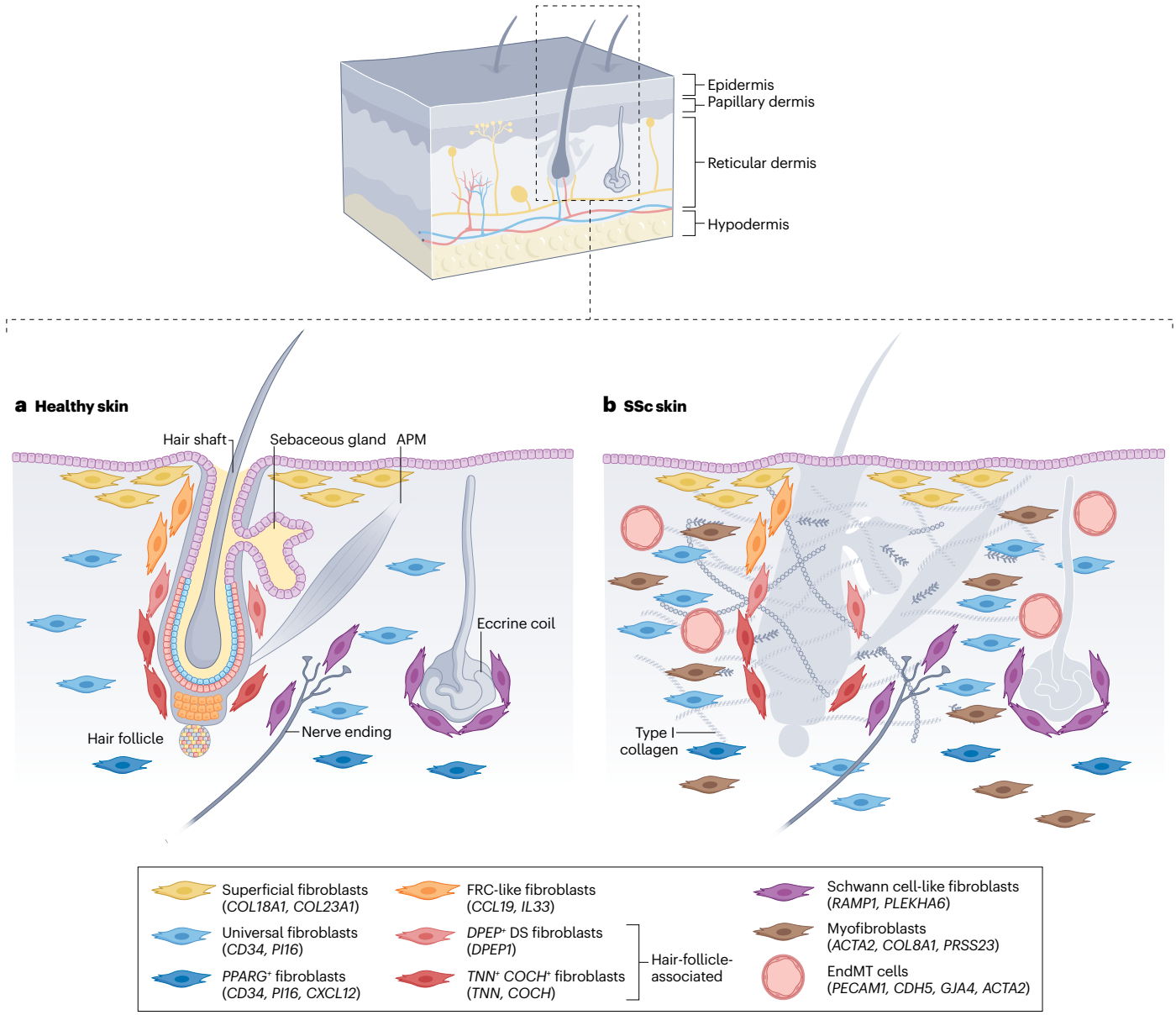

Fig. 1 | Localization and diversity of fibroblast subsets in healthy skin and skin with systemic sclerosis. a, Fibroblast subpopulations in the skin have distinct spatial distributions. Superficial fibroblasts (yellow) are located in the papillary dermis, whereas universal fibroblasts (light blue) are distributed throughout the dermis, with *PPARG*$^+$ fibroblasts (dark blue) enriched in the deeper layers of the dermis. Several fibroblast subsets localize to hair follicles, including fibroblastic reticular cell (FRC)-like fibroblasts (orange) around the follicle opening, and two other subsets (shown in dark red and light red) are located along the follicular shaft and bulge region. Other specialized fibroblasts are found near eccrine glands or nerve endings, such as Schwann cell-like fibroblasts (purple), underscoring the functional and positional heterogeneity of dermal fibroblasts. **b**, In systemic sclerosis (SSc), several fibroblast subsets expand, particularly αSMA$^+$ (α smooth-muscle actin) myofibroblasts (brown) and endothelial-to-mesenchymal transition (EndMT) cells, both of which contribute to type I collagen production and deposition in the skin. Fibrosis in SSc skin is often accompanied by loss of adnexal structures, including hair follicles, sebaceous and eccrine sweat glands. APM, arrector pili muscle; DS, dermal sheath.

a myofibroblast phenotype, but could not be separated from other populations by expression of αSMA and FAP alone. This population is increased in frequency in those patients with SSc and progression of skin fibrosis[31].

The activation of fibroblasts in SSc is driven by a core set of signalling pathways. Traditionally, core signalling pathways of fibroblast activation have been defined as stimuli that can induce a myofibroblast phenotype in resting fibroblasts with upregulation of ECM proteins such as type I collagen and induction of αSMA positive stress fibres that mediate contractility. However, this definition might miss pathways that drive the progression of fibrosis by inducing shifts from homeostatic subpopulations to pro-inflammatory or profibrotic subpopulations and those that promote the differentiation of disease-associated fibroblast populations. Although omics-based profiling shows unique patterns of signalling for each of these fibroblast subpopulations, a deeper understanding of the effects of core fibrosis pathways on individual subpopulations is lacking and how targeting these core pathways affects the numbers and function of fibroblasts remains unclear.

Vasculature–fibroblast crosstalk in systemic sclerosis

The first manifestation of SSc is apoptosis of the microvascular endothelium. Apoptotic microvascular endothelial cells are detected in preclinical models of SSc before the onset of typical clinical manifestations and before inflammatory and fibrotic changes[32]. The precipitating trigger and the molecular mechanisms underlying the induction of apoptosis remain enigmatic. Whether the induction of apoptosis in endothelial cells is a direct consequence of this trigger or a consequence of a misdirected autoimmune response against endothelial cells is unclear; however, autoantibodies directed against different antigens expressed on endothelial cells are reported in SSc[33,34]. These antibodies might maintain chronic vascular injury even after clearance of the trigger. An increase in granzyme-expressing cytotoxic $CD4^+$ and $CD8^+$ T cells colocalizing with apoptotic endothelial cells is described in the skin of patients with early dcSSc, suggesting a direct role of cytotoxic T cells in endothelial cell death[35].

Evidence indicates that vascular injury promotes fibroblast activation in SSc. Platelets are activated at sites of vascular injury in SSc, which leads to the release of platelet granules into the blood. Platelet granules contain large amounts of serotonin (5-hydroxytryptamine (5-HT)) and lower concentrations of other profibrotic mediators including PDGF[36]. 5-HT has been implicated in the pathogenesis of fibrotic tissue remodelling in multiple organs[37]. Stimulating mesenchymal cells with 5-HT in vitro can induce collagen production. These effects are mediated by 5-HT2 receptors, particularly the 5-HT2B receptor, which can activate TGFβ–SMAD3 signalling[38]. Pharmacological or genetic inactivation of the 5-HT2B receptor or knockout of *TPH1*, which encodes tryptophan hydroxylase (the rate-limiting enzyme for 5-HT synthesis in non-neuronal tissues), ameliorates experimental dermal and pulmonary fibrosis[38,39]. Moreover, activated platelets upregulate thymic stromal lymphopoietin (TSLP) in microvascular endothelial cells and might thereby contribute to the increased levels of TSLP found in the blood of patients with SSc[40]. TSLP promotes fibroblast activation, thus providing another link between platelet activation and fibrotic tissue remodelling in SSc.

Increased coagulation might also promote fibrotic tissue remodelling in different organs, although there is no direct evidence of this mechanism in SSc thus far. Thrombin induces the expression of connective tissue growth factor, stimulates proliferation of fibroblasts and promotes fibroblast-to-myofibroblast transition[41]. Moreover, the thrombin inhibitor dabigatran ameliorates experimental fibrosis in multiple organs[42].

The atypical chemokine receptor 1 (ACKR1), also known as Duffy antigen receptor, has been implicated in tissue inflammation across various organs in SSc. ACKR1 is expressed on postcapillary venules and facilitates chemokine transport[43]. Increased ACKR1 expression is found in lesional SSc skin, where it promotes immune cell recruitment[44]. In the bleomycin model of skin fibrosis, elevated ACKR1 levels are associated with immune cell infiltration and fibrosis, whereas ACKR1 inhibition attenuates this effect[44]. Expansion of venous $ACKR1^+$ endothelial cells also occurs in patients with idiopathic pulmonary fibrosis (IPF)[45]. In fibrotic lungs, $ACKR1^+$ endothelial cells are spatially localized within immune cell aggregates, fibroblastic foci and aberrant basaloid cell regions, consistent with their pro-inflammatory and profibrotic functions.

Endothelial-to-mesenchymal transition describes a phenotypic and functional change of endothelial cells, which includes gradual loss of endothelial markers and expression of mesenchymal cell markers. Cells that co-express endothelial cell markers (vascular endothelial-cadherin and von Willebrand factor) and mesenchymal cell markers (αSMA, collagen and fibroblast-specific protein 1 (also known as S100A4)) have been identified in the skin and lungs of people with SSc[46,47]. Cells that undergo endothelial-to-mesenchymal transition are reported to originate from $GJA4^+$ arteriolar endothelial cells, and Hippo signalling promotes this transition[25]. Spatial proteomics analyses of SSc skin support these findings, revealing an increase in $CD34^+$ $αSMA^+$ $CD31^+$ triple-positive cells that express markers of endothelial-to-mesenchymal transition in SSc vascular niches[48]. These niches are also enriched in immune cells and myofibroblasts, and the density of these cells correlates with progressive fibrotic remodelling in patients with SSc[48]. Endothelial-to-mesenchymal transition might therefore add to the pool of profibrotic fibroblast populations that drive fibrotic remodelling in SSc.

Pericytes are stromal cells that warp around endothelial cells in capillaries and post-capillary venules, and together with vascular smooth muscle cells make up the mural cells that support blood vessels in tissues. Pericytes are mainly found around pre-capillary, capillary and post-capillary vessels where they regulate vessel tone and integrity, and influence chemotaxis and diapedesis of leukocytes[49]. In people with early SSc, pericytes have an activated phenotype, possibly owing to a PDGF–PDGF receptor-β autocrine or paracrine loop that involves endothelial cells[50,51] Pericytes might also directly contribute to the production of ECM upon acquisition of a myofibroblast phenotype (pericyte-to-myofibroblast transdifferentiation) or indirectly by promoting fibroblast activation via PDGF-AB or PDGF-BB interacting with the PDGFβ receptor[51].

Autoimmune and inflammation-mediated fibroblast activation in systemic sclerosis

Inflammation is thought to be a key driver of fibroblast activation and fibrosis. Although SSc is not a classical inflammatory disease and markers of systemic inflammation, such as C-reactive protein, are not elevated in two-thirds of patients, low-grade inflammation in affected tissues is essential for disease initiation and a central driver of disease progression.

B cells and T cells

Accumulating evidence highlights a central role of B cells in the pathogenesis of SSc. B cell activation is dysregulated in SSc at multiple levels,

including a bias towards effector B cells with an activated phenotype and impaired regulatory B (B_{reg}) cell function[52,53]. B cells promote fibroblast activation and fibrotic remodelling through multiple mechanisms including release of cytokines, chemokines, autoantibodies and direct cellular interactions with fibroblasts and other effector cells[54] (Fig. 2).

In SSc, naive, transitional and $CD21^{low}CD38^{low}$ peripheral B cell subsets are increased, whereas memory B cells, switched memory B cells and IL-10-producing B_{reg} cells are reduced[53,55]. Memory B cells in SSc express increased levels of activation markers such as CD80, CD86 and CD95, and transitional B cells have increased expression of TIM1. Decreased expression of CD22 and elevated CD19 expression further dysregulate B cell receptor signalling[56], skewing B cell populations towards an activated phenotype in SSc.

B cells and plasma cells are increased in tissue samples obtained from the skin, lung and gastrointestinal tract of people with SSc[57,58]. Consistently, pronounced B cell signatures enriched in immunoglobulin genes are observed in SSc skin, particularly in patients with early dcSSc[59]. Dermal B cell extravasation probably involves endothelial E-selectin interacting with cutaneous lymphocyte antigen and α4β1 integrin. In SSc-related interstitial lung disease (SSc-ILD) and pulmonary arterial hypertension $CD19^{+}$ B cells are increased, and some of

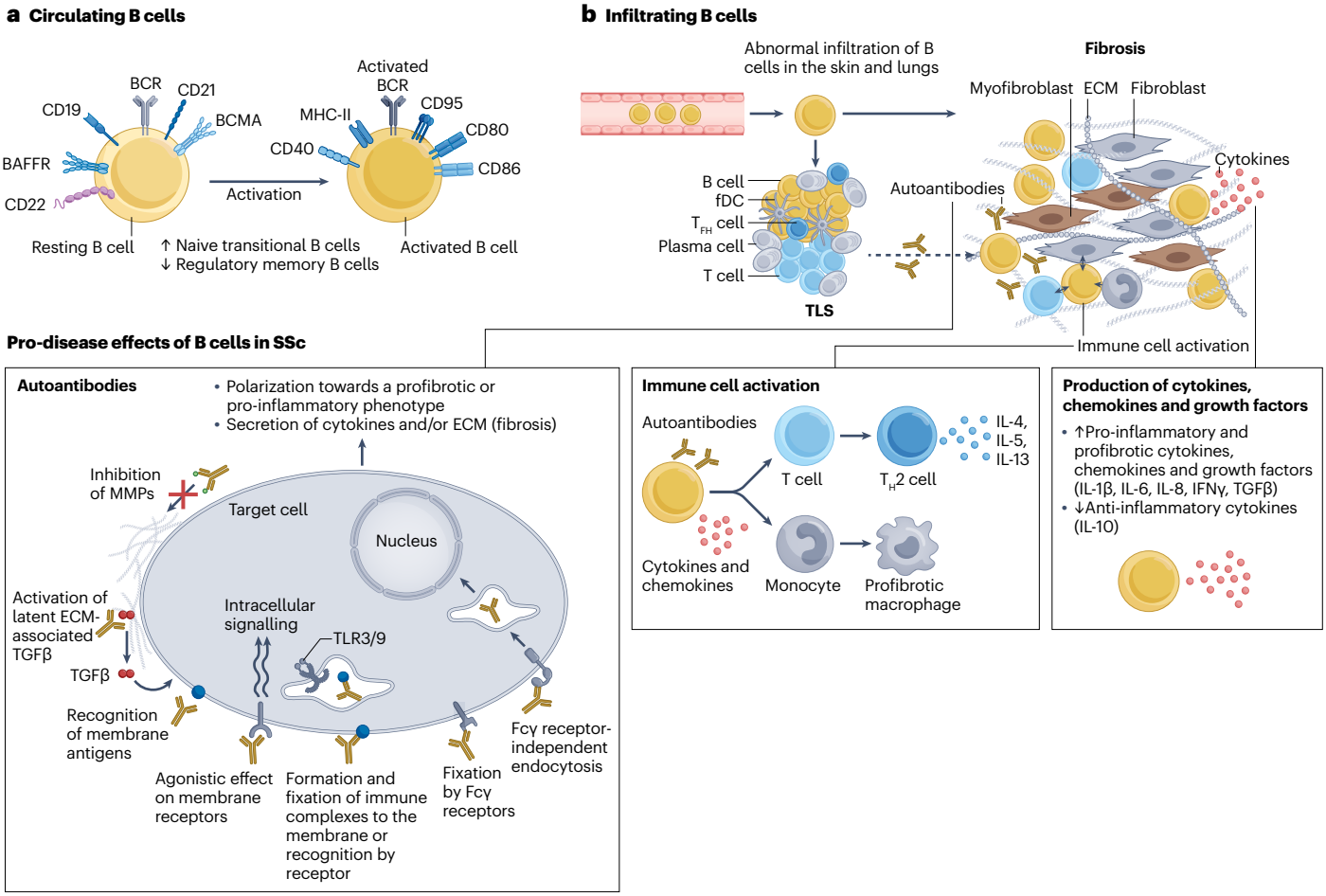

Fig. 2 | Role of B cells in the pathophysiology of systemic sclerosis. **a**, Peripheral B cell populations in systemic sclerosis (SSc) are skewed towards increased naive and transitional B cells, with reduced memory B cells and IL-10-producing regulatory B cells. B cells, particularly memory subsets, exhibit elevated expression of activation markers (CD80, CD86, CD95), decreased regulatory CD22 expression and increased CD19 expression. Those receptors shown in blue are increased on B cells in SSc and those shown in purple are decreased. **b**, Abnormal infiltration of B cells characterizes skin and lung tissues in SSc and these cells can form immune-cell aggregates that might resemble tertiary lymphoid structures (TLSs). In the skin, B cell extravasation probably involves E-selectin expressed on dermal endothelial cells, E-selectin ligands (such as cutaneous lymphocyte antigen) and α4β1 integrin on B cells. Through secretion of pro-inflammatory cytokines (including IL-6, TNF and IL-13) and chemokines, infiltrating B cells activate fibroblasts, endothelial cells and other immune cells. Tissue-resident B cells also interact with non-immune cells, modulating SSc-related fibrosis. Additionally, infiltrating B cells perpetuate disease through autoantibody production. B cells produce autoantibodies, including autoantibodies that activate fibroblasts and polarize them towards profibrotic or pro-inflammatory, disease-promoting phenotypes. B cell and T cell interactions contribute to sustained inflammation and autoimmunity in SSc. B cells present self-antigens and provide co-stimulatory signals to $CD4^{+}$ T cells, promoting a T helper 2 (T_H2) cell immune response characterized by IL-4, IL-5 and IL-13 production. B cells also stimulate macrophages to adopt a profibrotic phenotype. B cells release pro-inflammatory and profibrotic cytokines, chemokines and growth factors that further promote fibrosis. BAFFR, BAFF receptor; BCR, B cell receptor; ECM, extracellular matrix; fDC, follicular dendritic cell; MMPs, matrix metalloproteinases; T_{FH} cell, T follicular helper cell; TGFβ, transforming growth factor-β.

these cells are then organized into tertiary lymphoid structures[60,61]. Lung-resident B cells in SSc include $CD19^+CD21^{low/neg}$, IgM^+ and $CD138^+CX3CR1^+$ plasma cells[62].

Secretion of cytokines is a central mechanism by which B cells activate fibroblasts and other immune cells. Elevated expression of IL-6 in B cells correlates with progressive fibrotic remodelling, particularly in patients with early SSc[63]. High levels of IL-8, IL-1β, B cell activating factor (BAFF), CXCL13 and granulocyte–macrophage colony-stimulating factor (GM–CSF) are also associated with severe fibrosis[52,64]. Ex vivo studies show that B cells derived from people with SSc can infiltrate healthy skin and induce a pro-inflammatory fibroblast phenotype reminiscent of pro-inflammatory fibroblast subpopulations in SSc skin via TNF signalling[65]. In the lung, B cell–fibroblast interactions promote fibrotic remodelling via cytokines such as TNF and IL-1β[66].

Autoantibodies contribute to the pathophysiology of SSc via multiple mechanisms[67]. Functional autoantibodies that recognize platelet-derived growth factor receptor, endothelin receptor type A or type 1 angiotensin II receptor can bind to cell-surface receptors to activate profibrotic intracellular signalling cascades in fibroblasts and other target cells. Anti-Scl70 antibodies (also known as anti-topoisomerase I antibodies) can disrupt DNA cleavage complexes to promote fibroblast activation[68,69]. Moreover, anti-Scl70 IgG antibody could interfere with the normal interaction between Scl70 autoantigen and CCR7 on fibroblasts[70]. Immune complexes formed by anti-Scl70 antibodies and other autoantibodies can also engage Toll-like receptors on fibroblasts, subsequently triggering pro-inflammatory and profibrotic signalling cascades[71]. Consistent with these findings, IgG anti-Scl70 antibodies from patients with SSc can induce pro-inflammatory and profibrotic transcriptomic and proteomic shifts in healthy fibroblasts[72] and in endothelial cells[73]. Moreover, immunization of mice with human Scl70 antigen and complete Freud's adjuvant induces the production of anti-Scl70 antibodies and subsequent development of dermal and pulmonary fibrosis[74]. B cells with high affinity for Scl70 induce more pronounced upregulation of profibrotic cytokines and more extensive fibrotic remodelling, whereas low-affinity antibodies or inhibition of cytokine production ameliorate fibrosis[75]. Translation of these findings from bench to bedside and clinical trials that target B cells and autoantibodies in SSc have been reviewed elsewhere[13].

T cells also have a key role in SSc. Activated T cells in SSc are predominantly T helper 2 (T_H2) cells, which produce IL-4 and IL-13 and can trigger the activation of adjacent fibroblasts to promote fibrosis[76]. Cytotoxic $CD4^+$ T cells accumulate in the skin of patients with SSc and can induce endothelial-cell apoptosis[35]. A heterogeneous subset of effector memory $CD8^+KLRB1^+IL\text{-}7R^+$ cells characterized by increased cytolytic Tc2 and Tc17 effector functions were identified in early dcSSc skin lesions and seemed to induce tissue damage and fibrosis[77]. Although the pathophysiological role of T_H17 cell cytokines is currently less well understood, IL-17 producing T_H17 cells are upregulated in dcSSc, which contributes to the immune imbalance in SSc.

Interactions between B cells and T cells perpetuate inflammation and autoimmunity in SSc. B cells present antigens and provide co-stimulation to $CD4^+$ T cells, enhancing follicular helper T (T_{FH}) cell activation, IL-21 secretion and autoantibody production[78]. In SSc, T_{FH} cells are hyperactivated, express elevated levels of immunostimulatory molecules such as inducible T cell co-stimulator (ICOS) and PD-1 and promote type 2 humoral immune responses. A unique $CD4^+$ T cell subset characterized by the expression of CXCL13 and IL-21 in addition to a T_{FH} cell-like gene expression signature has been identified using scRNA-seq; this subset seemed poised to promote B cell responses within the inflamed skin of patients with SSc[79].

Thus, B cells and T cells have important roles in the pathophysiology of SSc. In particular, B cell activation and accumulation in organs is key for the activation of resident cells such as fibroblasts and endothelial cells.

Monocytes and macrophages

Activated monocyte and macrophages are key contributors to fibrosis via the release of profibrotic mediators, contact-dependent fibroblast activation and ECM remodelling[80,81] (Fig. 3). Owing to their plasticity, monocytes can dynamically adapt to their tissue environment and exert a broad spectrum of pro-inflammatory and profibrotic responses. Patients with SSc have abnormal circulating monocyte populations characterized by an increased proportion of cells that co-express both pro-inflammatory ($CD80^+$ and $CD86^+$) and profibrotic ($CD204^+$, $CD163^+$ and $CD206^+$) markers[82]. Notably, patients with SSc and lung involvement exhibit a higher percentage of these abnormal monocytes than those without lung involvement.[83]. Profibrotic macrophage polarization, which is defined by the expression of the scavenger receptor macrophage receptor with collagenous structure (MARCO) and elevated expression of arginase 1, IL-10 and TGFβ, has also been reported in patients with asbestos-induced fibrosis[84]. Experimental studies in mice have confirmed the requirement of MARCO for the development of chrysotile-induced pulmonary fibrosis[84]. Similarly, an increase in $MARCO^+$ monocytes and macrophages have been identified in the circulation and lesional skin and lungs of patients with SSc and in the bleomycin-induced mouse model of fibrosis[85]. Preclinical studies further show that administration of poly(lactic-co-glycolic acid) nanoparticles attenuate fibrosis, at least in part, by targeting $MARCO^+$ monocytes and macrophages. Although understanding of monocyte and macrophage biology in SSc is still evolving, current studies highlight substantial phenotypic heterogeneity within the myeloid compartment.

The interplay between macrophages and fibroblasts is a central feature of SSc pathogenesis[86]. Soluble mediators present in SSc plasma or secreted via SSc fibroblast-derived exosomes can induce a profibrotic and pro-inflammatory phenotype in monocytes and macrophages[87,88]. Macrophages in turn, particularly those with a profibrotic (formerly referred to as 'M2-like') phenotype, produce cytokines such as TGFβ, IL-6 and CCL2 that activate fibroblasts[87,88]. Circulating monocytes from patients with SSc express low levels of the Friend leukaemia integration 1 (FLI1) transcription factor[89]. FLI1-deficient macrophages can stimulate the expression of collagen in co-cultures with fibroblasts; however, marked phenotypic heterogeneity exists in macrophages, which can make phenotypic classification of these cells challenging.

Activated endothelial cells might also promote macrophage polarization. An increased presence of sialylated IgG that binds to dendritic cell-specific intercellular adhesion molecule-3-grabbing non-integrin$^+$ (DC-SIGN, also known as CD209) and $CD68^+$ macrophages has been observed in the perivascular regions of those patients with SSc and a high modified Rodnan skin score[90]. Corresponding in vitro studies show that conditioned medium from IL-1β-treated SSc-derived microvascular endothelial cells induced elevated secretion of IL-6 and endothelin-1. These secreted factors promote the differentiation of monocytes into DC-$SIGN^+$ macrophages that produced high levels of CCL2 and CXCL8 but low levels of IL-10. Furthermore, SSc

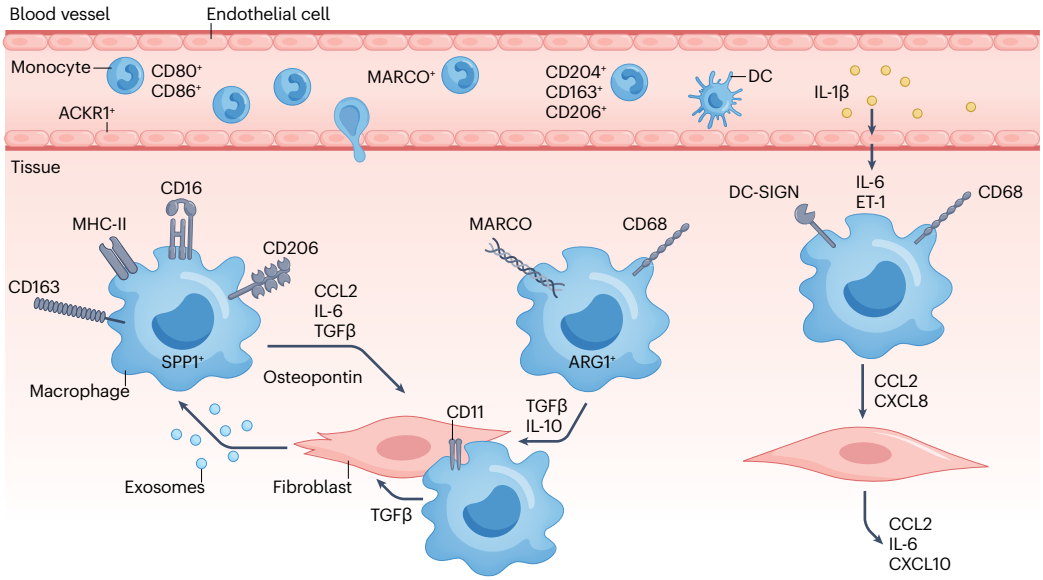

Fig. 3 | Macrophage–fibroblast interactions in fibrotic tissue remodelling in SSc. In systemic sclerosis (SSc), circulating monocytes express both pro-inflammatory (CD80$^+$ and CD86$^+$) and profibrotic (CD204$^+$, CD163$^+$ and CD206$^+$) markers. ACKR1$^+$ endothelial cells facilitate chemokine-mediated recruitment of leukocytes, including monocytes. In tissues, fibroblasts interact with macrophages via direct cell-to-cell contact, as well as soluble mediators. Exosomes derived from SSc fibroblasts stimulate macrophages by increasing surface expression of CD163, CD206, MHC-II and CD16. In turn, activated macrophages (SPP1$^+$ and ARG1$^+$ macrophages) secrete profibrotic cytokines that promote collagen and fibronectin production. Endothelial cells exposed to pro-inflammatory cytokines such as IL-1β also promote differentiation of DC-SIGN$^+$ and CD68$^+$ macrophages, which activate fibroblasts via CCL2 and CXCL8. ACKR1; atypical chemokine receptor 1; DC-SIGN, dendritic cell-specific intercellular adhesion molecule-3-grabbing non-integrin; MARCO, macrophage receptor with collagenous structure.

microvascular endothelial cell-activated DC-SIGN$^+$ macrophages enhanced a pro-inflammatory phenotype in fibroblasts in co-culture experiments[90].

Beyond soluble mediator signalling, macrophages can also activate fibroblasts through direct adhesion via cadherin-11, a transmembrane adhesion molecule expressed on macrophages and fibroblasts in fibrotic skin and lung tissue[91,92]. Cadherin-11 engagement triggers TGFβ signalling, enhancing fibroblast contractility and ECM production.

Several novel monocyte and macrophage subsets associated with SSc have been identified using scRNA-seq. SPP1^{hi} macrophages have emerged as key drivers of fibrosis and immune dysregulation[93–96]. *SPP1* encodes osteopontin, a highly phosphorylated, secreted glycoprotein that can function as both a pro-inflammatory and a profibrotic molecule depending on the disease-specific context. Osteopontin levels are elevated in the serum of patients with SSc and correlate with lung fibrosis and reduced pulmonary function[94]. Notably, a genetic predisposition can contribute to the accumulation of SPP1^{hi} macrophages in SSc. People with SSc who carry a hypofunctional variant of *NCF1*, which encodes the p47phox subunit of the nicotinamide adenine dinucleotide phosphate oxidase complex, are at an increased risk of developing lung fibrosis. Reduced *NCF1* activity is associated with an expansion of SPP1$^+$ macrophages in both patients with SSc and in a bleomycin-induced model of lung fibrosis[96].

Nerve–fibroblast axis

Autonomic and sensory nerves have been studied in the setting of inflammation and immune-cell activation. Noradrenaline produced by the adrenergic nerves in the lungs transmits fibrotic signals to myofibroblasts that express adrenoreceptor α-1D (ADRA1D) in alveolar lung fibrosis in mice[97,98]. This effect can be reversed by administration of the ADRA1D antagonist terazosin. In one study, thus far only available as a preprint, incubation with terazosin also induced the downregulation of fibrotic markers in human precision-cut lung slices[98]. ADRA1D$^+$ alveolar myofibroblasts are detected in lung tissues of patients with SSc-ILD and IPF, and deletion of *Adra1d* in myofibroblasts in vivo in mice attenuates alveolar fibrosis[98]. Netrin-1, derived from macrophages, induces lung fibrosis in mice through neuronal guidance function and by increasing noradrenaline levels, and this profibrotic effect can be blocked by ADRA1D inactivation. Moreover, in a longitudinal IPF cohort, ADRA1D blockade improved patient survival[99]. In addition to noradrenaline, nerve growth factor (NGF) might be implicated in the pathogenesis of fibrosis. NGF enhances fibroblast migration, transition to myofibroblasts and gel contraction (an in vitro model of fibroblast contractibility)[100]; however, NGF can also be antifibrotic as continuous administration of NGF induces myofibroblast apoptosis[100]. In addition, activation of the sympathetic nervous system and production of neuropeptides can indirectly activate fibroblasts by promoting inflammation and production of cytokines from inflammatory cells as shown in cardiac remodelling[101] and other tissues[102,103]. Taken together, these studies implicate sympathetic nerve–fibroblast communication in the pathophysiology of fibrosis.

Matrikines and matricryptins

ECM components including collagens, elastin, fibronectin and laminin are cleaved by different enzymes including cathepsins, matrix metalloproteinases (MMPs), bone morphogenetic proteins and a disintegrin

and metalloproteinases (ADAMs) to release biologically active peptides known as matrikines, which have an important role in tissue remodelling and repair that differs from the role of the parent molecule. The matrikines released as products of partial proteolysis exert pleiotropic effects that modulate cell proliferation, apoptosis, angiogenesis and migration (Supplementary Fig. 1).

Matrikines can exert profibrotic and antifibrotic effects; for example, the cleavage product of collagen type VI, endotrophin, is profibrotic[104], whereas the cleavage product of collagen type XVIII, endostatin, is antifibrotic[105]. Endostatin and an endostatin-derived peptide can reduce fibrosis in experimental dermal and pulmonary fibrosis in mice and in ex vivo cultures of human biopsy-obtained skin and lung samples[105,106]. Although endostatin levels are elevated in the serum of patients with SSc[107], reduced levels of cathepsin L (the main enzyme responsible for cleavage of and also the sequestration of endostatin in extracellular vesicles) might explain why concentrations of endostatin do not reach antifibrotic levels in SSc[108]. Deficiency in certain MMPs that generate matrikines, such as MMP12, might also reduce dermal fibrosis[109]. Thus, targeting pathogenic matrikines using antibodies and/or the enzymes responsible for their generation or boosting the production of beneficial matrikines in fibrosis (such as endostatin) presents a potential novel therapeutic avenue[104].

In addition to the generation of matrikines, enzymatic fragments of ECM molecules can become exposed and bioactive; these sites are referred to as matricryptins[110]. The generation of matricryptins occurs in response to mechanical forces, reactive oxygen species and other processes. Matrikines and matricryptins derived from the same molecule can exert opposite effects; for example, matrikines and matricryptins from SPARC can exert pro-angiogenic and anti-angiogenic effects[110]. To add further complexity, some of these effects are cell-type dependent. Thus, the balance and activity of different matrikines and matricryptins depends on the factors responsible for their release and the tissue and cell context[110].

Senescence

Fibrosis shares features of early or premature senescence. Senescence of activated fibroblasts and myofibroblasts has been described in different fibrosing conditions[111]. Activated fibroblast subpopulations and myofibroblasts can obtain a senescence-associated secretory phenotype (SASP), which includes the release of pro-inflammatory and profibrotic factors (such as IL-1α, IL-1β, IL-6, TGFβ, PDGF and plasminogen activator inhibitor-1)[112]. These factors can promote persistence of the activated fibroblasts by inducing a permissive, profibrotic milieu. Targeted elimination of senescent cells improves pulmonary function in mice[113]. Although the mechanisms leading to the senescent phenotype are incompletely understood, emerging data suggest that senotherapeutics, including senomorphics and senolytics, might be effective for the treatment of fibrosis in SSc. In a study of dasatinib (a multityrosine kinase inhibitor that also has senolytic effects) in patients with SSc, re-analysis of the skin gene-expression profile of those who responded to treatment showed a decrease in the SASP gene signature[114]. Additional research is needed to understand how senescent cells emerge in fibrosis, their exact role in the initiation and/or perpetuation of fibrosis, and the therapeutic potential of eliminating senescent cells in diseased tissues.

Profibrotic transcription factors

Profibrotic signals induce the activation of a network of transcription factors that translate upstream signals into a profibrotic phenotype.

JAK–STAT signalling

Janus kinase 2 (JAK2) has been characterized as a downstream mediator of TGFβ in fibroblasts (Fig. 4). Phosphorylation of JAK2 at 1007/1008 Tyr residues causes fibroblasts to accumulate in skin of patients with SSc. Stimulation of resting fibroblasts with TGFβ induces this JAK2 phosphorylation[115], which provides evidence that TGFβ contributes to the activation of JAK2–signal transducer and activator of transcription 3 (STAT3) signalling in SSc skin. JAK2 activation promotes TGFβ-induced fibroblast-to-myofibroblast transition, which can be prevented by pharmacological or genetic inhibition. Furthermore, inhibiting JAK2 reverses the active phenotype of SSc cells and can also attenuate experimental dermal fibrosis[115]. However, JAK2 can evade inhibition by highly specific JAK2 inhibitors, as JAK1 can *trans*-phosphorylate JAK2, resulting in JAK2 activation. This escape mechanism can be inhibited by using combined JAK1 and JAK2 inhibitors, or selective JAK2 inhibitors in combination with heat shock protein 90 inhibitors, which increase JAK2 degradation[116].

Alternative ways to target TGFβ-induced JAK2–STAT3 signalling in fibrosis might involve the tyrosine phosphatase SHP2 (Src homology 2 domain-containing protein tyrosine phosphatase-2) and the serine-threonine kinase CKII. TGFβ enhances SHP2 recruitment to JAK2 and stimulates tyrosine phosphatase activity, which leads to the dephosphorylation of the inhibitory phosphorylation site Y570 of JAK2 and activation of STAT3. Inactivating SHP2 increases Y570 phosphorylated JAK2, decreases JAK2–STAT3 signalling, suppresses TGFβ-induced fibroblast activation and improves experimental dermal and pulmonary fibrosis[117]. CKII expression is also upregulated in SSc fibroblasts[118]. Inhibiting CKII reduces TGFβ-induced JAK2 phosphorylation and STAT3 accumulation in fibroblasts, which prevents fibroblast-to-myofibroblast transition and experimental fibrosis[118].

STAT3 is an essential downstream mediator of JAK1 and JAK2, but it also integrates signals from other profibrotic kinases such as SMAD3, SRC, ABL and JNK[115,119–122]. Consistently, fibroblast-specific inducible knockout or pharmacological inhibition of STAT3 reduces TGFβ-induced fibroblast-to-myofibroblast transition and collagen release in vitro and ameliorates experimental skin fibrosis[123]. Thus, inhibition of JAK–STAT3 signalling can limit fibroblast activation and fibrotic tissue remodelling in SSc. Translation of these findings into clinical trials is reviewed elsewhere[13].

PU.1

PU.1, also known as SPI1, is a transcription factor of the E26 transformation-specific family. Under homeostatic conditions, the expression of PU.1 is largely restricted to macrophages, and resting fibroblasts lack PU.1 owing to epigenetic repression. However, the tight epigenetic control of PU.1 in fibroblasts is perturbed in fibrotic tissues, such as the skin in SSc, leading to PU.1 expression in certain fibroblast subpopulations. PU.1 induces the expression of profibrotic genes in fibroblasts and promotes fibroblast-to-myofibroblast transition as it can regulate profibrotic gene-expression programmes[124]. Notably, forced overexpression of PU.1 is not only sufficient to induce a fibroblast-to-myofibroblast differentiation in resting fibroblasts but also induces a fibrotic phenotype in inflammatory fibroblasts isolated from inflamed joints of patients with rheumatoid arthritis. Fibroblast-specific, inducible knockout of PU.1 prevents fibroblast-to-myofibroblast transition and ameliorates experimental fibrosis in multiple organs. Small molecule inhibitors of PU.1 can exert potent antifibrotic effects[124]; however, PU.1 inhibitors with sufficient pharmacokinetics for use in humans are currently not available.

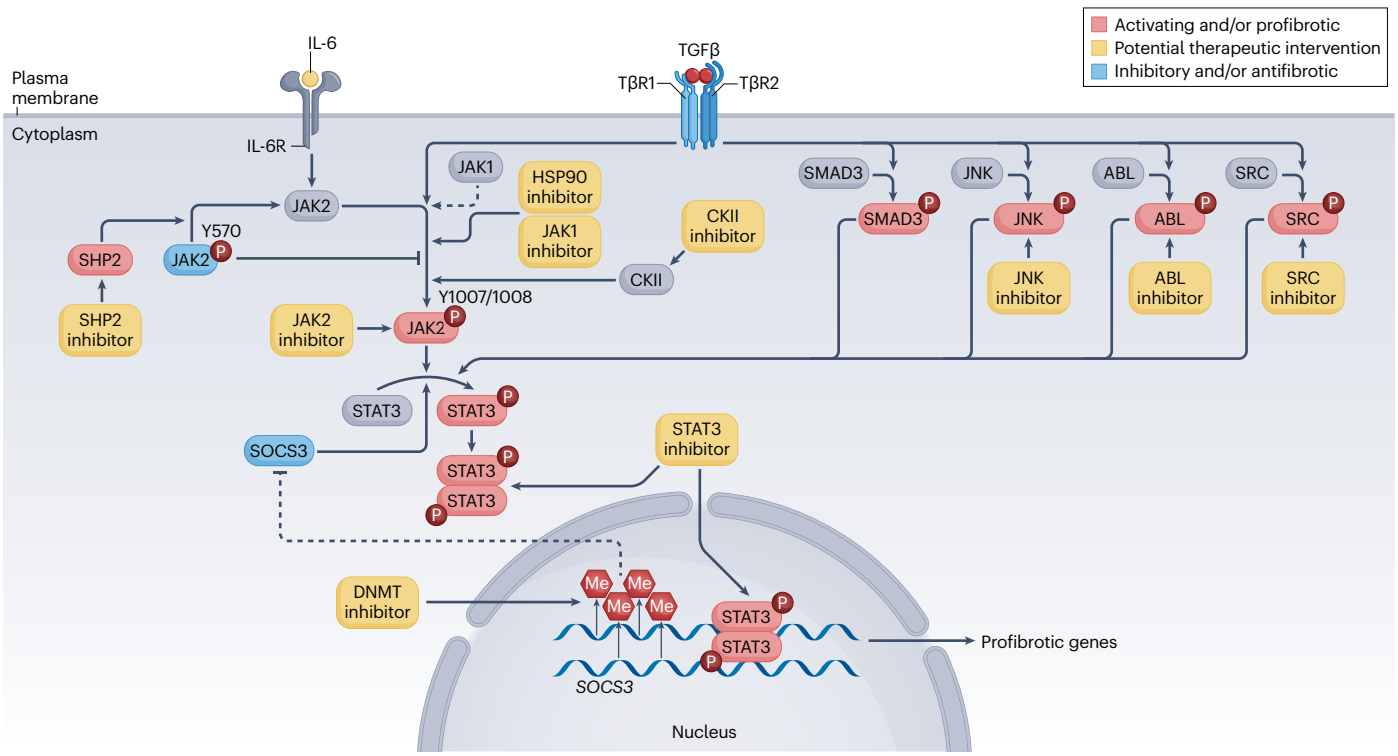

Fig. 4 | Dysregulated JAK–STAT signalling as a core pathway of fibroblast activation in systemic sclerosis. Janus kinase (JAK)–signal transducer and activator of transcription (STAT) signalling is dysregulated in systemic sclerosis (SSc) fibroblasts on various levels and many potential interventions (shown in yellow) can be used to therapeutically target this dysregulated signalling. JAK1, JAK2, JAK3 and TYK2 together form the JAK family. JAKs are receptor-associated tyrosine kinases that transmit signals of various cytokine and growth-factor receptors. Activation of the upstream receptors (such as the IL-6 receptor (IL-6R) and the transforming growth factor-β (TGFβ) receptors (TβR1 and TβR2)) induces recruitment of JAK proteins and promotes their phosphorylation at 1007/1008 Tyr residues. Activated JAKs then phosphorylate the receptors, thereby generating docking sites for STAT proteins. Upon binding to these phosphorylated binding sites of the receptors, STAT proteins are phosphorylated, dimerize and translocate into the nucleus, where they activate transcription of target genes[212]. DNMT, DNA methyltransferase; HSP90, heat shock protein 90; Me, methyl group; SHP2, Src homology 2 domain-containing protein tyrosine phosphatase-2; SOCS3, suppressor of cytokine signalling 3.

Nuclear receptors

Nuclear receptors, a superfamily of transcriptional regulators, have crucial roles in fibrotic tissue remodelling. Several nuclear receptors can modulate fibrotic tissue remodelling by regulating different molecular pathways and on different cell types (Fig. 5).

NR1C3 (also known as PPARγ) competes with SMAD3 for the coactivator p300, thereby inhibiting SMAD-dependent transcription of profibrotic genes[125]. NR1C3 expression is reduced in fibrotic tissues and cultured fibroblasts from patients with SSc; this downregulation is mediated by TGFβ signalling[126]. In adipocytes, the downregulation of NR1C3 requires the corepressor NCoR[127]. NR1C3 agonists mitigate TGFβ-induced fibroblast activation, collagen secretion and bleomycin-induced fibrosis. Moreover, single-nucleotide polymorphisms in NR1C3 might be implicated in SSc susceptibility; however, a pan-PPAR agonist (lanifibranor) failed to demonstrate efficacy in a phase II study in patients with dcSSc (NCT02921971).

NR4A1 (alternatively known as Nur77 or TR3) also functions as an antifibrotic nuclear receptor, the expression of which is diminished in fibrotic diseases[128,129]. Under normal wound-healing conditions, transient TGFβ signalling upregulates NR4A1, which then represses profibrotic gene expression via SP1-dependent *trans*-repression. In chronic fibrotic states, prolonged TGFβ exposure undermines the inhibitory functions of NR4A1 via histone deacetylase-mediated epigenetic silencing and through AKT-induced phosphorylation[22,128]. NR4A1 agonists have demonstrated antifibrotic properties in multiple models of experimental fibrosis[128,130–132], but small molecules with suitable pharmacokinetic profiles for clinical use have not yet been developed.

NR1I1 (also known as the vitamin D receptor) has a role in fibrotic remodelling in multiple organs[133]. Activation of NR1I1 inhibits TGFβ–SMAD signalling by binding to phosphorylated SMAD3 and preventing its transcriptional activity[134]. This mechanism is particularly relevant to SSc, in which reduced NR1I1 expression in the skin, along with common vitamin D deficiency, might contribute to fibrogenesis.

Other members of the nuclear receptor family that alter TGFβ signalling in fibroblasts and have been implicated in the pathogenesis of SSc are NR0B1 (also known as DAX1), NR2C1 (also known as testicular receptor 4 (TR4)), NR1F1 (also known as RAR-related orphan receptor-α (RORα,)) and NR1I3 (also known as the constitutive androstane receptor (CAR))). The expression of NR0B1, NR2C1 and NR1F1 is upregulated in fibroblasts from patients with SSc[135–137]. NR0B1 and NR2C1 are upregulated in a TGFβ-dependent manner, whereas the expression of NR1F1 is induced by canonical WNT signalling[135–137]. NR0B1, NR2C1 and NR1F1 regulate distinct intracellular pathways in fibroblasts. NR0B1 promotes activation of WNT–β-catenin signalling

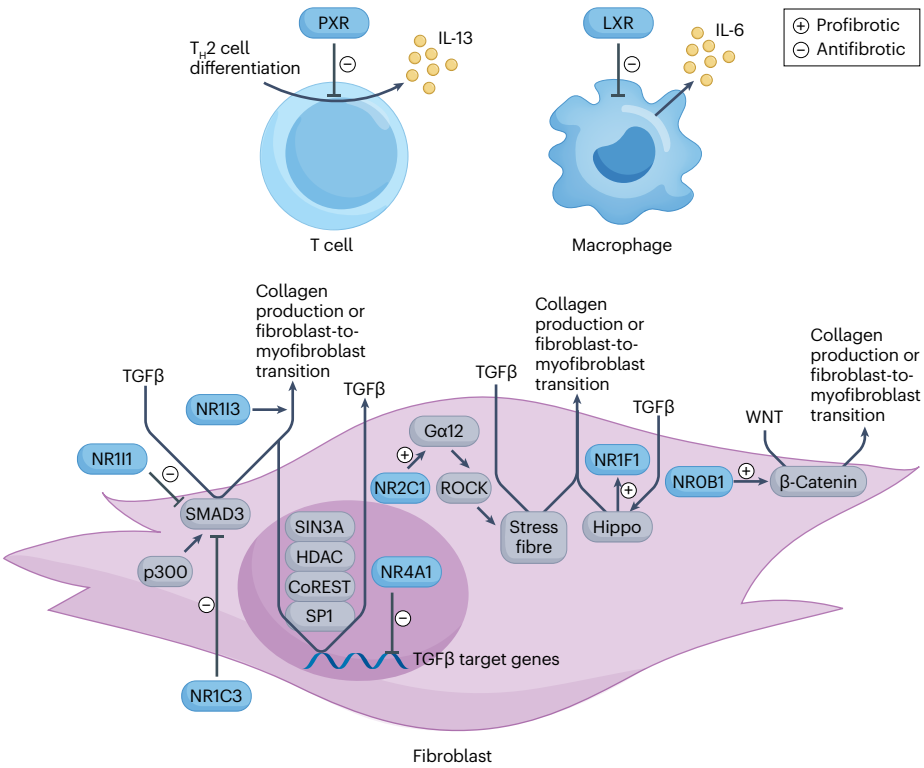

Fig. 5 | The multifaceted roles of nuclear receptors in fibrotic tissue remodelling. Nuclear receptors (shown in blue) function on different target cells (such as T cells, macrophages and fibroblasts) to modulate inflammatory and fibrotic pathways in the pathogenesis of fibrotic tissue remodelling. The expression levels of individual nuclear receptors are often modulated by pro-inflammatory and profibrotic mediators that are commonly implicated in the pathogenesis of systemic sclerosis (SSc). Dysregulation of nuclear receptor signalling in turn regulates core pathways of SSc, including transforming growth factor-β (TGFβ), WNT or IL-6 signalling, to promote fibrotic tissue remodelling. HDAC, histone deacetylase; LXR, liver X receptor; PXR, pregnane X receptor; ROCK, RHO-associated protein kinase; T_H2 cell, T helper 2 cell.

to facilitate fibroblast-to-myofibroblast differentiation[135]. Inactivation of NR0B1 ameliorates collagen release in cultured human dermal fibroblasts, in an in vitro model of human skin and in mouse models of dermal fibrosis[135]. Inhibition of NR0B1 also reduces the expression of disease-relevant genes, including genes associated with WNT–β-catenin signalling in precision-cut slices of skin from patients with SSc[135]. NR2C1 regulates Gα12 and RHO-associated protein kinase (ROCK) signalling to control the expression of numerous genes implicated in cytoskeletal remodelling and thereby promotes fibroblast-to-myofibroblast transition[137]. Inactivation of NR2C1 reduces collagen release and prevents experimental dermal and pulmonary fibrosis in mouse models[137]. NR1F1 is required for TGFβ-induced activation of Hippo signalling in fibroblasts. Inactivation of NR1F1 inhibits Hippo signalling, reduces fibroblast-to-myofibroblast transition and ameliorates experimental dermal, pulmonary and hepatic fibrosis[136]. The role of NR1I3 is less well-defined. Activation of NR1I3 by synthetic NR1I3 agonists fosters activation of canonical TGFβ signalling and exacerbates experimental fibrosis[138]. However, the exact molecular mechanisms and potential therapeutic implications of NR1I3 inhibition have not yet been investigated.

In contrast to the nuclear receptors discussed thus far, liver X receptor (LXR) and pregnane X receptor (PXR) regulate the release of profibrotic mediators from macrophages or T cells, respectively, rather than targeting fibroblasts directly. LXR agonists inhibit macrophage activation and IL-6 release in mouse models of dermal fibrosis[139]. PXR activation inhibits the release of IL-13 from T_H2 cells, which results in reduced fibrotic remoulding in inflammatory mouse models of SSc[140].

Thus, several nuclear receptors have been implicated in the pathogenesis of fibrotic tissue remodelling at different molecular and cellular levels and might offer potential for therapeutic intervention.

Developmental pathways

Hedgehog and WNT signalling pathways are integral to organ development in the embryo and are thus often referred to as developmental pathways. Under physiological conditions, these developmental pathways regulate stem-cell function but are silenced in most other cell types in adults. However, these developmental pathways are reactivated in the context of fibrosis and seem to have crucial roles in tissue remodelling[141].

Hedgehog signalling

The expression levels of the sonic hedgehog (SHH) ligand and the transcription factor GLI2 are increased in skin from patients with SSc and in other fibrotic tissues[142]. Serum levels of SHH are also upregulated in SSc and correlate with the extent of fibrosis[143]. TGFβ contributes to hedgehog pathway activation by inducing SHH expression, upregulating the expression of the hedgehog acyltransferase (also known as skinny hedgehog, which catalyses the attachment of palmitate to SHH, thereby enabling the multimerization of SHH proteins) and also by directly activating the GLI2 promoter in fibroblasts[144–146]. Crosstalk between hedgehog signalling and activator protein 1 signalling might also contribute to aberrant GLI2 activity in SSc[147]. Hedgehog signalling promotes fibroblast-to-myofibroblast differentiation and is sufficient to induce skin fibrosis in mice[144,148]. Moreover, its inactivation, either pharmacologically or genetically, attenuates experimental fibrosis in the skin, lungs and other organs[148–150].

Canonical WNT signalling

Canonical (β-catenin-dependent) WNT signalling is upregulated in various fibrotic conditions including in SSc skin, as indicated by increased expression of WNT ligands, reduced levels of endogenous WNT inhibitors, nuclear accumulation of β-catenin and overexpression

of WNT–β-catenin-regulated target genes[151–155]. Stimulation with recombinant WNT proteins upregulates the expression of myofibroblast markers and the release of collagen in fibroblasts. Moreover, activation of canonical WNT signalling, either by overexpression of WNT ligands (such as WNT10b) or fibroblast-specific, inducible overexpression of β-catenin is sufficient to induce dermal fibrosis in mice[152,156,157]. Targeted inactivation of canonical WNT signalling by several different genetic or pharmacological approaches consistently demonstrated antifibrotic effects in preclinical models[158–163]. TGFβ activates canonical WNT signalling in fibroblasts, promoting nuclear translocation of β-catenin and upregulation of WNT target genes[157]. These stimulatory effects of TGFβ on canonical WNT signalling are at least in part mediated by TGFβ-dependent suppression of the transcription of endogenous WNT antagonists such as Dickkopf-1 (DKK1) and secreted frizzled-related protein 1 (SFRP1) through p38-dependent mechanisms and epigenetic silencing[164], but also by downregulation of axin-2 (ref. 165). The stimulatory effects of TGFβ on canonical WNT signalling contribute to its profibrotic effects as inhibition of canonical WNT signalling ameliorates fibrosis induced by aberrant TGFβ signalling in mice[157]. Collectively, these findings position canonical WNT signalling as a central pathway in fibrotic remodelling (Fig. 6).

Non-canonical WNT signalling

Non-canonical (β-catenin-independent) WNT signalling is defined as signalling events induced by WNT proteins that are transmitted to the nucleus independently of β-catenin. These non-canonical WNT signals are often triggered by specific WNT proteins such as WNT5A. Non-canonical WNT signalling is also perturbed in SSc, with upregulation of WNT5A reported in skin of patients with SSc[166]. Recombinant WNT5A induces collagen release and fibroblast-to-myofibroblast transition in cultured fibroblasts. Overexpression of WNT5A is sufficient to induce fibrosis in organotypic skin models of mouse skin and lungs. These profibrotic effects are mediated by WNT5A-induced activation of latent TGFβ[166]. WNT5A activates JNK and ROCK signalling to induce cytoskeletal rearrangements and clustering of integrin αV, which promotes activation of latent TGFβ stored in large amounts in the ECM. Inhibition of WNT5A or its downstream mediators prevents activation of latent TGFβ, rebalances TGFβ signalling and ameliorates experimental fibrosis[166]. In contrast to canonical WNT signalling and hedgehog signalling, non-canonical signalling via WNT5A is thus an upstream regulator of TGFβ signalling in SSc (Fig. 6).

These findings highlight the close interaction of TGFβ signalling with canonical and non-canonical WNT and hedgehog signalling and

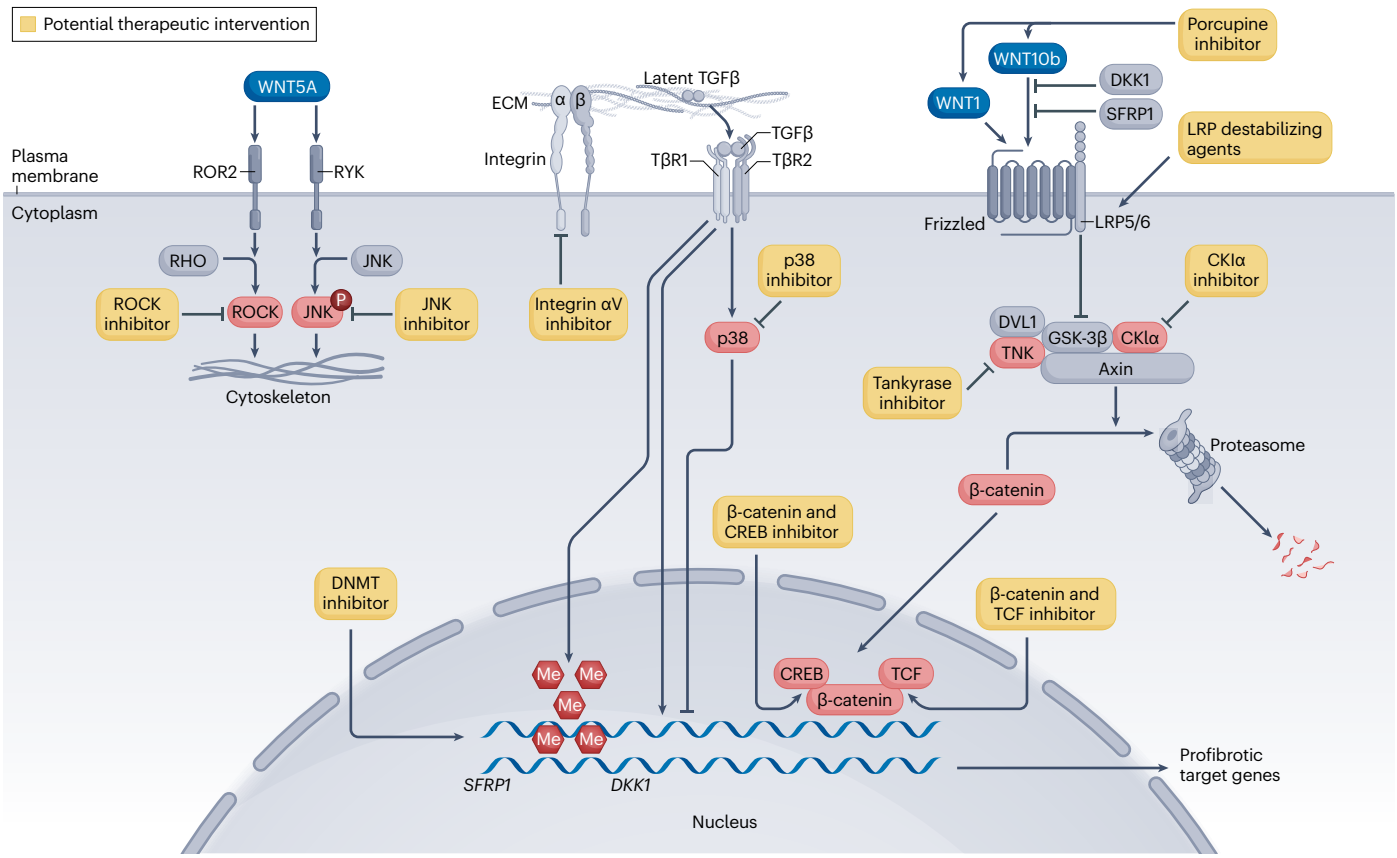

Fig. 6 | Canonical and non-canonical WNT signalling as mediators of fibrotic tissue remodelling in systemic sclerosis. In systemic sclerosis (SSc), WNT signalling in fibroblasts is dysregulated, and molecules within this pathway are potential therapeutic targets (targets are shown in red and potential interventions in yellow). In SSc, changes in the expression of WNT ligands, endogenous inhibitors and intracellular mediators synergize to promote the hyperactivation of canonical as well as non-canonical WNT signalling. The profibrotic effects of WNT signalling can be targeted at multiple levels. CREB, cAMP response element-binding protein; DKK1, Dickkopf 1; DNMT, DNA methyltransferase; ECM, extracellular matrix; LRP, low-density lipoprotein receptor-related protein; Me, methyl group; ROCK, RHO-associated protein kinase; SFRP1, secreted frizzled-related protein 1; TCF, ternary complex factor; TGFβ, transforming growth factor-β; TβR, TGFβ receptor.

provide evidence that these signalling cascades synergize to promote fibrotic tissue remodelling in SSc.

Epigenetic changes and fibrotic tissue memory

Fibroblasts in SSc undergo epigenetic changes as a result of chronic exposure to the profibrotic environment[167]. These epigenetic modifications consolidate the activated phenotype of SSc fibroblasts and render them at least in part independent of external stimuli, such as those delivered by immune cells[168]. This finding is reflected in the chronically active phenotype of SSc fibroblasts with increased release of ECM and elevated expression of myofibroblast markers even after several passages in in vitro monocultures. This stabilization of the activated phenotype of tissue-resident cells by epigenetic modifications is also referred to as 'tissue memory'[169,170]. Tissue memory in SSc is encoded by a complex combination of different epigenetic alterations involving changes in DNA methylation, histone methylation, histone acetylation, epigenetic readers of the bromodomain (BRD) family and non-coding RNAs[164,167,171–187]. We discuss selected examples of DNA and histone modifications that contribute to fibroblast activation; changes in the expression of non-coding RNAs have been reviewed elsewhere[188].

DNA methylation

Three DNA methyltransferases (DNMTs), DNMT1, DNMT3A and DNMT3B, can methylate DNA at position C5 of the pyrimidine ring of cytosine[189]. When methylated cytosine residues are grouped in what are known as CpG islands, binding sites for methyl-CpG-binding domain (MBD) proteins form. MBD protein binding promotes the recruitment of repressor complexes to inhibit transcription[190]. Numerous studies show that fibroblast activation in SSc is promoted by altered DNA methylation[164,186,191–193]. Notably, TGFβ induces the expression of DNMT3A with consecutive increases in DNMT1 in fibroblasts, thereby providing a molecular link between aberrant TGFβ signalling and DNA-methylation-mediated tissue memory[194]. The first target shown to be dysregulated by DNA methylation in SSc was the transcription factor FLI1 (refs. 186,195,196). FLI1 can limit TGFβ signalling[197]; however, in SSc, aberrant DNA methylation silences FLI1 expression. Other targets of DNA methylation are suppressor of cytokine signalling 3 (SOCS3), an endogenous inhibitor of JAK–STAT signalling, and the endogenous WNT antagonists DKK1 and SFRP1. Silencing of SOCS3 expression in fibroblasts facilitates prolonged activation of JAK2–STAT3 signalling and promotes fibroblast activation and tissue remodelling[198]. Silencing of DKK1 and SFRP1 might synergize with overexpression of WNT ligands to induce aberrant WNT signalling in SSc[164]. DNMT inhibitors can partially reverse the activated phenotype of SSc fibroblasts and demonstrate antifibrotic effects across multiple organs[164,199,200].

Methylation analysis of the X chromosome in peripheral blood mononuclear cells (PBMCs) from monozygotic twins discordant for SSc identified differential methylation of genes involved in transcription, proliferation, inflammation, apoptosis and oxidative stress[201]. Global methylation analysis in PBMCs of both monozygotic and dizygotic twins discordant for SSc identified distinct methylation sites in patients with lcSSc compared with those with dcSSc[202]. A global analysis of differential methylation and expression conducted using primary dermal fibroblasts from monozygotic and dizygotic twins with SSc demonstrated the differential regulation of the transcription factor KLF4 (ref. 180). Functional studies in fibroblasts and conditional knockout mice revealed that KLF4 (the expression of which is suppressed in fibroblasts from patients with SSc compared with their healthy twin) regulates *TBX5* and *TFAP2A*, and that lower levels of KLF4 promote fibrosis[180]. Together, these studies highlight the functional impact of differential methylation in SSc, both systemically and in affected tissues, and indicate a potential benefit of using epigenetic modifiers for the treatment of SSc.

Histone acetylation and methylation

TGFβ can also alter the epigenetic memory of SSc fibroblasts by modulating the histone code. Histone modifications include acetylation and methylation. Early reports demonstrated that histone deacetylation inhibitors attenuate the activated phenotype of SSc fibroblasts and ameliorate bleomycin-induced dermal fibrosis in mice[174]. Follow-up studies show that TGFβ downregulates the expression of the H4K16 histone acetyltransferase MYST1 in a SMAD-dependent manner. MYST1 provides epigenetic control of autophagy by suppressing the transcription of core components of the autophagy machinery. Plasmid-induced re-expression of MYST1 abrogates the stimulatory effects of TGFβ on autophagy and ameliorates TGFβ-induced fibroblast activation and experimental fibrosis[203]. Histone modifications are also implicated in the regulation of PU.1 expression[124]. In resting fibroblasts, repressive H3K9me3 and H3K27me3 marks dominate the promoter and upstream regulatory element of the PU.1 gene. In SSc fibroblasts, however, the upstream regulatory element of the PU.1 locus becomes permissive with increased H3K27 acetylation and loss of H3K9me3 and H3K27me3, thereby facilitating transcription of PU.1 (ref. 124). Histone modifications are thus a central component of the profibrotic tissue memory.

Other epigenetic modifications

Epigenetic modifications with an open chromatin state also maintain constitutive activation of a *TGFB2* enhancer in SSc fibroblasts[179]. Although most other in vitro studies in SSc use recombinant TGFβ1, this study demonstrated that the upregulation of TGFβ2 signalling might contribute to endogenous activation of SSc fibroblasts in a BRD4-dependent manner. Inhibition of the epigenetic reader protein BRD4 alleviated the hyperactivation of the *TGFB2* enhancer, mitigated profibrotic gene expression in fibroblasts and ameliorated dermal fibrosis in explant cultures of the skin of patients with SSc.

Epigenetic modifications are not restricted to fibroblasts in SSc but also contribute to the activated phenotype of other cell types such as macrophages. Combined scRNA-seq and single-cell assay for transposase-accessible chromatin sequencing (scATAC-seq) of SSc-ILD and healthy lungs revealed that the opening of chromatin promotes the activation of a specific set of transcription factors that promote SPP1 macrophage differentiation in SSc-ILD[204].

Although some epigenetic modulators such as histone deacetylase inhibitors or DNMT inhibitors are already in clinical use in oncology and thus offer potential for direct translation to SSc, the use of others such as bromodomain and extra terminal domain protein inhibitors is limited by adverse events. Cell-type specific delivery, such as coupling to antibodies or topical application, might offer opportunities for translation of those therapies to the clinic, but these are currently unavailable.

Other self-maintaining activation loops

The excessive deposition of ECM alters the biomechanical properties of fibrotic tissues, resulting in increased stiffness. Moreover, fibrotic tissues in SSc are hypoxic. Such changes, which are highly conserved across different fibrotic organs, trigger molecular signals that promote fibroblast activation and generate matricryptins, and might thus drive disease progression, particularly in later disease stages.

Tissue stiffness

Stiff substrates promote fibroblast activation, as evidenced by increased expression of contractile proteins and collagen production of fibroblasts cultured on stiff surfaces (such as standard cell culture dishes)[205]. Integrin receptors have a major role in how cells sense mechanical cues from the ECM, including changes in stiffness, and can convert them into intracellular signals that influence cell behaviour. Many of the downstream signalling pathways of integrin receptors are implicated in fibrosis[206]. The transcriptional coactivators Yes-associated protein-1 (YAP1) and transcriptional coactivator with PDZ-binding motif (TAZ) are key downstream effectors of the Hippo pathway. They function as mechanosensors and have central roles in transducing stiffness into cellular responses[207]. Inhibition of YAP–TAZ signalling attenuates both stiffness-induced and TGFβ-induced fibroblast-to-myofibroblast transformation, whereas constitutive YAP activation drives fibroblast activation and ECM synthesis[205]. Additional factors such as p300 and α6 integrin might also be implicated in stiffness-induced myofibroblast differentiation.

Hypoxia

Hypoxia-inducible factor 1α (HIF-1α) is the principal mediator of cellular responses to low oxygen levels[208]. Under normoxic conditions, HIF-1α undergoes hydroxylation and acetylation, which promotes its proteasomal degradation. In hypoxic environments, the lack of oxygen prevents HIF-1α hydroxylation, enabling its accumulation, nuclear translocation, dimerization with HIF-1β (also known as aryl hydrocarbon receptor nuclear translocator) and subsequent activation of target genes with hypoxia-responsive elements[209]. Hypoxia promotes fibroblast-to-myofibroblast differentiation and enhances ECM protein transcription via HIF-1α-dependent and -independent mechanisms[210]. The stimulatory effects of hypoxia on fibroblasts and ECM release are in part mediated by TGFβ[211]. Thus, hypoxia can promote fibroblast activation and progression of fibrosis, particularly in later stages of SSc with advanced vasculopathy and excessive accumulation of ECM.

Conclusions

The pathogenesis of SSc is characterized by a complex interplay of vascular injury, inflammation and misdirected tissue repair, which interact at multiple levels to drive disease progression. The intense crosstalk also makes defining of individual pathways such as drivers, amplifiers or modulators of disease challenging. Despite advances in understanding of fibrotic tissue remodelling, the pathogenesis of SSc remains incompletely understood; for example, the early, disease-initiating mechanisms remain largely unknown, mechanisms of disease progression in the absence of inflammation are understudied and specific cellular niches and localized differences in signalling activity within affected tissues are unclear. This lack of understanding is partly due to preclinical models that do not fully recapitulate the diverse features of SSc. Emerging human model systems, such as organoids, organ-on-chip platforms and ex vivo tissue cultures combined with unbiased multi-level omics approaches, hold promise for uncovering novel molecular and cellular targets for the treatment of SSc. Therapies aimed at disrupting the self-sustaining cycle of vasculopathy, inflammation and fibrosis offer potential for development of truly disease-modifying therapeutics that target not only certain manifestations but also the underlying core pathophysiology to treat the full spectrum of manifestations of SSc and other fibrotic diseases.

Published online: 26 January 2026

References

1. Rieder, F. et al. Fibrosis: cross-organ biology and pathways to development of innovative drugs. *Nat. Rev. Drug Discov.* **24**, 543–569 (2025).
2. Distler, J. H. W. et al. Shared and distinct mechanisms of fibrosis. *Nat. Rev. Rheumatol.* **15**, 705–730 (2019).
3. Thannickal, V. J. et al. Fibrosis: ultimate and proximate causes. *J. Clin. Invest.* **124**, 4673–4677 (2014).
4. Wynn, T. A. Cellular and molecular mechanisms of fibrosis. *J. Pathol.* **214**, 199–210 (2008).
5. Dees, C., Chakraborty, D. & Distler, J. H. W. Cellular and molecular mechanisms in fibrosis. *Exp. Dermatol.* **30**, 121–131 (2021).
6. Truchetet, M. E., Brembilla, N. C. & Chizzolini, C. Current concepts on the pathogenesis of systemic sclerosis. *Clin. Rev. Allergy Immunol.* **64**, 262–283 (2023).
7. Volkmann, E. R., Andréasson, K. & Smith, V. Systemic sclerosis. *Lancet* **401**, 304–318 (2023).
8. Distler, J. H. et al. Review: frontiers of antifibrotic therapy in systemic sclerosis. *Arthritis Rheumatol.* **69**, 257–267 (2017).
9. Limandjaja, G. C. et al. Hypertrophic scars and keloids: overview of the evidence and practical guide for differentiating between these abnormal scars. *Exp. Dermatol.* **30**, 146–161 (2021).
10. De Luca, D. A. et al. Lichen sclerosus: the 2023 update. *Front. Med.* **10**, 1106318 (2023).
11. Keum, H. et al. Incidence and prevalence of morphea. *JAMA Dermatol.* **160**, 1128–1130 (2024).
12. van Straalen, K. R. et al. Single-cell sequencing reveals Hippo signaling as a driver of fibrosis in hidradenitis suppurativa. *J. Clin. Invest.* **134**, e169225 (2024).
13. Distler, J. H. W. et al. Emerging therapies for the treatment of systemic sclerosis. *Nat. Rev. Rheumatol.* **21**, 612–625 (2025).
14. Leask, A., Naik, A. & Stratton, R. J. Back to the future: targeting the extracellular matrix to treat systemic sclerosis. *Nat. Rev. Rheumatol.* **19**, 713–723 (2023).
15. Ho, Y. Y. et al. Fibrosis — a lethal component of systemic sclerosis. *Nat. Rev. Rheumatol.* **10**, 390–402 (2014).
16. Davidson, S. et al. Fibroblasts as immune regulators in infection, inflammation and cancer. *Nat. Rev. Immunol.* **21**, 704–717 (2021).
17. Pradhan, R. N. et al. A bird's eye view of fibroblast heterogeneity: a pan-disease, pan-cancer perspective. *Immunol. Rev.* **302**, 299–320 (2021).
18. Buechler, M. B. et al. Cross-tissue organization of the fibroblast lineage. *Nature* **593**, 575–579 (2021).
19. Gao, Y. et al. Cross-tissue human fibroblast atlas reveals myofibroblast subtypes with distinct roles in immune modulation. *Cancer Cell* **42**, 1764–1783.e10 (2024).
20. Steele, L. et al. A single-cell and spatial genomics atlas of human skin fibroblasts reveals shared disease-related fibroblast subtypes across tissues. *Nat. Immunol.* **26**, 1807–1820 (2025).
21. Sole-Boldo, L. et al. Single-cell transcriptomes of the human skin reveal age-related loss of fibroblast priming. *Commun. Biol.* **3**, 188 (2020).
22. Philippeos, C. et al. Spatial and single-cell transcriptional profiling identifies functionally distinct human dermal fibroblast subpopulations. *J. Invest. Dermatol.* **138**, 811–825 (2018).
23. Korosec, A. et al. Lineage identity and location within the dermis determine the function of papillary and reticular fibroblasts in human skin. *J. Invest. Dermatol.* **139**, 342–351 (2019).
24. Tabib, T. et al. SFRP2/DPP4 and FMO1/LSP1 define major fibroblast populations in human skin. *J. Invest. Dermatol.* **138**, 802–810 (2018).
25. Ma, F. et al. Systems-based identification of the hippo pathway for promoting fibrotic mesenchymal differentiation in systemic sclerosis. *Nat. Commun.* **15**, 210 (2024).
26. Li, Y. N. et al. Spatially informed phenotyping by cyclic-in-situ-hybridisation identifies novel fibroblast populations and their pathogenic niches in systemic sclerosis. *Ann. Rheum. Dis.* **84**, 1852–1864 (2025).
27. Zhu, H. et al. Fibroblast subpopulations in systemic sclerosis: functional implications of individual subpopulations and correlations with clinical features. *J. Invest. Dermatol.* **144**, 1251–1261.e13 (2024).
28. Gur, C. et al. LGR5 expressing skin fibroblasts define a major cellular hub perturbed in scleroderma. *Cell* **185**, 1373–1388.e20 (2022).
29. Merrick, D. et al. Identification of a mesenchymal progenitor cell hierarchy in adipose tissue. *Science* **364**, eaav2501 (2019).
30. Rius Rigau, A. et al. Imaging mass cytometry-based characterization of fibroblast subsets and their cellular niches in systemic sclerosis. *Ann. Rheum. Dis.* https://doi.org/10.1136/ard-2024-226336 (2024).
31. Devakumar, V. et al. Single cell mapping of the metabolic landscape of skin fibrosis in systemic sclerosis. Preprint at *bioRxiv* https://doi.org/10.1101/2025.04.14.648761 (2025).
32. Sgonc, R. et al. Endothelial cell apoptosis is a primary pathogenetic event underlying skin lesions in avian and human scleroderma. *J. Clin. Invest.* **98**, 785–792 (1996).
33. Riemekasten, G. et al. Involvement of functional autoantibodies against vascular receptors in systemic sclerosis. *Ann. Rheum. Dis.* **70**, 530–536 (2011).
34. Sgonc, R. et al. Endothelial cell apoptosis in systemic sclerosis is induced by antibody-dependent cell-mediated cytotoxicity via CD95. *Arthritis Rheum.* **43**, 2550–2562 (2000).
35. Maehara, T. et al. Cytotoxic CD4+ T lymphocytes may induce endothelial cell apoptosis in systemic sclerosis. *J. Clin. Invest.* **130**, 2451–2464 (2020).
36. Gremmel, T., Frelinger, A. L. 3rd & Michelson, A. D. Platelet physiology. *Semin. Thromb. Hemost.* **42**, 191–204 (2016).

37. Mann, D. A. & Oakley, F. Serotonin paracrine signaling in tissue fibrosis. *Biochim. Biophys. Acta* **1832**, 905–910 (2013).
38. Dees, C. et al. Platelet-derived serotonin links vascular disease and tissue fibrosis. *J. Exp. Med.* **208**, 961–972 (2011).
39. Trinh-Minh, T. et al. Antifibrotic effects of specific targeting of the 5-hydroxytryptamine 2B receptor (5-HT_{2B}R) in murine models and ex vivo models of scleroderma skin. *Arthritis Rheumatol.* **77**, 1063–1076 (2025).
40. Truchetet, M. E. et al. Platelets induce thymic stromal lymphopoietin production by endothelial cells: contribution to fibrosis in human systemic sclerosis. *Arthritis Rheumatol.* **68**, 2784–2794 (2016).
41. Howell, D. C. et al. Direct thrombin inhibition reduces lung collagen, accumulation, and connective tissue growth factor mRNA levels in bleomycin-induced pulmonary fibrosis. *Am. J. Pathol.* **159**, 1383–1395 (2001).
42. de Ridder, G. G., Lundblad, R. L. & Pizzo, S. V. Actions of thrombin in the interstitium. *J. Thromb. Haemost.* **14**, 40–47 (2016).
43. Crawford, K. S. & Volkman, B. F. Prospects for targeting ACKR1 in cancer and other diseases. *Front. Immunol.* **14**, 1111960 (2023).
44. Huang, Y. et al. Atypical chemokine receptor 1-positive endothelial cells mediate leucocyte infiltration and synergize with secreted frizzled-related protein 2/asporin-positive fibroblasts to promote skin fibrosis in systemic sclerosis. *Br. J. Dermatol.* **191**, 964–978 (2024).
45. Raslan, A. A. et al. Lung injury-induced activated endothelial cell states persist in aging-associated progressive fibrosis. *Nat. Commun.* **15**, 5449 (2024).
46. Romano, E. et al. Recent insights into cellular and molecular mechanisms of defective angiogenesis in systemic sclerosis. *Biomedicines* **12**, 1331 (2024).
47. Piera-Velazquez, S., Mendoza, F. A. & Jimenez, S. A. Endothelial to mesenchymal transition (EndoMT) in the pathogenesis of human fibrotic diseases. *J. Clin. Med.* **5**, 45 (2016).
48. Rius Rigau, A. et al. Characterization of vascular niche in systemic sclerosis by spatial proteomics. *Circ. Res.* **134**, 875–891 (2024).
49. Talotta, R. et al. Certainties and uncertainties concerning the contribution of pericytes to the pathogenesis of systemic sclerosis. *J. Scleroderma Relat. Disord.* **3**, 14–20 (2018).
50. Iwayama, T. & Olson, L. E. Involvement of PDGF in fibrosis and scleroderma: recent insights from animal models and potential therapeutic opportunities. *Curr. Rheumatol. Rep.* **15**, 304 (2013).
51. Rajkumar, V. S. et al. Activation of microvascular pericytes in autoimmune Raynaud's phenomenon and systemic sclerosis. *Arthritis Rheum.* **42**, 930–941 (1999).
52. Sanges, S. et al. Soluble markers of B cell activation suggest a role of B cells in the pathogenesis of systemic sclerosis-associated pulmonary arterial hypertension. *Front. Immunol.* **13**, 954007 (2022).
53. Forestier, A. et al. Altered B lymphocyte homeostasis and functions in systemic sclerosis. *Autoimmun. Rev.* **17**, 244–255 (2018).
54. Sanges, S. et al. Role of B cells in the pathogenesis of systemic sclerosis. *Rev. Med. Interne* **38**, 113–124 (2017).
55. Matsushita, T. et al. Decreased levels of regulatory B cells in patients with systemic sclerosis: association with autoantibody production and disease activity. *Rheumatology* **55**, 263–267 (2016).
56. Melissaropoulos, K. & Liossis, S. N. Decreased CD22 expression and intracellular signaling aberrations in B cells of patients with systemic sclerosis. *Rheumatol. Int.* **38**, 1225–1234 (2018).
57. Le Maitre, M. et al. Beyond circulating B cells: characteristics and role of tissue-infiltrating B cells in systemic sclerosis. *Autoimmun. Rev.* **24**, 103782 (2025).
58. Bosello, S. et al. Characterization of inflammatory cell infiltrate of scleroderma skin: B cells and skin score progression. *Arthritis Res. Ther.* **20**, 75 (2018).
59. Whitfield, M. L. et al. Systemic and cell type-specific gene expression patterns in scleroderma skin. *Proc. Natl Acad. Sci.* **100**, 12319–12324 (2003).
60. Lafyatis, R. et al. B cell infiltration in systemic sclerosis-associated interstitial lung disease. *Arthritis Rheum.* **56**, 3167–3168 (2007).
61. Sanges, S. et al. B-cells in pulmonary arterial hypertension: friend, foe or bystander? *Eur. Respir. J.* **63**, 2301949 (2024).
62. Hoffmann-Vold, A. M. et al. Augmented concentrations of CX3CL1 are associated with interstitial lung disease in systemic sclerosis. *PLoS ONE* **13**, e0206545 (2018).
63. Taher, T. E. et al. Association of defective regulation of autoreactive interleukin-6-producing transitional B lymphocytes with disease in patients with systemic sclerosis. *Arthritis Rheumatol.* **70**, 450–461 (2018).
64. Thoreau, B., Chaigne, B. & Mouthon, L. Role of B-cell in the pathogenesis of systemic sclerosis. *Front. Immunol.* **13**, 933468 (2022).
65. Le Maitre, M. et al. Characteristics and impact of infiltration of B-cells from systemic sclerosis patients in a 3D healthy skin model. *Front. Immunol.* **15**, 1373464 (2024).
66. Kondo, K. et al. Establishment and characterization of a human B cell line from the lung tissue of a patient with scleroderma; extraordinary high level of IL-6 secretion by stimulated fibroblasts. *Cytokine* **13**, 220–226 (2001).
67. Benfaremo, D. et al. Putative functional pathogenic autoantibodies in systemic sclerosis. *Eur. J. Rheumatol.* **7**, S181–S186 (2020).
68. Chepy, A. et al. Autoantibodies in systemic sclerosis: From disease bystanders to pathogenic players. *J. Transl. Autoimmun.* **10**, 100272 (2025).
69. Chepy, A. et al. Can antinuclear antibodies have a pathogenic role in systemic sclerosis? *Front. Immunol.* **13**, 930970 (2022).
70. Arcand, J. et al. The autoantigen DNA topoisomerase I interacts with chemokine receptor 7 and exerts cytokine-like effects on dermal fibroblasts. *Arthritis Rheum.* **64**, 826–834 (2012).
71. Raschi, E. et al. Immune complexes containing scleroderma-specific autoantibodies induce a profibrotic and proinflammatory phenotype in skin fibroblasts. *Arthritis Res. Ther.* **20**, 187 (2018).
72. Chepy, A. et al. Effects of immunoglobulins g from systemic sclerosis patients in normal dermal fibroblasts: a multi-omics study. *Front. Immunol.* **13**, 904631 (2022).
73. Chepy, A. et al. Immunoglobulins G from patients with systemic sclerosis modify the molecular signatures of endothelial cells. *RMD Open* **11**, e004290 (2025).
74. Yoshizaki, A. et al. Immunization with DNA topoisomerase I and Freund's complete adjuvant induces skin and lung fibrosis and autoimmunity via interleukin-6 signaling. *Arthritis Rheum.* **63**, 3575–3585 (2011).
75. Fukasawa, T. et al. Single-cell-level protein analysis revealing the roles of autoantigen-reactive B lymphocytes in autoimmune disease and the murine model. *eLife* **10**, e67209 (2021).
76. Sakkas, L. I., Chikanza, I. C. & Platsoucas, C. D. Mechanisms of Disease: the role of immune cells in the pathogenesis of systemic sclerosis. *Nat. Clin. Pract. Rheumatol.* **2**, 679–685 (2006).
77. Gaydosik, A. M. et al. Dysfunctional KLRB1^{+}CD8^{+} T-cell responses are generated in chronically inflamed systemic sclerosis skin. *Ann. Rheum. Dis.* **84**, 798–809 (2025).
78. Ricard, L. et al. Circulating follicular helper T cells are increased in systemic sclerosis and promote plasmablast differentiation through the IL-21 pathway which can be inhibited by ruxolitinib. *Ann. Rheum. Dis.* **78**, 539–550 (2019).
79. Gaydosik, A. M. et al. Single-cell transcriptome analysis identifies skin-specific T-cell responses in systemic sclerosis. *Ann. Rheum. Dis.* **80**, 1453–1460 (2021).
80. Al-Adwi, Y. et al. Macrophages as determinants and regulators of fibrosis in systemic sclerosis. *Rheumatology* **62**, 535–545 (2023).
81. Toledo, D. M. & Pioli, P. A. Macrophages in systemic sclerosis: novel insights and therapeutic implications. *Curr. Rheumatol. Rep.* **21**, 31 (2019).
82. Soldano, S. et al. Increase in circulating cells coexpressing M1 and M2 macrophage surface markers in patients with systemic sclerosis. *Ann. Rheum. Dis.* **77**, 1842–1845 (2018).
83. Trombetta, A. C. et al. A circulating cell population showing both M1 and M2 monocyte/macrophage surface markers characterizes systemic sclerosis patients with lung involvement. *Respir. Res.* **19**, 186 (2018).
84. Murthy, S. et al. Alternative activation of macrophages and pulmonary fibrosis are modulated by scavenger receptor, macrophage receptor with collagenous structure. *FASEB J.* **29**, 3527–3536 (2015).
85. Xu, D. et al. PLG nanoparticles target fibroblasts and MARCO+ monocytes to reverse multiorgan fibrosis. *JCI Insight* **7**, e151037 (2022).
86. Taroni, J. N. et al. A novel multi-network approach reveals tissue-specific cellular modulators of fibrosis in systemic sclerosis. *Genome Med.* **9**, 27 (2017).
87. Bhandari, R. et al. Profibrotic activation of human macrophages in systemic sclerosis. *Arthritis Rheumatol.* **72**, 1160–1169 (2020).
88. Bhandari, R. et al. Human dermal fibroblast-derived exosomes induce macrophage activation in systemic sclerosis. *Rheumatology* **62**, SI114–SI124 (2023).
89. Bujor, A. M. et al. Fli1 downregulation in scleroderma myeloid cells has profibrotic and proinflammatory effects. *Front. Immunol.* **11**, 800 (2020).
90. Laurent, P. et al. Interleukin-1β-activated microvascular endothelial cells promote DC-SIGN-positive alternatively activated macrophages as a mechanism of skin fibrosis in systemic sclerosis. *Arthritis Rheumatol.* **74**, 1013–1026 (2022).
91. To, S. & Agarwal, S. K. Macrophages and cadherins in fibrosis and systemic sclerosis. *Curr. Opin. Rheumatol.* **31**, 582–588 (2019).
92. Lodyga, M. et al. Cadherin-11-mediated adhesion of macrophages to myofibroblasts establishes a profibrotic niche of active TGF-β. *Sci. Signal.* **12**, eaao3469 (2019).
93. Ouyang, J. F. et al. Systems level identification of a matrisome-associated macrophage polarisation state in multi-organ fibrosis. *eLife* **12**, e85530 (2023).
94. Gao, X. et al. Osteopontin links myeloid activation and disease progression in systemic sclerosis. *Cell Rep. Med.* **1**, 100140 (2020).
95. Morse, C. et al. Proliferating SPP1/MERTK-expressing macrophages in idiopathic pulmonary fibrosis. *Eur. Respir. J.* **54**, 1802441 (2019).
96. Yuan, X. et al. Human hypofunctional NCF1 variants promote pulmonary fibrosis in the bleomycin-induced mouse model and patients with systemic sclerosis via expansion of SPP1^{+} monocytes-derived macrophages. *Ann. Rheum. Dis.* **84**, 294–306 (2025).
97. Ishikawa, G. et al. α1 Adrenoreceptor antagonism mitigates extracellular mitochondrial DNA accumulation in lung fibrosis models and in patients with idiopathic pulmonary fibrosis. *Am. J. Physiol. Lung Cell Mol. Physiol* **324**, L639–L651 (2023).
98. Ishikawa, G. et al. A nerve-fibroblast axis in mammalian lung fibrosis. Preprint at *bioRxiv* https://doi.org/10.1101/2024.09.09.611003 (2025).
99. Gao, R. et al. Macrophage-derived netrin-1 drives adrenergic nerve-associated lung fibrosis. *J. Clin. Invest.* **131**, e136542 (2021).
100. Micera, A. et al. New insights on the involvement of nerve growth factor in allergic inflammation and fibrosis. *Cytokine Growth Factor. Rev.* **14**, 369–374 (2003).
101. Levick, S. P. et al. Sympathetic nervous system modulation of inflammation and remodeling in the hypertensive heart. *Hypertension* **55**, 270–276 (2010).
102. Pongratz, G. & Straub, R. H. The sympathetic nervous response in inflammation. *Arthritis Res. Ther.* **16**, 504 (2014).
103. Koenecke, A. et al. Alpha-1 adrenergic receptor antagonists to prevent hyperinflammation and death from lower respiratory tract infection. *eLife* **10**, e61700 (2021).
104. An, Y. A. et al. Endotrophin neutralization through targeted antibody treatment protects from renal fibrosis in a podocyte ablation model. *Mol. Metab.* **69**, 101680 (2023).

105. Yamaguchi, Y. et al. A peptide derived from endostatin ameliorates organ fibrosis. *Sci. Transl. Med.* **4**, 136ra71 (2012).
106. Sharma, S. et al. E4 engages uPAR and enolase-1 and activates urokinase to exert antifibrotic effects. *JCI Insight* **6**, e144935 (2021).
107. Hebbar, M. et al. Increased concentrations of the circulating angiogenesis inhibitor endostatin in patients with systemic sclerosis. *Arthritis Rheum.* **43**, 889–893 (2000).
108. Mouawad, J. E. et al. Reduced Cathepsin L expression and secretion into the extracellular milieu contribute to lung fibrosis in systemic sclerosis. *Rheumatology* **62**, 1306–1316 (2023).
109. Stawski, L. et al. MMP-12 deficiency attenuates angiotensin II-induced vascular injury, M2 macrophage accumulation, and skin and heart fibrosis. *PLoS ONE* **9**, e109763 (2014).
110. Ricard-Blum, S. & Salza, R. Matricryptins and matrikines: biologically active fragments of the extracellular matrix. *Exp. Dermatol.* **23**, 457–463 (2014).
111. O'Reilly, S., Tsou, P. S. & Varga, J. Senescence and tissue fibrosis: opportunities for therapeutic targeting. *Trends Mol. Med.* **30**, 1113–1125 (2024).
112. Merkt, W. et al. Senotherapeutics: targeting senescence in idiopathic pulmonary fibrosis. *Semin. Cell Dev. Biol.* **101**, 104–110 (2020).
113. Schafer, M. J. et al. Cellular senescence mediates fibrotic pulmonary disease. *Nat. Commun.* **8**, 14532 (2017).
114. Martyanov, V., Whitfield, M. L. & Varga, J. Senescence signature in skin biopsies from systemic sclerosis patients treated with senolytic therapy: potential predictor of clinical response? *Arthritis Rheumatol.* **71**, 1766–1767 (2019).
115. Dees, C. et al. JAK-2 as a novel mediator of the profibrotic effects of transforming growth factor β in systemic sclerosis. *Arthritis Rheum.* **64**, 3006–3015 (2012).
116. Zhang, Y. et al. JAK1-dependent transphosphorylation of JAK2 limits the antifibrotic effects of selective JAK2 inhibitors on long-term treatment. *Ann. Rheum. Dis.* **76**, 1467–1475 (2017).
117. Zehender, A. et al. The tyrosine phosphatase SHP2 controls TGFβ-induced STAT3 signaling to regulate fibroblast activation and fibrosis. *Nat. Commun.* **9**, 3259 (2018).
118. Zhang, Y. et al. Inhibition of casein kinase II reduces TGFβ induced fibroblast activation and ameliorates experimental fibrosis. *Ann. Rheum. Dis.* **74**, 936–943 (2015).
119. Pedroza, M. et al. Role of STAT3 in skin fibrosis and transforming growth factor beta signalling. *Rheumatology* **57**, 1838–1850 (2017).
120. Skhirtladze, C. et al. Src kinases in systemic sclerosis: central roles in fibroblast activation and in skin fibrosis. *Arthritis Rheum.* **58**, 1475–1484 (2008).
121. Akhmetshina, A. et al. Dual inhibition of c-abl and PDGF receptor signaling by dasatinib and nilotinib for the treatment of dermal fibrosis. *FASEB J.* **22**, 2214–2222 (2008).
122. Reich, N. et al. Jun N-terminal kinase as a potential molecular target for prevention and treatment of dermal fibrosis. *Ann. Rheum. Dis.* **71**, 737–745 (2012).
123. Chakraborty, D. et al. Activation of STAT3 integrates common profibrotic pathways to promote fibroblast activation and tissue fibrosis. *Nat. Commun.* **8**, 1130 (2017).
124. Wohlfahrt, T. et al. PU.1 controls fibroblast polarization and tissue fibrosis. *Nature* **566**, 344–349 (2019).
125. Wei, J. et al. PPARγ downregulation by TGFβ in fibroblast and impaired expression and function in systemic sclerosis: a novel mechanism for progressive fibrogenesis. *PLoS ONE* **5**, e13778 (2010).
126. Wei, J. et al. Regulation of matrix remodeling by peroxisome proliferator-activated receptor-gamma: a novel link between metabolism and fibrogenesis. *Open. Rheumatol. J.* **6**, 103–115 (2012).
127. Korman, B. et al. Adipocyte-specific repression of PPAR-gamma by NCoR contributes to scleroderma skin fibrosis. *Arthritis Res. Ther.* **20**, 145 (2018).
128. Palumbo-Zerr, K. et al. Orphan nuclear receptor NR4A1 regulates transforming growth factor-β signaling and fibrosis. *Nat. Med.* **21**, 150–158 (2015).
129. Chen, J. et al. Nur77 deficiency exacerbates cardiac fibrosis after myocardial infarction by promoting endothelial-to-mesenchymal transition. *J. Cell Physiol.* **236**, 495–506 (2021).
130. Pulakazhi Venu, V. K. et al. Nr4A1 modulates inflammation-associated intestinal fibrosis and dampens fibrogenic signaling in myofibroblasts. *Am. J. Physiol. Gastrointest. Liver Physiol.* **321**, G280–G297 (2021).
131. Tao, Y. et al. Nr4a1 promotes renal interstitial fibrosis by regulating the p38 MAPK phosphorylation. *Mol. Med.* **29**, 63 (2023).
132. Ma, M. F. et al. Orphan nuclear receptor 4 A1 involvement in transforming growth factor beta1-induced myocardial fibrosis in diabetic mice. *J. Physiol. Pharmacol.* https://doi.org/10.26402/jpp.2023.6.04 (2023).
133. Shany, S., Sigal-Batikoff, I. & Lamprecht, S. Vitamin D and myofibroblasts in fibrosis and cancer: at cross-purposes with TGF-β/SMAD signaling. *Anticancer. Res.* **36**, 6225–6234 (2016).
134. Zerr, P. et al. Vitamin D receptor regulates TGF-β signalling in systemic sclerosis. *Ann. Rheum. Dis.* **74**, e20 (2015).
135. Shen, L. et al. POS0007 The nuclear receptor Dax1 regulates Wnt/B-catenin signaling to promote fibroblast activation and skin fibrosis in systemic sclerosis. *Ann. Rheumatic Dis.* **83**, 286 (2024).
136. Tran-Manh, C. et al. POS1013 Retinoic acid-related orphan receptor-a as an upstream regulator of Hippo signaling and a therapeutic target in fibrotic tissue remodeling. *Ann. Rheumatic Dis.* **84**, 1121 (2025).
137. Shen, L. et al. POS0476 The nuclear receptor tr4 orchestrates cytoskeletal organization in a gα12/rock-dependent manner to promote myofibroblast differentiation and tissue fibrosis in systemic sclerosis. *Ann. Rheumatic Dis.* **81**, 492–493 (2022).
138. Avouac, J. et al. The nuclear receptor constitutive androstane receptor/NR1I3 enhances the profibrotic effects of transforming growth factor β and contributes to the development of experimental dermal fibrosis. *Arthritis Rheumatol.* **66**, 3140–3150 (2014).
139. Beyer, C. et al. Activation of liver X receptors inhibits experimental fibrosis by interfering with interleukin-6 release from macrophages. *Ann. Rheum. Dis.* **74**, 1317–1324 (2015).
140. Beyer, C. et al. Activation of pregnane X receptor inhibits experimental dermal fibrosis. *Ann. Rheum. Dis.* **72**, 621–625 (2013).
141. Beyer, C., Dees, C. & Distler, J. H. Morphogen pathways as molecular targets for the treatment of fibrosis in systemic sclerosis. *Arch. Dermatol. Res.* **305**, 1–8 (2013).
142. Beyer, C. & Distler, J. H. Morphogen pathways in systemic sclerosis. *Curr. Rheumatol. Rep.* **15**, 299 (2013).
143. Beyer, C. et al. Elevated serum levels of sonic hedgehog are associated with fibrotic and vascular manifestations in systemic sclerosis. *Ann. Rheum. Dis.* **77**, 626–628 (2018).
144. Horn, A. et al. Hedgehog signaling controls fibroblast activation and tissue fibrosis in systemic sclerosis. *Arthritis Rheum.* **64**, 2724–2733 (2012).
145. Liang, R. et al. The transcription factor GLI2 as a downstream mediator of transforming growth factor-β-induced fibroblast activation in SSc. *Ann. Rheum. Dis.* **76**, 756–764 (2017).
146. Liang, R. et al. Acyltransferase skinny hedgehog regulates TGFβ-dependent fibroblast activation in SSc. *Ann. Rheum. Dis.* **78**, 1269–1273 (2019).
147. Bergmann, C. et al. Mutual amplification of GLI2/hedgehog and transcription factor JUN/AP-1 signaling in fibroblasts in systemic sclerosis: potential implications for combined therapies. *Arthritis Rheumatol.* **77**, 92–98 (2025).
148. Horn, A. et al. Inhibition of hedgehog signalling prevents experimental fibrosis and induces regression of established fibrosis. *Ann. Rheum. Dis.* **71**, 785–789 (2012).
149. Distler, A. et al. Combined inhibition of morphogen pathways demonstrates additive antifibrotic effects and improved tolerability. *Ann. Rheum. Dis.* **73**, 1264–1268 (2014).
150. Zerr, P. et al. Inhibition of hedgehog signaling for the treatment of murine scleredermatous chronic graft-versus-host disease. *Blood* **120**, 2909–2917 (2012).
151. Bergmann, C. & Distler, J. H. Canonical Wnt signaling in systemic sclerosis. *Lab. Invest.* **96**, 151–155 (2016).
152. Wei, J. et al. Canonical Wnt signaling induces skin fibrosis and subcutaneous lipoatrophy: a novel mouse model for scleroderma? *Arthritis Rheum.* **63**, 1707–1717 (2011).
153. Zhang, Y. et al. Targeting of canonical WNT signaling ameliorates experimental scleredermatous chronic graft-versus-host disease. *Blood* **137**, 2403–2416 (2021).
154. Fakhouri, S. C. et al. Disturbed spatial WNT activation — a potential driver of the reticularized skin phenotype in systemic sclerosis. *Arthritis Rheumatol.* **77**, 740–749 (2025).
155. Daoussis, D. et al. Dickkopf-1 is downregulated early and universally in the skin of patients with systemic sclerosis despite normal circulating levels. *Clin. Exp. Rheumatol.* **36**, 45–49 (2018).
156. Bergmann, C. et al. Inhibition of glycogen synthase kinase 3β induces dermal fibrosis by activation of the canonical Wnt pathway. *Ann. Rheum. Dis.* **70**, 2191–2198 (2011).
157. Akhmetshina, A. et al. Activation of canonical Wnt signalling is required for TGF-β-mediated fibrosis. *Nat. Commun.* **3**, 735 (2012).
158. Bergmann, C. et al. X-linked inhibitor of apoptosis protein (XIAP) inhibition in systemic sclerosis (SSc). *Ann. Rheum. Dis.* **80**, 1048–1056 (2021).
159. Beyer, C. et al. Blockade of canonical Wnt signalling ameliorates experimental dermal fibrosis. *Ann. Rheum. Dis.* **72**, 1255–1258 (2013).
160. Distler, A. et al. Inactivation of tankyrases reduces experimental fibrosis by inhibiting canonical Wnt signalling. *Ann. Rheum. Dis.* **72**, 1575–1580 (2013).
161. Beyer, C. et al. β-catenin is a central mediator of pro-fibrotic Wnt signaling in systemic sclerosis. *Ann. Rheum. Dis.* **71**, 761–767 (2012).
162. Chen, C. W. et al. Pharmacological inhibition of porcupine induces regression of experimental skin fibrosis by targeting Wnt signalling. *Ann. Rheum. Dis.* **76**, 773–778 (2017).
163. Distler, A. et al. Inactivation of evenness interrupted (EVI) reduces experimental fibrosis by combined inhibition of canonical and non-canonical Wnt signalling. *Ann. Rheum. Dis.* **73**, 624–627 (2014).
164. Dees, C. et al. The Wnt antagonists DKK1 and SFRP1 are downregulated by promoter hypermethylation in systemic sclerosis. *Ann. Rheum. Dis.* **73**, 1232–1239 (2014).
165. Gillespie, J. et al. Transforming growth factor β activation primes canonical wnt signaling through down-regulation of axin-2. *Arthritis Rheumatol.* **70**, 932–942 (2018).
166. Trinh-Minh, T. et al. Noncanonical WNT5A controls the activation of latent TGF-β to drive fibroblast activation and tissue fibrosis. *J. Clin. Invest.* **134**, e159884 (2024).
167. Tsou, P. S., Varga, J. & O'Reilly, S. Advances in epigenetics in systemic sclerosis: molecular mechanisms and therapeutic potential. *Nat. Rev. Rheumatol.* **17**, 596–607 (2021).
168. Henderson, J., Distler, J. & O'Reilly, S. The role of epigenetic modifications in systemic sclerosis: a druggable target. *Trends Mol. Med.* **25**, 395–411 (2019).
169. Tsou, P. S. Epigenetic control of scleroderma: current knowledge and future perspectives. *Curr. Rheumatol. Rep.* **21**, 69 (2019).
170. Bergmann, C. & Distler, J. H. Epigenetic factors as drivers of fibrosis in systemic sclerosis. *Epigenomics* **9**, 463–477 (2017).
171. Pachera, E. et al. Long noncoding RNA H19X is a key mediator of TGF-β-driven fibrosis. *J. Clin. Invest.* **130**, 4888–4905 (2020).
172. Kramer, M. et al. Inhibition of H3K27 histone trimethylation activates fibroblasts and induces fibrosis. *Ann. Rheum. Dis.* **72**, 614–620 (2013).
173. Bergmann, C. et al. The histone demethylase Jumonji domain-containing protein 3 (JMJD3) regulates fibroblast activation in systemic sclerosis. *Ann. Rheum. Dis.* **77**, 150–158 (2018).
174. Huber, L. C. et al. Trichostatin a prevents the accumulation of extracellular matrix in a mouse model of bleomycin-induced skin fibrosis. *Arthritis Rheum.* **56**, 2755–2764 (2007).

175. Maurer, B. et al. MicroRNA-29, a key regulator of collagen expression in systemic sclerosis. *Arthritis Rheum.* **62**, 1733–1743 (2010).
176. Ramahi, A., Altorok, N. & Kahaleh, B. Epigenetics and systemic sclerosis: an answer to disease onset and evolution? *Eur. J. Rheumatol.* **7**, S147–S156 (2020).
177. Abd-Elmawla, M. A. et al. Deregulation of long noncoding RNAs ANCR, TINCR, HOTTIP and SPRY4-IT1 in plasma of systemic sclerosis patients: SPRY4-IT1 as a novel biomarker of scleroderma and its subtypes. *Cytokine* **133**, 155124 (2020).
178. Martinez-Lopez, J. et al. A strong dysregulated myeloid component in the epigenetic landscape of systemic sclerosis: an integrated DNA methylome and transcriptome analysis. *Arthritis Rheumatol.* **77**, 439–449 (2025).
179. Shin, J. Y. et al. Epigenetic activation and memory at a TGFB2 enhancer in systemic sclerosis. *Sci. Transl. Med.* **11**, eaaw0790 (2019).
180. Malaab, M. et al. Antifibrotic factor KLF4 is repressed by the miR-10/TFAP2A/TBX5 axis in dermal fibroblasts: insights from twins discordant for systemic sclerosis. *Ann. Rheum. Dis.* **81**, 268–277 (2022).
181. Tsou, P. S. et al. Histone deacetylase 5 is overexpressed in scleroderma endothelial cells and impairs angiogenesis via repression of proangiogenic factors. *Arthritis Rheumatol.* **68**, 2975–2985 (2016).
182. Ciechomska, M. et al. Histone demethylation and Toll-like receptor 8-dependent cross-talk in monocytes promotes transdifferentiation of fibroblasts in systemic sclerosis Via Fra-2. *Arthritis Rheumatol.* **68**, 1493–1504 (2016).
183. Li, T. et al. Epigenomics and transcriptomics of systemic sclerosis CD4+ T cells reveal long-range dysregulation of key inflammatory pathways mediated by disease-associated susceptibility loci. *Genome Med.* **12**, 81 (2020).
184. Lu, T. et al. Whole-genome bisulfite sequencing in systemic sclerosis provides novel targets to understand disease pathogenesis. *BMC Med. Genomics* **12**, 144 (2019).
185. van der Kroef, M. et al. Histone modifications underlie monocyte dysregulation in patients with systemic sclerosis, underlining the treatment potential of epigenetic targeting. *Ann. Rheum. Dis.* **78**, 529–538 (2019).
186. Wang, Y., Fan, P. S. & Kahaleh, B. Association between enhanced type I collagen expression and epigenetic repression of the FLI1 gene in scleroderma fibroblasts. *Arthritis Rheum.* **54**, 2271–2279 (2006).
187. Ghosh, A. K. et al. p300 is elevated in systemic sclerosis and its expression is positively regulated by TGF-β: epigenetic feed-forward amplification of fibrosis. *J. Invest. Dermatol.* **133**, 1302–1310 (2013).
188. Liu, Y. et al. The roles of noncoding RNAs in systemic sclerosis. *Front. Immunol.* **13**, 856036 (2022).
189. Razin, A. & Riggs, A. D. DNA methylation and gene function. *Science* **210**, 604–610 (1980).
190. Nan, X. et al. Transcriptional repression by the methyl-CpG-binding protein MeCP2 involves a histone deacetylase complex. *Nature* **393**, 386–389 (1998).
191. Chen, X. et al. Suppression of SUN2 by DNA methylation is associated with HSCs activation and hepatic fibrosis. *Cell Death Dis.* **9**, 1021 (2018).
192. Sanders, Y. Y. et al. Thy-1 promoter hypermethylation: a novel epigenetic pathogenic mechanism in pulmonary fibrosis. *Am. J. Respir. Cell Mol. Biol.* **39**, 610–618 (2008).
193. Zhang, Y. et al. Poly(ADP-ribose) polymerase-1 regulates fibroblast activation in systemic sclerosis. *Ann. Rheum. Dis.* **77**, 744–751 (2018).
194. Asano, Y., Czuwara, J. & Trojanowska, M. Transforming growth factor-β regulates DNA binding activity of transcription factor Fli1 by p300/CREB-binding protein-associated factor-dependent acetylation. *J. Biol. Chem.* **282**, 34672–34683 (2007).
195. Noda, S. et al. Simultaneous downregulation of KLF5 and Fli1 is a key feature underlying systemic sclerosis. *Nat. Commun.* **5**, 5797 (2014).
196. Asano, Y., Bujor, A. M. & Trojanowska, M. The impact of Fli1 deficiency on the pathogenesis of systemic sclerosis. *J. Dermatol. Sci.* **59**, 153–162 (2010).
197. Asano, Y. & Trojanowska, M. Fli1 represses transcription of the human α2(I) collagen gene by recruitment of the HDAC1/p300 complex. *PLoS ONE* **8**, e74930 (2013).
198. Dees, C. et al. TGF-β-induced epigenetic deregulation of SOCS3 facilitates STAT3 signaling to promote fibrosis. *J. Clin. Invest.* **130**, 2347–2363 (2020).
199. Zhao, S. et al. 5-aza-2′-deoxycytidine inhibits the proliferation of lung fibroblasts in neonatal rats exposed to hyperoxia. *Pediatr. Neonatol.* **58**, 122–127 (2017).
200. Bechtel, W. et al. Methylation determines fibroblast activation and fibrogenesis in the kidney. *Nat. Med.* **16**, 544–550 (2010).
201. Selmi, C. et al. X chromosome gene methylation in peripheral lymphocytes from monozygotic twins discordant for scleroderma. *Clin. Exp. Immunol.* **169**, 253–262 (2012).
202. Ramos, P. S. et al. Integrative analysis of DNA methylation in discordant twins unveils distinct architectures of systemic sclerosis subsets. *Clin. Epigenetics* **11**, 58 (2019).
203. Zehender, A. et al. TGFβ promotes fibrosis by MYST1-dependent epigenetic regulation of autophagy. *Nat. Commun.* **12**, 4404 (2021).
204. Papazoglou, A. et al. Epigenetic regulation of profibrotic macrophages in systemic sclerosis-associated interstitial lung disease. *Arthritis Rheumatol.* **74**, 2003–2014 (2022).
205. Liu, F. et al. Mechanosignaling through YAP and TAZ drives fibroblast activation and fibrosis. *Am. J. Physiol. Lung Cell Mol. Physiol* **308**, L344–L357 (2015).
206. Conroy, K. P., Kitto, L. J. & Henderson, N. C. αv integrins: key regulators of tissue fibrosis. *Cell Tissue Res.* **365**, 511–519 (2016).
207. Panciera, T. et al. Mechanobiology of YAP and TAZ in physiology and disease. *Nat. Rev. Mol. Cell Biol.* **18**, 758–770 (2017).
208. Choudhry, H. & Harris, A. L. Advances in hypoxia-inducible factor biology. *Cell Metab.* **27**, 281–298 (2018).
209. Beyer, C. et al. Hypoxia. Hypoxia in the pathogenesis of systemic sclerosis. *Arthritis Res. Ther.* **11**, 220 (2009).
210. Distler, J. H. et al. Hypoxia-induced increase in the production of extracellular matrix proteins in systemic sclerosis. *Arthritis Rheum.* **56**, 4203–4215 (2007).
211. Xiong, A. & Liu, Y. Targeting hypoxia inducible factors-1α as a novel therapy in fibrosis. *Front. Pharmacol.* **8**, 326 (2017).
212. Baker, S. J., Rane, S. G. & Reddy, E. P. Hematopoietic cytokine receptor signaling. *Oncogene* **26**, 6724–6737 (2007).

Acknowledgements

J.H.W.D. acknowledges the following grants: DI 1537/20-1, DI 1537/22-1, DI 1537/23-1, DI1537/27-1, DI 1537/28-1 from the German Research Foundation and projects from the research council (Forschungskommission) of the Medical Faculty of the Heinrich-Heine-University, as well as an unrestricted research grant from the Hiller-Foundation. D.L. acknowledges unrestricted research grants from GCS G4 and AVIESAN; grants from the European Union through the European Regional Development Fund (ERDF) within the framework of the Contrat de Plan Etat-Région (CPER) 2021–2027 for the Hauts-de-France region, France; as well as an unrestricted research grant from the University of Lille (Cross Disciplinary Program). A.-E.M. acknowledges the following grants: MA 9219/2-1 and 493659010 of the German Research Foundation, grants 2021_EKEA.03 and 2022_EKMS.02 of the Else-Kröner-Fresenius-Foundation, The Edith Busch and World Scleroderma Foundation Research Grant Programme 2022–2023 and the Research Committee of the Medical Faculty of the Heinrich-Heine University Düsseldorf (Forschungskommission; ID 2023-33). J.E.G. acknowledges an unrestricted research grant from the Taubman Medical Research Institute.

Author contributions

The authors contributed equally to all aspects of the article.

Competing interests

J.H.W.D. has consulted for Active Biotech, Anamar, ARXX, AstraZeneca, Bayer Pharma, Boehringer Ingelheim, Bristol Myers Squibb, Callidatas, Calluna, Galapagos, GSK, Janssen, Kyverna, Novartis, Pfizer, Quell Therapeutics and UCB; has received research funding from Anamar, ARXX, BMS, Boehringer Ingelheim, Cantargia, Celgene, CSL Behring, Exo Therapeutics, Galapagos, GSK, Incyte, Inventiva, Kiniksa, Kyverna, Lassen Therapeutics, Mestag, Sanofi-Aventis, SpicaTx, RedX, UCB and ZenasBio; is the CEO of 4D Science and scientific lead of FibroCure. D.L. has consulted for AstraZeneca, Boehringer Ingelheim, CSL Behring, Biocryst, Takeda; has received research funding from Boehringer Ingelheim, Roche, CSL Behring, Biocryst and Servier. J.E.G. has consulted for Eli Lilly, Janssen, Johnson & Johnson, Incyte, BMS, Sanofi, Prometheus, Almirall, Kyowa-Kirin, Novartis, AnaptysBio, Boehringer Ingelheim, GSK, AbbVie and Galderma; has research funding from Almirall, AbbVie, Boehringer Ingelheim, GSK, Galderma, Novartis, Johnson & Johnson and Eli Lilly.

Additional information

Supplementary information The online version contains supplementary material available at https://doi.org/10.1038/s41584-025-01349-z.

Peer review information *Nature Reviews Rheumatology* thanks Lazaros Sakkas, who co-reviewed with Vasiliki Syrmou; David Abraham; Michael Whitfield; and the other, anonymous, reviewer(s) for their contribution to the peer review of this work.

nature reviews rheumatology

https://doi.org/10.1038/s41584-026-01352-y

Review article

Check for updates

Metabolic masqueraders of paediatric and adult rheumatic diseases

Steven H. Lang[1,2], Cher Sha[1], Chelsi M. Rose[1,2], V. Reid Sutton[1,2], Tiphanie P. Vogel[2,3,4] ✉ & Lindsay C. Burrage[1,3,4] ✉

Abstract

Inborn errors of metabolism comprise a clinically diverse group of conditions that arise from the decreased activity of an enzyme or metabolite transporter and subsequent blockade in a metabolic pathway. These disorders are typically considered in the differential diagnosis of critically ill neonates or young children presenting with hypoglycaemia, metabolic acidosis or hyperammonaemia. However, beyond these classic presentations, a broader group of inborn errors of metabolism can manifest more subtly, with progressive articular and multi-systemic involvement that mimics or overlaps with typical features of rheumatological disease. Consequently, these conditions might be misdiagnosed for years as rheumatological diseases, including juvenile idiopathic arthritis, systemic sclerosis, idiopathic inflammatory myopathies and systemic lupus erythematosus. Moreover, these disorders provide unique opportunities to understand the complex interplay between metabolism and immune function. With the growing availability of disease-modifying therapies for inborn errors of metabolism, rheumatologists must be able to recognize these disorders, particularly in patients with atypical features or treatment-refractory disease.

Sections

Introduction

Inborn errors of metabolism with joint manifestations

Metabolic myopathies

Inborn errors of metabolism with autoinflammatory or autoimmune manifestations

Outlook

Conclusion

[1]Department of Molecular & Human Genetics, Baylor College of Medicine, Houston, TX, USA. [2]Texas Children's Hospital, Houston, TX, USA. [3]Division of Rheumatology, Department of Paediatrics, Baylor College of Medicine and William T. Shearer Center for Human Immunobiology, Houston, TX, USA. [4]These authors contributed equally: Tiphanie P. Vogel, Lindsay C. Burrage. ✉e-mail: tpvogel@bcm.edu; burrage@bcm.edu

Key points

- Metabolic 'mimickers' of rheumatological disease provide unique opportunities to understand the complex interplay between metabolism and immune function.
- Chronic activation of the innate immune system in lysosomal storage disorders results from the accumulation of lysosomal substrates and leads to joint manifestations mimicking arthritis.
- Metabolic myopathies, which have overlapping features with immune-mediated inflammatory myopathies, include disorders that impact glycogen metabolism, fatty acid oxidation and mitochondrial respiration.
- Inborn errors of metabolism with systemic symptoms highlight diverse mechanisms — including defects of amino acid transport, oligosaccharide processing and lipid and cholesterol metabolism — by which metabolic alterations drive immune dysregulation.
- Genetic testing should be considered in the evaluation of atypical or treatment-refractory juvenile idiopathic arthritis and other early-onset and/or atypical rheumatological presentations given the overlap between metabolic 'mimickers' and rheumatological disorders.

Introduction

Inborn errors of metabolism are traditionally defined as conditions that result from reduced activity of an enzyme or impaired function of a metabolite transporter, leading to disruption of specific biochemical pathways[1]. Although individually rare, these conditions are collectively common, with an estimated global prevalence of 50.9 per 100,000 live births[2]. Many disorders of intermediary metabolism — such as organic acidaemias, aminoacidopathies and urea cycle defects — present early in life with acute encephalopathy that requires immediate intervention. By contrast, other inborn errors of metabolism, including those affecting complex molecule and organelle metabolism, lipid metabolism and nucleic acid metabolism, can present more insidiously. These conditions can manifest with progressive dysfunction of non-neurological systems, including osteoarticular, connective tissue and systemic involvement. Such presentations can closely mimic primary rheumatological diseases, including juvenile idiopathic arthritis (JIA), systemic sclerosis, idiopathic inflammatory myopathies and systemic autoimmune or autoinflammatory disorders[3–9]. Rheumatologists are therefore uniquely positioned to make an early and accurate diagnosis for these individuals. However, surveys consistently show that rheumatologists often have a limited awareness of common inborn errors of metabolism that present with osteoarticular involvement[10,11].

Where available, newborn screening facilitates early recognition of some inborn errors of metabolism amenable to immediate intervention in the newborn period. However, the overwhelming majority of the nearly 1,500 known inborn errors of metabolism remain undetected by current newborn screening protocols[12,13]. Therefore, maintaining a high clinical index of suspicion is paramount for accurate and timely diagnosis and treatment, when available, particularly within the therapeutic window of opportunity. The rarity and complexity of these disorders pose substantial diagnostic challenges, particularly in cases with mild or non-neurological presentations that resemble more common conditions.

In this Review, we aim to familiarize the reader with inborn errors of metabolism that might first present to the rheumatologist's office with signs and symptoms reminiscent of JIA, systemic sclerosis, idiopathic inflammatory myopathies or systemic autoimmune or autoinflammatory disorders — including systemic lupus erythematosus (SLE)-like disease (Table 1 and Supplementary Table 1). The disorders discussed have been selected based on our collective experience caring for children and adults with inborn errors of metabolism at a large tertiary care centre, supplemented by an extensive review of the literature. Although not classical clinical 'mimickers', mevalonate kinase deficiency and laccase domain-containing 1 (LACC1) deficiency are included as prototypical examples of rheumatic diseases caused by immunometabolic dysfunction. Deficiency of adenosine deaminase 2 (DADA2), a pertinent metabolic cause of vasculitis, is excluded, as this disorder has been recently reviewed in detail elsewhere in this journal[14]. Disorders that primarily present with non-musculoskeletal pain, as well as disorders that result from defects in metal metabolism or electrolyte homeostasis, fall outside the scope of this Review. Finally, ultra-rare disorders described in only single case reports have not been included.

In addition to clinical presentation, we also highlight emerging insights into the inflammatory pathophysiology of many metabolic 'masqueraders'. These disorders offer a unique lens through which to explore immunometabolism, illuminating how metabolic processes sustain the energetic demands of immune cells and orchestrate their activation, differentiation and effector functions[15].

Inborn errors of metabolism with joint manifestations

Overall, a major diagnostic category among the metabolic 'mimickers' of rheumatological disease are the disorders that mimic arthritis. Many of the disorders in this category are lysosomal storage disorders, which often present with prominent skeletal and connective tissue manifestations. Although each lysosomal storage disorder is defined by a unique enzyme deficiency leading to accumulation of distinct substrates, their converging phenotypes point to a common underlying pathomechanism of chronic activation of the innate immune system. Although much attention has focused on the direct pro-inflammatory effects of accumulated bioactive substrates — such as glycosaminoglycan in the mucopolysaccharidoses or globotriaosylceramide in Fabry disease, both of which can activate canonical pathways such as Toll-like receptor 4 (TLR4) signalling (Box 1) — emerging evidence also implicates the lysosome itself as a key mediator of inflammation. Indeed, in the context of lysosomal dysfunction and impaired autophagy, cellular stress signals such as potassium efflux, reactive oxygen species generation, and cytoplasmic release of lysosomal cathepsins can promote inflammasome assembly and activation, culminating in the maturation and secretion of IL-1β[16,17]. Despite promising preclinical data and the limited benefit of enzyme replacement therapy and haematopoietic stem cell transplant (HSCT) in addressing the skeletal phenotypes of many lysosomal storage disorders, the clinical use of immunomodulatory agents remains limited and is an important area for future work. This section highlights lysosomal storage disorders as well as other metabolic mimickers of arthritis.

Farber disease

Farber disease is an autosomal-recessive lysosomal storage disorder caused by minimal or absent activity of acid ceramidase, a lysosomal

Table 1 | Key clinical features of inborn errors of metabolism that might mimic rheumatic diseases

Disease	Gene	Clinical findings
Inborn errors of metabolism with joint manifestations		
Alkaptonuria	*HGD*	Ankylosing spondylitis-like arthritis Dark urine, particularly after standing, or alkalization; darkened sebum (earwax) Darkening of the sclerae and auricles Aortic valve stenosis
Fabry disease	*GLA*	Episodic pain affecting the distal extremities Small red-to-black papular skin lesions
Farber disease	*ASHA1*	Subcutaneous nodules Dysphonia
Gaucher disease	*GBA1*	Bone and/or joint pain Thrombocytopenia Hepatosplenomegaly Radiographic evidence of Erlenmeyer flask deformity
HGprt-related hyperuricaemia	*HPRT1*	Gout Renal calculi
LACC1 deficiency	*LACC1*	Family history of juvenile arthritis Consanguinity
Mucolipidosis type III	*GNPTAB* or *GNPTG*	Hand deformities (such as claw hand, carpal tunnel and restricted range of motion) Progressive hip dysplasia Radiographic evidence of dysostosis multiplex
Mucopoly-saccharidosis type I	*IDUA*	Joint contractures of the hands and shoulders Carpal tunnel syndrome Umbilical or inguinal hernia Distinctive facial features including a flat face, depressed nasal bridge, frontal bossing and macroglossia Corneal clouding Recurrent respiratory infections Cardiac murmur Radiographic evidence of dysostosis multiplex
Mucopoly-saccharidosis type IVA	*GALNS*	Wrist laxity Short trunk Pectus carinatum Radiographic evidence of dysostosis multiplex
PRPS1 superactivity	*PRPS1*	Gout
Metabolic myopathies		
Danon disease	*LAMP2*	Severe cardiomyopathy
Glycogen storage disease type II, late onset	*GAA*	Left ventricular hypertrophy Dysrhythmias including Wolf–Parkinson–White syndrome
Glycogen storage disease type V	*PYGM*	Experience of a 'second wind' approximately 10 min into physical activity
Inborn errors of metabolism with autoimmune or autoinflammatory manifestations		
α-Mannosidosis	*MAN2B1*	Various autoimmune manifestations, including SLE Hearing loss Coarse facial features Dysostosis multiplex on radiographs
Lysinuric protein intolerance	*SLC7A7*	SLE-like disease Haemophagocytic lymphohistiocytosis Persistent pulmonary alveolar proteinosis Post-prandial hyperammonaemia
Mevalonate kinase deficiency	*MVK*	High fevers lasting 3–7 days
Prolidase deficiency	*PEPD*	Chronic, painful lower extremity ulcers Splenomegaly
Acid sphingo-myelinase deficiency type B	*SMPD1*	Hepatosplenomegaly Thrombocytopenia Interstitial lung disease

HGprt, hypoxanthine-guanine phosphoribosyltransferase; LACC1, laccase domain-containing 1; PRPS1, phosphoribosylpyrophosphate synthase 1; SLE, systemic lupus erythematosus.

enzyme encoded by *ASAH1* (ref. 18). Acid ceramidase catalyses the hydrolysis of the bioactive lipid molecule ceramide into sphingosine and free fatty acid (Supplementary Fig. 1). The pathological hallmark of Farber disease is the presence of granulomatous lesions composed of foamy macrophages and histiocytes containing characteristic lysosomal 'banana body' inclusions[19]. Circulating plasma levels of MCP1 — a potent recruiter of monocytes and macrophages — are elevated up to tenfold in individuals with Farber disease compared with healthy individuals[20]. The central role of macrophage-mediated inflammation is further supported by findings from a double-knockout murine model, in which deletion of both acid ceramidase and MCP1 resulted in prolonged survival, delayed onset of weight loss and reduced pulmonary and hepatic inflammation[21]. Although the precise role of specific ceramide species in promoting this inflammatory response in Farber disease is still poorly understood, ceramide-1-phosphate has been shown to induce MCP1 release via activation of PI3K–AKT, MEK–ERK1/2 and p38 signalling pathways[22].

The classic triad of findings in Farber disease are subcutaneous nodules, polyarticular joint abnormalities — including contractures — and dysphonia resulting from laryngeal involvement[23,24] (Fig. 1). Neurological manifestations are common, but severity ranges from absent to progressive neurodegeneration, amyotrophy, cognitive impairment and epilepsy[23,24]. Clinical features might also include recurrent sterile fevers, whereas laboratory findings can reveal elevations in inflammatory markers and abnormal lymphocyte subsets[25,26]. Symptom onset typically occurs between 1 and 9 months of age, yet diagnosis is frequently delayed, with a median lag exceeding 12 months after initial presentation. In one series, 71% of patients were initially misdiagnosed with a form of JIA[27]. Median survival is approximately 3 years, with respiratory insufficiency being the most common cause of death. However, disease severity is heterogeneous, with variable rates of progression and multisystem involvement. Notably, some patients survive into the sixth and seventh decades without neurological sequelae[23].

Genetic sequencing of *ASAH1* is the preferred diagnostic approach for Farber disease. Although in vitro assays of ceramidase activity are not widely available, these assays might offer valuable prognostic insight. Notably, residual enzyme activity exceeding 5.1% has been associated with a milder disease course and prolonged survival[23].

Allogenic HSCT has demonstrated efficacy in resolving inflammatory granulomas, improving joint mobility and reversing hoarseness in patients with Farber disease[28]. However, this approach does not seem to

Box 1 | Pro-inflammatory signalling in mucopolysaccharidoses

Cartilage pathology in mucopolysaccharidosis is characterized by thickening, with vacuolated and enlarged chondrocytes, disruption of the columnar architecture and impaired endochondral ossification[217,218]. Accumulation of glycosaminoglycans (GAGs) in mucopolysaccharidosis has been linked to activation of inflammatory cascades, potentially owing to their structural similarity to lipopolysaccharide, a potent activator of Toll-like receptor 4 (TLR4). Glycosaminoglycans present in the tissues or peripheral circulation can activate TLR4 receptors on synoviocytes and chondrocytes, leading to the release of the major inflammatory cytokines TNF and IL-1β[219–221]. TNF signalling promotes chondrocyte apoptosis by suppressing the activity of the pro-survival lipid sphingosine-1-phosphate (S1P) and upregulating the production of the apoptotic lipid ceramide. Conversely, in the synovium, these cytokines trigger the release of sphingosine-1-phosphate and suppress the expression of ceramide. This shift promotes synovial-cell survival and proliferation, leading to hyperplastic synovial tissue. Additionally, TNF and IL-1β promote osteoclastogenesis by inducing the expression and secretion of RANKL, ultimately leading to increased bone erosion and osteopenia. Increased TNF levels have been directly associated with increased pain, decreased physical function and decreased quality of life in individuals with a diagnosis of mucopolysaccharidosis[222]. TNF inhibition has been shown to improve skeletal disease in animal models[221,223], and had beneficial effects on physical function, and possibly pain, in very limited case series of patients with mucopolysaccharidosis[224,225].

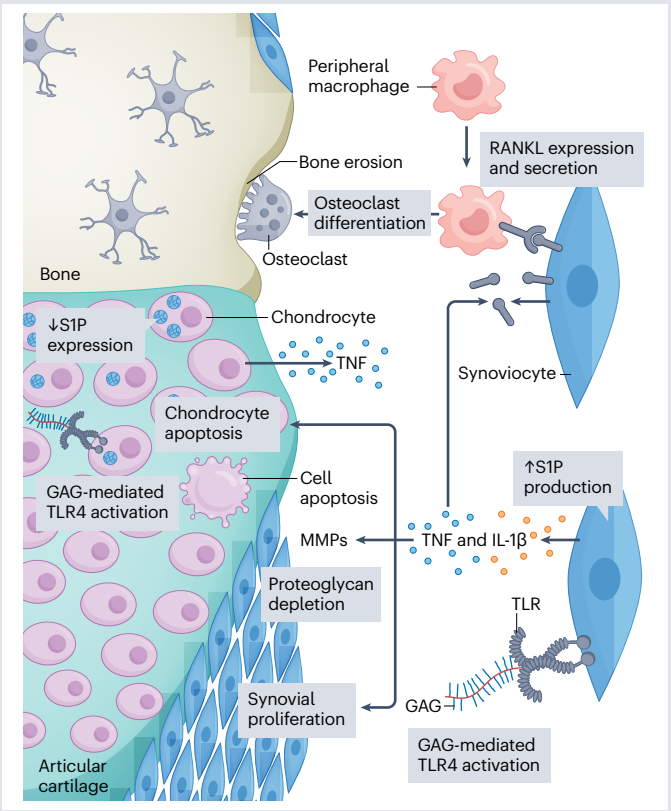

MMP, matrix metalloproteinase.

alleviate central nervous system manifestations when present[28]. Owing to prominent joint involvement, many patients receive treatment with DMARDs. Anecdotal reports suggest clinical improvement with these agents, including a case series presented in abstract form describing five patients treated with tocilizumab who showed notable clinical responses[29]. However, no formal recommendations are currently available for immune modulation in Farber disease[20]. NSAIDs are also commonly used, despite the absence of established evidence supporting their benefit. Partial or transient responses to these therapies might contribute to diagnostic delay by reinforcing initial misdiagnoses.

Mucolipidosis type III

Mucolipidosis type III is an autosomal-recessive lysosomal storage disorder characterized by impaired intracellular trafficking of lysosomal hydrolases[30]. This defect arises from reduced activity of N-acetylglucosamine-1-phosphotransferase (GlcNAc-PTase), an enzyme encoded by *GNPTAB* and *GNPTG*. Lysosomal hydrolases require a specific post-translational modification — most notably, the addition of mannose-6-phosphate — to be correctly targeted to the lysosome. GlcNAc-PTase, a membrane-bound heterohexamer composed of $\alpha_2\beta_2\gamma_2$ subunits, catalyses an important step of this modification process[31]. In the absence of this modification, lysosomal enzymes are misdirected, leading to accumulation of undegraded glycoproteins and glycolipids within lysosomes and tissues, and giving rise to the clinical manifestations of the disease.

Hand deformities (including claw hands, carpal tunnel syndrome and restricted range of motion) are the most common presenting features of mucolipidosis type III, occurring in nearly half of patients[32]. These manifestations frequently lead to misdiagnosis as JIA or systemic sclerosis[3,4]. Progressive hip dysplasia and vertebral anomalies are also common[33]. Gross motor delays might be observed; however, cognitive development is typically preserved[34]. Radiographic imaging often reveals characteristic features of dysostosis multiplex[35,36] (Fig. 2). Although survival data are limited, the median lifespan is estimated at 62 years, with cardiorespiratory compromise being the most frequent cause of death[32].

Plasma levels of most lysosomal acid hydrolases are highly elevated in mucolipidosis type III; however, this biochemical finding does not discriminate between mucolipidosis subtypes[30]. Definitive classification requires targeted genetic sequencing of *GNPTAB* and *GNPTG*. No effective disease-modifying interventions currently exist for mucolipidosis type III. Supportive interventions, however, can alleviate symptoms and improve quality of life. Low-impact physiotherapy is generally well tolerated, and orthopaedic procedures — hip and knee replacements — have yielded favourable outcomes in selected cases[37,38]. Night-time casting of hands might help to preserve function over time.

In a limited case series, intravenous pamidronate reduced bone pain, lowered analgesic requirements and improved mobility[39].

Fabry disease

Fabry disease, an X-linked disorder, is one of the most common lysosomal storage disorders[40–42]. This disease is caused by pathogenic variants in *GLA*, which result in defective activity of α-galactosidase A, an enzyme responsible for cleaving galactose from globotriaosylceramide and related glycosphingolipids (Supplementary Fig. 1). Accumulation of globotriaosylceramide occurs across multiple cell types, with mortality primarily driven by progressive nephropathy and vasculopathy. Similar to other lysosomal storage disorders discussed in this Review, the pathophysiology of Fabry disease is increasingly recognized to involve inflammatory processes[43,44]. For example, globotriaosylceramide has been shown to function as a damage-associated molecular pattern (DAMP) and stimulate production of IL-1β and TNF in monocytes and dendritic cells via TLR4-mediated signalling[45]. Additionally, altered levels of vascular endothelial adhesion molecules and coagulation factors have been reported in Fabry disease, and probably contribute to the vasculopathy alongside globotriaosylceramide and lyso-globotriaosylceramide accumulation in endothelial cells and vascular smooth-muscle cells[46].

Neuropathic pain, including episodic pain crises in the distal extremities and acroparaesthesias, is the most common presenting symptom in approximately half of patients with Fabry disease, typically emerging in the first decade of life[47]. This presentation might be misinterpreted as inflammatory arthritis. Gastrointestinal symptoms, including abdominal pain and diarrhoea, are the second most common presenting symptom, followed by angiokeratomas in a characteristic 'bathing suit' distribution, which might be mistaken for purpura[47].

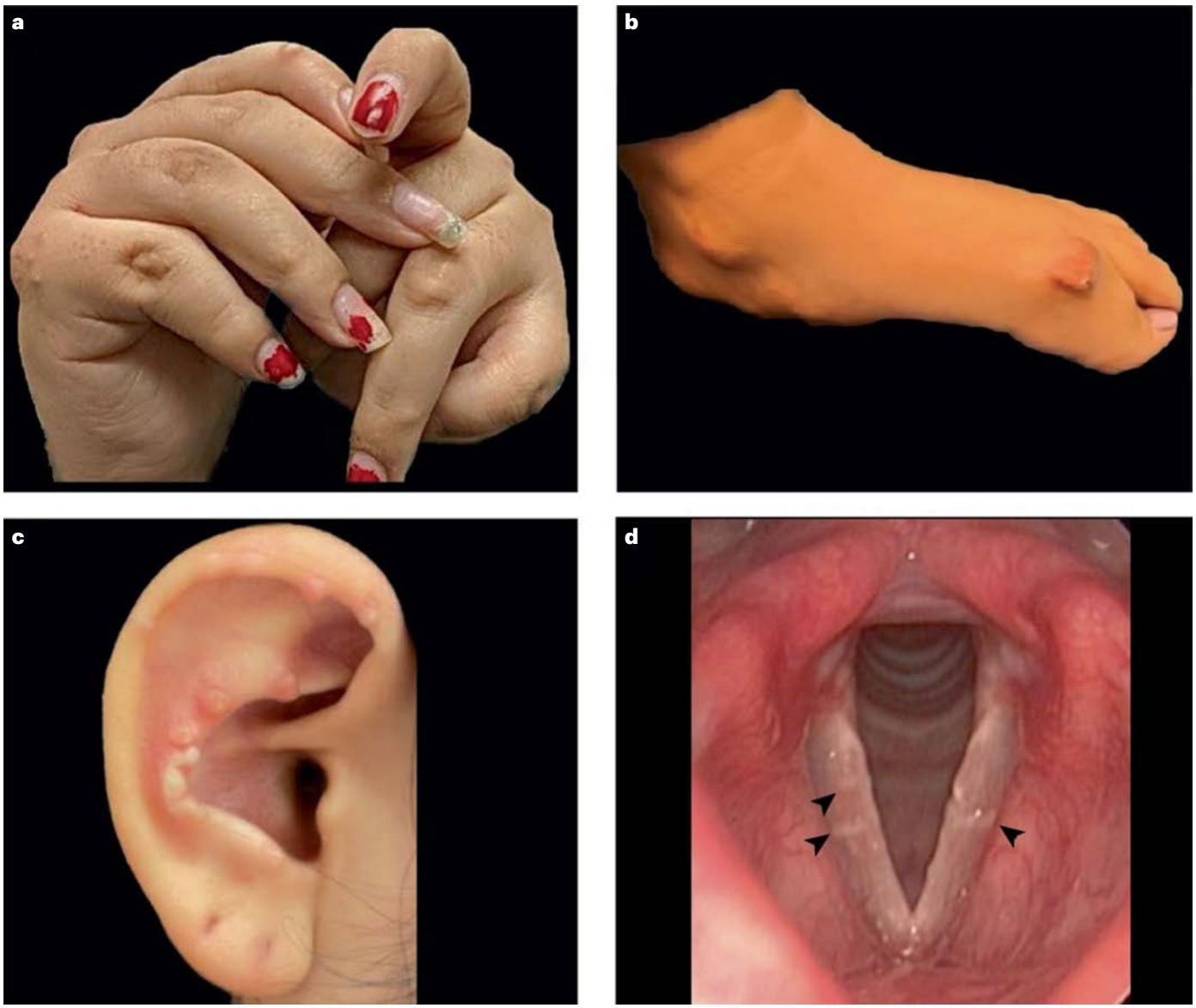

Fig. 1 | Clinical features of Farber disease in a paediatric patient. a–d, Clinical presentation of a 14-year-old female patient with Farber disease. Characteristic findings include chronic polyarthritis (**a**,**b**) and subcutaneous nodules (**a**–**c**). Direct laryngoscopy revealed laryngeal nodules (arrowheads; **d**).

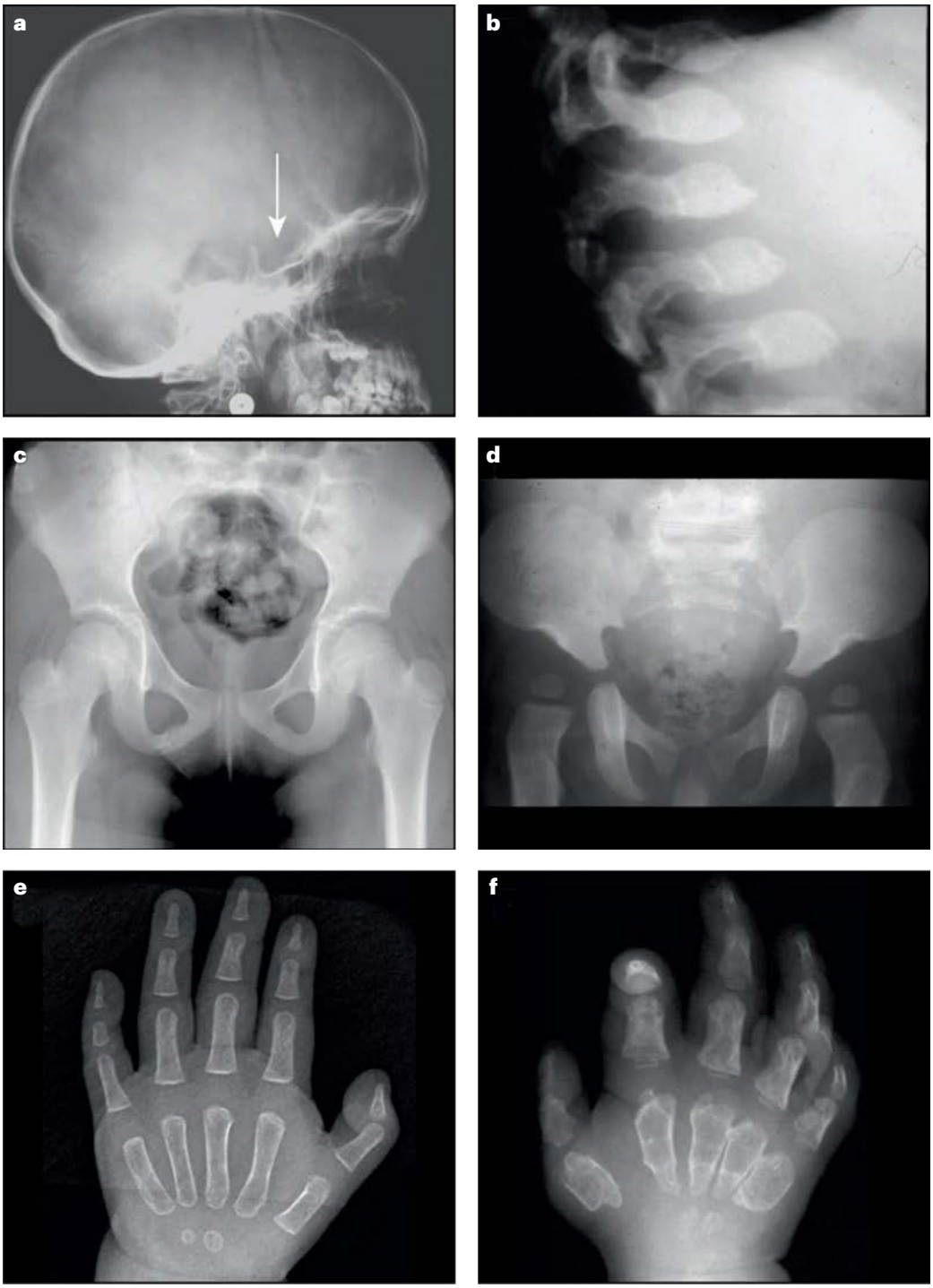

Fig. 2 | Typical radiographic findings of dysostosis multiplex. a–**f**, Characteristic skeletal abnormalities in dysostosis multiplex. Panel **a** shows a lateral skull radiograph with a characteristic 'J-shaped' sella turcica (arrow). In panel **b**, a lateral view of the spine reveals oval-shaped vertebral bodies with inferior 'beaking'. Panel **c** presents a normal anterior–posterior view of a pelvis for comparison. In panel **d**, the pelvis demonstrates the classic 'wine glass' appearance, marked by rounded iliac wings and tapering of the inferior ilium, which gives the ilium the shape of a ping-pong paddle. The acetabulum is also poorly developed, and the proximal femoral epiphyses are small. Panel **e** shows a normal hand radiograph from a patient of similar age to the individual in panel **f**, showing severe proximal tapering of the metacarpals with broad and dysplastic metacarpals and phalanges.

Recurrent sterile fevers occur in up to 20% of patients[48]. Interestingly, inflammatory markers are typically within normal limits during febrile episodes, supporting the theory that elevated temperatures in this condition arise from impaired heat dissipation secondary to autonomic dysfunction (specifically, anhidrosis)[48,49]. Major organ manifestations do not typically develop until the fourth and fifth decades and are consequences of both chronic microvascular disease and storage pathology leading to cardiac disease — including left ventricular hypertrophy and arrhythmias — stroke and progressive renal disease[50]. Knowledge of Fabry disease among rheumatologists seems to be limited. In a survey of 120 rheumatologists, only 6% correctly recognized Fabry disease when provided with a narrative history, physical examination describing a typical presentation and positive family history[11]. The most frequently proposed differential diagnoses included connective tissue disorders, unspecified enzyme deficiencies and rheumatoid arthritis[11].

Diagnosis of Fabry disease in male patients is confirmed by measuring α-galactosidase A activity in leukocytes, with levels below 5% considered diagnostic[51]. In female patients, however, enzyme activity can be highly variable owing to X chromosome inactivation, necessitating molecular confirmation through identification of a pathogenic variant in *GLA*[51]. Therapeutic options include enzyme replacement therapy and pharmacological chaperone. Agalsidase beta is an enzyme replacement therapy administered via intravenous infusion every other week[52]. A Cochrane review established that enzyme replacement therapy improves pain-related quality-of-life scores and reduces the incidence of cardiovascular and cerebrovascular events and renal disease[53,54]. Migalastat is a small-molecule chaperone therapy for individuals with amenable *GLA* variants and has been shown to stabilize renal function and improve left-ventricular mass index[55]. These therapies represent important advances in disease management, although long-term outcomes and optimal treatment strategies continue to be areas of active investigation.

Gaucher disease

Gaucher disease is a lysosomal storage disorder characterized by defective sphingolipid catabolism[56]. Deficient activity of the acid hydrolase glucocerebrosidase leads to accumulation of its substrate glucosylceramide, primarily within macrophages (Supplementary Fig. 1). These cells are preferentially affected owing to their physiological role in clearing cellular debris, which exposes them to a high flux of sphingolipid-containing cell membranes[57]. Lipid-laden macrophages, known as Gaucher cells, infiltrate the bone marrow, liver and spleen, disrupting normal tissue architecture and contributing to an inflammatory microenvironment. Individuals with Gaucher disease have an altered serum inflammatory profile, with high levels of macrophage inflammatory protein 1α (MIP-1α) and MIP-1β, which directly correlate with bone disease activity[58–60]. Chitotriosidase, an enzyme secreted by macrophages, is used as a biomarker for diagnosis and response to therapy[61].

Both innate and adaptive immune mechanisms are implicated in Gaucher disease pathophysiology. Continuous uptake and processing of glucosylceramide released by Gaucher cells leads to the differentiation of plasma cells that produce glucosylceramide-specific IgG autoantibodies[62]. These autoantibodies form immune complexes with glucosylceramide, activating the classical complement pathway and leading to robust production of C5a. Engagement of C5a receptors on Gaucher cells further perpetuates the production and release of glucosylceramide, driving additional immune-complex formation. Concurrent activation of C5a receptors on dendritic cells upregulates the expression of co-stimulatory molecules, promoting T cell activation and sustaining a pro-inflammatory milieu[62,63]. Strikingly, in a chemically induced model of Gaucher disease, mice deficient in the C5a receptor showed only minimal signs of disease, with normalization of cytokine profiles, underscoring the important role of complement-mediated inflammation in disease progression[62].

Type 1 (the non-neuronopathic form) is the most common phenotype of Gaucher disease and frequently presents during childhood[64]. The classic triad comprises hepatosplenomegaly, thrombocytopenia (secondary to splenic sequestration) and skeletal disease, which can lead to pain and disability. Skeletal complications include decreased bone mineral density, Erlenmeyer flask deformity, osteonecrosis and bone crisis[57]. The Erlenmeyer flask deformity is a radiographic hallmark characterized by loss of normal metaphyseal concavity and widening of a long bone metaphysis, attributed to infiltration of Gaucher cells within the bone marrow[65]. Bone crises are acute episodes of severe bone or joint pain that most commonly involve long bones, but can also affect the hands and feet[66]. Bone crises can be associated with clinical and laboratory signs[57,67].

Diagnosis of Gaucher disease is established through enzymatic assay of glucocerebrosidase activity in peripheral blood lymphocytes or leukocytes, complemented by *GBA1* sequencing[68]. Therapeutic strategies include enzyme replacement therapy (using recombinant glucocerebrosidase formulations such as imiglucerase, velaglucerase alfa and taliglucerase alfa) and substrate reduction therapy using glucosylceramide synthase inhibitors (such as miglustat and eliglustat)[69]. Emerging therapeutic avenues, including complement pathway inhibition, are currently under investigation in preclinical models[70].

Mucopolysaccharidoses

The mucopolysaccharidoses are a heterogeneous group of lysosomal storage disorders that arise from defects in 1 of 11 lysosomal enzymes involved in the degradation of glycosaminoglycans, historically known as mucopolysaccharides (Supplementary Fig. 1). These disorders are typically inherited in an autosomal-recessive manner, except for mucopolysaccharidosis II (known as Hunter syndrome), which follows an X-linked inheritance pattern. The contribution of glycosaminoglycan accumulation in joint tissues to inflammatory processes has been investigated (Box 1).

Seven separate subtypes of mucopolysaccharidoses have been described, with considerable phenotypic overlap across forms. A comprehensive review of mucopolysaccharidosis nosology is beyond the scope of this Review, but many mucopolysaccharidoses have shared musculoskeletal features. This section focuses on attenuated mucopolysaccharidosis I (known as Scheie syndrome) and mild mucopolysaccharidosis IVA (known as Morquio A disease), which can present as isolated connective tissue diseases with preserved cognition. In mucopolysaccharidosis I, umbilical and inguinal hernias are typically the earliest presenting features (mean age at onset 4.6 years), followed by joint contractures of the hands and shoulders (mean age at onset 7.6 years) and dysostosis multiplex (mean age at onset 8 years)[71,72]. Patients have characteristic coarse facial features, including a flat face, a depressed nasal bridge, frontal bossing and macroglossia[71]. Mucopolysaccharidosis IVA is classically characterized by short trunk dwarfism, pectus carinatum, odontoid hypoplasia, kyphoscoliosis, genu valgum (knock-knees) and hip dysplasia with an abnormal 'waddling gait'[73]. Uniquely, this subtype is the only form of mucopolysaccharidosis associated with hypermobility of the distal joints, contrasting with proximal stiffness. The wrist is most severely affected by joint laxity, resulting in a

weak grip and difficulty with fine motor skills[74]. Mild mucopolysaccharidosis IVA might not present until late in childhood, with individuals exhibiting a normal stature and subtle skeletal involvement[75].

In a survey of rheumatologists presented with a prototypical case of mucopolysaccharidosis, only 13% included mucopolysaccharidosis in the differential diagnosis, and just 20% identified the appropriate next step in evaluation once provided with the suspected diagnosis[10]. This survey prompted the development of a rheumatology-based diagnostic algorithm. Key clinical features that should prompt consideration of mucopolysaccharidosis include corneal clouding, a history of umbilical or inguinal hernia, cardiac murmurs secondary to valvular thickening and dysfunction, recurrent upper respiratory or ear infections and carpal tunnel syndrome. Notably, mucopolysaccharidosis is the most common cause of carpal tunnel syndrome in children and adolescents[76]. Unfortunately, despite efforts to increase clinician awareness, time to diagnosis in mucopolysaccharidosis I has not improved since the introduction of enzyme replacement therapy[77,78].

Diagnostic evaluation of mucopolysaccharidoses should integrate both biochemical and molecular approaches. Urinary glycosaminoglycan analysis, preferably by tandem mass spectrometry, enables differentiation of specific glycosaminoglycan species and can guide subtype identification[79]. Enzyme activity assays performed on cultured peripheral blood cells or fibroblasts provide functional confirmation of a suspected diagnosis[80]. Concurrently, molecular diagnosis can be pursued with a multi-gene mucopolysaccharidosis panel to confirm diagnosis and facilitate genetic counselling. Additionally, radiographic imaging remains an important adjunct, with skeletal surveys often revealing features of dysostosis multiplex[81] (Fig. 2). Finally, enzyme-based newborn screening for mucopolysaccharidosis I is now implemented across most US states and in several other countries, enabling earlier detection and intervention.

Enzyme replacement therapy is currently available for most mucopolysaccharidoses, with the exception of mucopolysaccharidosis III, mucopolysaccharidosis IVB and mucopolysaccharidosis IX. This approach generally leads to improvement in biochemical parameters, organomegaly, respiratory function and exercise capacity[82–86]. However, the effects of enzyme replacement therapy on skeletal disease in mucopolysaccharidosis are limited owing to the limited penetration of replacement enzyme into avascular cartilage and bone. Very early initiation of enzyme replacement therapy might partially prevent the development of orthopaedic manifestations; impressive differences in disease progression have been observed in a sibship trio who commenced therapy at different ages[87]. Despite promising preclinical data (Box 1) and the limited benefit of enzyme replacement therapy and HSCT on the skeletal phenotype of mucopolysaccharidoses[88], the clinical use of TNF inhibitors as an adjunctive therapy is not currently formally recommended, owing to limited clinical data.

Laccase domain-containing 1 deficiency

LACC1 deficiency is an autosomal-recessive cause of JIA and the first monogenic form of the disorder to be described[89]. LACC1 is highly expressed in classically activated macrophages, and accumulating evidence supports a multifaceted role for this enzyme in immunometabolism[90–92]. Emerging data have positioned LACC1 as a molecular link between pro-inflammatory, arginine-mediated nitric oxide synthesis and anti-inflammatory polyamine synthesis[93]. Specifically, LACC1 can catalyse the conversion of citrulline — generated by nitric oxide synthase 2 during arginine metabolism — to ornithine and isocyanic acid, thereby feeding directly into the anti-inflammatory polyamine synthesis pathway[93]. This novel pathway of arginine metabolism in classically activated macrophages, in which citrulline is typically recycled back to arginine, provides a direct mechanism by which LACC1 can negatively regulate inflammation.

In a large cohort of 52 individuals with LACC1 deficiency, symptom onset occurred by the age of 2 years in the majority of cases, with 61.5% displaying a polyarticular pattern and 26.9% meeting criteria for systemic-onset JIA, including fever and rash[94]. No extra-articular manifestations have been consistently reported. Although no biochemical tests are currently available for LACC1 deficiency, diagnosis can be confirmed through molecular testing that identifies biallelic pathogenic variants in *LACC1*.

Most patients exhibit a poor or partial response to DMARDs, and fewer than one-third achieve remission[94]. Therefore, paediatric rheumatologists should consider LACC1 deficiency in early-onset, refractory disease, particularly in individuals from consanguineous families. One reported case involved a patient who developed acute lymphocytic leukaemia and experienced flares of arthritis during chemotherapy. Notably, following HSCT, the patient achieved complete remission of JIA, further supporting the pathophysiological role of macrophage-mediated inflammation in the pathogenesis of LACC1-associated disease[90].

Alkaptonuria

Alkaptonuria is an autosomal-recessive disease caused by deficiency of homogentisate-1,2-dioxygenase, encoded by *HGD*[95]. This enzyme catalyses the cleavage of the aromatic ring of homogentisic acid, an intermediate in the catabolic pathway of phenylalanine and tyrosine[95]. Alkaptonuria holds the historical distinction of being the first human disease described according to Mendelian inheritance, and served as the foundational model for the concept of inborn errors of metabolism[96].

In alkaptonuria, persistently high levels of homogentisic acid are maintained in the blood and extracellular spaces despite effective excretion into the urine. Metabolites of homogentisic acid produce a dark ochronotic pigment that is deposited in connective tissues. Although the precise immunopathogenic mechanisms remain obscure, one body of evidence suggests that oxidation of homogentisic acid produces free radicals that lead to lipid peroxidation and chronic inflammation[97–99]. Supporting this hypothesis, in a large study evaluating serum biomarkers in alkaptonuria, serum amyloid A and chitotriosidase were considerably increased compared with healthy individuals[99]. Although overall markers of oxidative stress did not notably differ between groups, oxidative stress levels correlated positively with severity of disease[99].

In his seminal work *Inborn Errors of Metabolism*, the father of inborn errors of metabolism, Archibald Garrod, remarks that "in early life [alkaptonuria] is a trifling matter, inconvenient rather than harmful… an infant stains its clothing or the urine has an unusual appearance"[100]. Indeed, although dark urine and sebum (particularly earwax) might be clinically apparent in infancy, the classic triad of dark urine, darkened connective tissue, including the sclerae and auricle (ochronosis), and arthritis does not fully manifest until the fourth or fifth decade. Importantly, freshly voided urine appears normal and only darkens to dark brown over several hours as homogentisic acid undergoes oxidation upon exposure to air[101]. Therefore, in the modern era of flush toilets and disposable nappies, this pathognomonic finding might go unnoticed. The arthritis of alkaptonuria is clinically similar to ankylosing spondylitis, with back pain that typically begins in the lumbar and thoracic spine followed by the cervical spine[102].

Arthropathy of the knee, hip and shoulder is common. Radiographic findings include intervertebral disc space narrowing, calcification and fusion[102]. Valvular complications, particularly aortic stenosis, are common[102–104]. Although severe manifestations do not typically manifest until adulthood, in a prospective cohort study of 13 children, 6 complained of joint pains at least weekly, despite the absence of degenerative changes on knee MRI[105,106].

Diagnostic confirmation of alkaptonuria relies on biochemical and molecular analyses. Alkalinization of the urine results in immediate brown discoloration owing to rapid oxidation of homogentisic acid. Quantitative detection of homogentisic acid can be performed through gas chromatography–mass spectrometry-based analysis of urinary organic acids[16]. Molecular confirmation is achieved through sequencing of *HGD*. In terms of therapy, nitisinone, an inhibitor of p-hydroxyphenylpyruvate dioxygenase (the enzyme that catalyses the formation of homogentisic acid), can slow the development of ochronosis and progression of disease[17,107]. However, complications of this therapy include tyrosinaemia, which can lead to keratopathy[17]. This adverse effect is typically managed with a protein-restricted diet[17]. Despite evidence supporting the role of oxidative stress in the pathophysiology of alkaptonuria, little is known about the clinical utility of antioxidant therapy in addition to traditional treatment approaches. In a single case report, a patient treated with only a low protein diet and ascorbic acid achieved complete clinical and radiographic resolution of disease, but further studies are necessary to confirm this finding[108]. Given the challenges of maintaining a low protein diet and potential for possible side effects with nitisinone, especially in the absence of adherence to this diet, investigations of alternative treatment options are warranted.

Disorders of purine metabolism

Uric acid is the end-product of purine degradation in humans (Supplementary Fig. 2). Purine metabolism also includes two other pathways: the de novo synthesis pathway, which relies on the activity of phosphoribosylpyrophosphate synthase 1 (PRPS1), and the purine salvage pathway, in which hypoxanthine-guanine phosphoribosyltransferase (HGprt) catalyses the reutilization of purine bases. Hyperuricaemia and its sequelae, including gouty arthritis, are commonly encountered in adults and often attributed to reduced renal urate clearance in the context of a purine-rich diet, compounded by other co-morbidities[109]. By contrast, the presentation of gout in childhood is rare and should prompt investigation for underlying disorders of purine metabolism.

In PRPS1 superactivity, excessive purine production arises from gain-of-function variants in *PRPS1* or from increased transcription and production of structurally normal PRPS1 protein through a currently unknown mechanism[110]. By contrast, Lesch–Nyhan disease is caused by pathogenic variants in *HPRT1*, resulting in absent or extremely low activity of HGprt that leads to impaired purine salvage[111]. Instead of being recycled, the purines are shunted to the degradation pathway and oxidized to uric acid. Additionally, decreased activity of HGprt increases the availability of substrates for de novo purine synthesis[112]. As *HPRT1* is on the X chromosome, male individuals are almost exclusively affected. *PRPS1* is similarly X-linked; however, unlike Lesch–Nyhan disease (and many other X-linked conditions), female individuals are commonly affected by PRSP1 superactivity owing to the gain-of-function mechanism.

The classic clinical presentation of Lesch–Nyhan disease includes hyperuricaemia, choreoathetoid cerebral palsy, intellectual disability and severe self-mutilating behaviour[113]. However, clinical variation exists. In some patients with attenuated disease, hyperuricaemia is the predominant feature and neurocognitive and behavioural manifestations might be absent or elicited only on careful examination[114]; these patients have been described as having HGprt-related hyperuricaemia. Along the spectrum of HGprt-related hyperuricaemia to Lesch–Nyhan disease is a third phenotype designated HGprt-related neurological dysfunction. Individuals with this phenotype exhibit hyperuricaemia alongside overt neurological or behavioural abnormalities, but without the classic self-mutilating behaviours observed in Lesch–Nyhan disease[115,116].

In male patients, PRPS1 superactivity is associated with severe hyperuricaemia and a clinical spectrum of neurodevelopmental phenotypes, including intellectual disability, hypotonia and deafness[110]. A clear genotype–phenotype relationship has been established: severely affected male patients typically harbour pathogenic variants in *PRPS1* that affect allosteric sites, resulting in enzyme gain-of-function through loss of feedback inhibition[110]. By contrast, male patients with mild disease do not exhibit detectable sequence variants or duplications of *PRPS1*, but instead show increased rates of *PRPS1* transcription and elevated levels of the PRPS1 protein[110]. Female patients with PRPS1 superactivity might be affected by either mechanism, and generally present with only hyperuricaemia. One reported case described a 13-year-old girl who presented with polyarthritis initially misdiagnosed as JIA[117].

Elevated levels of uric acid in the blood or urine should raise suspicion of an underlying disorder of purine metabolism. However, normal uric acid levels do not exclude such diagnoses, particularly in children, who physiologically have higher rates of renal clearance of uric acid than adults[118]. In such cases, urine purine analysis using high-performance liquid chromatography coupled with tandem mass spectrometry provides a more sensitive biochemical screen for detecting purine metabolic abnormalities[118].

For HGprt-related hyperuricaemia, molecular diagnosis is typically established through sequence analysis of *HPRT1*. If no pathogenic variants are identified, gene-targeted duplication and deletion analysis should be considered. Measurement of HGprt enzyme activity also serves as a useful clinical diagnostic assay[115]. For PRPS1 superactivity, diagnostic approaches differ by phenotype and sex. In male patients with mild disease, diagnosis relies on assessing PRPS1 enzyme activity, as these individuals generally lack detectable sequence or copy number variants[110,119]. For male patients with severe disease, sequence analysis of *PRPS1* can establish the diagnosis. For female patients, PRPS1 enzyme activity with or without *PRPS1* sequence analysis can establish the diagnosis[110,119]. If initial testing is inconclusive, other rare defects of purine metabolism should be considered. Additionally, inherited renal diseases such as familial juvenile hyperuricaemic nephropathy and primary hyperoxaluria (which can present with oxalate arthropathy mimicking gout) should be included in the differential diagnosis[120]. Glycogen storage disease type I is another important consideration, as this disease has been reported to present with hyperuricaemia and gout in some cases[121].

The xanthine oxidase inhibitor allopurinol is effective in reducing the hyperuricaemia of HGprt deficiency and PRPS1 superactivity, although this inhibitor does not improve neurological outcomes[119,122]. Febuxostat, another xanthine oxidase inhibitor, is considered a second-line therapy for individuals who are intolerant to allopurinol[119,123]. Acute gout flares are generally managed with non-steroidal anti-inflammatory agents, colchicine or glucocorticoids, but the IL-1β inhibitor canakinumab might be used as a second-line agent[124].

Metabolic myopathies

Metabolic myopathies are a group of disorders caused by defects in glycogen utilization, fatty acid oxidation, or mitochondrial respiration that render the cell unable to maintain adequate levels of adenosine triphosphate for contraction and relaxation. These conditions share overlapping features with immune-mediated inflammatory myopathies — including proximal muscle weakness, elevated creatine kinase levels, fatigue and myalgia — and should be considered in the differential diagnosis of individuals with atypical or treatment-refractory idiopathic inflammatory myopathy. In this section, we discuss two common glycogenoses and Danon disease, all of which can closely mimic idiopathic inflammatory myopathy. For a more comprehensive overview — including defects of fatty acid oxidation and mitochondrial myopathies — readers are referred to existing reviews on metabolic myopathies as mimickers of idiopathic inflammatory myopathy[125,126].

Glycogen storage disease type V

At rest, muscle primarily utilizes fatty acid oxidation as a source of acetyl-CoA to feed into the Krebs cycle. However, during periods of intense exercise, anaerobic glycolysis becomes the dominant metabolic pathway, utilizing glucose generated from the breakdown of muscle glycogen within the cytosol[127]. This process requires the action of glycogen phosphorylase. Glycogen storage disease type V (known as McArdle disease) is an autosomal-recessive disorder caused by mutations in *PYGM*, which encodes the muscle-specific isoform of glycogen phosphorylase (myophosphorylase). As hepatic and cardiac isoforms remain unaffected, glycogen storage disease type V typically manifests as a 'pure' skeletal muscle myopathy[128].

The classic presentation of glycogen storage disease type V is intolerance to activities involving isometric muscle contraction, such as weightlifting, or high-intensity dynamic exercises, such as sprinting[129]. Patients might present with episodes of severe muscle contractures, rhabdomyolysis and myoglobinuria with acute renal failure secondary to pigment nephropathy. A 'second wind' phenomenon is described by most patients wherein individuals experience a sudden improvement in exercise capacity about 10 min into activity, attributed to enhanced utilization of circulating blood glucose[130]. Data from a large European cohort of 282 individuals with glycogen storage disease type V provide insights into disease phenotypes[131]. Fixed weakness was observed in 51.4% of patients, primarily affecting the upper limbs and trunk, and 82% of patients reported the 'second wind' phenomenon. Baseline creatine kinase levels were elevated in most patients, although 6.8% of patients had values within the normal range. Misdiagnosis remains common, with one study reporting a median diagnostic delay of 29 years[5]. Notably, rheumatological conditions were the third most common misdiagnosis, following 'growing pains' and 'laziness'[5].

Molecular testing by sequence analysis of *PYGM* is important for glycogen storage disease type V diagnosis, followed by gene-targeted duplication and deletion analysis if sequence analysis is inconclusive. Historically, physicians have recommended avoidance of all forms of exercise owing to the risk of rhabdomyolysis. However, emerging evidence supports the efficacy of light-intensity aerobic exercise in improving aerobic capacity, decreasing creatine kinase levels, and improving clinical symptoms in individuals with glycogen storage disease type V[132]. Therefore, a carbohydrate-rich drink prior to exercise and a professionally supervised exercise programme with gradual progression of intensity is the current standard[133,134].

Glycogen storage disease type II

Although cytosolic glycogen might be degraded to meet cellular energy demands, glycogen is also degraded within lysosomes. Lysosomal degradation is an important part of the physiological turnover of cellular components critical to the homeostasis of terminally differentiated cells, such as myocytes. Glycogen storage disease type II (known as Pompe disease) is an autosomal-recessive disorder caused by deficiency of α-glucosidase (acid maltase), encoded by *GAA*. This enzyme is responsible for the complete hydrolysis of glycogen within lysosomes. In the absence of α-glucosidase, glycogen accumulates within lysosomes, making glycogen storage disease type II a lysosomal storage disorder too. Excessive glycogen accumulation leads to lysosomal rupture and the eventual replacement of the muscle fibre contractile elements with non-functional glycogen deposits. In addition to this mechanical model of disease pathogenesis, accumulating evidence points to global perturbations in vesicle trafficking and intracellular signalling as key contributors to disease pathogenesis[135,136].

Glycogen storage disease type II presents across a clinical spectrum, ranging from the classic infantile form to late-onset forms. The classic infantile form typically presents within the first few months of life with global hypotonia and hypertrophic cardiomyopathy, followed by death by 1 year owing to cardiopulmonary insufficiency if untreated[137]. By contrast, late-onset Pompe disease typically presents with fatigue and creatine kinase elevation, and a slowly progressive lower-limb girdle, axial and diaphragmatic muscle weakness that leads to restrictive lung disease. A history of delayed motor development is often reported[138,139]. Axial muscle weakness, in particular, is a hallmark feature that might be overlooked; in one cohort of 24 patients, nearly all participants reported an inability to perform sit-ups during their early school years[140]. Cardiac manifestations are less common but, when present, might manifest as left ventricular hypertrophy, aortopathy and/or as specific arrhythmias including Wolf–Parkinson–White syndrome[141,142]. Clinicians have identified disease in some children before symptoms appear, based solely on creatine kinase levels; in one study, 10 out of 31 children with late-onset disease were diagnosed in this way[143]. Diagnostic delay is common, with a median of 5–12 years from the onset of symptoms[6,140]. Common misdiagnoses include polymyositis and ankylosing spondylitis, as well as fibromyalgia[6–8,79].

Clinicians can screen symptomatic individuals for glycogen storage disease type II by measuring α-glucosidase activity using a dried-blood spot assay[144,145]. This method has enabled the inclusion of glycogen storage disease type II in the newborn screening programmes across most US states and several other countries[146]. Molecular testing is used to confirm a diagnosis. In 2010, the enzyme replacement therapy alglucosidase alfa was approved for use in late-onset Pompe disease following the results of a randomized controlled trial that demonstrated improvement in 6-min walk tests and stabilization of pulmonary function in treated patients[147,148]. In 2021, a second-generation enzyme replacement therapy, avalglucosidase alfa-ngpt, was approved for the treatment of late-onset Pompe disease. The COMET trial showed that avalglucosidase alfa-ngpt provided superior outcomes compared with alglucosidase alfa, including greater improvement in pulmonary function and enhanced performance in the 6-min walk test[149].

Danon disease

Danon disease is an X-linked dominant condition caused by deficiency of the lysosomal-associated membrane 2 (LAMP2) protein, encoded by *LAMP2*. LAMP2 is expressed within the lysosomal membranes of cardiac, muscle and nerve cells and is required for the maturation of

autophagosomes by fusion with lysosomes[150]. Although the precise pathomechanism remains incompletely elucidated, deficiency of LAMP2 leads to the accumulation of autophagic vacuoles, myofibrillar disarray and fibrosis[151].

The classic triad of findings in affected male patients includes severe cardiomyopathy, skeletal myopathy and mild intellectual disability. Skeletal myopathy is present in 76% of male patients, with a median age at onset of 13 years, and causes impaired ambulation in 30% of patients[152]. Proximal myopathy is most common (46% of male patients), although distal and generalized myopathy have also been reported[152]. Serum creatine kinase levels are frequently elevated, with a median of 867.6 U/l (normal range: 22–198 U/l)[152]. Skeletal myopathy seems to precede the development of hypertrophic cardiomyopathy, which has a median age at onset of 14 years. Structural and electrical cardiac pathology is ultimately the primary cause of morbidity and mortality in Danon disease, with most male patients progressing to end-stage cardiomyopathy by 20 years of age[152]. Female patients with *LAMP2* variants are less likely to present with skeletal myopathy (affecting only 13% of female patients), with a median age at onset of 23 years, and impaired ambulation in only 2% of patients[152]. However, approximately 73% of female patients develop cardiomyopathy, albeit with slower progression than in male patients.

Diagnosis requires molecular testing via sequence analysis of *LAMP2*, followed by gene-targeted duplication and deletion analysis if initial results are inconclusive[153]. Currently, no disease-specific therapies are available for Danon disease. However, one phase I study of RP-A501, a recombinant adeno-associated virus serotype 9-based gene therapy, showed promising improvements in cardiac biomarkers, cardiac imaging findings and clinician-reported and patient-reported outcomes[154].

Inborn errors of metabolism with autoinflammatory or autoimmune manifestations

Several inborn errors of metabolism have manifestations that overlap with autoinflammatory or autoimmune rheumatological conditions. These inborn errors of metabolism with systemic symptoms highlight the diverse mechanisms by which metabolic alterations — including defects of amino acid transport, oligosaccharide processing and complex lipid and cholesterol metabolism — can drive immune dysregulation.

Lysinuric protein intolerance

Lysinuric protein intolerance is an autosomal-recessive aminoaciduria caused by pathogenic variants in *SLC7A7*, which encodes y^+LAT1, one component of a transporter complex that facilitates efflux of the dibasic amino acids arginine, lysine and ornithine[155]. In polarized intestinal and renal tubular epithelia, the y^+LAT1-containing transporter is expressed on the basolateral membrane and is required for absorption of dibasic amino acids. Impaired absorption leads to depletion of the key urea cycle intermediates arginine and ornithine, resulting in a secondary urea cycle defect. y^+LAT1 is also expressed in monocytes and macrophages, but the mechanisms underlying immune dysregulation in lysinuric protein intolerance remain incompletely understood. One proposed mechanism suggests that impaired efflux of arginine increases intracellular arginine availability, promoting nitric oxide production via inducible nitric oxide synthase[156]. However, further studies have demonstrated that *SLC7A7* downregulation induces the expression of inflammatory mediators independent of intracellular arginine availability[157]. Investigations using a murine model of atherosclerosis have also revealed a critical role for y^+LAT1 in promoting macrophage restorative functions by facilitating glutamine influx and feeding the glutaminolysis needed to sustain flux through the Krebs cycle[158].

Lysinuric protein intolerance is a multisystem disorder with heterogeneous clinical manifestations. Failure to thrive is the most common presenting symptom (52% of cases), followed by non-specific gastrointestinal symptoms including emesis (30%) and diarrhoea (14%), which typically emerge after weaning from breast milk[159]. Patients might feel ill after consuming protein-rich meals and develop dietary aversions (36%)[159]. These symptoms are probably driven by post-prandial hyperammonaemia resulting from a secondary urea cycle defect. Rheumatological complications of lysinuric protein intolerance portend a poorer prognosis and include SLE-like disease, haemophagocytic lymphohistiocytosis and early and persistent pulmonary alveolar proteinosis[159].

The biochemical hallmark of lysinuric protein intolerance is low-to-normal plasma levels of arginine, ornithine and lysine, alongside elevated urinary excretion of these amino acids[160]. Cysteine levels typically remain unaffected. Molecular confirmation involves sequencing and deletion and duplication analysis of *SLC7A7*. Therapeutic management focuses on preventing hyperammonaemia and addressing nutritional deficiencies, similar to strategies used in primary urea cycle disorders. Treatment includes supplementation with the urea cycle intermediate citrulline, as well as nitrogen-scavenging agents such as glycerol phenylbutyrate, sodium phenylbutyrate and sodium benzoate[160]. These strategies alone, however, do not correct the chronic lysine deficiency, which might be a driver of growth failure and bone disease in lysinuric protein intolerance[161]. Low-dose lysine supplementation has been shown to improve plasma lysine levels, although gastrointestinal intolerance can limit its use[162,163]. Thus, further studies are needed to understand the long-term benefits of lysine administration[162]. Management of inflammatory complications is specific to individual clinical manifestations. In one reported case, HSCT successfully reversed the progression of disease in a patient with SLE-like disease, pulmonary alveolar proteinosis and haemophagocytic lymphohistiocytosis[164].

Mevalonate kinase deficiency

Mevalonate kinase deficiency is an autosomal-recessive recurrent fever syndrome that exemplifies the direct impact of a single metabolic pathway on immune function. This disorder highlights the role of the bioactive cholesterol intermediates, isoprenoids, in the regulation of the innate immune system. Physiologically, isoprenoids are generated during cholesterol biosynthesis, a pathway that begins with the synthesis of mevalonate. Mevalonate is then phosphorylated in two subsequent steps, by mevalonate kinase and phosphomevalonate kinase, to produce mevalonate pyrophosphate. This intermediate is then further modified to become the so-called activated isoprene units[165], which serve as building blocks for larger isoprenoid compounds.

Prenylation refers to a post-translational modification in which isoprenoids are covalently attached to proteins. Rho GTPases that function as inflammatory signalling components require prenylation with geranylgeranyl pyrophosphate for proper association with regulatory elements. In mevalonate kinase deficiency, reduced synthesis of geranylgeranyl pyrophosphate disrupts this processing, leading to ectopic activation of Rho GTPases. This aberrant signalling initiates a cascade that results in the formation of the pyrin inflammasome and the release of pro-inflammatory IL-1β, explaining the inflammatory phenotype of mevalonate kinase deficiency[165]. The episodic nature of inflammatory attacks in mevalonate kinase deficiency might be partially attributed to the temperature sensitivity of mevalonate kinase. In vitro studies have

shown that enzyme activity decreases 2-fold to 8-fold in cultured cells exposed to elevated temperatures[166]. Events such as minor infections, vaccinations or vigorous exercise, which mildly raise body temperature, are frequently associated with triggering attacks[166].

Mevalonate kinase deficiency encompasses two distinct phenotypes: hyperimmunoglobulin D syndrome and mevalonic aciduria, caused by partial and complete deficiency of mevalonate kinase, respectively. The information presented in this Review primarily pertains to hyperimmunoglobulin D syndrome as mevalonic aciduria is associated with severe, early-onset neurological presentations. Episodes of high, sterile fevers, often >40°C, are the most common presenting symptom in hyperimmunoglobulin D syndrome, typically commencing within the first year of life with flares lasting approximately 3–7 days[167,168]. Fevers might occur spontaneously or might be precipitated by vaccination (which often triggers the first attack), routine childhood infections, exercise or emotional stress[167,168]. Febrile episodes are irregular and might occur at intervals of 2–8 weeks. Febrile attacks are often accompanied by painful cervical lymphadenopathy, severe abdominal pain (sometimes mimicking an acute abdomen) and inflammatory arthritis of the large peripheral joints. Mucocutaneous manifestations are variable and include maculopapular rashes, erythema nodosum, and oral and genital aphthous ulcers[167,169]. Inflammatory biomarkers, including erythrocyte sedimentation rate, C-reactive protein and white blood cell count, are highly elevated during attacks. Interestingly, the frequency of febrile attacks typically decreases with age, although complete remission is not observed. Diagnostic delay is common, with an average lag of 7 years[168], and this disorder can be misdiagnosed as systemic-onset JIA, Behcet disease, periodic fever, aphthous stomatitis, pharyngitis, adenitis (PFAPA) syndrome, familial Mediterranean fever or recurrent viral illnesses[168].

Although elevated levels of circulating IgD antibodies were reported in the original Dutch cohort of individuals with hyperimmunoglobulin D syndrome, leading to the name hyper IgD syndrome, this marker has limited diagnostic value and is no longer recommended for clinical evaluation or disease monitoring[170,171]. By contrast, elevated urinary mevalonate levels during disease flares offer greater specificity, although definitive diagnosis relies on molecular confirmation through *MVK* sequencing and mevalonate kinase assays[172]. Importantly, biallelic variants in *PMVK*, encoding the kinase immediately distal to mevalonate kinase in the isoprene biosynthesis pathway, have been reported to cause a mevalonate kinase deficiency-like phenotype. Phosphomevalonate kinase deficiency should be considered in individuals with clinical features suggestive of mevalonate kinase deficiency but lacking pathogenic variants in *MVK*[173,174].

The IL-1 inhibitor canakinumab is approved to treat mevalonate kinase deficiency. In the CLUSTER trial, 35% of patients met the primary end point of resolution of baseline flare within 15 days of treatment, with no new flares for 16 weeks[175]. On-demand use of anakinra, another IL-1 inhibitor, has also been shown to reduce the severity and duration of febrile attacks[176]. Beyond IL-1 inhibition, expert opinion from the 2021 European Alliance of Associations for Rheumatology–American College of Rheumatology consensus guidelines suggest that glucocorticoids and anti-TNF agents might also be helpful[171].

α-Mannosidosis

α-Mannosidosis is an autosomal-recessive lysosomal storage disorder that results from deficient activity of lysosomal α-mannosidase encoded by *MAN2B1*. This enzyme is needed for the cleavage of mannose residues present in N-linked glycoproteins. α-Mannosidase deficiency results in the intra-lysosomal accumulation of unbranched oligosaccharides[177,178]. Although immune dysfunction is a recognized feature, the specific underlying inflammatory mechanisms remain poorly defined.

α-Mannosidosis is a multi-system, highly clinically heterogeneous disease. The characteristic features of α-mannosidosis include intellectual disability, recurrent infections, hearing loss and facial and skeletal abnormalities, as well as hypotonia and cerebellar ataxia[179–181]. Early psychomotor development is typically normal. Facial coarsening is progressive, with the gradual development of a prominent forehead, rounded eyebrows, flattened nasal bridge and macroglossia reminiscent of the mucopolysaccharidoses. Skeletal abnormalities include dysostosis multiplex (Fig. 2), scoliosis, chest-wall deformities and severe coxarthrosis. One patient seen at our centre developed severe erosive knee arthropathy (Fig. 3). Immune deficiency is common, with many patients demonstrating poor humoral immune responses and often experiencing recurrent infections, especially during the first decade of life[179,180]. Autoimmune manifestations have also been documented, including SLE, Sjögren syndrome, pancytopenia, hypothyroidism and primary biliary cirrhosis[180–183].

Biochemical and molecular testing should be pursued simultaneously. Mannose-rich oligosaccharides can be detected in urine using thin-layer liquid chromatography or high-performance liquid chromatography. The most efficient and reliable method for establishing a diagnosis is the measurement of acidic α-mannosidase activity in leukocytes[179]. Molecular testing should begin with targeted sequencing analysis of *MAN2B1*, followed by gene-targeted duplication and deletion analysis, if initial results are inconclusive[184].

In 2018, velmanase alfa was approved as the first enzyme replacement therapy for the treatment of the non-central nervous system manifestations of α-mannosidosis. This drug has been shown to reduce serum oligosaccharide levels, improve functional capacity and increase serum immunoglobulin levels[185]. HSCT has been reported anecdotally throughout the literature, with the largest case series involving 17 patients[186]. In this retrospective analysis, most patients experienced developmental improvement following transplantation, as well as improvement in auditory function and skeletal disease in some patients[186].

Prolidase deficiency

Prolidase deficiency is an autosomal-recessive disorder caused by pathogenic variants in *PEPD*, encoding the enzyme prolidase. Prolidase is a member of the peptidase family and forms a homodimer that hydrolyses dipeptides or tripeptides with a C-terminal proline or hydroxyproline residue[187]. Prolidase has an important role in the recycling of proline and is suspected to be the rate-limiting step in the production of collagen[188]. The accumulation of proline or hydroxyproline dipeptides might lead to cell death, causing inflammation and skin problems.

Prolidase deficiency has a range of phenotypic manifestations including intellectual disability, recurrent infections, autoimmunity, dysmorphic features, skin lesions (including severe and chronic painful skin ulcers of the lower extremities and telangiectasias on the hands and the face), splenomegaly, elevated liver enzymes and skeletal anomalies[187]. This disorder is a recognized mimic of SLE, predominantly presenting with cutaneous features and systemic autoimmunity.

Laboratory findings often include thrombocytopenia, hypocomplementaemia and hypergammaglobulinaemia[189]. Biochemical findings include increased levels of proline metabolites in both serum and urine. The 'hallmark' feature is massive imidopeptiduria, characterized by the presence of dipeptides containing proline and hydroxyproline in

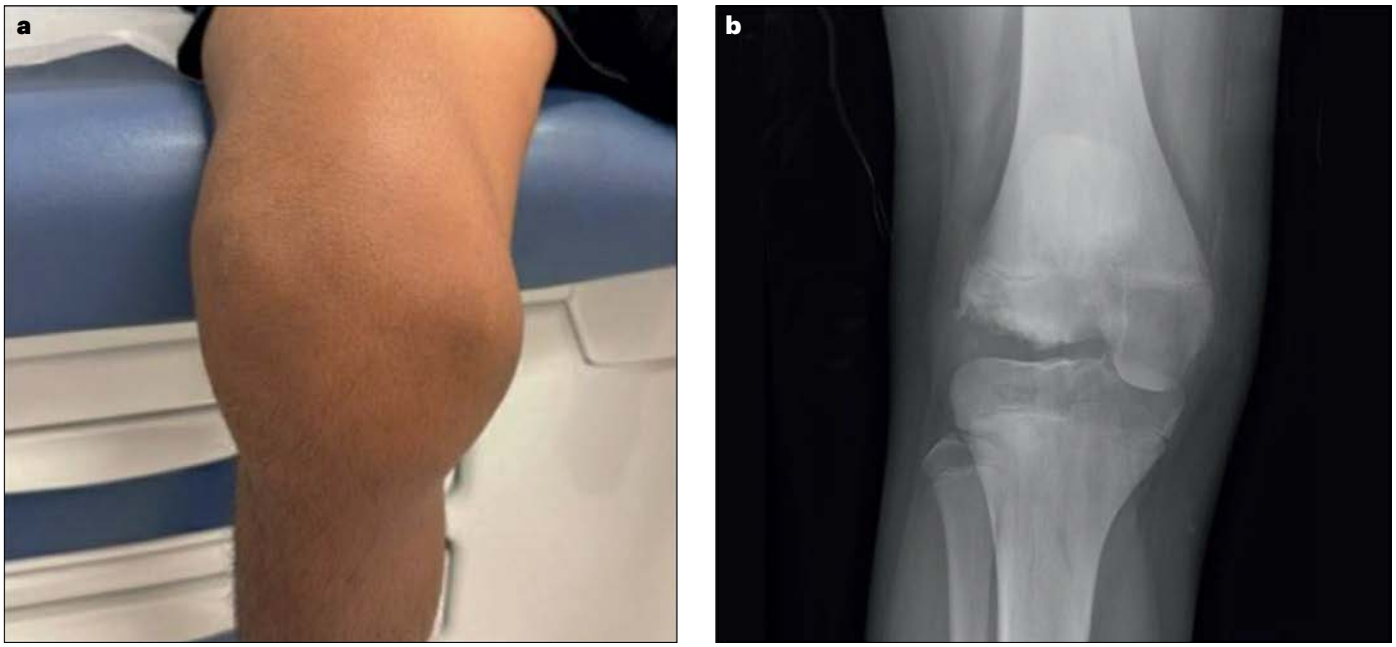

Fig. 3 | Knee arthrosis in a paediatric patient with α-mannosidosis. a,**b**, Clinical and radiographic findings in a 17-year-old male patient with α-mannosidosis. Panel **a** shows the external appearance of the affected knee. Panel **b** shows near-complete destruction of the right lateral femoral condyle on radiographic imaging. Interestingly, microscopic examination of the synovium obtained during subsequent surgery did not reveal notable inflammatory cell infiltration.

the urine. Importantly, the clinical laboratory should be informed when prolidase deficiency is suspected as specialized analytical techniques might be needed for the detection of urine imidodipeptides. Although no standardized diagnostic criteria or testing algorithms currently exist for this condition, definitive diagnosis can be established by identifying biallelic pathogenic variants in *PEPD* through molecular genetic testing[190].

No disease-specific treatment is currently available for prolidase deficiency. Therapies depend on the clinical manifestations but might include a combination of intravenous immunoglobulin, low-molecular-weight heparin, vitamin C, topical proline and topical tacrolimus[187].

Acid sphingomyelinase deficiency type B

Acid sphingomyelinase deficiency type B (ASMD type B; previously known as Niemann–Pick Type B) is a lysosomal storage disorder caused by biallelic pathogenic variants in *SMPD1*, encoding sphingomyelin phosphodiesterase 1 (SMPD1). These variants result in reduced SMPD1 activity, resulting in a milder phenotype than ASMD type A, where enzyme activity is completely abolished[191,192]. In lysosomes, SMPD1 hydrolyses sphingomyelin into ceramide and phosphocholine[192]. Reduced SMPD1 activity results in sphingomyelin accumulation in the lysosomes of macrophages, hepatocytes and vascular endothelial cells[192], forming lipid-laden foam cells that affect organs of the reticuloendothelial system[192]. In *Smpd1*-knockout mice, elevated levels of MIP-1α and MIP-2 in bronchoalveolar fluid, along with increased neutrophil infiltration in the lungs, suggest the role of pulmonary inflammation in disease pathogenesis[193].

Most individuals with ASMD type B develop hepatosplenomegaly in early childhood, although some patients receive a diagnosis in adulthood[194,195]. Other presenting features include thrombocytopenia secondary to hypersplenism[194,195], pulmonary complications due to the onset of interstitial lung disease[194,195], hyperlipidaemia, growth restriction and osteopenia[194,195]. Patients might have ocular abnormalities including macular halos and cherry-red macula[194,195]. In contrast to ASMD type A, ASMD type B is defined by little to no neurological involvement, although a few individuals might experience peripheral neuropathy, ataxia and intellectual disability[196,197]. Common misdiagnoses of ASMD type B include ASMD type C, haematological malignancy and Gaucher disease[198].

Clinicians should confirm a suspected diagnosis of ASMD type B by measuring acid sphingomyelinase activity in leukocytes or fibroblasts[197]. If enzyme activity is reduced, sequencing of *SMPD1* can validate the biochemical findings and identify pathogenic variants[197]. In terms of therapy, the enzyme replacement therapy olipudase alfa provides an exogenous source of acid sphingomyelinase, and is available for non-central nervous system complications owing to its inability to cross the blood–brain barrier[199]. In the ASCEND clinical trial, adults with ASMD type B treated with olipudase alfa for 2 years showed improvements in pulmonary function — as measured by percentage predicted diffusing capacity for carbon monoxide — as well as reductions in hepatosplenomegaly and lipid parameters compared with placebo treatment[200,201]. In the ASCEND-Peds clinical trial, children with ASMD type B also showed clinical improvement[199,202]. HSCT has also been shown to correct non-central nervous system complications, but given the associated morbidity and mortality risks with this approach, olipudase alfa is typically the preferred therapeutic approach[197].

Outlook

Genomic technologies are increasingly utilized in paediatric rheumatology, primarily in the setting of undiagnosed autoinflammatory disease and early onset SLE, where exome and genome sequencing have

demonstrated increasing diagnostic utility[159,203–209]. By contrast, genetic testing is less frequently used in the diagnosis of JIA, which remains a clinical diagnosis with few monogenic aetiologies. However, given the subtle presentations of the inborn errors of metabolism described herein, and the difficulty of clinical diagnosis, we propose that exome or genome sequencing should be considered a critical step in the evaluation of atypical or treatment-refractory JIA and perhaps in other similar early-onset and/or atypical rheumatological presentations, especially when single gene testing and/or gene panel testing have failed to yield a diagnosis. Exome and genome sequencing have the benefit of trio analysis, which can assist with phasing of variants and identification of de novo variation. Moreover, curated gene panels might become quickly outdated as new genetic causes are described, whereas exome and genome sequencing data remain available for re-analysis over time.

Biochemical testing remains a critical adjunct to genetic testing, especially in the context of variants of uncertain significance, when molecular testing is unavailable, or in the setting of non-diagnostic genetic testing results despite high clinical suspicion. Ultimately, confirming a diagnosis of an inborn error of metabolism is necessary not just for guiding management, but also for facilitating genetic counselling and testing of at-risk relatives. However, substantial disparities exist worldwide in the diagnosis of inborn errors of metabolism. In resource-limited settings, access to diagnostic testing might only be available through international collaboration with specialized research laboratories. Likewise, there is similar disparity in the availability of therapies for inborn errors of metabolism. The overwhelming majority of investigational or approved therapies are available only in high-resource regions such as Europe, North America, Israel, Japan and Australia. Thus, access to disease-modifying therapies in resource-limited settings might rely on charitable expanded access programmes where available[210,211].

Conclusion

This Review is aimed at encouraging clinicians and researchers to consider inborn errors of metabolism in the differential diagnosis of atypical or treatment-refractory presentations of rheumatological disease. Each disorder discussed could conceivably present initially to a rheumatology clinic. Although the title refers to these inborn errors of metabolism as 'masqueraders' of rheumatological disease, this framing — although useful diagnostically — oversimplifies their mechanistic complexity. These disorders highlight how a broad repertoire of metabolites can directly influence immune-cell regulation. Immunometabolism has been historically viewed through the lens of the major pathways of intermediary metabolism. These pathways include bioenergetic shifts from oxidative phosphorylation to anaerobic glycolysis (known as the Warburg effect) as well as the fragmentation of the Krebs cycle and subsequent diversion of its intermediates both for the biosynthesis of inflammatory mediators and for the regulation of inflammatory gene expression[212–216]. However, the disorders reviewed here show that immune-cell function depends on a much wider array of metabolic processes[15].

Published online: 25 February 2026

References

1. Morava, E. et al. Quo vadis: the re-definition of "inborn metabolic diseases". *J. Inherit. Metab. Dis.* **38**, 1003–1006 (2015).
2. Waters, D. et al. Global birth prevalence and mortality from inborn errors of metabolism: a systematic analysis of the evidence. *J. Glob. Health* **8**, 021102 (2018).
3. Kasapkara, C. S., Akcaboy, M., Kara Eroglu, F. & Derinkuyu, B. E. Mucolipidosis type III: a rare disease in differential diagnosis of joint stiffness in pediatric rheumatology. *Arch. Rheumatol.* **33**, 93–98 (2018).
4. Brik, R. et al. Mucolipidosis III presenting as a rheumatological disorder. *J. Rheumatol.* **20**, 133–136 (1993).
5. Scalco, R. S. et al. Misdiagnosis is an important factor for diagnostic delay in McArdle disease. *Neuromuscul. Disord.* **27**, 852–855 (2017).
6. Lagler, F. B. et al. Extent, impact, and predictors of diagnostic delay in Pompe disease: a combined survey approach to unveil the diagnostic odyssey. *JIMD Rep.* **49**, 89–95 (2019).
7. Marotto, D. et al. Late-onset Pompe disease with normal creatine kinase levels: the importance of rheumatological suspicion. *Int. J. Mol. Sci.* **24**, 15924 (2023).
8. Yuce Inel, T., Koken Avsar, A., Teke Kisa, P., Ozer, E. & Sari, I. A challenging etiology of myopathy: the late-onset Pompe disease. *Eur. J. Rheumatol.* **10**, 26–28 (2023).
9. Loret, A. et al. Joint manifestations revealing inborn metabolic diseases in adults: a narrative review. *Orphanet J. Rare Dis.* **18**, 239 (2023).
10. Cimaz, R. et al. Joint contractures in the absence of inflammation may indicate mucopolysaccharidosis. *Pediatr. Rheumatol. Online J.* **7**, 18 (2009).
11. Cimaz, R. et al. Awareness of Fabry disease among rheumatologists — current status and perspectives. *Clin. Rheumatol.* **30**, 467–475 (2011).
12. Fabie, N. A. V., Pappas, K. B. & Feldman, G. L. The current state of newborn screening in the United States. *Pediatr. Clin. North. Am.* **66**, 369–386 (2019).
13. Ferreira, C. R., Rahman, S., Keller, M., Zschocke, J. & Group, I. A. An international classification of inherited metabolic disorders (ICIMD). *J. Inherit. Metab. Dis.* **44**, 164–177 (2021).
14. Gul, A. et al. The pathogenesis, clinical presentations and treatment of monogenic systemic vasculitis. *Nat. Rev. Rheumatol.* **21**, 414–425 (2025).
15. Ryan, D. G. & O'Neill, L. A. J. Krebs cycle reborn in macrophage immunometabolism. *Annu. Rev. Immunol.* **38**, 289–313 (2020).
16. Scott, D., Clinton Frazee, C. 3rd & Garg, U. Screening of organic acidurias by gas chromatography-mass spectrometry (GC-MS). *Methods Mol. Biol.* **2546**, 321–333 (2022).
17. Ranganath, L. R. et al. Nitisinone arrests ochronosis and decreases rate of progression of alkaptonuria: evaluation of the effect of nitisinone in the United Kingdom national alkaptonuria centre. *Mol. Genet. Metab.* **125**, 127–134 (2018).
18. Koch, J. et al. Molecular cloning and characterization of a full-length complementary DNA encoding human acid ceramidase. Identification Of the first molecular lesion causing Farber disease. *J. Biol. Chem.* **271**, 33110–33115 (1996).
19. Zappatini-Tommasi, L., Dumontel, C., Guibaud, P. & Girod, C. Farber disease: an ultrastructural study. Report of a case and review of the literature. *Virchows Arch. A Pathol. Anat. Histopathol.* **420**, 281–290 (1992).
20. Dworski, S. et al. Acid ceramidase deficiency is characterized by a unique plasma cytokine and ceramide profile that is altered by therapy. *Biochim. Biophys. Acta Mol. Basis Dis.* **1863**, 386–394 (2017).
21. Yu, F. P. S., Dworski, S. & Medin, J. A. Deletion of MCP-1 impedes pathogenesis of acid ceramidase deficiency. *Sci. Rep.* **8**, 1808 (2018).
22. Arana, L. et al. Ceramide 1-phosphate induces macrophage chemoattractant protein-1 release: involvement in ceramide 1-phosphate-stimulated cell migration. *Am. J. Physiol. Endocrinol. Metab.* **304**, E1213–E1226 (2013).
23. Zielonka, M., Garbade, S. F., Kolker, S., Hoffmann, G. F. & Ries, M. A cross-sectional quantitative analysis of the natural history of Farber disease: an ultra-orphan condition with rheumatologic and neurological cardinal disease features. *Genet. Med.* **20**, 524–530 (2018).
24. Yu, F. P. S., Amintas, S., Levade, T. & Medin, J. A. Acid ceramidase deficiency: Farber disease and SMA-PME. *Orphanet J. Rare Dis.* **13**, 121 (2018).
25. Kostik, M. M. et al. Farber lipogranulomatosis with predominant joint involvement mimicking juvenile idiopathic arthritis. *J. Inherit. Metab. Dis.* **36**, 1079–1080 (2013).
26. Bonafe, L. et al. Brief report: peripheral osteolysis in adults linked to ASAH1 (Acid Ceramidase) mutations: a new presentation of Farber's disease. *Arthritis Rheumatol.* **68**, 2323–2327 (2016).
27. Solyom, A. et al. Farber disease (acid ceramidase deficiency) epidemiology: literature review and patient cohort data indicate moderate and attenuated phenotypes are likely underrepresented in the medical literature and are underdiagnosed. *Mol. Genet. Metab.* **120**, S124–S125 (2016).
28. Ehlert, K. et al. Allogeneic hematopoietic cell transplantation in Farber disease. *J. Inherit. Metab. Dis.* **42**, 286–294 (2019).
29. Mitchell, J. et al. Farber disease: implications of anti-inflammatory treatment. *Mol. Genet. Metab.* **117**, S82 (2016).
30. Mueller, O. T., Honey, N. K., Little, L. E., Miller, A. L. & Shows, T. B. Mucolipidosis II and III. The genetic relationships between two disorders of lysosomal enzyme biosynthesis. *J. Clin. Invest.* **72**, 1016–1023 (1983).
31. Khan, S. A. & Tomatsu, S. C. Mucolipidoses overview: past, present, and future. *Int. J. Mol. Sci.* **21**, 6812 (2020).
32. Dogterom, E. J. et al. Mucolipidosis type II and type III: a systematic review of 843 published cases. *Genet. Med.* **23**, 2047–2056 (2021).
33. Hetherington, C., Harris, N. J. & Smith, T. W. Orthopaedic management in four cases of mucolipidosis type III. *J. R. Soc. Med.* **92**, 244–246 (1999).
34. Cathey, S. S. et al. Phenotype and genotype in mucolipidoses II and III alpha/beta: a study of 61 probands. *J. Med. Genet.* **47**, 38–48 (2010).
35. David-Vizcarra, G. et al. The natural history and osteodystrophy of mucolipidosis types II and III. *J. Paediatr. Child. Health* **46**, 316–322 (2010).
36. Melhem, R., Dorst, J. P., Scott, C. I. Jr. & McKusick, V. A. Roentgen findings in mucolipidosis III (Pseudo-Hurler polydystrophy). *Radiology* **106**, 153–160 (1973).
37. Raas-Rothschild, A. & Spiegel, R. Mucolipidosis III gamma. In *GeneReviews* (eds Adam, M. P. et al.) (2019).

38. Tuysuz, B. et al. Mucolipidosis type III gamma: three novel mutation and genotype-phenotype study in eleven patients. *Gene* **642**, 398–407 (2018).
39. Robinson, C. et al. The osteodystrophy of mucolipidosis type III and the effects of intravenous pamidronate treatment. *J. Inherit. Metab. Dis.* **25**, 681–693 (2002).
40. Gragnaniello, V. et al. Newborn screening for Fabry disease in northeastern Italy: results of five years of experience. *Biomolecules* **11**, 951 (2021).
41. Burton, B. K. et al. Newborn screening for lysosomal storage disorders in Illinois: the initial 15-month experience. *J. Pediatr.* **190**, 130–135 (2017).
42. Hopkins, P. V. et al. Incidence of 4 lysosomal storage disorders from 4 years of newborn screening. *JAMA Pediatr.* **172**, 696–697 (2018).
43. Kurdi, H., Lavalle, L., Moon, J. C. C. & Hughes, D. Inflammation in Fabry disease: stages, molecular pathways, and therapeutic implications. *Front. Cardiovasc. Med.* **11**, 1420067 (2024).
44. Rozenfeld, P. & Feriozzi, S. Contribution of inflammatory pathways to Fabry disease pathogenesis. *Mol. Genet. Metab.* **122**, 19–27 (2017).
45. De Francesco, P. N., Mucci, J. M., Ceci, R., Fossati, C. A. & Rozenfeld, P. A. Fabry disease peripheral blood immune cells release inflammatory cytokines: role of globotriaosylceramide. *Mol. Genet. Metab.* **109**, 93–99 (2013).
46. DeGraba, T. et al. Profile of endothelial and leukocyte activation in Fabry patients. *Ann. Neurol.* **47**, 229–233 (2000).
47. Hopkin, R. J. et al. Characterization of Fabry disease in 352 pediatric patients in the Fabry registry. *Pediatr. Res.* **64**, 550–555 (2008).
48. Verrecchia, E. et al. The impact of fever/hyperthermia in the diagnosis of Fabry: a retrospective analysis. *Eur. J. Intern. Med.* **32**, 26–30 (2016).
49. Luo, Y., Wu, D. & Shen, M. Recurrent fever of unknown origin: an overlooked symptom of Fabry disease. *Mol. Genet. Genomic Med.* **8**, e1454 (2020).
50. Eng, C. M. et al. Fabry disease: baseline medical characteristics of a cohort of 1765 males and females in the Fabry registry. *J. Inherit. Metab. Dis.* **30**, 184–192 (2007).
51. Gal, A., Hughes, D. A. & Winchester, B. Toward a consensus in the laboratory diagnostics of Fabry disease — recommendations of a European expert group. *J. Inherit. Metab. Dis.* **34**, 509–514 (2011).
52. Germain, D. P. et al. Consensus recommendations for diagnosis, management and treatment of Fabry disease in paediatric patients. *Clin. Genet.* **96**, 107–117 (2019).
53. El Dib, R. et al. Enzyme replacement therapy for Anderson-Fabry disease. *Cochrane Database Syst. Rev.* **7**, CD006663 (2016).
54. El Dib, R. et al. Enzyme replacement therapy for Anderson-Fabry disease: a complementary overview of a Cochrane publication through a linear regression and a pooled analysis of proportions from cohort studies. *PLoS ONE* **12**, e0173358 (2017).
55. Germain, D. P. et al. Treatment of Fabry's disease with the pharmacologic chaperone migalastat. *N. Engl. J. Med.* **375**, 545–555 (2016).
56. Brady, R. O., Kanfer, J. N. & Shapiro, D. Metabolism of glucocerebrosides. ii. evidence of an enzymatic deficiency in Gaucher's Disease. *Biochem. Biophys. Res. Commun.* **18**, 221–225 (1965).
57. Hughes, D. et al. Gaucher disease in bone: from pathophysiology to practice. *J. Bone Min. Res.* **34**, 996–1013 (2019).
58. van Breemen, M. J. et al. Increased plasma macrophage inflammatory protein (MIP)-1α and MIP-1β levels in type 1 Gaucher disease. *Biochim. Biophys. Acta* **1772**, 788–796 (2007).
59. Campeau, P. M. et al. Characterization of Gaucher disease bone marrow mesenchymal stromal cells reveals an altered inflammatory secretome. *Blood* **114**, 3181–3190 (2009).
60. Boven, L. A. et al. Gaucher cells demonstrate a distinct macrophage phenotype and resemble alternatively activated macrophages. *Am. J. Clin. Pathol.* **122**, 359–369 (2004).
61. Hollak, C. E., van Weely, S., van Oers, M. H. & Aerts, J. M. Marked elevation of plasma chitotriosidase activity. A novel hallmark of Gaucher disease. *J. Clin. Invest.* **93**, 1288–1292 (1994).
62. Pandey, M. K. et al. Complement drives glucosylceramide accumulation and tissue inflammation in Gaucher disease. *Nature* **543**, 108–112 (2017).
63. Pandey, M. K., Grabowski, G. A. & Kohl, J. An unexpected player in Gaucher disease: the multiple roles of complement in disease development. *Semin. Immunol.* **37**, 30–42 (2018).
64. Castillon, G., Chang, S. C. & Moride, Y. Global incidence and prevalence of Gaucher disease: a targeted literature review. *J. Clin. Med.* **12**, 85 (2022).
65. Faden, M. A., Krakow, D., Ezgu, F., Rimoin, D. L. & Lachman, R. S. The Erlenmeyer flask bone deformity in the skeletal dysplasias. *Am. J. Med. Genet. A* **149A**, 1334–1345 (2009).
66. Weizman, Z., Tennenbaum, A. & Yatziv, S. Interphalangeal joint involvement in Gaucher's disease, type I, resembling juvenile rheumatoid arthritis. *Arthritis Rheum.* **25**, 706–707 (1982).
67. Weinreb, N. J. et al. Long-term clinical outcomes in type 1 Gaucher disease following 10 years of imiglucerase treatment. *J. Inherit. Metab. Dis.* **36**, 543–553 (2013).
68. Dardis, A. et al. Patient centered guidelines for the laboratory diagnosis of Gaucher disease type 1. *Orphanet J. Rare Dis.* **17**, 442 (2022).
69. Kishnani, P. S. et al. Screening, patient identification, evaluation, and treatment in patients with Gaucher disease: results from a Delphi consensus. *Mol. Genet. Metab.* **135**, 154–162 (2022).
70. Serfecz, J. C. et al. C5a Activates a pro-inflammatory gene expression profile in human Gaucher iPSC-derived macrophages. *Int. J. Mol. Sci.* **22**, 9912 (2021).
71. Beck, M. et al. The natural history of MPS I: global perspectives from the MPS I Registry. *Genet. Med.* **16**, 759–765 (2014).
72. Cimaz, R. et al. Attenuated type I mucopolysaccharidosis in the differential diagnosis of juvenile idiopathic arthritis: a series of 13 patients with Scheie syndrome. *Clin. Exp. Rheumatol.* **24**, 196–202 (2006).
73. Montano, A. M., Tomatsu, S., Gottesman, G. S., Smith, M. & Orii, T. International Morquio A registry: clinical manifestation and natural course of Morquio A disease. *J. Inherit. Metab. Dis.* **30**, 165–174 (2007).
74. Aslam, R., van Bommel, A. C. M., Hendriksz, C. J. & Jester, A. Subjective and objective assessment of hand function in mucopolysaccharidosis IVa patients. *JIMD Rep.* **9**, 59–65 (2013).
75. Yi, M., Shen, P. & Zhang, H. Delayed diagnosis of mild mucopolysaccharidosis type IVA. *BMC Med. Genomics* **17**, 151 (2024).
76. Lamberti, P. M. & Light, T. R. Carpal tunnel syndrome in children. *Hand Clin.* **18**, 331–337 (2002).
77. Giugliani, R., Muschol, N., Keenan, H. A., Dant, M. & Muenzer, J. Improvement in time to treatment, but not time to diagnosis, in patients with mucopolysaccharidosis type I. *Arch. Dis. Child.* **106**, 674–679 (2021).
78. Bruni, S., Lavery, C. & Broomfield, A. The diagnostic journey of patients with mucopolysaccharidosis I: a real-world survey of patient and physician experiences. *Mol. Genet. Metab. Rep.* **8**, 67–73 (2016).
79. Mathis, D. et al. Specific GAG ratios in the diagnosis of mucopolysaccharidoses. *JIMD Rep.* **65**, 116–123 (2024).
80. Strovel, E. T. et al. Measurement of lysosomal enzyme activities: a technical standard of the American College of Medical Genetics and Genomics (ACMG). *Genet. Med.* **24**, 769–783 (2022).
81. Spranger, J. R. W. et al. *Bone Dysplasias: An Atlas of Genetic Disorders of Skeletal Development* 3rd edn (Oxford University Press, 2012).
82. Jameson, E., Jones, S. & Remmington, T. Enzyme replacement therapy with laronidase (Aldurazyme®) for treating mucopolysaccharidosis type I. *Cochrane Database Syst. Rev.* **6**, CD009354 (2019).
83. Wikman-Jorgensen, P. E. et al. Enzyme replacement therapy for the treatment of Hunter disease: a systematic review with narrative synthesis and meta-analysis. *Mol. Genet. Metab.* **131**, 206–210 (2020).
84. Jones, S. A. et al. A phase 1/2 study of intrathecal heparan-N-sulfatase in patients with mucopolysaccharidosis IIIA. *Mol. Genet. Metab.* **118**, 198–205 (2016).
85. Hendriksz, C. J. et al. Efficacy and safety of enzyme replacement therapy with BMN 110 (elosulfase alfa) for Morquio A syndrome (mucopolysaccharidosis IVA): a phase 3 randomised placebo-controlled study. *J. Inherit. Metab. Dis.* **37**, 979–990 (2014).
86. Harmatz, P. et al. Direct comparison of measures of endurance, mobility, and joint function during enzyme-replacement therapy of mucopolysaccharidosis VI (Maroteaux-Lamy syndrome): results after 48 weeks in a phase 2 open-label clinical study of recombinant human N-acetylgalactosamine 4-sulfatase. *Pediatrics* **115**, e681–e689 (2005).
87. Laraway, S., Breen, C., Mercer, J., Jones, S. & Wraith, J. E. Does early use of enzyme replacement therapy alter the natural history of mucopolysaccharidosis I? Experience in three siblings. *Mol. Genet. Metab.* **109**, 315–316 (2013).
88. Chen, H. H. et al. Enzyme replacement therapy for mucopolysaccharidoses; past, present, and future. *J. Hum. Genet.* **64**, 1153–1171 (2019).
89. Wakil, S. M. et al. Association of a mutation in LACC1 with a monogenic form of systemic juvenile idiopathic arthritis. *Arthritis Rheumatol.* **67**, 288–295 (2015).
90. Kallinich, T. et al. Juvenile arthritis caused by a novel FAMIN (LACC1) mutation in two children with systemic and extended oligoarticular course. *Pediatr. Rheumatol. Online J.* **14**, 63 (2016).
91. Omarjee, O. et al. LACC1 deficiency links juvenile arthritis with autophagy and metabolism in macrophages. *J. Exp. Med.* **218**, e20201006 (2021).
92. Li, Y. et al. Crohn's Disease-associated variant in laccase domain containing 1 (LACC1) modulates T cell gene expression, metabolism and T cell function. *Nat. Commun.* **16**, 2577 (2025).
93. Wei, Z., Oh, J., Flavell, R. A. & Crawford, J. M. LACC1 bridges NOS2 and polyamine metabolism in inflammatory macrophages. *Nature* **609**, 348–353 (2022).
94. Wu, Y., Wang, S., Yin, W., Yin, W. & Ding, Y. Clinical characteristics and genotype analysis of a Chinese patient with juvenile arthritis due to novel LACC1 frameshift mutation and literature review. *Mol. Genet. Genomic Med.* **11**, e2175 (2023).
95. Fernandez-Canon, J. M. et al. The molecular basis of alkaptonuria. *Nat. Genet.* **14**, 19–24 (1996).
96. Garrod, A. E. The incidence of alkaptonuria: a study in chemical individuality. 1902. *Mol. Med.* **2**, 274–282 (1996).
97. Braconi, D. et al. Evaluation of anti-oxidant treatments in an in vitro model of alkaptonuric ochronosis. *Rheumatology* **49**, 1975–1983 (2010).
98. Millucci, L. et al. Amyloidosis in alkaptonuria. *J. Inherit. Metab. Dis.* **38**, 797–805 (2015).
99. Braconi, D. et al. Inflammatory and oxidative stress biomarkers in alkaptonuria: data from the DevelopAKUre project. *Osteoarthritis Cartilage* **26**, 1078–1086 (2018).
100. Harris, H. *Garrod's Inborn Errors of Metabolism* (Oxford University Press,1963).
101. Milch, R. A., Titus, E. D. & Loo, T. L. Atmospheric oxidation of homogentisic acid: spectrophotometric studies. *Science* **126**, 209–210 (1957).
102. Mannoni, A. et al. Alkaptonuria, ochronosis, and ochronotic arthropathy. *Semin. Arthritis Rheum.* **33**, 239–248 (2004).
103. Ranganath, L. R. & Cox, T. F. Natural history of alkaptonuria revisited: analyses based on scoring systems. *J. Inherit. Metab. Dis.* **34**, 1141–1151 (2011).
104. Phornphutkul, C. et al. Natural history of alkaptonuria. *N. Engl. J. Med.* **347**, 2111–2121 (2002).

105. Kujawa, M. J. et al. Clinical presentation of 13 children with alkaptonuria. *J. Inherit. Metab. Dis.* **46**, 916–930 (2023).
106. Akbaba, A. I., Ozgul, R. K. & Dursun, A. Presentation of 14 alkaptonuria patients from Turkey. *J. Pediatr. Endocrinol. Metab.* **33**, 289–294 (2020).
107. Mayrink, F. D., Dorneles, G., da Silva, I. M. & Areda, C. A. Efficacy and safety of nitisinone for patients with alkaptonuria: a systematic review with metanalysis. *Mol. Genet. Metab.* **145**, 109099 (2025).
108. Morava, E., Kosztolanyi, G., Engelke, U. F. & Wevers, R. A. Reversal of clinical symptoms and radiographic abnormalities with protein restriction and ascorbic acid in alkaptonuria. *Ann. Clin. Biochem.* **40**, 108–111 (2003).
109. Dehlin, M., Jacobsson, L. & Roddy, E. Global epidemiology of gout: prevalence, incidence, treatment patterns and risk factors. *Nat. Rev. Rheumatol.* **16**, 380–390 (2020).
110. de Brouwer, A. P. et al. PRPS1 mutations: four distinct syndromes and potential treatment. *Am. J. Hum. Genet.* **86**, 506–518 (2010).
111. Nyhan, W. L. The recognition of Lesch-Nyhan syndrome as an inborn error of purine metabolism. *J. Inherit. Metab. Dis.* **20**, 171–178 (1997).
112. Pareek, V., Pedley, A. M. & Benkovic, S. J. Human de novo purine biosynthesis. *Crit. Rev. Biochem. Mol. Biol.* **56**, 1–16 (2021).
113. Lesch, M. & Nyhan, W. L. A familial disorder of uric acid metabolism and central nervous system function. *Am. J. Med.* **36**, 561–570 (1964).
114. Jinnah, H. A. et al. Attenuated variants of Lesch-Nyhan disease. *Brain* **133**, 671–689 (2010).
115. Fu, R., Chen, C. J. & Jinnah, H. A. Genotypic and phenotypic spectrum in attenuated variants of Lesch-Nyhan disease. *Mol. Genet. Metab.* **112**, 280–285 (2014).
116. Madeo, A. et al. Clinical, biochemical and genetic characteristics of a cohort of 101 French and Italian patients with HPRT deficiency. *Mol. Genet. Metab.* **127**, 147–157 (2019).
117. Zikanova, M. et al. Clinical manifestations and molecular aspects of phosphoribosylpyrophosphate synthetase superactivity in females. *Rheumatology* **57**, 1180–1185 (2018).
118. Jurecka, A. & Tylki-Szymanska, A. Inborn errors of purine and pyrimidine metabolism: a guide to diagnosis. *Mol. Genet. Metab.* **136**, 164–176 (2022).
119. de Brouwer, A. P. M. & Christodoulou, J. Phosphoribosylpyrophosphate synthetase superactivity. In *GeneReviews* (eds Adam, M. P. et al.) (2022).
120. Baum, M. A., Mandel, M. & Somers, M. J. G. Understanding rare kidney stone diseases: a review. *Am. J. Kidney Dis.* **86**, 236–244 (2025).
121. Xu, N. et al. Clinical features of gout in adult patients with type Ia glycogen storage disease: a single-centre retrospective study and a review of literature. *Arthritis Res. Ther.* **24**, 58 (2022).
122. Torres, R. J., Prior, C. & Puig, J. G. Efficacy and safety of allopurinol in patients with hypoxanthine-guanine phosphoribosyltransferase deficiency. *Metabolism* **56**, 1179–1186 (2007).
123. Jinnah, H. A. *HPRT1* disorders. In *GeneReviews* (eds Adam, M. P. et al.) (2020).
124. Schlesinger, N. et al. Canakinumab for acute gouty arthritis in patients with limited treatment options: results from two randomised, multicentre, active-controlled, double-blind trials and their initial extensions. *Ann. Rheum. Dis.* **71**, 1839–1848 (2012).
125. Wortmann, R. L. & DiMauro, S. Differentiating idiopathic inflammatory myopathies from metabolic myopathies. *Rheum. Dis. Clin. North. Am.* **28**, 759–778 (2002).
126. Smith, E. C., El-Gharbawy, A. & Koeberl, D. D. Metabolic myopathies: clinical features and diagnostic approach. *Rheum. Dis. Clin. North. Am.* **37**, 201–217 (2011).
127. Jensen, J., Rustad, P. I., Kolnes, A. J. & Lai, Y. C. The role of skeletal muscle glycogen breakdown for regulation of insulin sensitivity by exercise. *Front. Physiol.* **2**, 112 (2011).
128. Santalla, A. et al. Genotypic and phenotypic features of all Spanish patients with McArdle disease: a 2016 update. *BMC Genomics* **18**, 819 (2017).
129. Lucia, A. et al. Clinical practice guidelines for glycogen storage disease V & VII (McArdle disease and Tarui disease) from an international study group. *Neuromuscul. Disord.* **31**, 1296–1310 (2021).
130. Haller, R. G. & Vissing, J. Spontaneous "second wind" and glucose-induced second "second wind" in McArdle disease: oxidative mechanisms. *Arch. Neurol.* **59**, 1395–1402 (2002).
131. Scalco, R. S. et al. Data from the European registry for patients with McArdle disease and other muscle glycogenoses (EUROMAC). *Orphanet J. Rare Dis.* **15**, 330 (2020).
132. Preisler, N., Haller, R. G. & Vissing, J. Exercise in muscle glycogen storage diseases. *J. Inherit. Metab. Dis.* **38**, 551–563 (2015).
133. Lucia, A., Quinlivan, R., Wakelin, A., Martin, M. A. & Andreu, A. L. The 'McArdle paradox': exercise is a good advice for the exercise intolerant. *Br. J. Sports Med.* **47**, 728–729 (2013).
134. Nogales-Gadea, G. et al. Exercise and preexercise nutrition as treatment for McArdle disease. *Med. Sci. Sports Exerc.* **48**, 673–679 (2016).
135. Meena, N. K. & Raben, N. Pompe disease: new developments in an old lysosomal storage disorder. *Biomolecules* **10**, 1339 (2020).
136. Raben, N., Roberts, A. & Plotz, P. H. Role of autophagy in the pathogenesis of Pompe disease. *Acta Myol.* **26**, 45–48 (2007).
137. Kishnani, P. S. et al. A retrospective, multinational, multicenter study on the natural history of infantile-onset Pompe disease. *J. Pediatr.* **148**, 671–676.
138. Ausems, M. G. et al. A diagnostic protocol for adult-onset glycogen storage disease type II. *Neurology* **52**, 851–853 (1999).
139. Lefeuvre, C. et al. Characteristics of patients with late-onset Pompe disease in France: insights from the French Pompe Registry in 2022. *Neurology* **101**, e966–e977 (2023).
140. Yue, D. et al. Diagnostic delay in late-onset Pompe disease among Chinese patients: a retrospective study. *JIMD Rep.* **65**, 39–46 (2024).
141. Dasouki, M. et al. Pompe disease: literature review and case series. *Neurol. Clin.* **32**, 751–776 (2014). ix.
142. Schuller, A., Wenninger, S., Strigl-Pill, N. & Schoser, B. Toward deconstructing the phenotype of late-onset Pompe disease. *Am. J. Med. Genet. C. Semin. Med. Genet.* **160C**, 80–88 (2012).
143. van Capelle, C. I. et al. Childhood Pompe disease: clinical spectrum and genotype in 31 patients. *Orphanet J. Rare Dis.* **11**, 65 (2016).
144. Chamoles, N. A., Niizawa, G., Blanco, M., Gaggioli, D. & Casentini, C. Glycogen storage disease type II: enzymatic screening in dried blood spots on filter paper. *Clin. Chim. Acta* **347**, 97–102 (2004).
145. Dajnoki, A. et al. Newborn screening for Pompe disease by measuring acid α-glucosidase activity using tandem mass spectrometry. *Clin. Chem.* **54**, 1624–1629 (2008).
146. Klug, T. L., Swartz, L. B., Washburn, J., Brannen, C. & Kiesling, J. L. Lessons learned from Pompe disease newborn screening and follow-up. *Int. J. Neonatal Screen.* **6**, 11 (2020).
147. van der Ploeg, A. T. et al. A randomized study of alglucosidase alfa in late-onset Pompe's disease. *N. Engl. J. Med.* **362**, 1396–1406 (2010).
148. Cupler, E. J. et al. Consensus treatment recommendations for late-onset Pompe disease. *Muscle Nerve* **45**, 319–333 (2012).
149. Diaz-Manera, J. et al. Safety and efficacy of avalglucosidase alfa versus alglucosidase alfa in patients with late-onset Pompe disease (COMET): a phase 3, randomised, multicentre trial. *Lancet Neurol.* **20**, 1012–1026 (2021).
150. Tanaka, Y. et al. Accumulation of autophagic vacuoles and cardiomyopathy in LAMP-2-deficient mice. *Nature* **406**, 902–906 (2000).
151. Endo, Y., Furuta, A. & Nishino, I. Danon disease: a phenotypic expression of LAMP-2 deficiency. *Acta Neuropathol.* **129**, 391–398 (2015).
152. Brambatti, M. et al. Danon disease: gender differences in presentation and outcomes. *Int. J. Cardiol.* **286**, 92–98 (2019).
153. Hong, K. N. et al. International consensus on differential diagnosis and management of patients with Danon disease: JACC state-of-the-art review. *J. Am. Coll. Cardiol.* **82**, 1628–1647 (2023).
154. Greenberg, B. et al. Phase 1 study of AAV9.LAMP2B gene therapy in Danon disease. *N. Engl. J. Med.* **392**, 972–983 (2024).
155. Borsani, G. et al. SLC7A7, encoding a putative permease-related protein, is mutated in patients with lysinuric protein intolerance. *Nat. Genet.* **21**, 297–301 (1999).
156. Mannucci, L. et al. Increased NO production in lysinuric protein intolerance. *J. Inherit. Metab. Dis.* **28**, 123–129 (2005).
157. Rotoli, B. M. et al. Downregulation of SLC7A7 triggers an inflammatory phenotype in human macrophages and airway epithelial cells. *Front. Immunol.* **9**, 508 (2018).
158. Benhmammouch, S. et al. Slc7a7 licenses macrophage glutaminolysis for restorative functions in atherosclerosis. *Nat. Metab.* **7**, 1924–1938 (2025).
159. Contreras, J. L. et al. Immune dysregulation mimicking systemic lupus erythematosus in a patient with lysinuric protein intolerance: case report and review of the literature. *Front. Pediatr.* **9**, 673957 (2021).
160. Ogier de Baulny, H., Schiff, M. & Dionisi-Vici, C. Lysinuric protein intolerance (LPI): a multi organ disease by far more complex than a classic urea cycle disorder. *Mol. Genet. Metab.* **106**, 12–17 (2012).
161. Sperandeo, M. P. et al. Slc7a7 disruption causes fetal growth retardation by downregulating Igf1 in the mouse model of lysinuric protein intolerance. *Am. J. Physiol. Cell Physiol* **293**, C191–C198 (2007).
162. Tanner, L. M., Nanto-Salonen, K., Niinikoski, H., Huoponen, K. & Simell, O. Long-term oral lysine supplementation in lysinuric protein intolerance. *Metabolism* **56**, 185–189 (2007).
163. Lukkarinen, M., Nanto-Salonen, K., Pulkki, K., Aalto, M. & Simell, O. Oral supplementation corrects plasma lysine concentrations in lysinuric protein intolerance. *Metabolism* **52**, 935–938 (2003).
164. Zhou, Y. et al. Reversal of SLE and hemophagocytic lymphohistiocytosis caused by lysinuric protein intolerance through allogeneic hematopoietic stem cell transplantation. *J. Allergy Clin. Immunol.* **151**, 1673–1674 (2023).
165. Akula, M. K. et al. Control of the innate immune response by the mevalonate pathway. *Nat. Immunol.* **17**, 922–929 (2016).
166. Houten, S. M. et al. Temperature dependence of mutant mevalonate kinase activity as a pathogenic factor in hyper-IgD and periodic fever syndrome. *Hum. Mol. Genet.* **11**, 3115–3124 (2002).
167. Zhang, S. Natural history of mevalonate kinase deficiency: a literature review. *Pediatr. Rheumatol. Online J.* **14**, 30 (2016).
168. Berody, S., Galeotti, C., Kone-Paut, I. & Piram, M. A retrospective survey of patients's journey before the diagnosis of mevalonate kinase deficiency. *Jt Bone Spine* **82**, 240–244 (2015).
169. van der Hilst, J. C. & Frenkel, J. Hyperimmunoglobulin D syndrome in childhood. *Curr. Rheumatol. Rep.* **12**, 101–107 (2010).
170. Ammouri, W. et al. Diagnostic value of serum immunoglobulinaemia D level in patients with a clinical suspicion of hyper IgD syndrome. *Rheumatology* **46**, 1597–1600 (2007).
171. Romano, M. et al. The 2021 EULAR/American College of Rheumatology points to consider for diagnosis, management and monitoring of the interleukin-1 mediated autoinflammatory diseases: cryopyrin-associated periodic syndromes, tumour necrosis factor receptor-associated periodic syndrome, mevalonate kinase deficiency, and deficiency of the interleukin-1 receptor antagonist. *Arthritis Rheumatol.* **74**, 1102–1121 (2022).
172. Jeyaratnam, J. et al. Diagnostic value of urinary mevalonic acid excretion in patients with a clinical suspicion of mevalonate kinase deficiency (MKD). *JIMD Rep.* **27**, 33–38 (2016).
173. Berner, J. et al. Phosphomevalonate kinase deficiency expands the genetic spectrum of systemic autoinflammatory diseases. *J. Allergy Clin. Immunol.* **152**, 1025–1031.e2 (2023).

174. Jairaman, A. et al. A novel homozygous variant in PMVK is associated with enhanced IL1β secretion and a hyper-IgD syndrome-like phenotype. *Clin. Genet.* **105**, 302–307 (2024).
175. De Benedetti, F. et al. Canakinumab for the treatment of autoinflammatory recurrent fever syndromes. *N. Engl. J. Med.* **378**, 1908–1919 (2018).
176. Bodar, E. J. et al. On-demand anakinra treatment is effective in mevalonate kinase deficiency. *Ann. Rheum. Dis.* **70**, 2155–2158 (2011).
177. Stinchi, S. et al. Targeted disruption of the lysosomal α-mannosidase gene results in mice resembling a mild form of human α-mannosidosis. *Hum. Mol. Genet.* **8**, 1365–1372 (1999).
178. Michalski, J. C., Haeuw, J. F., Wieruszeski, J. M., Montreuil, J. & Strecker, G. In vitro hydrolysis of oligomannosyl oligosaccharides by the lysosomal α-D-mannosidases. *Eur. J. Biochem.* **189**, 369–379 (1990).
179. Malm, D. & Nilssen, O. Alpha-mannosidosis. *Orphanet J. Rare Dis.* **3**, 21 (2008).
180. Malm, D., Riise Stensland, H. M., Edvardsen, O. & Nilssen, O. The natural course and complications of alpha-mannosidosis — a retrospective and descriptive study. *J. Inherit. Metab. Dis.* **37**, 79–82 (2014).
181. Saad, A. K. et al. Retrospective study of clinical and genetic profiles of alpha-mannosidosis patients from the UAE. *JIMD Rep.* **66**, e70001 (2025).
182. Urushihara, M. et al. Sisters with α-mannosidosis and systemic lupus erythematosus. *Eur. J. Pediatr.* **163**, 192–195 (2004).
183. Lipinski, P. et al. Long-term outcome of patients with alpha-mannosidosis — a single center study. *Mol. Genet. Metab. Rep.* **30**, 100826 (2022).
184. Riise Stensland, H. M. et al. amamutdb.no: a relational database for MAN2B1 allelic variants that compiles genotypes, clinical phenotypes, and biochemical and structural data of mutant MAN2B1 in α-mannosidosis. *Hum. Mutat.* **36**, 581–586 (2015).
185. Lander, J. M. et al. Velmanase alfa approved for treatment of non-central nervous system manifestations of alpha-mannosidosis: a therapeutics bulletin of the American College of Medical Genetics and Genomics (ACMG). *Genet. Med. Open.* **2**, 101832 (2024).
186. Mynarek, M. et al. Allogeneic hematopoietic SCT for alpha-mannosidosis: an analysis of 17 patients. *Bone Marrow Transpl.* **47**, 352–359 (2012).
187. Rossignol, F., Wang, H. & Ferreira, C. Prolidase deficiency. In *GeneReviews* (ed Adam, M. P. et al.) (2022).
188. Spodenkiewicz, M. et al. Clinical genetics of prolidase deficiency: an updated review. *Biology* **9**, 10 (2020).
189. Chasset, F. et al. Rare diseases that mimic systemic lupus erythematosus (Lupus mimickers). *Jt Bone Spine* **86**, 165–171 (2019).
190. Eni-Aganga, I., Lanaghan, Z. M., Balasubramaniam, M., Dash, C. & Pandhare, J. PROLIDASE: a review from discovery to its role in health and disease. *Front. Mol. Biosci.* **8**, 723003 (2021).
191. Schneider, P. B. & Kennedy, E. P. Sphingomyelinase in normal human spleens and in spleens from subjects with Niemann-Pick disease. *J. Lipid Res.* **8**, 202–209 (1967).
192. Schuchman, E. H. & Desnick, R. J. Types A and B Niemann-Pick disease. *Mol. Genet. Metab.* **120**, 27–33 (2017).
193. Dhami, R., He, X., Gordon, R. E. & Schuchman, E. H. Analysis of the lung pathology and alveolar macrophage function in the acid sphingomyelinase-deficient mouse model of Niemann-Pick disease. *Lab. Invest.* **81**, 987–999 (2001).
194. McGovern, M. M. et al. Prospective study of the natural history of chronic acid sphingomyelinase deficiency in children and adults: eleven years of observation. *Orphanet J. Rare Dis.* **16**, 212 (2021).
195. McGovern, M. M. et al. A prospective, cross-sectional survey study of the natural history of Niemann-Pick disease type B. *Pediatrics* **122**, e341–e349 (2008).
196. Wasserstein, M. P. et al. Acid sphingomyelinase deficiency: prevalence and characterization of an intermediate phenotype of Niemann-Pick disease. *J. Pediatr.* **149**, 554–559 (2006).
197. Geberhiwot, T. et al. Consensus clinical management guidelines for acid sphingomyelinase deficiency (Niemann–Pick disease types A, B and A/B). *Orphanet J. Rare Dis.* **18**, 85 (2023).
198. Doerr, A. et al. Diagnostic odyssey for patients with acid sphingomyelinase deficiency (ASMD): exploring the potential indicators of diagnosis using quantitative and qualitative data. *Mol. Genet. Metab. Rep.* **38**, 101052 (2024).
199. Diaz, G. A. et al. One-year results of a clinical trial of olipudase alfa enzyme replacement therapy in pediatric patients with acid sphingomyelinase deficiency. *Genet. Med.* **23**, 1543–1550 (2021).
200. Wasserstein, M. et al. A randomized, placebo-controlled clinical trial evaluating olipudase alfa enzyme replacement therapy for chronic acid sphingomyelinase deficiency (ASMD) in adults: one-year results. *Genet. Med.* **24**, 1425–1436 (2022).
201. Wasserstein, M. P. et al. Continued improvement in disease manifestations of acid sphingomyelinase deficiency for adults with up to 2 years of olipudase alfa treatment: open-label extension of the ASCEND trial. *Orphanet J. Rare Dis.* **18**, 378 (2023).
202. Diaz, G. A. et al. Long-term safety and clinical outcomes of olipudase alfa enzyme replacement therapy in pediatric patients with acid sphingomyelinase deficiency: two-year results. *Orphanet J. Rare Dis.* **17**, 437 (2022).
203. Kosukcu, C. et al. Whole exome sequencing in unclassified autoinflammatory diseases: more monogenic diseases in the pipeline? *Rheumatology* **60**, 607–616 (2021).
204. Batu, E. D. et al. Whole exome sequencing in early-onset systemic lupus erythematosus. *J. Rheumatol.* **45**, 1671–1679 (2018).
205. Fathalla, B. M., Alsarhan, A., Afzal, S., El Naofal, M. & Abou Tayoun, A. The genomic landscape of pediatric rheumatology disorders in the Middle East. *Hum. Mutat.* **42**, e1–e14 (2021).
206. Lee, W. F. et al. Characteristics and genetic analysis of patients suspected with early-onset systemic lupus erythematosus. *Pediatr. Rheumatol. Online J.* **20**, 68 (2022).
207. Tirosh, I. et al. Whole exome sequencing in childhood-onset lupus frequently detects single gene etiologies. *Pediatr. Rheumatol. Online J.* **17**, 52 (2019).
208. Li, G. et al. Genetic heterogeneity in Chinese children with systemic lupus erythematosus. *Clin. Exp. Rheumatol.* **39**, 214–222 (2021).
209. Karacan, I. et al. Diagnostic utility of a targeted next-generation sequencing gene panel in the clinical suspicion of systemic autoinflammatory diseases: a multi-center study. *Rheumatol. Int.* **39**, 911–919 (2019).
210. Mehta, A. et al. A charitable access program for patients with lysosomal storage disorders in underserved communities worldwide. *Orphanet J. Rare Dis.* **16**, 8 (2021).
211. Mansoor, S., Qamar, R. & Azam, M. Inborn errors of metabolism: historical perspectives to contemporary management. *Clin. Chim. Acta* **562**, 119883 (2024).
212. Hard, G. C. Some biochemical aspects of the immune macrophage. *Br. J. Exp. Pathol.* **51**, 97–105 (1970).
213. Palsson-McDermott, E. M. & O'Neill, L. A. The Warburg effect then and now: from cancer to inflammatory diseases. *Bioessays* **35**, 965–973 (2013).
214. West, A. P. et al. TLR signalling augments macrophage bactericidal activity through mitochondrial ROS. *Nature* **472**, 476–480 (2011).
215. Tannahill, G. M. et al. Succinate is an inflammatory signal that induces IL-1β through HIF-1α. *Nature* **496**, 238–242 (2013).
216. Seim, G. L. et al. Two-stage metabolic remodelling in macrophages in response to lipopolysaccharide and interferon-γ stimulation. *Nat. Metab.* **1**, 731–742 (2019).
217. Jiang, Z., Byers, S., Casal, M. L. & Smith, L. J. Failures of endochondral ossification in the mucopolysaccharidoses. *Curr. Osteoporos. Rep.* **18**, 759–773 (2020).
218. Peck, S. H. et al. Molecular profiling of failed endochondral ossification in mucopolysaccharidosis VII. *Bone* **128**, 115042 (2019).
219. Simonaro, C. M., Haskins, M. E. & Schuchman, E. H. Articular chondrocytes from animals with a dermatan sulfate storage disease undergo a high rate of apoptosis and release nitric oxide and inflammatory cytokines: a possible mechanism underlying degenerative joint disease in the mucopolysaccharidoses. *Lab. Invest.* **81**, 1319–1328 (2001).
220. Simonaro, C. M. et al. Mechanism of glycosaminoglycan-mediated bone and joint disease: implications for the mucopolysaccharidoses and other connective tissue diseases. *Am. J. Pathol.* **172**, 112–122 (2008).
221. Simonaro, C. M. et al. Involvement of the Toll-like receptor 4 pathway and use of TNF-alpha antagonists for treatment of the mucopolysaccharidoses. *Proc. Natl Acad. Sci.* **107**, 222–227 (2010).
222. Polgreen, L. E. et al. Elevated TNF-α is associated with pain and physical disability in mucopolysaccharidosis types I, II, and VI. *Mol. Genet. Metab.* **117**, 427–430 (2016).
223. Eliyahu, E. et al. Anti-TNF-alpha therapy enhances the effects of enzyme replacement therapy in rats with mucopolysaccharidosis type VI. *PLoS ONE* **6**, e22447 (2011).
224. Polgreen, L. E. et al. Pilot study of the safety and effect of adalimumab on pain, physical function, and musculoskeletal disease in mucopolysaccharidosis types I and II. *Mol. Genet. Metab. Rep.* **10**, 75–80 (2017).
225. Buchinskaya, N. V. et al. Evaluation of etanercept (a tumor necrosis factor alpha inhibitor) as an effective treatment for joint disease in mucopolysaccharidosis type I. A case report with whole-body magnetic resonance imaging. *Front. Med.* **10**, 1252704 (2023).

Acknowledgements
L.C.B. is supported by a Burroughs Wellcome Fund Career Award for Medical Scientists.

Author contributions
S.H.L., C.M.R. and C.S. researched data for the article. T.P.V., S.H.L., V.R.S. and L.C.B. contributed substantially to discussion of the content. S.H.L., C.M.R. and C.S. wrote the article. All authors reviewed and/or edited the manuscript before submission.

Competing interests
The authors declare no competing interests.

Additional information
Supplementary information The online version contains supplementary material available at https://doi.org/10.1038/s41584-026-01352-y.

Peer review information *Nature Reviews Rheumatology* thanks François Maillot, Klaus Tenbrock and Dirk Foell for their contribution to the peer review of this work.

nature reviews rheumatology

https://doi.org/10.1038/s41584-026-01353-x

Review article

Check for updates

Advances in cartilage imaging techniques

Ali Guermazi[1,2] ✉, Felix Eckstein[3,4], Garry Gold[5], Daichi Hayashi[6], Mohamed Jarraya[7], Feliks Kogan[5], Xiaojuan Li[8], Thomas M. Link[9], Sven Nebelung[10], Edwin H. G. Oei[11], Patrick Omoumi[12], Simo Saarakkala[13,14], Siegfried Trattnig[15], Wolfgang Wirth[4] & Frank W. Roemer[2,16,17]

Abstract

Articular cartilage is crucial for joint function; however, it has limited regenerative capacity when damaged, a hallmark of many rheumatic diseases. Non-invasive imaging is essential for early diagnosis, therapeutic monitoring and prognostication. MRI remains the reference standard, offering detailed assessment of both morphological and compositional cartilage changes. Technological advances, including high-resolution and compositional MRI techniques such as T2 mapping, T1ρ, delayed gadolinium-enhanced MRI of cartilage, sodium imaging, diffusion imaging and ultra-short echo-time imaging, enable early detection of matrix alterations that precede structural breakdown. CT arthrography, although it involves radiation, serves as a valuable alternative when MRI is contra-indicated, offering high performance in the detection and evaluation of cartilage surface lesions. Emerging modalities, such as ultrasonography and PET, offer additional functional insights but are currently limited in scope. Artificial intelligence is poised to transform cartilage imaging through accelerated acquisition, automated segmentation, improved interpretation and enhanced efficiency, with growing clinical adoption. Advanced cartilage imaging will probably have an increasingly important role in clinical rheumatology, particularly for the optimization of individualized management of cartilage pathology.

Sections

Introduction

MRI technical considerations

Semi-quantitative MRI cartilage assessment

Segmentation-based cartilage morphometry

Cartilage MRI at 3 T and 7 T versus 1.5 T

Compositional MRI

CT imaging techniques

PET imaging techniques

Ultrasonography imaging of articular cartilage

Artificial intelligence

Clinical and research applications

Conclusions

A full list of affiliations appears at the end of the paper. ✉e-mail: guermazi@bu.edu

Key points

- MRI is the primary imaging technique used to directly visualize articular cartilage. All MRI field strengths can be used for cartilage imaging, whereas higher magnetic field strength allows for greater spatial resolution and shorter acquisition times.
- Semi-quantitative MRI assessment allows for evaluation of cartilage surface damage regarding area extent and depth, but also covers other articular structures, such as subchondral bone and menisci.
- Quantitative cartilage morphometry involves cartilage tissue segmentation from MRI and computation of diverse 3D measures; this technique is highly sensitive to change over time.
- Compositional MRI techniques allow for the evaluation of the cartilage ultrastructure prior to the presence of surface damage and can be used as biomarkers for early cartilage degeneration.
- Advances in the CT field include the advent of spectral, photon-counting and weight-bearing CT, whereas the application of PET and other nuclear medicine techniques to cartilage has been limited.
- Artificial intelligence is increasingly used in cartilage evaluation to accelerate MRI acquisition and improve image quality. Artificial intelligence-based automated segmentation enables precise cartilage quantification.

Introduction

Articular cartilage has a central role in maintaining joint function by providing a low-friction, load-bearing surface[1]. Damage to cartilage, whether traumatic, degenerative or as a result of intra-articular inflammation, is a common feature of many rheumatic diseases, including osteoarthritis (OA), with limited potential for spontaneous regeneration and healing[2].

Imaging techniques have evolved substantially over the past two decades, offering clinicians and researchers a range of tools for the visualization and quantification of cartilage pathology[3]. MRI remains the cornerstone of non-invasive cartilage assessment[4]. As the primary modality for evaluating both traumatic and degenerative lesions, MRI enables detailed visualization of morphological (surface damage) and compositional changes (intrachondral tissue alterations). Continuous refinement of pulse sequences over the past two decades, including fast spin-echo (FSE), gradient-recalled echo (GRE), and composite and high-resolution 3D sequences, have markedly improved the detection of focal defects, delaminating cartilage lesions and widespread surface damage. Beyond structural evaluation based on semi-quantitative multi-tissue and quantitative segmentation-based approaches[5,6], compositional MRI techniques such as T2 mapping, T1ρ, delayed gadolinium-enhanced MRI of cartilage (dGEMRIC), sodium imaging, diffusion-weighted imaging and Ultra-short echo-time imaging (UTE) have emerged as powerful tools for assessing cartilage ultrastructure[7]. These modalities enable the non-invasive assessment of matrix integrity, hydration status, collagen organization and collagen and proteoglycan content, factors that often precede morphological breakdown and could potentially serve as early biomarkers for disease onset or progression.

CT and CT arthrography remain widely used in clinical practice, particularly when MRI is contraindicated or unavailable. Although conventional CT has limited use in assessing non-calcified tissues, CT arthrography, through direct intra-articular contrast medium injection, provides excellent spatial resolution and is particularly adept at delineating cartilage surface lesions[8]. Despite the radiation exposure, its diagnostic accuracy, rapid acquisition and compatibility with metallic implants make it a viable alternative in selected clinical scenarios[9].

Other modalities, such as ultrasonography and nuclear medicine techniques, are increasingly being explored for cartilage assessment, but their current clinical application remains limited. Although some cartilage surfaces, particularly those deep within the joint, might not be easily accessible to ultrasonography, its accessibility and potential for dynamic evaluation render it promising for selected clinical or research tasks. PET, particularly when combined with MRI (PET–MRI), might offer insights into cartilage metabolism and inflammation, opening up new avenues for functional imaging in rheumatic diseases.

A transformative development in musculoskeletal radiology, particularly in cartilage imaging, is artificial intelligence (AI), with applications quickly expanding from research settings to clinical practice[10]. AI-driven tools might help to automate segmentation, enhance image interpretation and improve diagnostic consistency across imaging platforms. In addition, AI-based acceleration of image acquisition and image reconstruction has already become standard of care in the clinical environment and has led to marked time and cost savings, improved image quality, combined with increased patient comfort owing to shorter examination times[11].

This Review provides a comprehensive overview of contemporary and emerging cartilage imaging and analysis techniques. The goal is to equip rheumatologists with a current understanding of the evolving imaging landscape, ultimately facilitating more precise and individualized care for patients with cartilage disease. We highlight key advances in cartilage imaging, with a particular emphasis on their technical development, clinical use and potential for integration into routine rheumatology practice.

MRI technical considerations

The evaluation of articular cartilage with MRI depends on intrinsic cartilage characteristics, such as T1 recovery time, T2 decay time and proton density, all of which can be altered in early cartilage damage, and extrinsic parameters that are machine and protocol-dependent, such as field strength, repetition time, echo time and flip angle[12]. MRI at a high magnetic field strength of 3 T offers substantial technical advantages over 1.5 T, primarily through its nearly doubled signal-to-noise ratio (SNR), which can be invested in higher spatial resolution, thinner slice acquisition and reduced scan duration[13]. This improvement can translate into superior detection of focal cartilage defects, as demonstrated in several studies[14–16]. Ultra-high-field (7 T) MRI provides an additional improvement in SNR; however, numerous challenges and limitations prevent the widespread use of this technique, including limited availability, coil design requirements and patient comfort[17]. Comparisons of cartilage assessment in the wrist at 3 T and 7 T MRI in a multireader exercise show slight superiority of 7 T, but only for some features[18]. Figure. 1 illustrates a direct comparison of 3 T versus 7 T imaging for the wrist and knee joint.

Coil selection is a key factor that influences image quality. For knee cartilage imaging in particular, dedicated knee coils or multichannel

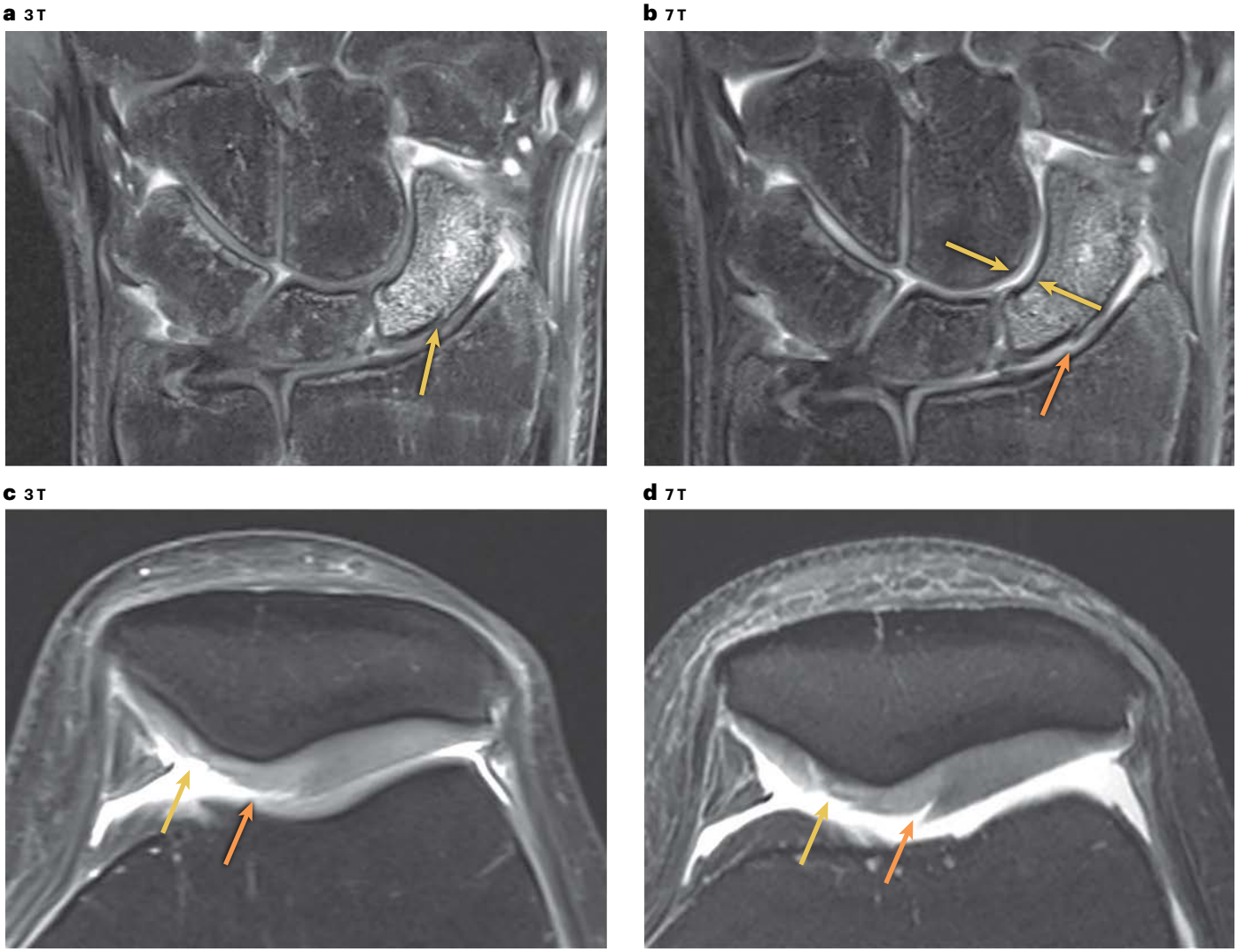

Fig. 1 | Direct comparison between 3 T and 7 T MRI. Increased field strength can be used for acceleration of image acquisition or increase in spatial resolution. **a**, 3 T MRI (coronal intermediate fat-suppressed image) shows a scaphoid fracture with marked bone contusion and a small step-off of the proximal cortex. The proximal fracture location is depicted by the yellow arrow. It is unclear whether the cartilage surface is intact or not. **b**, Corresponding coronal 7 T image similarly shows a definitive small step-off of the proximal articular surface (orange arrow). In addition, superior delineation of the capitate and scaphoid cartilaginous surfaces occurs at 7 T compared with 3 T (yellow arrows), probably reflected by enhanced visualization of joint fluid. **c**, Axial intermediate-weighted fat-suppressed image of the knee at 3 T shows discrete superficial surface irregularities at the medial patella (yellow arrow) and the patellar apex (orange arrow). **d**, Corresponding 7 T MRI shows a definite delaminating surface defect at the apex that is not appreciated at 3 T MRI (orange arrow). The medial surface damage is depicted with comparable quality on 3 T and 7 T MRI (yellow arrow). The trochlear cartilage is not adequately visualized owing to a slightly different knee flexion angle.

extremity coils are preferred[19]. For smaller joints, such as the wrist, a flexible surface coil is preferred as it can be positioned closely to the anatomical region of interest. Parallel imaging techniques supported by multichannel coils help to reduce scanning time while maintaining spatial resolution[20].

2D FSE sequences are the clinical standard for evaluating cartilage morphology. Among the various sequences available, fat-suppressed intermediate-weighted sequences offer the best contrast within the cartilaginous tissue and between the cartilage and surrounding tissues, such as synovial fluid and subchondral bone[21]. Additionally, they provide the advantage of depicting other joint structural lesions, including meniscal or ligamentous tears and bone marrow oedema.

Several 3D sequences have been developed, each with different strengths and weaknesses. 3D GRE sequences, such as dual-echo steady state (DESS), offer excellent contrast between cartilage and surrounding structures and are the reference for cartilage morphometry. However, they are less sensitive to detecting focal cartilage damage than fat-suppressed intermediate-weighted MRI and are mostly used in the research setting or in clinical trials[21] (Fig. 2). 3D FSE sequences have demonstrated good diagnostic performance for cartilage lesion

diagnosis, but their widespread clinical use has been hindered by limitations, including long acquisition times, lower in-plane resolution compared with 2D sequences and some degree of blurring[21,22].

Semi-quantitative MRI cartilage assessment

Semi-quantitative MRI assessment in osteoarthritic joints offers ways of understanding OA disease progression across the entire joint[23], and can be performed with the help of several available scoring systems[24–37] (Table 1).

Semi-quantitative MRI analysis of knee OA features including cartilage damage has helped to better understand associations between structural damage, disease progression (including prediction of joint replacement) and clinical pain and symptoms[38,39]. Available evidence from the literature supports the reliability, validity and responsiveness of semi-quantitative MRI evaluation in observational studies and clinical trials of OA[5,39–41]. Examples of the application of semi-quantitative grading for the evaluation of therapeutic effects of a given intervention include the evaluation of the efficacy of autologous protein solution in 53 patients with varying degrees of knee OA, with statistically significant improvement in cartilage damage grades reported after treatment[42]. In the randomized controlled STARR trial, worsening of semi-quantitative cartilage grades compared with baseline was observed in 40% ($n = 16$) of the arthroscopic partial meniscectomy group compared with 22% ($n = 9$) of the physical therapy group, possibly indicating worsening of cartilage defects in the arthroscopic partial meniscectomy group in young patients with isolated traumatic meniscal tears without radiographic OA[43]. A post hoc analysis of the VIDEO trial, which investigated the effects of vitamin D on OA, indicated that vitamin D supplementation in patients with OA and 25-hydroxyvitamin D levels greater than 43 nmol/l might slow the progression of cartilage lesions, as assessed by semi-quantitative grading[44].

One possible reason for the failure of disease-modifying OA drug (DMOAD) trials might be the heterogeneity of the disease. OA investigators have thus been calling for a stratification of study populations by performing MRI-based screening for clinical trial eligibility[45]. Various structural phenotypes of knee OA have been proposed in the literature and can be defined based on semi-quantitative MRI[23]. These semi-quantitative MRI-based phenotypes include subchondral bone, cartilage–meniscus, inflammatory, atrophic and hypertrophic phenotypes[46]. For example, one study of 733 participants from the Osteoarthritis Initiative (OAI) study with Kellgren–Lawrence grade 2 knee OA showed that the cartilage–meniscus phenotype was associated with the progression of osteophytes and sclerosis at 24 months' follow-up, and was not associated with shorter time to subsequent total knee replacement[47].

Different definitions of a cartilage–meniscus phenotype have been suggested[48]. Based on data from the Foundation for National Institute of Health OA Biomarkers study, the study showed that there was an increased likelihood of cartilage damage progression over 48 months for those with Kellgren–Lawrence grade 2 knee OA for all definitions, but the same result was not observed for those with Kellgren–Lawrence grade 3 knee OA[48].

Overall, current evidence suggests that MRI-based semi-quantitative imaging research (most commonly on knee OA), including assessment of articular cartilage in OA-affected joints,

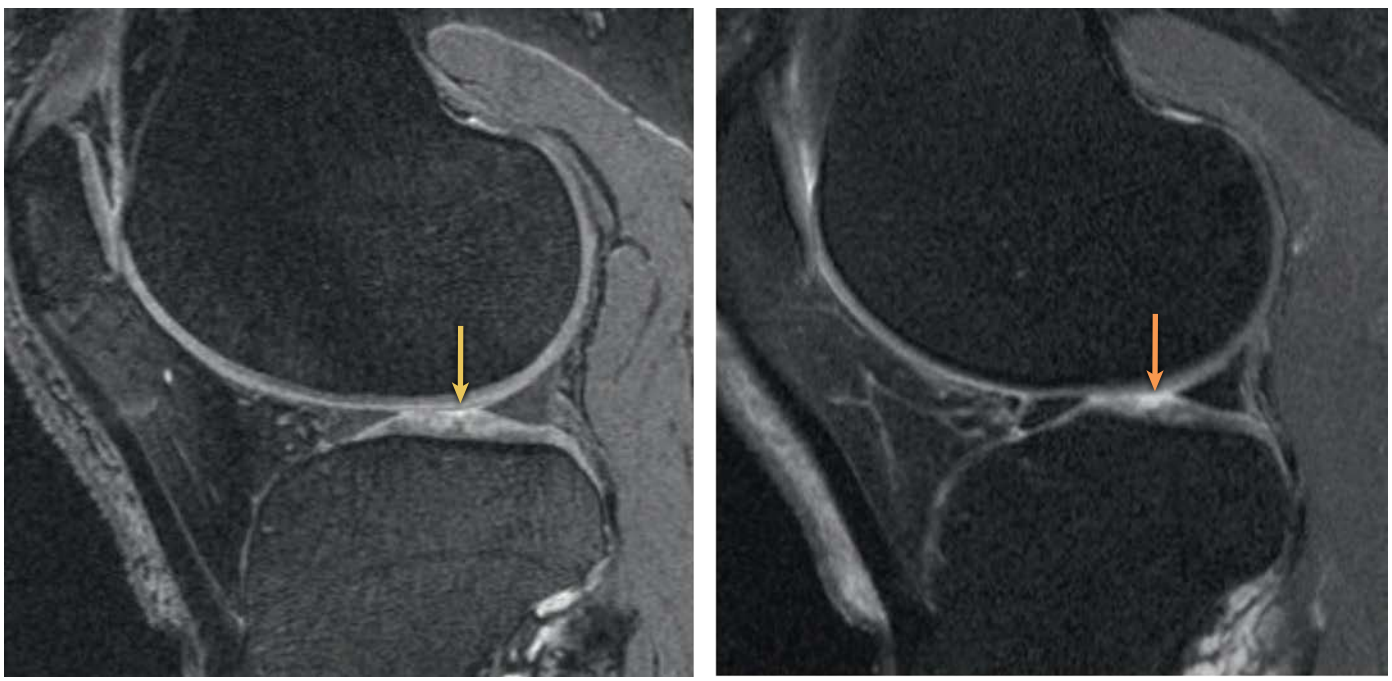

Fig. 2 | Relevance of sequence selection for evaluation of focal cartilage defects. a, Sagittal 3D T2-weighted dual-echo steady state (DESS) sequence shows a small hypointense signal change within the central aspect of the lateral tibial plateau (yellow arrow). No definite surface damage is apparent. **b**, Corresponding sagittal intermediate-weighted fat-suppressed turbo spin echo (FS TSE) sequence shows a definite surface lesion at the central lateral tibia (orange arrow). High-resolution 3D gradient echo-type sequences are less sensitive for the detection of focal cartilage damage than standard 2D turbo spin echo sequences.

Table 1 | Semi-quantitative MRI scoring systems for the whole joint including assessment of cartilage damage

Scoring system	Publication year	Cartilage scoring	Ref.
Knee			
WORMS	2004	Cartilage signal and morphology: 0 (normal thickness and signal); 1 (normal thickness but increased signal on T2-weighted images); 2.0 (partial-thickness focal defect <1 cm at greatest width); 2.5 (full-thickness focal defect <1 cm at greatest width); 3 (multiple areas of partial-thickness (grade 2.0) defects intermixed with areas of normal thickness, or a grade 2.0 defect wider than 1 cm but <75% of the region); 4 (diffuse (≥75% of the region) partial-thickness loss); 5 (multiple areas of full-thickness loss (grade 2.5) or a grade 2.5 lesion wider than 1 cm but <75% of the region); 6 (diffuse (≥75% of the region) full-thickness loss)	24
KOSS	2005	The depth of a cartilaginous defect: 0 (absent, that is, no abnormality in signal intensity or morphology); 1 (less than 50% reduction of cartilage thickness); 2 (50% or greater reduction of cartilage thickness); 3 (full-thickness or near-full-thickness cartilage defect)	25
		The surface extent is estimated by its maximal diameter: 0 (absent); 1 (minimal, <5 mm); 2 (moderate, 5–10 mm); 3 (severe, >10 mm)	
BLOKS	2008	Size of any cartilage loss as a percentage of surface area as related to the size of each individual region: 0 (none); 1 (<10% of the region of cartilage surface area); 2 (10–75% of region of cartilage surface area); 3 (>75% of the region of cartilage surface area)	26
		Percentage of full-thickness cartilage loss of the region: 0 (none); 1 (<10% of the region of cartilage surface area); 2 (10–75% of the region of cartilage surface area); 3 (>75% of the region of cartilage surface area)	
MOAKS	2011	Size of any cartilage loss as a percentage of surface area as related to the size of each individual region: 0 (none); 1 (<10% of the region of cartilage surface area); 2 (10–75% of region of cartilage surface area); 3 (>75% of the region of cartilage surface area)	27
		Percentage full-thickness cartilage loss of the region: 0 (none); 1 (<10% of the region of cartilage surface area); 2 (10–75% of the region of cartilage surface area); 3 (>75% of the region of cartilage surface area)	
Meredith et al.	2009	Degree of cartilage damage: 0 (normal); 1 (increased signal heterogeneity without surface disruption); 2 (fraying (superficial only)); 3 (fissuring (full thickness lesions <1 mm in width)); 4 (thinning <50% of cartilage thickness); 5 (thinning >50% of cartilage thickness); 6 (full thickness cartilage loss)	28
		Greatest diameter of lesion of greatest severity: 0 (normal); 1 (<1 cm); 2 (1–2 cm); 3 (2–3 cm); 4 (>3 cm)	
		Degree of cartilage damage and lesion size scores summed over 17 regions (hypothetical range 0–102): 0 (none); 0–30 (mild); 30–60 (moderate); >60 (severe)	
ACLOAS	2014	Cartilage damage: 0 (normal cartilage); 2.0 (focal partial-thickness defect <10% of the subregional area affected); 2.5 (focal full-thickness defect, ≥10% of the subregional area affected); 3 (multiple areas of partial-thickness (grade 2.0) defects and areas of normal thickness in the subregion, or a grade 2.0 defect ≥10% but <75% of the subregion); 4 (diffuse partial-thickness loss, ≥75% of the subregion); 5 (multiple areas of full-thickness loss (grade 2.5) or a grade 2.5 lesion ≥10% but <75% of the subregion); 6 (diffuse full-thickness loss, ≥75% of subregion)	29
CROAKS	2014	Cartilage damage: each articular cartilage region is graded for area extent of loss and percentage loss in this subregion that is affected by full-thickness loss. Thus, a two-digit score is applied, with the first digit describing the area size of the lesion and the second digit describing the percentage of the subregion that is affected by full-thickness loss. Possible scores: 1.0; 1.1; 2.0; 2.1; 2.2; 3.0; 3.1; 3.2; 3.3	30
ROAMES	2020	Cartilage damage: 0 (normal cartilage surface), 1 (maximum grade in the compartment is a focal defect, that is WORMS 2 and 2.5), 2 (maximum grade in the compartment is superficial diffuse damage, that is, WORMS 3 and 4), 3 (maximum grade in the compartment is diffuse full-thickness damage, that is, WORMS 5 and 6); combined lesions (diffuse superficial plus small full-thickness component) grades 2.1 and 3.1 in MOAKS are categorized as 2 and 3	31
Uppstrom et al.	2025	Chondral loss: high-grade partial thickness (>50%) or full thickness and the size of the chondral lesions (<10 mm^2, 10–14 mm^2 or 15 mm^2; the extent of chondral loss was scored as 0 (absent), 1 (mild, 10–14 mm^2), or 2 (severe, ≥15 mm^2); small chondral lesions <10 mm^2 were scored as 0	32
Hip			
HOAMS	2011	Cartilage integrity or damage: assessed using a single score that is based on a percentage of affected area of any given subregion, focal defects are differentiated from more diffuse damage; in addition, the depth of the cartilage lesion is taken into account; any subregion is scored according to worst grade within that subregion (0 (normal cartilage), 1 (focal partial thickness defect, ≤25% of the subregional area affected), 2 (focal full-thickness defect, ≤25% of the subregional area affected), 3 (several partial-thickness defects or a single but larger superficial defect, >25% of subregional area affected), 4 (several large full-thickness defects or a single full-thickness defect, >25% of the subregional area affected))	33
SHOMRI	2015	Articular cartilage lesions: scored in each of the ten subregions using a three-point scale (0 (no loss), 1 (partial-thickness loss), 2 (full-thickness loss)); for large lesions that span more than one region (>1 cm in maximal diameter), a lesion is scored in both subregions; if the lesion is <1 cm it is scored in the subregion where more than 50% of the lesion is located; each of the ten subregions is scored separately and added for a total cartilage score	34

Table 1 (continued) | Semi-quantitative MRI scoring systems for the whole joint including assessment of cartilage damage

Scoring system	Publication year	Cartilage scoring	Ref.
Hand and thumb base			
OHOA-MRI	2011	JSN is used as a surrogate measure of cartilage loss: 0 (no JSN); 1 (mild JSN); 2 (bone-to-bone contact in part of the joint); 3 (bone-to-bone contact in the whole joint)	35
HOAMRIS	2014	Cartilage space loss in hand OA: 0 (normal); 1 (mild, loss of cartilage space without bone-to-bone contact); 2 (moderate, focal complete loss of cartilage space); 3 (severe, complete cartilage space loss affecting >50% of the articulating joint area)	36
TOMS	2017	Loss of cartilage, or loss of cartilage space based on the inter-bone distance in thumb base OA; if the assessment of cartilage and cartilage space are in conflict, direct visualization of the cartilage should be prioritized (0 (no loss of cartilage or cartilage space), 1 (mild cartilage loss without complete denuding, or cartilage space loss without bone-to-bone contact), 2 (moderate cartilage loss with 50% denuding of the joint surface or focal complete cartilage space loss with bone-to-bone contact that spans 50% of the articulating area), 3 (severe cartilage loss with >50% denuding of the joint surface or complete cartilage space loss over >50% of the articulating area))	191

ACLOAS, Anterior Cruciate Ligament Osteoarthritis Score; BLOKS, Boston–Leeds Osteoarthritis Knee Score; CROAKS, Cartilage Repair Osteoarthritis Knee Score; HOAMRIS, Hand Osteoarthritis MRI Scoring System; HOAMS, Hip Osteoarthritis MRI Score; JSN, joint space narrowing; KOSS, Knee Osteoarthritis Scoring System; MOAKS, MRI Osteoarthritis Knee Score; OA, osteoarthritis; OHOA-MRI, Oslo Hand Osteoarthritis MRI score; ROAMES, Rapid Osteoarthritis MRI Eligibility Score; SHOMRI, Scoring Hip Osteoarthritis with MRI; TOMS, Thumb base Osteoarthritis MRI Scoring System; WORMS, Whole Organ Magnetic Resonance Score.

continues to have an important role in observational and clinical studies of OA[49].

Segmentation-based cartilage morphometry

Unlike semi-quantitative evaluation, segmentation-based quantitative MRI, also known as cartilage morphometry, involves cartilage tissue segmentation from MRI, and computation of diverse 3D morphometric measures. These measures include cartilage thickness, volume, subchondral bone size, denuded areas and others[6]. Commonly used MRI sequences include spoiled GRE (also termed fast low-angle shot or fast field echo or DESS) and quantitative DESS (qDESS)[6] (Fig. 3).

Although not used routinely for clinical OA diagnosis, cartilage morphometry is highly sensitive to subtle changes over time and therefore particularly valuable for research and clinical trials. Cartilage morphometry is primarily used in epidemiological studies of OA risk factors and disease progression, and interventional trials that assess therapeutic effects[6]. As quantitative cartilage biomarkers are targeted for use as responsive surrogate endpoints in clinical trials, cartilage loss has been successfully related to knee pain and radiographic change[50,51], surgical knee replacement[52–54] and a pain-based end point of virtual knee replacement[55,56]. The ROCCELLA trial enrolled over 800 people across ~100 clinical sites. Although the drug under investigation (S201086/GLPG1972, an ADAMTS-5 inhibitor) did not show any positive effects for cartilage loss, morphometry revealed high sensitivity to disease-related change over 1 year[57]. Satisfactory test–retest reproducibility and low 'smallest detectable changes' were reported in this trial, confirming high methodological reliability and precision[58].

Cartilage morphometry has been applied in numerous other OA treatment trials, spanning pharmacological (such as sprifermin)[59–65], lifestyle (IDEA study)[66], regenerative therapy[67] and surgical intervention[68–71]. Sprifermin (FGF18) increased cartilage thickness versus placebo over 2 years[59] and this effect was maintained over 3 years post-treatment[61,63]. No benefits for OA-related pain were observed in this cohort, but post hoc analyses show improvements in pain for patients with severe disease 3–5 years after treatment[60,62]. Furthermore, 2 months of knee joint distraction (a joint-preserving treatment) increased cartilage thickness over 1 year[68], and was associated with considerable improvement in pain and lasting structural effects observed up to and over 10 years[69–71]. High tibial osteotomy markedly reduced cartilage thickness loss versus placebo over a period of 1 year, accompanied by strong parallel improvements in clinical outcomes[72].

Future directions include the use of qDESS with short acquisition time for combined assessment of cartilage morphometry and composition (T2 mapping)[73–75]. AI and convolutional neural network (CNN)-based segmentation methodologies are increasing the feasibility of automated cartilage morphology and T2 mapping or T1ρ analysis in early disease[76–78] and that of denuded bone and cartilage loss at advanced stages[79,80]. Location-independent approaches permit measuring cartilage change and treatment effects independent of specific joint locations, with improved sensitivity[63,81]. Cartilage morphometry has been shown to perform comparably at 1.5 T and 3 T[82,83].

Cartilage MRI at 3 T and 7 T versus 1.5 T

Interest in cartilage imaging using high-field (3 T) and ultra-high-field whole-body systems (7 T and above) is growing as higher SNR with increasing magnetic field strength can be used to improve spatial and temporal resolution. To ensure the optimal performance of cartilage examination using ultra-high-field MRI, using well-optimized sequences and dedicated coils is required. Analysis of SNR gain at 7 T versus 3 T using a series of clinical protocols for the knee, including two 2D sequences (proton density-weighted turbo spin echo and T1-weighted spin echo) and three isotropic 3D sequences (true fast imaging with steady-state free precession, fast low-angle shot and proton density-weighted turbo spin-echo sampling perfection with application optimized contrast using different flip-angle evolution)[84], showed that the higher SNR of the 7 T MRI machine can be used to either substantially decrease the scan time or increase the in-plane resolution (by a mean factor of 2, with signal-intense sequences even by a factor of 4). 3 T MRI offers greater diagnostic accuracy than 1.5 T MRI for articular cartilage lesions[85].

High spatial resolution at 3 T and 7 T enables examination of the thin cartilage layers in ankle and wrist joints and subtle abnormalities such as early delamination of cartilage[86–88]. In addition to morphological imaging, one of the main strengths of high-field and ultra-high-field MRI is compositional MRI, which enables the detection of biochemical and ultrastructural changes in the cartilage extracellular matrix (discussed in a later section).

In summary, current evidence supports that 7 T offers potential research-level advantages in spatial resolution and compositional imaging, whereas 3 T currently remains clinically adequate (Fig. 1 and Fig. 4).

Compositional MRI

Compositional MRI techniques enable the evaluation of the cartilage matrix composition and quality at a stage where abnormal findings are early and potentially reversible, which enables intervention to halt disease progression. Quantitative compositional techniques might also facilitate sensitive monitoring of therapeutic interventions. Over the past two decades, several technologies have been developed.

T2 relaxation time measurements

T2 relaxation time is a quantitative MRI technique that has been used to characterize hyaline cartilage quality. T2 measurements provide information on the water content and the integrity of the collagen architecture of the extracellular cartilage matrix[89]. In the early stages of cartilage degeneration, the water content increases and the collagen architecture deteriorates, both of which increase T2 values. Notably, T2 measurements are useful when cartilage thickness is relatively maintained but is limited when disease is more advanced and cartilage loss occurs[90].

The technique was validated in previous studies, which documented a definite association between cartilage matrix composition and T2 values[91]. T2 measurements can predict the progression of cartilage loss[92] and worsening structural OA based on radiographic Kellgren–Lawrence scores[93]. Using AI-based algorithms, T2 values from the entire OAI cohort were obtained. Those individuals in the highest 25% quartile of tibiofemoral T2 values were at a five-times higher risk of radiographic OA incidence after 2 years[94]. T2 values predicted the development of pain[95] and have been used to monitor interventions such as weight loss[96].

T1ρ relaxation time measurements

Although T2 relaxation time measurements provide information on the cartilage water content and collagen architecture, T1ρ relaxation time, defined as the spin lattice relaxation time in the rotating frame, characterizes the proteoglycan concentration within the cartilage matrix by probing the interactions between motion-restricted water molecules with their local macromolecular environment[89]. Early stages of cartilage degeneration are characterized by decreasing proteoglycan content in the cartilage matrix, which results in high T1ρ measurements[97].

T1ρ measurements have been validated using cartilage samples obtained from total knee arthroplasties, which show that T1ρ values correlate with proteoglycan content and Mankin scores[98]. Reproducibility was high[99] and clinical studies show that T1ρ values can predict progressive cartilage degeneration[92] and can also be used to monitor therapeutic interventions with viscosupplementation[100] and allogeneic human adipose-derived mesenchymal progenitor cells[101]. T1ρ seems to be a promising biomarker for the diagnosis and prediction of post-traumatic OA after anterior cruciate ligament reconstruction surgery[102,103] (Supplementary Fig. 1).

Although T1ρ MRI has long been proposed as a non-invasive biomarker of proteoglycan content, emerging research is increasingly emphasizing that the specificity of this technique remains controversial. For example, anisotropy mapping at 3 T showed that continuous wave T1ρ varies with sample orientation and spin-lock amplitude, implying collagen structure dependence[104]. Furthermore, the use of different spin-lock time protocols shows that T1ρ estimates vary meaningfully with the choice of spin-lock time combinations, undermining cross-study comparability[105].

Ultra-short echo-time imaging

UTE sequences with an echo time of less than 100 µs are capable of detecting signals from both fast- and slow-relaxing water protons in cartilage. This detection enables comprehensive evaluation of all cartilage layers, including the deep and calcified zones. In a study of patients with early OA different quantitative UTE-based techniques were applied, including macromolecular fraction, magnetization transfer ratio and UTE-T2*, moderate correlations were observed between UTE-magnetization transfer measurements in the osteochondral junction and corresponding Kellgren–Lawrence grades, whereas UTE-T2* measurements showed a weaker correlation with

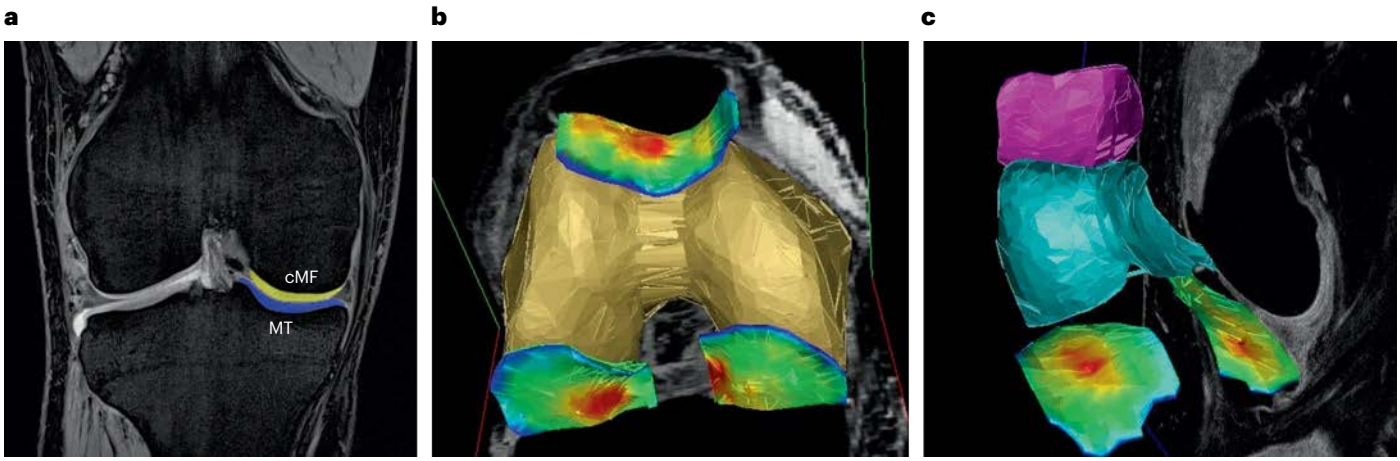

Fig. 3 | Cartilage morphometry based on MRI. a, Coronal quantitative dual-echo at steady state (qDESS) sequence. Cartilage segmentation is shown for the medial tibia (MT, blue) and the weight-bearing, central medial femur (cMF, yellow). **b**, 3D reconstruction of the joint from coronal images. The cartilage thickness distribution is shown for the patella and for the medial and lateral tibia. Cartilage thickness in the medial and lateral tibia is displayed by false colours; red denotes thick and dark blue indicates very thin cartilage. **c**, 3D reconstruction of the joint from sagittal images. The cartilage surface areas of the femoropatellar cartilage plates are shown in purple and teal; the cartilage thickness distribution is shown for the medial and lateral tibia.

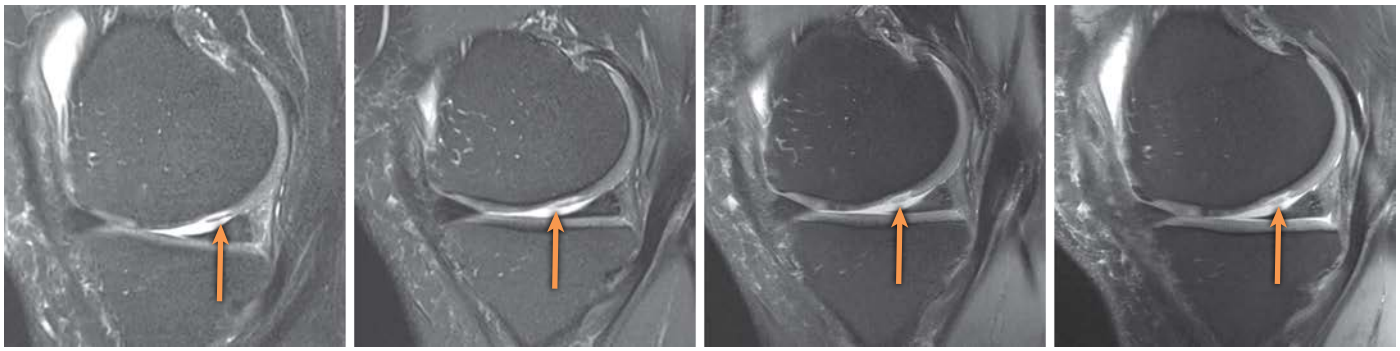

Fig. 4 | Direct comparison of different magnetic field strengths for cartilage surface damage evaluation. All images are intermediate-weighted fat-suppressed and acquired in the sagittal plane. The medial tibiofemoral compartment of the knee joint is shown with orange arrows indicating a delaminating surface lesion. **a**, 0.55 T; **b**, 1.5 T; **c**, 3 T; and **d**, 7 T MRI. All images were acquired with similar acquisition time (around 4 min), whereas the increase in field strength has been used for higher spatial resolution for 3 T and 7 T MRI. However, the delaminating cartilage flap at the medial femur is shown for all field strengths. Higher field strength might translate into superior image quality but not necessarily always into an increase in diagnostic accuracy.

Kellgren–Lawrence grades. Among the evaluated imaging biomarkers, macromolecular fraction showed the highest diagnostic sensitivity and specificity, followed closely by the MTR, whereas UTE-T2* showed lower discriminatory performance[106].

UTE magnetization transfer quantifies the macromolecular content relative to water in cartilage by leveraging magnetization transfer effects, which enable indirect detection of macromolecular protons with extremely short UTE-T2* values[107]. These results suggest a potential role for macromolecular fraction and magnetization transfer ratio in the assessment of the osteochondral junction. UTE quantitative susceptibility mapping of articular cartilage and cortical bone facilitates simultaneous mapping of cartilage and bone in the knee joint[108,109]. These developments support the potential of UTE MRI for the assessment of compositional features of the calcified layer of cartilage and might help to evaluate and understand early OA, particularly the role of the deep calcified layer of cartilage.

Diffusion imaging

As is the case with all compositional MRI techniques, diffusion imaging, including diffusion-weighted imaging and diffusion tensor imaging (DTI), can enable the visualization and quantification of early cartilage degeneration before morphological surface damage becomes apparent. Water mobility is restricted in healthy hyaline cartilage. In cartilage degeneration, which includes disruption of collagen networks and decreased proteoglycan content, increased water mobility occurs, which can be measured by diffusion imaging. DTI assesses water mobility in multiple directions to estimate a tensor, from which mean diffusivity and fractional anisotropy are derived, providing microstructural insights beyond conventional MRI[110]. Diffusion MRI of cartilage using standard single-shot echo-planar imaging is challenging owing to fast signal dephasing (T2 ~30 ms), thin tissue that requires high resolution and susceptibility artefacts in joints[111].

Ex vivo DTI studies have shown cartilage zonal patterns[112] as well as increased mean diffusivity and decreased fractional anisotropy in degenerated cartilage, in which mean diffusivity primarily reflects proteoglycan content and fractional anisotropy reflects collagen architecture[113]. In vivo cartilage diffusion MRI can distinguish healthy people from those with OA[114,115] (Supplementary Fig. 2). In a small cohort of people with and without OA, DTI exhibited a specificity and sensitivity that enabled the differentiation of people with OA from those without (apparent diffusion coefficient values of 1.0 and 0.8, respectively, and values of 0.88 and 0.8 for fractional anisotropy, respectively)[116].

Diffusion kurtosis imaging and other high-order models offer additional microstructural sensitivity by quantifying non-Gaussian diffusion and heterogeneity. A 2024 methods paper proposed axisymmetric modelling, spatial regularization and efficient direction b-value schemes to potentially increase sensitivity to cytoarchitectural changes that occur at various cellular spatial scales[117]. Model-based multi-compartment and regularized fitting, combined with robust motion correction and standardized acquisition protocols, constitute a potential path to reproducible, microstructure-sensitive cartilage diffusion MRI[118].

Other compositional MRI techniques

dGEMRIC uses repulsive forces between a negatively charged contrast agent (gadopentetate dimeglumine) and negative charges on glycosaminoglycans (GAGs) to indirectly measure GAG content[119]. The contrast agent, typically administered intravenously 90 min before MRI acquisition using a double dose (0.2 mmol/kg), accumulates in the cartilage in an inverse relationship with GAG content following exercise[120]. The quantitative outcome measure of dGEMRIC is T1 relaxation time, which is reduced in areas with decreased GAG content compared with healthy cartilage[119]. dGEMRIC has been validated both in vitro and in vivo, demonstrating good correlation with GAG content[121] and good reproducibility[122]. Owing to the robustness of this technique, dGEMRIC has been successfully applied in many clinical studies, such as in femoroacetabular impingement[123] and cartilage repair[124]. Disadvantages of dGEMRIC mainly relate to the contrast agent and the examination time being extremely long because of the required delay between contrast agent administration and image acquisition.

Glycosaminoglycan chemical exchange saturation transfer (gagCEST) MRI exploits an asymmetry in the MRI spectrum created by GAG biochemistry. The asymmetry is most pronounced on high-field MRI, so the methodology works best at 7 T[125]. Faster 3D as well as B0- and

B1-corrected gagCEST protocols at 3 T have increased SNR and clinical feasibility. Small clinical studies show a correlation with arthroscopy or dGEMRIC, but sensitivity is still limited by field inhomogeneity, low effect size at 3 T and long scan and processing demands[126]. Overall, limited studies have been performed with gagCEST[127].

Sodium MRI uses an MRI system that can excite at the sodium frequency and a special coil tuned to receive signal at this frequency. Non-invasive sodium MRI can directly quantify the positively charged sodium content that is proportional to the negatively charged cartilage GAG content. Low sodium content results in low SNR. Thus, sodium MRI works best with high-field MRI (7 T) but can be performed at 3 T with long scan times[128]. The use of sodium MRI in people with early OA showed differences between cartilage sodium measures in patients with early OA and healthy volunteers[129]. One study determined sodium relaxation times and concentrations of the human wrist on 3 T MRI, with the authors pointing out the inherent limitation of low spatial resolution of sodium imaging[130]. Despite the challenging nature of sodium MRI for cartilage evaluation, several studies have used sodium MRI as a quantitative marker for cartilage degeneration[131] and monitoring cartilage transplantation[132]. Supplementary Fig. 2 represents an example of sodium imaging in a patient with patellofemoral OA.

Challenges of compositional MRI

Although quantitative cartilage imaging biomarkers have been under development for more than 20 years, their clinical application remains limited[133,134]. One reason in the context of cartilage imaging is the orientation dependence of both T2 and T1ρ[134]. In one study, magic angle effects in histologically confirmed normal and abnormal regions were investigated using a clinical whole-body 3 T scanner, providing information on the angular dependence of T1ρ and T2. Strong magic angle effects for both T1ρ and T2 relaxation in articular cartilage were observed, especially in the deeper layers[135]. The deeper layers of cartilage are more susceptible to magic angle effects owing to the highly ordered collagen fibres oriented perpendicular to the bone–cartilage interface as opposed to the increasingly random orientation of collagen fibres in the more superficial layers of cartilage. Both measures, therefore, can misrepresent biochemical change if orientation is ignored.

Several challenges have been addressed in the past few years that make these biomarkers more technically accessible. These include machine-learning-based cartilage segmentation and analysis[136], faster imaging times, which enable better and more efficient implementation in clinical MRI protocols[137], and the development of standardized and reproducible protocols[99,138]. The Quantitative Imaging Biomarker Alliance (supported by the Radiological Society of North America) has provided recommendations on patient selection, handling and positioning, data acquisition (including scan parameters), hardware and image reconstruction for T1ρ and T2 techniques[139]. Using these criteria, standardized cartilage compositional imaging is feasible with reproducibility percentages of 4–5% using scanners of the same type and manufacturer[139]. Two major challenges prevent routine clinical application of quantitative imaging biomarkers: the limited availability of reference databases and the lack of effective pharmacotherapies to treat OA[140]. Objective data are needed to demonstrate that early detection of cartilage matrix degeneration adds value to patient care[133]. With the development of effective pharmacotherapies, quantitative compositional cartilage imaging biomarkers could be used to stratify patients for treatment and monitor response to therapy.

CT imaging techniques

CT imaging provides high contrast between mineralized tissues and soft tissues and offers high spatial resolution. Furthermore, the acquisition times for CT imaging are within the range of a few seconds, thereby increasing patient comfort while minimizing the risk of movement artefacts. In the context of OA, this technique is used for the assessment of bone changes, including subchondral bone structural changes, osteophytes and calcium crystal deposits; however, CT inherently lacks contrast resolution between the different soft tissues, which impedes the accurate assessment of intra-articular structures. Therefore, CT arthrography has been used to visualize both mineralized and non-mineralized articular structures. This technique involves the intra-articular injection of contrast material, thereby creating contrast between the low attenuation of intra-articular tissues, particularly cartilage and menisci, and the high attenuation of synovial fluid provided by the contrast agent[141]. CT arthrography is considered the imaging reference standard for the in vivo assessment of cartilage thickness in joints with both thin and thick cartilage, and for the depiction of cartilage surface lesions[142–144] (Fig. 5). In addition, CT arthrography is used for the assessment of meniscal pathology, especially in the post-operative setting, when metal artefacts are often present that are usually better controlled by CT than by MRI[145]. However, its performance in evaluating ligaments does not match that of MRI[146]. Additionally, CT is limited by radiation exposure, although this exposure is minimal for peripheral joints, and the risks and discomfort associated with contrast agent injection into the joint.

Major technical developments in the field of CT include the advent of spectral CT as well as photon-counting CT (PCCT) and weight-bearing CT. Spectral CT relies on tissue attenuation that is influenced by density, atomic number and photon energy, allowing material characterization and tissue quantification[147]. Additional applications include image contrast optimization and metal artefact reduction. Dual-energy CT, a subset of spectral CT, uses two X-ray spectra and has been used in the diagnosis of crystal arthropathies and the detection of bone marrow lesions (a feature not achievable with conventional CT)[148].

PCCT is the newest generation of spectral CT technology. It uses photon-counting detectors that rely on a single-step direct conversion process in which semiconductor materials convert individual X-ray photons directly into electrical signals, enabling true multi-energy acquisition with improved energy discrimination and image quality. PCCT offers higher spatial resolution, dose reduction and, in theory, better material differentiation[149]. Ongoing research is aimed at addressing remaining technical challenges associated with PCCT.

Weight-bearing CT is another area of development that offers the possibility of extending the strengths of conventional CT and CT arthrography to more biomechanically relevant conditions[150], which is particularly interesting for mobile articular structures such as menisci.

Finally, advancements in generating CT-like images from MRI, using specific sequences and AI-based synthetic methods, enable the examination of mineralized tissues without radiation exposure. Additionally, acquiring standard MRI sequences enables comprehensive assessment of other articular structures, thereby combining the strengths of both imaging modalities[151].

Although no CT-based biomarkers are currently validated for OA, quantitative bone parameters from CT could potentially serve as biomarkers. These biomarkers include subchondral bone mineral density or structure, osteophyte volume assessment or the B-score, which has been validated for both CT and MRI[152–154]. PCCT enhances bone structure analysis by offering an in-plane resolution as fine as 0.11 mm,

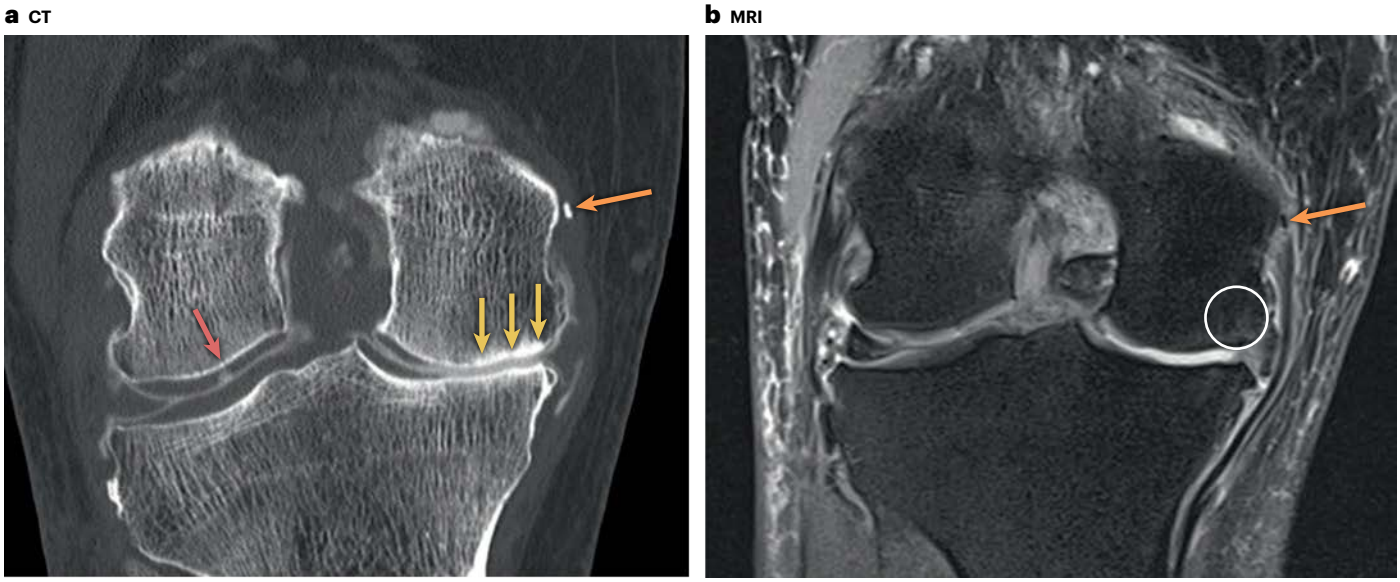

Fig. 5 | Comparison between CT arthrography and MRI. a,**b**, A 75-year-old man with bone-on-bone medial femorotibial osteoarthritis, as imaged by a coronal CT arthrography (**a**) and corresponding coronal intermediate-weighted fat-suppressed MRI (**b**). CT arthrography offers superior spatial and contrast resolution, facilitating the identification of small cartilage lesions (red arrow). Additionally, CT arthrography enables detailed analysis of bone structures, highlighting areas of increased subchondral bone density (yellow arrows), and allows for the depiction of crystal deposits, probably basic calcium phosphate crystals, within the medial collateral ligament, which is superiorly depicted on the CT image compared with MRI (orange arrows). Importantly, an area of subtle bone marrow oedema (white circle) is visible only on the MRI.

compared with the 0.5–0.6 mm of conventional CT, allowing for more detailed information extraction[147,155]. The automation of segmentation through AI-based algorithms and advanced analysis methods could facilitate the use of CT-based biomarkers for OA[156].

PET imaging techniques

PET offers unparalleled sensitivity and specificity to molecular processes; however, as a largely avascular and acellular tissue, the application of PET and other nuclear medicine techniques to cartilage has been limited. One emerging application of PET imaging is the evaluation of chondrocyte cell senescence. Cellular senescence is a hallmark of aging that has been implicated in OA and is a target for DMOADs[157]. Senescent cells overexpress β-gal, which has made it a popular target for studying senescence in multiple organ systems[158]. Both a PET radiotracer ([^{18}F]FPyGal)[159] and an MRI contrast agent (β-gal-responsive gadolinium)[160] have been developed and used to study senescent cells in OA. In vitro, ex vivo and in in vivo porcine joints, both approaches showed sensitivity to the presence of senescent cells. Furthermore, β-gal tracer uptake differed considerably between cartilage Outerbridge scores. Although results are promising for this emerging area in OA research and therapies, in vivo human studies are needed to support the potential use of these technologies.

Beyond direct imaging of cartilage, simultaneous PET–MRI systems have been leveraged to evaluate the interaction between cartilage and bone at the osteochondral junction. PET imaging with ^{18}F-sodium fluoride (NaF) interrogates areas of newly mineralizing bone and correlates with bone histomorphometry[161,162]. ^{18}F-NaF PET activity is elevated in patients with OA compared with healthy people, both in regions of structural pathology and in regions of normal-appearing bone and adjacent cartilage evaluated on MRI[163]. Additionally, ^{18}F-NaF PET–MRI has consistently shown relationships between cartilage structure (from morphological MRI) or microstructure (from MRI T2 or T1ρ relaxation times) and adjacent metabolic bone activity. In patients with an anterior cruciate ligament-reconstructed knee, a positive correlation was observed between subchondral bone ^{18}F-NaF PET activity and adjacent cartilage T2 relaxation times compared with contralateral knees[164]. Similar bone ^{18}F-NaF uptake and cartilage T2 relaxation time relationships have been observed in idiopathic OA in the tibiofemoral[165] and patellofemoral[166] joints, particularly between subchondral bone and deep cartilage zones. As a marker of subchondral bone physiology, ^{18}F-NaF PET uptake seems to be responsive to mechanical loading applied to the joint[167,168]. This result suggests that ^{18}F-NaF PET–MRI might be sensitive to transmission of focally high loading stresses to the underlying subchondral bone owing to a breakdown in cartilage mechanical function[169] (Fig. 6). Although work in this area is expanding, more research is necessary to understand the underlying mechanisms and to demonstrate the potential of these technologies.

Ultrasonography imaging of articular cartilage

Traditionally, ultrasonography has not been considered a modality of choice when assessing localized cartilage lesions or cartilage biochemical composition. The primary reason being that achieving an acoustic window for weight-bearing cartilage areas in the knee or hip joints is widely believed to be impossible. However, when scanning knee joints in 90° flexion on the oblique transverse axial plane, assessing two-thirds of the articular cartilage in the medial femoral condyle and one-third in the lateral femoral condyle is possible when using MRI as the reference[170]. Clinically, the central portion of the medial femoral condyle is one of the most vulnerable locations for cartilage lesions. In addition to the

medial femoral condyles, femoral trochlear cartilage regions can be assessed with ultrasonography[171] (Supplementary Fig. 4).

When the acoustic window to the articular cartilage has been obtained using a suitable scanning technique, ultrasonography can be used to evaluate localized cartilage lesions at the medial femoral condyle and the central trochlear area in the knee joint[172,173]. When using total knee arthroplasty as the gold standard, the sensitivity of ultrasonography is excellent (over 90%) for detecting medial femoral cartilage lesions[174].

Studies have generally shown good agreement between ultrasonography and MRI when measuring the thickness of the femoral cartilage; however, it also seems that ultrasonography underestimates the cartilage thickness compared with MRI[170,175]. This underestimation might be a result of different imaging resolutions between ultrasonography and MRI and higher sound speed in cartilage[175].

In theory, ultrasonography is also sensitive to the biochemical composition of cartilage, which was demonstrated in an ex vivo study that investigated the potential of quantitative ultrasound parameters to assess the progressive loss of collagen and proteoglycans in cartilage explants[176]. Returning ultrasound echoes from articular cartilage depend on the cartilage internal structure and composition, such as the collagen and proteoglycan content and, especially, the collagen network organization. Degenerated articular cartilage seems to possess lower ultrasound echogenicity (reduced brightness) than healthy cartilage[171]. Thus, changes in echogenicity without visible cartilage lesions or thinning could indicate an early osteoarthritic stage in the cartilage, which will eventually develop to visible cartilage thinning or a localized lesion. However, quantification of echogenicity from ultrasonography images requires standardization of imaging settings and experience of the operator. In the future, AI-based algorithms might offer novel biomarkers to assess the cartilage internal microarchitecture and, potentially, articular cartilage composition.

Artificial intelligence

AI is rapidly permeating routine radiological practice. Joint imaging, workflow management and clinical decision-making in orthopaedics, traumatology and rheumatology are no exception. AI-based techniques have been used for image reconstruction and accelerating image acquisition[177]. We focus on advances that have been made in the past 5 years in AI-driven analysis of knee cartilage, concentrating on automated segmentation, lesion detection and grading. The Dice similarity coefficient (DSC) measures the spatial overlap between automated and manual outlines of segmented cartilage, with 1.0 indicating perfect agreement. Contemporary deep-learning methods can now achieve whole-joint DSCs of around 0.90 or higher in research cohorts. Traditional 2D U-Net architectures trained on OAI data can reach mean DSCs of 0.89–0.92 for femorotibial cartilage and perform similarly in other large OAI studies[178–180]. Standard CNNs remain the reference architecture[178]; however, hybrid CNN–Transformer models capture long-range context, such as concomitant meniscal tears, more effectively than CNNs alone and consistently outperform them in multi-centre evaluations[181]. These hybrid designs are poised to become the dominant backbone for future musculoskeletal segmentation[181–183].

Nonetheless, clinical adoption is still limited for several reasons. First, regional and subregional accuracy remain variable. Tibial cartilage yields lower DSCs (≈0.75–0.80) in real-world datasets[181,183]. The tibial surface is probably hard to delineate because it is covered by menisci, offers little intrinsic contrast with subchondral bone and its nearly horizontal geometry accentuates partial volume artefacts.

Second, even models that perform well tend to under-segment cartilage affected by pathology[184,185]. Conventional metrics, such as whole-joint DSCs, are averaged over entire cartilage volumes and do not convey accuracy in or near a lesion.

Third, many models are still trained on outdated cohorts, such as the OAI (2004–2010) and SKI10, which were acquired using outdated protocols[179]. These sequences differ from current standard morphological sequences, such as 3D proton-density, fat-saturated turbo spin-echo or 3D DESS and quantitative sequences, causing performance to drop when models are applied to contemporary studies[181]. This 'domain shift' problem is well-recognized and an active research topic[186]. Manual reference annotations used for training also suffer from substantial inter-rater variability[181,183].

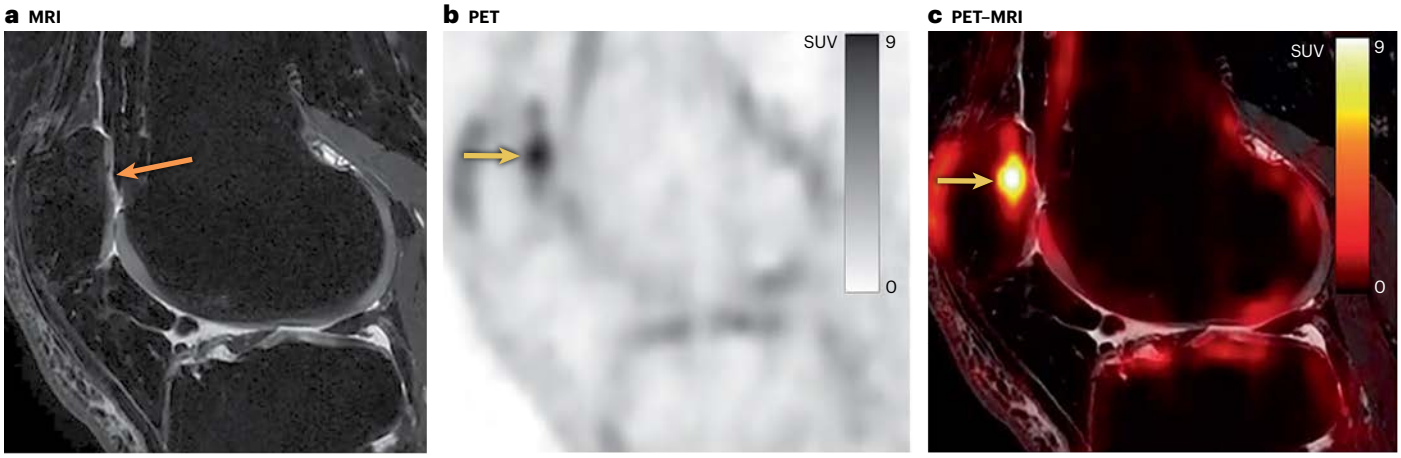

Fig. 6 | Metabolic imaging. a, T2-weighted sagittal intermediate-weighted fat-suppressed MRI shows superficial cartilage thinning at the superior aspect of the lateral patella facet (orange arrow). The subchondral bone is normal and does not show any signs of bone marrow oedema or other pathology. **b**, Corresponding ^{18}F-sodium fluoride (NaF) PET shows focal high metabolic bone activity adjacent to the cartilage defect (yellow arrow), suggestive of high mechanical stress in this region, albeit not visualized by MRI. **c**, The PET–MRI fusion image superiorly enables the assessment of metabolic–anatomical associations (yellow arrow points to increased tracer uptake in the subchondral bone). As a hybrid imaging technique, PET–MRI is able to investigate the interactions between cartilage mechanical function and subchondral bone loading. SUV, standardized uptake value.

Fourth, lesion-detection models are promising but present specific challenges. In a pioneering study, the authors used cascaded CNNs that sequentially segmented cartilage and classified potential lesions on sagittal 2D fat-suppressed T2-weighted FSE sequences, reporting good sensitivity and specificity[187]. Innovations made in the past 4 years include label-efficient training with semi-supervised teacher–student frameworks that reduce annotation effort while maintaining reliable defect grading[188]; architecture benchmarking in which a systematic comparison of different deep-learning architectures showed that hybrid networks delivered 90% agreement with human defect gradings[181]; and multimodal fusion that combines T1, T2, and proton-density-weighted images to improve defect gradings[182]. Despite these advances, most models remain vulnerable to advanced degeneration and are rarely validated against arthroscopic or histological references.

Fifth, downstream metrics such as cartilage thickness and volume, T2 relaxation times or subchondral bone shape can be reliably obtained from segmentation outlines[184]. However, the accuracy and validity of these metrics throughout the entire joint and in early OA (for which subtle changes matter the most) has yet to be confirmed.

Overall, AI-based analysis of knee cartilage MRI has progressed from proof-of-concept segmentation to integrated pipelines that approach expert performance and provide clinically meaningful quantitative outputs. To integrate these analyses into the clinic ongoing challenges needed be addressed, which include ensuring robustness across vendors, scanners and sequences, lesion-level validation, regional accuracy, ground truth reliability and regulatory approval.

Clinical and research applications

Modern cartilage imaging has become a vital component of rheumatology practice, substantially enhancing clinical diagnosis and supporting therapeutic decision making. Advances in imaging modalities, particularly MRI, ultrasonography and quantitative CT, have enabled detailed, non-invasive evaluation of cartilage structure and pathology. MRI remains the gold standard for assessing cartilage owing to the superior soft-tissue contrast and ability to visualize intrachondral biochemical changes. In routine clinical practice 1.5 T or 3 T systems together with modern multichannel coil technology that apply standard 2D and 3D sequences with and without fat suppression will be sufficient for cartilage assessment or suspected cartilage damage. The described compositional techniques, such as T2 mapping, dGEMRIC or T1ρ imaging enable early detection of cartilage degeneration, before morphological alterations become apparent. Owing to limitations in standardization and a lack of cartilage-regenerating therapies, these imaging modalities are currently not being used clinically but show potential. However, longitudinal MRI-based observational studies help to elucidate the natural history of cartilage degradation and the potential for cartilage repair, especially with regenerative treatments such as stem-cell therapy and biologic drugs.

Although ultrasonography is limited in visualizing anatomy deep within the joints, this technique is increasingly used for real-time evaluation of superficial cartilage damage, particularly in accessible joints such as the knee. The affordability and convenience of ultrasonography make it an attractive tool in outpatient settings. Intra-articular viscosupplementation is commonly applied using ultrasonography. In a clinical trial setting ultrasonography is being used to screen patients for the presence of synovitis and joint effusion, particularly in the context of therapeutic agents with an anti-inflammatory mode of action. Modern CT technology, including spectral and dual-energy CT, is currently being explored for the evaluation of inflammatory disorders such as spondyloarthritis[189,190] but to a lesser extent for cartilage imaging, owing to the inherent limitations with regard to soft-tissue visualization.

Glossary

Arthrography
Technique that is used for direct visualization of cartilage surface damage after intra-articular injection of either an iodine-based (CT) or gadolinium-based (MRI) contrast agent.

Compositional MRI
Umbrella term for MRI techniques that allow for evaluation of the cartilage ultrastructure including but not limited to assessment of collagen content and organization, water content and glycosaminoglycan content.

Convolutional neural network
(CNN). Type of deep-learning model commonly used in medical imaging to automatically detect and analyse patterns in images, such as identifying tumours or segmenting organs.

Delayed gadolinium-enhanced MRI of cartilage
(dGEMRIC). Compositional MRI technique that involves intra-articular administration of a gadolinium-based contrast agent using repulsive forces between a negatively charged contrast agent (commonly gadopentetate dimeglumine) and negative charges on glycosaminoglycans to indirectly measure glycosaminoglycan content.

Dice similarity coefficient
(DSC). Statistical measure used to evaluate the spatial overlap between two segmented regions, such as an automated segmentation and a ground truth (manual segmentation). It ranges from 0 (no overlap) to 1 (perfect overlap) and is commonly used to assess the accuracy of tissue or lesion segmentation in medical imaging.

Diffusion imaging
Compositional MRI technique that enables visualization of the mobility of water molecules within a given tissue. Increased mobility reflects early cartilage pathology.

PET
Imaging technique that uses different radioactive tracers that are administered intra-venously to visualize and measure metabolic activity of a given tissue.

Segmentation-based quantitative MRI
Using high-resolution 3D MRI sequences that offer a high contrast between cartilage, the subchondral bone and intra-articular joint fluid, quantitative assessment is based on manual, automated or semi-automated segmentation of cartilage. Several parameters are being extracted, including thickness, volume, amount of full-thickness damage or joint surface area.

Semi-quantitative MRI assessment
Applying ordinal grading scales, semi-quantitative cartilage assessment is performed by expert readers considering area extent and depth of cartilage damage in a specific anatomical subregion of a joint.

T1ρ
Compositional MRI technique, which is also termed spin-lattice relaxation time in the rotating frame, reflects the proteoglycan concentration within the cartilage matrix by probing the interactions between motion-restricted water molecules and their local macromolecular environment.

T2 mapping
Compositional MRI technique that quantifies the T2 relaxation time of a given tissue. In the context of cartilage imaging, T2 reflects collagen content and organization and water content.

Ultra-short echo-time imaging
(UTE). Very low echo times at MRI acquisition enable visualization of tissues that do not commonly exhibit a signal such as bone or tendons or the deep calcified layer of cartilage.

Conclusions

Marked advances in the visualization and assessment of articular cartilage have occurred over the past decade. The primary non-invasive instrument for assessing hyaline articular cartilage is MRI, with multiple techniques available that enable semi-quantitative or quantitative evaluation, as well as compositional MRI. Currently, compositional MRI techniques are primarily used in a research context as many of the techniques lack standardization and show high variability. Despite the success of several surgical cartilage repair techniques treatment of cartilage pathology remains a clinical challenge. Imaging enables the evaluation of potential treatment effects in a non-invasive manner. Additional techniques such as ultrasonography or PET imaging are increasingly evaluated but have shortcomings that hinder widespread application in a clinical context. In clinical practice and research settings, imaging has become essential for the evaluation of cartilage in both health and disease. As the field moves towards more individualized management of cartilage pathology, different imaging modalities are expected to assume complementary and distinct roles in the assessment of cartilage integrity, disease progression and response to treatment.

Published online: 3 February 2026

References

1. Joukar, A. et al. Correlation analysis of cartilage wear with biochemical composition, viscoelastic properties and friction. *J. Mech. Behav. Biomed. Mater.* **142**, 105827 (2023).
2. Pap, T. & Korb-Pap, A. Cartilage damage in osteoarthritis and rheumatoid arthritis — two unequal siblings. *Nat. Rev. Rheumatol.* **11**, 606–615 (2015).
3. Roemer, F. W. et al. State of the art: imaging of osteoarthritis — revisited 2020. *Radiology* **296**, 5–21 (2020).
4. Crema, M. D. et al. Articular cartilage in the knee: current MR imaging techniques and applications in clinical practice and research. *Radiographics* **31**, 37–61 (2011).
5. Roemer, F. W. et al. A perspective on the evolution of semi-quantitative MRI assessment of osteoarthritis: past, present and future. *Osteoarthritis Cartilage* **32**, 460–472 (2024).
6. Eckstein, F., Wluka, A. E., Wirth, W. & Cicuttini, F. 30 Years of MRI-based cartilage & bone morphometry in knee osteoarthritis: from correlation to clinical trials. *Osteoarthritis Cartilage* **32**, 439–451 (2024).
7. Guermazi, A. et al. Compositional MRI techniques for evaluation of cartilage degeneration in osteoarthritis. *Osteoarthritis Cartilage* **23**, 1639–1653 (2015).
8. Li, S. et al. Diagnostic value of MRI for detection of knee cartilage lesions vs. weight-bearing CT arthrography (WBCTa). *Skeletal Radiol.* **54**, 2795–2802 (2025).
9. Vande Berg, B. C., Lecouvet, F. E. & Malghem, J. Frequency and topography of lesions of the femoro-tibial cartilage at spiral CT arthrography of the knee: a study in patients with normal knee radiographs and without history of trauma. *Skeletal Radiol.* **31**, 643–649 (2002).
10. Guermazi, A. et al. How AI may transform musculoskeletal imaging. *Radiology* **310**, e230764 (2024).
11. Fritz, J., Guggenberger, R. & Del Grande, F. Rapid musculoskeletal MRI in 2021: clinical application of advanced accelerated techniques. *AJR Am. J. Roentgenol.* **216**, 718–733 (2021).
12. Buchanan, M. E. & Markhardt, B. K. Systematic review of techniques in cartilage imaging. *J. Cartil. Jt Preserv.* **4**, 100155 (2024).
13. Gold, G. E. et al. Musculoskeletal MRI at 3.0 T: relaxation times and image contrast. *Am. J. Roentgenol.* **183**, 343–351 (2004).
14. Link, T. M. et al. 3.0 vs 1.5 T MRI in the detection of focal cartilage pathology — ROC analysis in an experimental model. *Osteoarthritis Cartilage* **14**, 63–70 (2006).
15. Van Dyck, P. et al. Comparison of 1.5- and 3-T MR imaging for evaluating the articular cartilage of the knee. *Knee Surg. Sports Traumatol. Arthrosc.* **22**, 1376–1384 (2014).
16. Kijowski, R. et al. Comparison of 1.5- and 3.0-T MR imaging for evaluating the articular cartilage of the knee joint. *Radiology* **250**, 839–848 (2009).
17. Krug, R., Stehling, C., Kelley, D. A., Majumdar, S. & Link, T. M. Imaging of the musculoskeletal system in vivo using ultra-high field magnetic resonance at 7 T. *Invest. Radiol.* **44**, 613–618 (2009).
18. Heiss, R. et al. Clinical application of ultrahigh-field-strength wrist MRI: a multireader 3-T and 7-T comparison study. *Radiology* **307**, e220753 (2023).
19. Chang, G. et al. Comparison of a 28-channel receive array coil and quadrature volume coil for morphologic imaging and T2 mapping of knee cartilage at 7T. *J. Magn. Reson. Imaging* **35**, 441–448 (2012).
20. Deshmane, A., Gulani, V., Griswold, M. A. & Seiberlich, N. Parallel MR imaging. *J. Magn. Reson. Imaging* **36**, 55–72 (2012).
21. Omoumi, P., Mourad, C., Ledoux, J. B. & Hilbert, T. Morphological assessment of cartilage and osteoarthritis in clinical practice and research: intermediate-weighted fat-suppressed sequences and beyond. *Skeletal Radiol.* **52**, 2185–2198 (2023).
22. Shakoor, D. et al. Diagnostic performance of three-dimensional MRI for depicting cartilage defects in the knee: a meta-analysis. *Radiology* **289**, 71–82 (2018).
23. Collins, J. E., Roemer, F. W. & Guermazi, A. Approaches to optimize analyses of multidimensional ordinal MRI data in osteoarthritis research: a perspective. *Osteoarthr. Cartil. Open.* **6**, 100465 (2024).
24. Peterfy, C. G. et al. Whole-organ magnetic resonance imaging score (WORMS) of the knee in osteoarthritis. *Osteoarthritis Cartilage* **12**, 177–190 (2004).
25. Kornaat, P. R. et al. MRI assessment of knee osteoarthritis: knee osteoarthritis scoring system (KOSS) — inter-observer and intra-observer reproducibility of a compartment-based scoring system. *Skeletal Radiol.* **34**, 95–102 (2005).
26. Hunter, D. J. et al. The reliability of a new scoring system for knee osteoarthritis MRI and the validity of bone marrow lesion assessment: BLOKS (Boston Leeds Osteoarthritis Knee Score). *Ann. Rheum. Dis.* **67**, 206–211 (2008).
27. Hunter, D. J. et al. Evolution of semi-quantitative whole joint assessment of knee OA: MOAKS (MRI Osteoarthritis Knee Score). *Osteoarthritis Cartilage* **19**, 990–1002 (2011).
28. Meredith, D. S. et al. Empirical evaluation of the inter-relationship of articular elements involved in the pathoanatomy of knee osteoarthritis using magnetic resonance imaging. *BMC Musculoskelet. Disord.* **10**, 133 (2009).
29. Roemer, F. W., Frobell, R., Lohmander, L. S., Niu, J. & Guermazi, A. Anterior cruciate ligament osteoarthritis score (ACLOAS): longitudinal MRI-based whole joint assessment of anterior cruciate ligament injury. *Osteoarthritis Cartilage* **22**, 668–682 (2014).
30. Roemer, F. W. et al. Whole joint MRI assessment of surgical cartilage repair of the knee: cartilage repair osteoarthritis knee score (CROAKS). *Osteoarthritis Cartilage* **22**, 779–799 (2014).
31. Roemer, F. W. et al. MRI-based screening for structural definition of eligibility in clinical DMOAD trials: rapid osteoarthritis MRI eligibility score (ROAMES). *Osteoarthritis Cartilage* **28**, 71–81 (2020).
32. Uppstrom, T. J. et al. Reliability of a novel magnetic resonance imaging scoring system to evaluate patellofemoral osteoarthritis. *J. Knee Surg.* **38**, 555–562 (2025).
33. Roemer, F. W. et al. Hip osteoarthritis MRI scoring system (HOAMS): reliability and associations with radiographic and clinical findings. *Osteoarthritis Cartilage* **19**, 946–962 (2011).
34. Lee, S. et al. Scoring hip osteoarthritis with MRI (SHOMRI): a whole joint osteoarthritis evaluation system. *J. Magn. Reson. Imaging* **41**, 1549–1557 (2015).
35. Haugen, I. K. et al. Hand osteoarthritis and MRI: development and first validation step of the proposed Oslo hand osteoarthritis MRI score. *Ann. Rheum. Dis.* **70**, 1033–1038 (2011).
36. Haugen, I. K. et al. Iterative development and reliability of the OMERACT hand osteoarthritis MRI scoring system. *J. Rheumatol.* **41**, 386–391 (2014).
37. Kroon, F. P. B. et al. Longitudinal reliability of the OMERACT thumb base osteoarthritis magnetic resonance imaging scoring system (TOMS). *J. Rheumatol.* **46**, 1228–1231 (2019).
38. Roemer, F. W. et al. Can structural joint damage measured with MR imaging be used to predict knee replacement in the following year? *Radiology* **274**, 810–820 (2015).
39. Hafezi-Nejad, N., Zikria, B., Eng, J., Carrino, J. A. & Demehri, S. Predictive value of semi-quantitative MRI-based scoring systems for future knee replacement: data from the Osteoarthritis Initiative. *Skeletal Radiol.* **44**, 1655–1662 (2015).
40. Crema, M. D. et al. Cross-sectional and longitudinal reliability of semiquantitative osteoarthritis assessment at 1.0T extremity MRI: multi-reader data from the MOST study. *Osteoarthr. Cartil. Open.* **3**, 100214 (2021).
41. Hunter, D. J. et al. Responsiveness, effect size, and smallest detectable difference of Magnetic Resonance Imaging in knee osteoarthritis. *Osteoarthritis Cartilage* **14**, 112–115 (2006).
42. Fangzhou, C., Mochizuki, T., Ushiki, T. & Kawashima, H. Clinical outcomes and magnetic resonance imaging evaluation of autologous protein solution treatment for knee osteoarthritis. *Cureus* **17**, e84698 (2025).
43. van der Graaff, S. J. A. et al. Post-traumatic and OA-related lesions in the knee at baseline and 2 years after traumatic meniscal injury: secondary analysis of a randomized controlled trial. *Osteoarthritis Cartilage* **33**, 647–655 (2025).
44. Wang, T. et al. Baseline 25-hydroxyvitamin D levels predict the effects of vitamin D supplementation on joint symptoms and cartilage loss in patients with knee osteoarthritis. *Rheumatol. Adv. Pract.* **9**, rkaf061 (2025).
45. Guermazi, A., Roemer, F. W., Jarraya, M. & Hayashi, D. A call for screening MRI as a tool for osteoarthritis clinical trials. *Skeletal Radiol.* **52**, 2011–2019 (2023).
46. Roemer, F. W. et al. Structural phenotypes of knee osteoarthritis: potential clinical and research relevance. *Skeletal Radiol.* **52**, 2021–2030 (2023).
47. Liu, Y. et al. Association of MRI-based knee osteoarthritis structural phenotypes with short-term structural progression and subsequent total knee replacement. *J. Orthop. Surg. Res.* **19**, 699 (2024).
48. Roemer, F. W., Collins, J. E., Hunter, D. J., Demehri, S. & Guermazi, A. Patterns of progression differ between Kellgren-Lawrence 2 and 3 knees fulfilling different definitions of a cartilage-meniscus phenotype in the foundation for National Institutes of Health Osteoarthritis Biomarkers Study (FNIH). *Osteoarthr. Cartil. Open.* **4**, 100284 (2022).
49. Hayashi, D., Roemer, F. W. & Guermazi, A. Osteoarthritis year in review 2024: imaging. *Osteoarthritis Cartilage* **33**, 88–93 (2025).
50. Eckstein, F. et al. Brief report: cartilage thickness change as an imaging biomarker of knee osteoarthritis progression: data from the foundation for the National Institutes of Health Osteoarthritis Biomarkers Consortium. *Arthritis Rheumatol.* **67**, 3184–3189 (2015).
51. Hunter, D. J. et al. Multivariable modeling of biomarker data from the phase I Foundation for the National Institutes of Health Osteoarthritis Biomarkers Consortium. *Arthritis Care Res.* **74**, 1142–1153 (2021).

52. Eckstein, F. et al. Quantitative MRI measures of cartilage predict knee replacement: a case-control study from the Osteoarthritis Initiative. *Ann. Rheum. Dis.* **72**, 707–714 (2013).
53. Eckstein, F. et al. Trajectory of cartilage loss within 4 years of knee replacement — a nested case-control study from the Osteoarthritis Initiative. *Osteoarthritis Cartilage* **22**, 1542–1549 (2014).
54. Eckstein, F. et al. Comparison of radiographic joint space width and magnetic resonance imaging for prediction of knee replacement: a longitudinal case-control study from the osteoarthritis initiative. *Eur. Radiol.* **26**, 1942–1951 (2016).
55. Eckstein, F. et al. Quantitative cartilage thickness change preceding surgical and virtual knee replacement status – comparative analysis using data from the OAI. *Osteoarthritis Cartilage* **25**, S248–S249 (2017).
56. Eckstein, F. et al. Cartilage loss is greater in knees with virtual joint replacement status than in matched controls without. *Osteoarthr. Cartil. Open.* **7**, 100658 (2025).
57. Schnitzer, T. et al. Evaluation of S201086/GLPG1972, an ADAMTS-5 inhibitor, for the treatment of knee osteoarthritis in ROCCELLA: a phase 2 randomized clinical trial. *Osteoarthritis Cartilage* **31**, 985–994 (2023).
58. Eckstein, F., Deckx, B. K., Imbert, H., Lalande, O. & Wisser, A. A. Test-retest reliability and smallest detectable change (SDC) of MRI-based cartilage thickness analysis in a large multicenter randomized controlled clinical trial of knee osteoarthritis. *Osteoarthritis Cartilage* **29**, S327–S328 (2021).
59. Hochberg, M. C. et al. Effect of intra-articular sprifermin vs placebo on femorotibial joint cartilage thickness in patients with osteoarthritis: the FORWARD randomized clinical trial. *JAMA* **322**, 1360–1370 (2019).
60. Guehring, H. et al. The effects of sprifermin on symptoms and structure in a subgroup at risk of progression in the FORWARD knee osteoarthritis trial. *Semin. Arthritis Rheum.* **51**, 450–456 (2021).
61. Eckstein, F. et al. Unbiased analysis of knee cartilage thickness change over three years after sprifermin vs. placebo treatment – a post-hoc analysis from the phase 2B FORWARD study. *Osteoarthr. Cartil. Open.* **6**, 100513 (2024).
62. Eckstein, F. et al. Long-term structural and symptomatic effects of intra-articular sprifermin in patients with knee osteoarthritis: 5-year results from the FORWARD study. *Ann. Rheum. Dis.* **80**, 1062–1069 (2021).
63. Eckstein, F. et al. Intra-articular sprifermin reduces cartilage loss in addition to increasing cartilage gain independent of location in the femorotibial joint: post-hoc analysis of a randomised, placebo-controlled phase II clinical trial. *Ann. Rheum. Dis.* **79**, 525–528 (2020).
64. McAlindon, T. E. et al. Effect of intra-articular triamcinolone vs saline on knee cartilage volume and pain in patients with knee osteoarthritis: a randomized clinical trial. *JAMA* **317**, 1967–1975 (2017).
65. Conaghan, P. G. et al. Disease-modifying effects of a novel cathepsin k inhibitor in osteoarthritis: a randomized controlled trial. *Ann. Intern. Med.* **172**, 86–95 (2020).
66. Hunter, D. J. et al. The intensive diet and exercise for arthritis (IDEA) trial: 18-month radiographic and MRI outcomes. *Osteoarthritis Cartilage* **23**, 1090–1098 (2015).
67. Sekiya, I. et al. 3D-MRI analysis of cartilage thickness changes after PRP injection in medial knee osteoarthritis: a preliminary report. *PLoS ONE* **20**, e0321067 (2025).
68. Intema, F. et al. Tissue structure modification in knee osteoarthritis by use of joint distraction: an open 1-year pilot study. *Ann. Rheum. Dis.* **70**, 1441–1446 (2011).
69. Wiegant, K. et al. Sustained clinical and structural benefit after joint distraction in the treatment of severe knee osteoarthritis. *Osteoarthritis Cartilage* **21**, 1660–1667 (2013).
70. van der Woude, J. A. D. et al. Five-year follow-up of knee joint distraction: clinical benefit and cartilaginous tissue repair in an open uncontrolled prospective study. *Cartilage* **8**, 263–271 (2017).
71. Jansen, M. P., Mastbergen, S. C., MacKay, J. W., Turmezei, T. D. & Lafeber, F. Knee joint distraction results in MRI cartilage thickness increase up to 10 years after treatment. *Rheumatology* **61**, 974–982 (2022).
72. Birmingham, T. B. et al. High tibial osteotomy for medial compartment knee osteoarthritis: a randomized trial with parallel preference arm. *Ann. Intern. Med.* **178**, 1238–1248 (2025).
73. Chaudhari, A. S. et al. Five-minute knee MRI for simultaneous morphometry and T2 relaxometry of cartilage and meniscus and for semiquantitative radiological assessment using double-echo in steady-state at 3T. *J. Magn. Reson. Imaging* **47**, 1328–1341 (2018).
74. Eckstein, F. et al. The design of a sample rapid magnetic resonance imaging (MRI) acquisition protocol supporting assessment of multiple articular tissues and pathologies in knee osteoarthritis. *Osteoarthr. Cartil. Open.* **6**, 100505 (2024).
75. Williams, A. A. et al. Reproducibility of quantitative double-echo steady-state T_2 mapping of knee cartilage. *J. Magn. Reson. Imaging* **61**, 784–795 (2025).
76. Wirth, W. et al. Clinical validation of fully automated cartilage transverse relaxation time (T2) and thickness analysis using quantitative DESS magnetic resonance imaging. *MAGMA* **38**, 285–297 (2025).
77. Norman, B., Pedoia, V. & Majumdar, S. Use of 2D U-net convolutional neural networks for automated cartilage and meniscus segmentation of knee MR imaging data to determine relaxometry and morphometry. *Radiology* **288**, 177–185 (2018).
78. Xie, D. et al. Multi-vendor multi-site quantitative MRI analysis of cartilage degeneration 10 years after anterior cruciate ligament reconstruction: MOON-MRI protocol and preliminary results. *Osteoarthritis Cartilage* **30**, 1647–1657 (2022).
79. Wirth, W. & Eckstein, F. A fully-automated technique for cartilage morphometry in knees with severe radiographic osteoarthritis – method development and validation. *Osteoarthr. Cartil. Open.* **7**, 100645 (2025).
80. Yao, Y., Zhong, J., Zhang, L., Khan, S. & Chen, W. Cartimorph: a framework for automated knee articular cartilage morphometrics. *Med. Image Anal.* **91**, 103035 (2024).
81. Eckstein, F., Buck, R. & Wirth, W. Location-independent analysis of structural progression of osteoarthritis-taking it all apart, and putting the puzzle back together makes the difference. *Semin. Arthritis Rheum.* **46**, 404–410 (2017).
82. Wirth, W. et al. Test-retest precision and longitudinal cartilage thickness loss in the IMI-APPROACH cohort. *Osteoarthritis Cartilage* **31**, 238–248 (2023).
83. Eckstein, F. et al. Accuracy and precision of quantitative assessment of cartilage morphology by magnetic resonance imaging at 3.0T. *Arthritis Rheum.* **52**, 3132–3136 (2005).
84. Welsch, G. H. et al. Magnetic resonance imaging of the knee at 3 and 7 Tesla: a comparison using dedicated multi-channel coils and optimised 2D and 3D protocols. *Eur. Radiol.* **22**, 1852–1859 (2012).
85. Cheng, Q. & Zhao, F. C. Comparison of 1.5- and 3.0-T magnetic resonance imaging for evaluating lesions of the knee: a systematic review and meta-analysis (PRISMA-compliant article). *Medicine* **97**, e12401 (2018).
86. Juras, V. et al. Comparison of 3T and 7T MRI clinical sequences for ankle imaging. *Eur. J. Radiol.* **81**, 1846–1850 (2012).
87. Chang, G. et al. MRI of the wrist at 7 Tesla using an eight-channel array coil combined with parallel imaging: preliminary results. *J. Magn. Reson. Imaging* **31**, 740–746 (2014).
88. Friedrich, K. M. et al. In vivo 7.0-Tesla magnetic resonance imaging of the wrist and hand: technical aspects and applications. *Semin. Musculoskelet. Radiol.* **13**, 74–84 (2009).
89. Emanuel, K. S. et al. The relation between the biochemical composition of knee articular cartilage and quantitative MRI: a systematic review and meta-analysis. *Osteoarthritis Cartilage* **30**, 650–662 (2022).
90. Jungmann, P. M. et al. T_2 relaxation time measurements are limited in monitoring progression, once advanced cartilage defects at the knee occur: longitudinal data from the osteoarthritis initiative. *J. Magn. Reson. Imaging* **38**, 1415–1424 (2013).
91. Eck, B. L. et al. Quantitative MRI for evaluation of musculoskeletal disease: cartilage and muscle composition, joint inflammation, and biomechanics in osteoarthritis. *Invest. Radiol.* **58**, 60–75 (2023).
92. Prasad, A. P., Nardo, L., Schooler, J., Joseph, G. B. & Link, T. M. $T_1\rho$ and T_2 relaxation times predict progression of knee osteoarthritis. *Osteoarthritis Cartilage* **21**, 69–76 (2013).
93. Liebl, H. et al. Early T2 changes predict onset of radiographic knee osteoarthritis: data from the Osteoarthritis Initiative. *Ann. Rheum. Dis.* **74**, 1353–1359 (2015).
94. Razmjoo, A. et al. T2 analysis of the entire osteoarthritis initiative dataset. *J. Orthop. Res.* **39**, 74–85 (2021).
95. Joseph, G. B. et al. Elevated cartilage T2 and increased severity of cartilage defects at baseline are associated with the development of knee pain over 7 years. *Osteoarthritis Cartilage* **21**, S185–S186 (2013).
96. Gersing, A. S. et al. Progression of cartilage degeneration and clinical symptoms in obese and overweight individuals is dependent on the amount of weight loss: 48-month data from the Osteoarthritis Initiative. *Osteoarthritis Cartilage* **24**, 1126–1134 (2016).
97. Li, X. & Majumdar, S. Quantitative MRI of articular cartilage and its clinical applications. *J. Magn. Reson. Imaging* **38**, 991–1008 (2013).
98. Li, X. et al. Quantitative MRI using T1ρ and T2 in human osteoarthritic cartilage specimens: correlation with biochemical measurements and histology. *Magn. Reson. Imaging* **29**, 324–334 (2011).
99. Lartey, R. et al. Reproducibility of $T_{1\rho}$ and T_2 quantification in a multi-vendor multi-site study. *Osteoarthritis Cartilage* **31**, 249–257 (2023).
100. Shah, R. P. et al. T1rho magnetic resonance imaging at 3T detects knee cartilage changes after viscosupplementation. *Orthopedics* **38**, e604–e610 (2015).
101. Zhao, X. et al. Multi-compositional MRI evaluation of repair cartilage in knee osteoarthritis with treatment of allogeneic human adipose-derived mesenchymal progenitor cells. *Stem Cell Res. Ther.* **10**, 308 (2019).
102. Xie, D. et al. Baseline cartilage T1ρ and T2 predicted patellofemoral joint cartilage lesion progression and patient-reported outcomes after ACL reconstruction. *J. Orthop. Res.* **41**, 1310–1319 (2023).
103. O'Sullivan, O. et al. Knee MRI biomarkers associated with structural, functional and symptomatic changes at least a year from ACL injury — a systematic review. *Osteoarthr. Cartil. Open.* **5**, 100385 (2023).
104. Kantola, V. et al. Anisotropy of T_2 and $T_{1\rho}$ relaxation time in articular cartilage at 3 T. *Magn. Reson. Med.* **92**, 1177–1188 (2024).
105. Champagne, A. A. et al. Quantitative susceptibility and T1 rho mapping of knee articular cartilage at 3T. *Osteoarthr. Cartil. Open.* **6**, 100509. (2024).
106. Moazamian, D. et al. Quantitative ultrashort echo time magnetization transfer imaging of the osteochondral junction: an in vivo knee osteoarthritis study. *J. Imaging* **11**, 198 (2025).
107. Namiranian, B. et al. Assessment of mechanical properties of articular cartilage with quantitative three-dimensional ultrashort echo time (UTE) cones magnetic resonance imaging. *J. Biomech.* **113**, 110085 (2020).
108. Zhang, M. et al. Simultaneous quantitative susceptibility mapping of articular cartilage and cortical bone of human knee joint using ultrashort echo time sequences. *Front. Endocrinol.* **13**, 844351 (2022).
109. Nykanen, O. et al. T2* and quantitative susceptibility mapping in an equine model of post-traumatic osteoarthritis: assessment of mechanical and structural properties of articular cartilage. *Osteoarthritis Cartilage* **27**, 1481–1490 (2019).
110. Basser, P. J., Mattiello, J. & LeBihan, D. MR diffusion tensor spectroscopy and imaging. *Biophys. J.* **66**, 259–267 (1994).
111. Raya, J. G. Techniques and applications of in vivo diffusion imaging of articular cartilage. *J. Magn. Reson. Imaging* **41**, 1487–1504 (2015).

112. Filidoro, L. et al. High-resolution diffusion tensor imaging of human patellar cartilage: feasibility and preliminary findings. *Magn. Reson. Med.* **53**, 993–998 (2005).
113. Ferizi, U. et al. Diffusion tensor imaging of articular cartilage at 3T correlates with histology and biomechanics in a mechanical injury model. *Magn. Reson. Med.* **78**, 69–78 (2017).
114. Raya, J. G. et al. Feasibility of in vivo diffusion tensor imaging of articular cartilage with coverage of all cartilage regions. *Eur. Radiol.* **24**, 1700–1706 (2014).
115. Guha, A. et al. Spatial variations in magnetic resonance-based diffusion of articular cartilage in knee osteoarthritis. *Magn. Reson. Imaging* **33**, 1051–1058 (2015).
116. Raya, J. G. et al. Articular cartilage: in vivo diffusion-tensor imaging. *Radiology* **262**, 550–559 (2012).
117. Hamilton, J. et al. Robust frequency-dependent diffusional kurtosis computation using an efficient direction scheme, axisymmetric modelling, and spatial regularization. *Imaging Neurosci.* **2**, imag-2-00055 (2024).
118. Wang, F. et al. Motion-robust sub-millimeter isotropic diffusion imaging through motion corrected generalized slice dithered enhanced resolution (MC-gSlider) acquisition. *Magn. Reson. Med.* **80**, 1891–1906 (2018).
119. Bashir, A., Gray, M. L. & Burstein, D. Gd-DTPA2- as a measure of cartilage degradation. *Magn. Reson. Med.* **36**, 665–673 (1996).
120. Burstein, D. et al. Protocol issues for delayed Gd(DTPA)$^{2-}$-enhanced MRI (dGEMRIC) for clinical evaluation of articular cartilage. *Magn. Reson. Med.* **45**, 36–41 (2001).
121. van Tiel, J. et al. Is T1ρ mapping an alternative to delayed gadolinium-enhanced MR imaging of cartilage in the assessment of sulphated glycosaminoglycan content in human osteoarthritic knees? An in vivo validation study. *Radiology* **279**, 523–531 (2016).
122. van Tiel, J. et al. Reproducibility of 3D delayed gadolinium enhanced MRI of cartilage (dGEMRIC) of the knee at 3.0 T in patients with early stage osteoarthritis. *Eur. Radiol.* **23**, 496–504 (2013).
123. Mamisch, T. C. et al. Delayed gadolinium-enhanced magnetic resonance imaging of cartilage (dGEMRIC) in femoacetabular impingement. *J. Orthop. Res.* **29**, 1305–1311 (2011).
124. Domayer, S. E. et al. Delayed gadolinium-enhanced MRI of cartilage in the ankle at 3 T: feasibility and preliminary results after matrix-associated autologous chondrocyte implantation. *J. Magn. Reson. Imaging* **31**, 732–739 (2010).
125. Kogan, F., Hargreaves, B. A. & Gold, G. E. Volumetric multislice gagCEST imaging of articular cartilage: optimization and comparison with T1rho. *Magn. Reson. Med.* **77**, 1134–1141 (2017).
126. Watkins, L. E. et al. Rapid volumetric gagCEST imaging of knee articular cartilage at 3 T: evaluation of improved dynamic range and an osteoarthritic population. *NMR Biomed.* **33**, e4310 (2020).
127. Soellner, S. T. et al. gagCEST imaging at 3 T MRI in patients with articular cartilage lesions of the knee and intraoperative validation. *Osteoarthritis Cartilage* **29**, 1163–1172 (2021).
128. Zbyn, S. et al. Changes in tissue sodium concentration and sodium relaxation times during the maturation of human knee cartilage: ex vivo (23) Na MRI study at 10.5 T. *Magn. Reson. Med.* **91**, 1099–1114 (2024).
129. Newbould, R. D. et al. T1-weighted sodium MRI of the articulator cartilage in osteoarthritis: a cross sectional and longitudinal study. *PLoS ONE* **8**, e73067 (2013).
130. Muller-Lutz, A. et al. Sodium MRI of human articular cartilage of the wrist: a feasibility study on a clinical 3T MRI scanner. *MAGMA* **34**, 241–248 (2021).
131. Borthakur, A. et al. Sensitivity of MRI to proteoglycan depletion in cartilage: comparison of sodium and proton MRI. *Osteoarthritis Cartilage* **8**, 288–293 (2000).
132. Trattnig, S. et al. Na-23 MR imaging at 7 T after knee matrix-associated autologous chondrocyte transplantation: preliminary results. *Radiology* **257**, 175–184 (2010).
133. Mosher, T. J. Quantitative cartilage T2 and T1rho mapping: is there a clinical role? From the *AJR* special series on quantitative imaging. *Am. J. Roentgenol.* **224**, e2431655 (2025).
134. Li, X. et al. Cartilage compositional MRI — a narrative review of technical development and clinical applications over the past three decades. *Skeletal Radiol.* **53**, 1761–1781 (2024).
135. Shao, H. et al. Magic angle effect plays a major role in both T1rho and T2 relaxation in articular cartilage. *Osteoarthritis Cartilage* **25**, 2022–2030 (2017).
136. Desai, A. D. et al. The International Workshop on Osteoarthritis Imaging knee MRI segmentation challenge: a multi-institute evaluation and analysis framework on a standardized dataset. *Radiol. Artif. Intell.* **3**, e200078 (2021).
137. Li, H. et al. SuperMAP: deep ultrafast MR relaxometry with joint spatiotemporal undersampling. *Magn. Reson. Med.* **89**, 64–76 (2023).
138. Kim, J. et al. Multi-vendor multi-site $T_{1\rho}$ and T_2 quantification of knee cartilage. *Osteoarthritis Cartilage* **28**, 1539–1550 (2020).
139. Chalian, M. et al. The QIBA profile for MRI-based compositional imaging of knee cartilage. *Radiology* **301**, 423–432 (2021).
140. Link, T. M., Joseph, G. B. & Li, X. MRI-based $T_{1\rho}$ and T_2 cartilage compositional imaging in osteoarthritis: what have we learned and what is needed to apply it clinically and in a trial setting? *Skeletal Radiol.* **52**, 2137–2147 (2023).
141. Omoumi, P. Imaging of cartilage, meniscus, and beyond: role of magnetic resonance imaging (MRI) and computed tomography (CT). *Osteoarthr. Imaging* **5**, 1002268 (2025).
142. El-Khoury, G. Y. et al. Cartilage thickness in cadaveric ankles: measurement with double-contrast multi-detector row CT arthrography versus MR imaging. *Radiology* **233**, 768–773 (2004).
143. Wyler, A. et al. Comparison of MR-arthrography and CT-arthrography in hyaline cartilage-thickness measurement in radiographically normal cadaver hips with anatomy as gold standard. *Osteoarthritis Cartilage* **17**, 19–25 (2009).
144. Omoumi, P., Rubini, A., Dubuc, J. E., Vande Berg, B. C. & Lecouvet, F. E. Diagnostic performance of CT-arthrography and 1.5T MR-arthrography for the assessment of glenohumeral joint cartilage: a comparative study with arthroscopic correlation. *Eur. Radiol.* **25**, 961–969 (2015).
145. Mutschler, C. et al. Postoperative meniscus: assessment at dual-detector row spiral CT arthrography of the knee. *Radiology* **228**, 635–641 (2003).
146. Vande Berg, B. C. et al. Anterior cruciate ligament tears and associated meniscal lesions: assessment at dual-detector spiral CT arthrography. *Radiology* **223**, 403–409 (2002).
147. Mourad, C. et al. Chances and challenges of photon-counting CT in musculoskeletal imaging. *Skeletal Radiol.* **53**, 1889–1902 (2024).
148. Wilson, M. P. et al. Diagnostic accuracy of dual-energy CT for the detection of bone marrow edema in the appendicular skeleton: a systematic review and meta-analysis. *Eur. Radiol.* **31**, 1558–1568 (2021).
149. Bernabei, I. et al. Multi-energy photon-counting computed tomography versus other clinical imaging techniques for the identification of articular calcium crystal deposition. *Rheumatology* **60**, 2483–2485 (2021).
150. Turmezei, T. D. Quantitative assessment of the knee joint from weight bearing CT. *Osteoarthr. Imaging* **4**, 100177 (2024).
151. Hilbert, T., Omoumi, P., Raudner, M. & Kober, T. Synthetic contrasts in musculoskeletal MRI: a review. *Invest. Radiol.* **58**, 111–119 (2023).
152. Brett, A., Bowes, M. A. & Conaghan, P. G. Comparison of 3D quantitative osteoarthritis imaging biomarkers from paired CT and MR images: data from the IMI-APPROACH study. *BMC Musculoskelet. Disord.* **24**, 76 (2023).
153. Babel, H. et al. Three-dimensional quantification of bone mineral density in the distal femur and proximal tibia based on computed tomography: in vitro evaluation of an extended standardization method. *J. Clin. Med.* **10**, 160 (2021).
154. Omoumi, P. et al. Proximal tibial osteophyte volumes are correlated spatially and with knee alignment: a quantitative analysis suggesting the influence of biochemical and mechanical factors in the development of osteophytes. *Osteoarthritis Cartilage* **29**, 1691–1700 (2021).
155. Pena, J. A. et al. Dose-efficient assessment of trabecular microstructure using ultra-high-resolution photon-counting CT. *Z. Med. Phys.* **32**, 403–416 (2022).
156. Margain, P., Favre, J., Jolles, B. M. & Omoumi, P. Standardized maps — an emerging approach to leverage quantitative information in knee imaging. *Osteoarthr. Imaging* **4**, 100251 (2024).
157. Jeon, O. H. et al. Local clearance of senescent cells attenuates the development of post-traumatic osteoarthritis and creates a pro-regenerative environment. *Nat. Med.* **23**, 775–781 (2017).
158. Cai, Y. et al. Elimination of senescent cells by β-galactosidase-targeted prodrug attenuates inflammation and restores physical function in aged mice. *Cell Res.* **30**, 574–589 (2020).
159. Suryadevara, V. et al. [18F]FPyGal PET tracer detects senescence in human osteoarthritic specimens. *Osteoarthr. Imaging* **4**, 100205 (2024).
160. Nernekli, K. et al. MRI detection of senescent cells in porcine knee joints with a β-galactosidase responsive Gd-chelate. *npj Imaging* **3**, 18 (2025).
161. Piert, M. et al. Assessment of porcine bone metabolism by dynamic [18^F]-fluoride ion PET: correlation with bone histomorphometry. *J. Nucl. Med.* **42**, 1091–1100 (2001).
162. Messa, C. et al. Bone metabolic activity measured with positron emission tomography and [18F]fluoride ion in renal osteodystrophy: correlation with bone histomorphometry. *J. Clin. Endocrinol. Metab.* **77**, 949–955 (1993).
163. Watkins, L. et al. Assessment of quantitative [^{18}F]Sodium fluoride PET measures of knee subchondral bone perfusion and mineralization in osteoarthritic and healthy subjects. *Osteoarthritis Cartilage* **29**, 849–858 (2021).
164. Kogan, F. et al. Quantitative imaging of bone-cartilage interactions in ACL-Injured patients with PET-MRI. *Osteoarthritis Cartilage* **26**, 790–796 (2018).
165. Savic, D. et al. Imaging bone-cartilage interactions in osteoarthritis using [^{18}F]-NaF PET-MRI. *Mol. Imaging* **15**, 1–12 (2016).
166. Bhattacharjee, R. et al. The relationships between patellofemoral bone remodeling, cartilage composition, and vertical loading rate: PET/MRI in isolated patellofemoral osteoarthritis. *Osteoarthritis Cartilage* **32**, 1591–1600 (2024).
167. Haddock, B. et al. Assessment of acute bone loading in humans using [^{18}F]NaF PET/MRI. *Eur. J. Nucl. Med. Mol. Imaging* **46**, 2452–2463 (2019).
168. Bruce, O. L., Goyal, A., Gatti, A. A. & Kogan, F. Spatial correspondence between [^{18}F]NaF PET uptake and bone strain in the tibia. In *Proc. 34th Annual Meeting of ISMRM* (ISMRM, 2025).
169. Watkins, L. E. et al. [^{18}F]Sodium fluoride PET-MRI detects increased metabolic bone response to whole-joint loading stress in osteoarthritic knees. *Osteoarthritis Cartilage* **30**, 1515–1525 (2022).
170. Kauppinen, K. et al. Ultrasonographic assessment of the normal femoral articular cartilage of the knee joint: comparison with 3D MRI. *ScientificWorldJournal* **2021**, 9978819 (2021).
171. Harkey, M. S., Driban, J. B., Kuenze, C., Zhang, M. & Salzler, M. J. Pre-operative femoral cartilage ultrasound characteristics are altered in people who report symptoms at 1 year after anterior cruciate ligament reconstruction. *Ultrasound Med. Biol.* **47**, 1976–1984 (2021).
172. Saarakkala, S. et al. Diagnostic performance of knee ultrasonography for detecting degenerative changes of articular cartilage. *Osteoarthritis Cartilage* **20**, 376–381 (2012).
173. Podlipska, J. et al. Comparison of diagnostic performance of semi-quantitative knee ultrasound and knee radiography with MRI: Oulu Knee Osteoarthritis Study. *Sci. Rep.* **6**, 22365 (2016).
174. Nevalainen, M. T. et al. Ultrasonography of the late-stage knee osteoarthritis prior to total knee arthroplasty: comparison of the ultrasonographic, radiographic and intra-operative findings. *Sci. Rep.* **8**, 17742 (2018).

175. Torp-Pedersen, S., Bartels, E. M., Wilhjelm, J. & Bliddal, H. Articular cartilage thickness measured with US is not as easy as it appears: a systematic review of measurement techniques and image interpretation. *Ultraschall Med.* **32**, 54–61 (2011).
176. Sorriento, A. et al. Quantitative ultrasound classification of healthy and chemically degraded ex-vivo cartilage. *Sci. Rep.* **15**, 20760 (2025).
177. Fransen, S. J., Roest, C., Simonis, F. F., Yakar, D. & Kwee, T. C. The scientific evidence of commercial AI products for MRI acceleration: a systematic review. *Eur. Radiol.* **35**, 4736–4746 (2025).
178. Wirth, W. et al. Accuracy and longitudinal reproducibility of quantitative femorotibial cartilage measures derived from automated U-Net-based segmentation of two different MRI contrasts: data from the Osteoarthritis Initiative healthy reference cohort. *Magn. Reson. Mater. Phys. Biol. Med.* **34**, 337–354 (2021).
179. Yeoh, P. S. Q. et al. Emergence of deep learning in knee osteoarthritis diagnosis. *Computational Intell. Neurosci.* **2021**, 4931437 (2021).
180. Tack, A. & Zachow, S. Accurate automated volumetry of cartilage of the knee using convolutional neural networks: data from the Osteoarthritis Initiative. In *Proc. 2019 IEEE 16th International Symposium on Biomedical Imaging (ISBI 2019)* 40–43 (IEEE, 2019).
181. Guo, J. et al. Automated measurement and grading of knee cartilage thickness: a deep learning-based approach. *Front. Med.* **11**, 1337993 (2024).
182. Zhang, L. et al. Multi-level classification of knee cartilage lesion in multimodal MRI based on deep learning. *Biomed. Signal. Process. Control.* **83**, 104687 (2023).
183. Tang, X. et al. Fully automatic knee joint segmentation and quantitative analysis for osteoarthritis from magnetic resonance (MR) images using a deep learning model. *Med. Sci. Monit.* **28**, e936733–936731 (2022).
184. Goyal, A. et al. Automating imaging biomarker analysis for knee osteoarthritis using an open-source MRI-based deep learning pipeline. *Osteoarthr. Imaging* **5**, 100288 (2025).
185. Sun, C. et al. Evaluation of the consistency of the MRI-based AI segmentation cartilage model using the natural tibial plateau cartilage. *J. Orthop. Surg. Res.* **19**, 247 (2024).
186. Niu, Z., Ouyang, S., Xie, S., Chen, Y. -w & Lin, L. A survey on domain generalization for medical image analysis. Preprint at *arXiv* https://doi.org/10.48550/arXiv.2402.05035 (2024).
187. Liu, F. et al. Deep learning approach for evaluating knee MR images: achieving high diagnostic performance for cartilage lesion detection. *Radiology* **289**, 160–169 (2018).
188. Huo, J. et al. Automatic grading assessments for knee MRI cartilage defects via self-ensembling semi-supervised learning with dual-consistency. *Med. Image Anal.* **80**, 102508 (2022).
189. Marques, M. L. et al. Atlas for the CT Syndesmophyte Score (CTSS) in patients with axial spondyloarthritis. *RMD Open* **10**, e003702 (2024).
190. Wu, H. et al. Axial spondyloarthritis: dual-energy virtual noncalcium CT in the detection of bone marrow edema in the sacroiliac joints. *Radiology* **290**, 157–164 (2019).
191. Kroon, F. P. B. et al. development and reliability of the OMERACT thumb base osteoarthritis magnetic resonance imaging scoring system. *J. Rheumatol.* **44**, 1694–1698 (2017).

Author contributions

The authors contributed equally to all aspects of the article.

Competing interests

A.G. is the president and co-owner of Boston Core Imaging Lab (BICL), LLC., a company that provides image assessment devices to academia and the pharmaceutical industry; has received consulting fees from TissueGene, Novartis, ICM, Paradigm, Formation Bio, 4Moving, Scarcell Therapeutics, Pacira, Coval, Medipost, Levicept and Peptinov; is the co-editor-in-chief of *Skeletal Radiology*. F.E. is the co-owner and CEO of Chondrometrics GmbH, a company that provides MR image analysis services to academic researchers and to the pharmaceutical industry; has provided consulting services to MerckSerono, Galapagos/Servier, Kolon Tissue Gene, Novartis, Peptinov, Formation Bio, 4P Pharma, Sanofi and Artialis. D.H. has received publication royalties from Wolters Kluwer. S.N. has received lecture honoraria by Bayer Vital AG. E.H.G.O. has received research support from GE Healthcare. W.W. is in part-time employment with Chondrometrics GmbH and is a co-owner of Chondrometrics GmbH. F.W.R. is the CMO, director of research and shareholder of Boston Imaging Core Lab (BICL), LLC. F.W.R. is editor-in-chief of *Osteoarthritis Imaging*. G.G., M.J., F.K., X.L., T.M.L., P.O., S.S. and S.T. declare no competing interests.

Additional information

Supplementary information The online version contains supplementary material available at https://doi.org/10.1038/s41584-026-01353-x.

Peer review information *Nature Reviews Rheumatology* thanks Ichiro Sekiya, Vladimir Juras and Mikko Nissi for their contribution to the peer review of this work.

Review criteria A non-systematic literature search was performed using PubMed, starting with a list of terms including the title of the current manuscript, followed by multiple search terms including but not limited to "imaging", "cartilage", "quantitative", "semiquantitative", "joint", "whole organ", "joint tissue", "joint structure", "assessment", "score", "measure", "compositional MRI", "computed tomography", "ultrasound", "metabolic imaging", "PET", "ultrashort echo time imaging", "diffusion imaging", "T2 Mapping", "T1rho", "delayed gadolinium enhanced MRI of cartilage", "arthrography", "reliability", "artificial intelligence" and possible variants for each. The focus of the literature search was on articles published in the past 5 years. Results of the search were reviewed by the first and last authors to determine the relevance of the selected publications for the focus topic of this manuscript. All authors of this article made a joint decision on which articles to include and considered the most relevant. Finally, to receive broad and detailed input, informal (that is, non-structured) consultations were held with domain experts in various research areas. The identified methodologies, findings, concepts and recommendations were then organized into a systematic framework, providing an overview of advances in cartilage imaging, considering the state-of-the-art of current imaging science.

[1]Chobanian and Avedisian School of Medicine, Boston University, Boston, MA, USA. [2]Department of Radiology, VA Boston Healthcare System, West Roxbury, MA, USA. [3]Research Program for Musculoskeletal Imaging, Center for Anatomy and Cell Biology Paracelsus Medical University (PMU), Salzburg, Austria. [4]Chondrometrics GmbH, Freilassing, Germany. [5]Department of Radiology, Stanford University, Stanford, CA, USA. [6]Department of Radiology, Tufts University School of Medicine, Boston, MA, USA. [7]Department of Radiology, Massachusetts General Hospital, Harvard Medical School, Boston, MA, USA. [8]Program of Advanced Musculoskeletal Imaging, Departments of Biomedical Engineering and Diagnostic Radiology, Cleveland Clinic, Cleveland, OH, USA. [9]Department of Radiology, University of California at San Francisco, San Francisco, CA, USA. [10]Department of Diagnostic and Interventional Radiology, University Hospital Aachen, Aachen, Germany. [11]Department of Radiology and Nuclear Medicine, Erasmus MC, University Medical Center, Rotterdam, The Netherlands. [12]Department of Radiology, Lausanne University Hospital and University of Lausanne, Lausanne, Switzerland. [13]Research Unit of Health Sciences and Technology, University of Oulu, Oulu, Finland. [14]Department of Diagnostic Radiology, Oulu University Hospital, Oulu, Finland. [15]Department of Biomedical Imaging and Image Guided Therapy, Medical University of Vienna, Vienna, Austria. [16]Department of Radiology, Universitätsklinikum, Erlangen, Germany. [17]Friedrich-Alexander-Universität Erlangen-Nürnberg (FAU), Erlangen, Germany.

nature reviews rheumatology

https://doi.org/10.1038/s41584-025-01351-5

Expert recommendation

Check for updates

Recommendations for the use of CLASI as an outcome measure in cutaneous lupus erythematosus clinical trials

Grace Lu[1], Tyler Cepica[1], Catherine Barbey[2], Ilimbek Beketaev[3], Denesh Chitkara[4], Anthony P. Fernandez[5], Shimon Korish[6], Joseph F. Merola[1], Jill A. Lindstrom[7], Nikolay P. Nikolov[8], Hoang Nguyen[9], Christopher T. Richardson[10], Teodora P. Staeva[9], Victoria P. Werth[11,12] & Benjamin F. Chong[1] ✉ on behalf of the Lupus Accelerating Breakthroughs Consortium CLASI Working Group*

Abstract

Cutaneous lupus erythematosus (CLE) is an autoimmune skin condition associated with a considerable treatment burden and diminished quality of life. The absence of a consensus outcome measure to evaluate therapeutic response has posed a challenge to CLE drug development. The Cutaneous Lupus Erythematosus Disease Area and Severity Index (CLASI) was developed in response to this need, incorporating morphological components including erythema, scale, dyspigmentation and scarring, to reflect disease activity and damage. Numerous studies have demonstrated the utility of CLASI in capturing relevant aspects of disease from clinician- and patient-based perspectives; however, no regulatory precedent for use of clinical trial data employing CLASI to evaluate treatment response in CLE exists. Thus, the Lupus Accelerating Breakthroughs Consortium commissioned a working group of members from industry, academia, the US Food and Drug Administration (FDA) and CLE patient advocates to address the potential knowledge gaps with CLASI through evidence-based research. Upon reviewing and submitting these data to the FDA, the working group reached alignment that CLASI is a suitable outcome measure for CLE clinical trials, enabling a clearer regulatory path for clinical drug development. The group recognizes the need for additional information to assess what degree of change in CLASI captures clinically meaningful improvement.

Sections

Introduction

Creation of the CLASI working group

Rationale for use of the CLASI in clinical trials

Progress and recommendations of the Lupus ABC CLASI working group

Conclusions

A full list of affiliations appears at the end of the paper. *A list of authors and their affiliations appears at the end of the paper. ✉e-mail: Ben.Chong@UTSouthwestern.edu

Introduction

Cutaneous lupus erythematosus (CLE) is an inflammatory skin condition that poses a notable challenge for both clinicians and patients. Not only do people with CLE experience a lower quality of life[1] but they also face considerable barriers in treatment owing to limited therapeutic options. So far, hydroxychloroquine is the only medication that has been approved for CLE by the FDA in the past 70 years. Although numerous clinical trials are currently underway to address this need, there has been a lack of consensus regarding an outcome measure for evaluating CLE disease activity[2]. Having an agreed-upon outcome measure is critical for establishing consistency in inclusion criteria and for assessment of therapeutic response in CLE clinical trials. Various provider-reported outcome measures have been utilized in CLE clinical trials (Table 1), but several have limitations in their ability to capture partial response to therapy, differentiate the extent of disease severity and incorporate a diverse spectrum of CLE manifestations[3–5].

Of the existing candidate outcome measures, the Cutaneous Lupus Erythematosus Disease Area and Severity Index (CLASI) has been utilized in an increasing number of CLE clinical trials and clinical research studies[6–13]. This validated instrument evaluates CLE disease activity (CLASI-A) and damage (CLASI-D) on the basis of the severity and distribution of skin lesions. CLASI-A, which provides a score ranging from 0 to 70, assesses the severity of erythema and scale in 13 locations, non-scarring alopecia and mucosal involvement, with less weight applied to the latter two components. CLASI-D, which provides a score ranging from 0 to 56, assesses the severity of dyspigmentation and scarring and/or atrophy in 13 locations, and scarring alopecia, with the scores for dyspigmentation doubling when this feature has been

Table 1 | Recent clinical trials in CLE with corresponding outcome measures

Outcome measure	Investigational drugs	Description	Advantages	Limitations
SLE disease activity instruments				
BILAG	Abatacept[52], anifrolumab[53], atacicept[54], belimumab[8], CNTO 136[55], dapirolizumab[56], etanercept[57], lifitilimab[58], M5049[59], milatuzumab[60], rituximab[61], tofacitinib[62]	Measures systemic activity across nine domains that are weighted by impression of disease progression Mucocutaneous manifestations include presence of skin eruption, mucosal ulcers, panniculitis/bullous lupus, chilblains, and alopecia	Comprehensive evaluation of organ involvement that incorporates rare skin manifestations, such as bullous lupus and panniculitis Widely used in research and clinical trials	Limited ability to capture partial response Improvement relies on assessor's recall of disease progression Time-consuming and complex to administer and has limited utility beyond research settings
SLEDAI, SLEDAI-2K, SELENA-SLEDAI	Belimumab[8], CNTO 136[55], dapirolizumab[56], etanercept[57], KRP203[63], lifitilimab[58,64], M5049[59], mezagitamab[65], tofacitinib[62], ustekinumab[50]	Measures systemic activity through physical examination findings and laboratory values that are weighted by type of manifestation Skin lesions are scored by the presence or absence of inflammatory-type rash, alopecia, and mucosal ulcers	Simple to score and can be utilized in clinical practice Widely used in research and clinical trials	Incorporates a limited spectrum of skin manifestations Cannot capture partial improvement in skin disease or classify disease severity
Skin-specific instruments				
CLASI	Anifrolumab[7,66], baricitinib[67], belimumab[8], branebrutinib[68], CNTO 136[55], dapirolizumab[56], daxdilimab[69], deucravacitinib[49], edecesertib[70], filgotinib[71], iberdomide[11], KRP203[63], lanraplenib[71], lifitilimab[58,64], M5049[59], mezagitamab[65], RSLV-132[72], SAR443122[73], tofacitinib[62], VIB7734[74], ustekinumab[50]	Scores disease activity and damage based on severity and distribution of skin lesions	Demonstrated strong content and construct validity, and inter- and intra-rater reliability Correlates with patient quality of life Can be used by dermatologists and non-dermatologists	Does not sufficiently capture disease activity in rare CLE subtypes such as bullous SLE and lupus panniculitis
CLA-IGA	Anifrolumab[66], edecesertib[70], lifitilimab[64], M5049[59], SAR443122[73]	Scores skin disease activity on a five-point Likert scale with defined gradations of erythema and other morphologies	Easily interpreted by clinicians and patients Can be utilized in presentations with a low body surface area or when assessing specific lesions	Unable to capture subtle changes in disease activity Needs more validation studies in CLE patient cohorts Minimum CLA-IGA erythema requirements might exclude patients with darker skin types
RCLASI	Fumaderm[75], GSK2646264[76]	Revised version of the CLASI that incorporates additional morphological components into the activity score	Incorporates morphology associated with rarer CLE subtypes, including tumid lupus and lupus panniculitis Demonstrated good inter- and intra-rater reliability	Extensive nature of the instrument limits its use in clinical trials Incomplete validation data

BILAG, British Isles Lupus Assessment Group Index; CLA-IGA, Cutaneous Lupus Activity Investigator Global Assessment; CLE, cutaneous lupus erythematosus; CLASI, Cutaneous Lupus Erythematosus Disease Area and Severity Index; RCLASI, Revised Cutaneous Lupus Erythematosus Disease Area and Severity Index; SELENA-SLEDAI, Safety of Estrogens in Lupus National Assessment–Systemic Lupus Erythematosus Disease Activity Index; SLE, systemic lupus erythematosus; SLEDAI, Systemic Lupus Erythematosus Disease Activity Index; SLEDAI-2K, Systemic Lupus Erythematosus Disease Activity Index 2000.

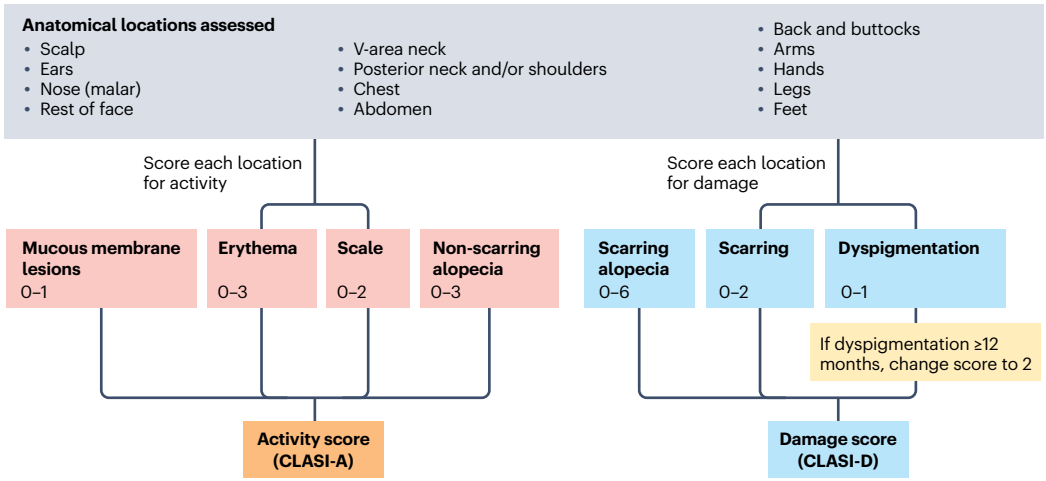

Fig. 1 | Overview of the CLASI. The Cutaneous Lupus Erythematosus Disease Activity and Severity Index (CLASI) is a clinician-assessed skin disease severity score consisting of activity and damage domains. The presence of erythema and scale and/or hypertrophy in 13 body locations (including the scalp, ears, nose, rest of face, V-area neck, posterior neck and/or shoulders, chest, abdomen, back and buttocks, arms, hands, legs and feet), mucous membrane lesions and alopecia contribute towards the activity score. The extent of dyspigmentation and scarring, atrophy, or panniculitis in the same 13 body locations, and scarring alopecia, contribute towards the damage score. Scoring of these activity and damage components are weighted more towards the head and neck areas, given the higher propensity of cutaneous lupus erythematosus in these body sites.

present for at least 12 months[14] (Fig. 1). The scoring of activity and damage is weighted more heavily for the head and neck than for other areas owing to the higher prevalence of CLE in these regions.

A growing body of evidence affirms the value of CLASI as a disease outcome measure. Multiple publications have demonstrated its excellent content validity, construct validity, as well as inter- and intra-rater reliability[5,14–16]. Studies have also affirmed its correlation with disease severity and with clinically meaningful improvement in disease activity[17]. CLASI has also been shown to reflect aspects of disease identified as important for patients in qualitative interviews and to correlate with numerous patient-reported outcome measures in several cohort studies[18–24]. Consequently, the existing literature provides a compelling case for the use of CLASI as an outcome measure in CLE clinical trials. In this Expert Recommendation, we describe the creation of the CLASI working group and its rationale for supporting the use of CLASI in clinical trials, including its ability to assess important clinical aspects of CLE, evaluate CLE lesion morphology, perform consistently across skin types and CLE subtypes and define clinically meaningful CLE improvement.

Creation of the CLASI working group

The Lupus Accelerating Breakthroughs Consortium (ABC), formed under the Lupus Research Alliance, is a public–private partnership with experts from industry and academia, patient advocates, FDA and NIH staff, and representatives of professional societies that seeks to address important challenges in lupus drug development[25]. From its inception, the consortium recognized that the lack of an endorsed primary outcome measure for CLE presents a substantial barrier to drug development and considered addressing this gap as one of its highest priorities. Lupus ABC commissioned a CLE exploratory committee composed of members from each of the aforementioned groups (see list of members in the Supplementary Information), which was first tasked to agree upon a primary outcome measure for assessing disease severity in CLE for further investigation. Multiple different outcome measures for assessing CLE disease activity were reviewed, including the British Isles Lupus Assessment Group Index (BILAG), Systemic Lupus Erythematosus Disease Activity Index (SLEDAI) and its derivatives, Cutaneous Lupus Activity Investigator Global Assessment (CLA-IGA), CLASI and the revised CLASI (RCLASI) (Table 1). BILAG and SLEDAI are composite disease activity instruments for systemic lupus erythematosus (SLE), whereas CLASI and CLA-IGA are skin-specific instruments. BILAG assesses mucocutaneous manifestations based on the investigator's impression of disease progression, measured by the presence of skin eruption, mucosal ulcers, panniculitis and/or bullous lupus, chilblains and alopecia[26]. SLEDAI and its derivatives have a fixed weight for each systemic manifestation, with skin lesions being scored by the presence or absence of inflammatory-type rash, alopecia and mucosal ulcers[27–29]. CLA-IGA scores global skin disease activity on a five-point Likert scale with defined gradations of erythema and other skin morphology[30]. RCLASI is a revised version of the CLASI that incorporates additional morphological components such as oedema and subcutaneous nodules into the activity score[31].

Upon consideration of these outcome measures, the CLE exploratory committee unanimously supported CLASI as the best outcome measure for evaluating therapeutic efficacy in CLE. Reasons cited by the group's members included its strong psychometric properties, sensitivity to changes in disease activity, ease of use by providers from multiple subspecialties, experience in multiple clinical studies and ability to assess a variety of skin manifestations of CLE. Furthermore, several limitations were identified in the other examined outcome measures, including an inability to capture a partial treatment response, extensive scoring metrics that limit potential use and incorporation of a limited spectrum of skin manifestations (Table 1). Consequently, a working group on CLASI was established with the primary objectives of understanding the potential limitations of CLASI, compiling research data to help to address the potential gaps and optimizing the use of CLASI as an outcome measure for CLE clinical trials (Fig. 2).

The working group seized the opportunity to collaborate and collectively identify and address the potential limitations of CLASI as

a primary end point in CLE clinical trials. These concerns included the ability of CLASI to address relevant clinical aspects of disease, given its emphasis on erythema; address CLE lesion morphology; perform consistently across the spectrum of skin pigmentation; assess disease activity across CLE subtypes; and define clinically meaningful CLE improvement (Table 2).

Rationale for use of the CLASI in clinical trials

The chairpersons of the working group (B.F.C. and D.C.) requested members (see Supplementary Information) to provide published and/or unpublished data and written responses pertinent to each of the five primary concerns listed above. These data and responses were presented at eight virtual working group meetings for review and feedback between January and November 2024 (Fig. 2). The following details represent a summary of the data compiled by the working group.

Erythema affects patient quality of life and mirrors other aspects of disease activity

Given that erythema is the most heavily weighted component in the scoring of CLASI-A, there were concerns regarding whether erythema reflected aspects of disease activity that were relevant to patients. However, data from qualitative studies, literature reviews and longitudinal cohort studies have affirmed its relevance from the patient perspective. Patient quality-of-life interviews and literature reviews identified erythema as the most cited indicator of disease[24,32]. In a prospective multi-centre study of 131 patients, CLASI-A erythema scores correlated directly with multiple patient-reported outcomes at baseline, including those examined in the CLE Quality of Life index (CLE-QoL)[33], Dermatology Life Quality Index (DLQI)[34], Analogue Pain, Itch, and Fatigue Score (APIFS)[35] and Patient Impression of Disease Progression[36]. These patient-reported outcome measures encompass various quality-of-life domains, including function, emotion and body image, as well as symptoms such as pain, itch and fatigue. Furthermore, change in erythema was associated with patient impression of disease progression after 6 months in a prospective cohort study of 107 patients with CLE, affirming its ability to capture important aspects of disease progression from the patient perspective[36].

Beyond patient outcomes, erythema has also been shown to correlate with other relevant aspects of disease. Immunohistochemical studies have demonstrated a direct correlation between higher CLASI-A total scores and increased cutaneous inflammation, as measured by several inflammatory biomarkers such as MxA and CD45[9]. Furthermore, both observational studies and clinical trial data have demonstrated that trends in CLASI-A erythema scores mirror those of CLASI-A scale and alopecia scores over time[37–39]. Consequently, the aggregate data affirm the association between erythema and patient-reported outcomes, as well as other relevant aspects of CLE disease, justifying its weight in CLASI-A scoring.

CLASI incorporates various morphological elements that represent activity and damage

The incorporation of meaningful and easily assessed morphological characteristics has been a priority in evaluating CLE lesions for both activity and damage since the development of CLASI in 2005[14]. As part of its scoring system, CLASI requires raters to assess erythema and scale for activity and pigmentary changes and scarring for damage across relevant body regions. In addition to erythema, scale and hypertrophy are key secondary characteristics observed in many CLE subtypes and indicate areas of active inflammation, whereas dyspigmentation and scarring represent damage resulting from prior inflammation[40].

These features convey important morphological information, with patients identifying them in qualitative interviews as important markers of CLE activity and damage[24]. To ensure broad usability among various providers and disciplines, the morphological features assessed by CLASI are designed to be easily recognizable, with good inter- and intra-rater reliability. Notably, CLASI-A and CLASI-D have demonstrated excellent inter- and intra-rater reliability among both dermatologists and rheumatologists[14,16,41].

Other morphological features of CLE such as crusting and erosions are less frequently observed during physical examinations, hold less importance for patients and are more challenging for non-dermatology-trained providers to identify. Consequently, the inclusion of scale, hypertrophy, pigmentary changes and scarring in CLASI provides a robust framework for assessing the morphology of CLE activity and damage.

CLASI performs consistently across the spectrum of skin pigmentation

Incorporating diverse patient populations in clinical trials is critical for the development of safe, equitable and efficacious pharmacological treatments. Consequently, having outcome measures that perform similarly in patients with varying degrees of skin pigmentation is an essential component of clinical trial design. Differences in erythema scoring have been noted in patients with CLE with different degrees of skin pigmentation in a cross-sectional study of 377 patients. Among patients with mild CLE, Black individuals were more likely to be scored as having pink erythema than red erythema than white individuals. However, in patients with moderate-to-severe CLE, most Black and white individuals were scored as having red erythema, indicating that CLASI adequately assesses moderate-to-severe disease across

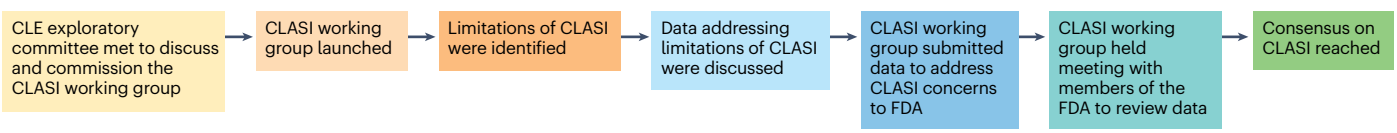

Fig. 2 | Key actions of the Lupus ABC CLASI working group. In November and December 2023, a cutaneous lupus erythematosus (CLE) exploratory committee commissioned by the Lupus Accelerating Breakthroughs Consortium (Lupus ABC) met to discuss and formally commission a Cutaneous Lupus Erythematosus Area and Severity Index (CLASI) working group. The Lupus ABC CLASI working group was officially launched in January 2024. Over the subsequent months, the CLASI working group compiled published data, unpublished data and written responses to address key points supporting the use of CLASI in clinical trials. These data were then submitted to the US Food and Drug Adminsitration (FDA) in June 2024 for the FDA's internal review. In August 2024, select representatives from the CLASI working group held a meeting with members of the FDA to further explain the data and responses as well as answer any additional questions, and consensus on CLASI was reached in November 2024. From the inception of the working group to a unified consensus on CLASI, the CLASI working group met officially on eight different occasions.

Table 2 | Addressing the potential limitations for the use of the CLASI in clinical trials

Potential knowledge gap	Summary of working group assessment	Refs.
Does erythema address the most important components of disease from the patient's perspective?	Erythema correlates with various patient-reported outcomes and mirrors other aspects of disease activity, including scale, alopecia and inflammation	9,36–39
Does CLASI address lesion morphology?	CLASI incorporates scale and hypertrophy; other elements of morphology are less important to patients, not frequently present and can be difficult to assess by non-dermatologists	24
Does CLASI perform consistently across the spectrum of skin pigmentation?	The degree of improvement in CLASI-A that reflects a meaningful improvement in a patient's quality of life is similar in Black and white patients; similar improvements in CLASI-A have also been noted across races and/or ethnicities in observational studies	37,42
Does CLASI assess disease severity across CLE subtypes?	Multiple publications support the use of CLASI across numerous CLE subtypes, including subacute and discoid CLE, which are the predominant subtypes examined in clinical trials	6,10,11, 45–48
What is the threshold for clinically meaningful improvement in CLASI?	CLASI-50 corresponds with meaningful improvement in patient-reported outcomes and impression of disease progression	19,37,43

CLASI, Cutaneous Lupus Erythematosus Disease Area and Severity Index; CLASI-A, CLASI activity; CLASI-50, CLASI-A score improvement of at least 50%; CLE, cutaneous lupus erythematosus.

different skin pigmentation subtypes[42]. Furthermore, the degree of improvement in CLASI-A that is meaningful to patients is similar in Black and white individuals in a retrospective analysis of a longitudinal database[43], and race and ethnicity have not been shown to significantly affect improvement in CLASI-A scores in observational studies[37]. As such, CLASI shows promise as an instrument that can perform consistently across diverse skin pigmentations, although additional studies would be beneficial in further demonstrating this capability.

CLASI can assess disease activity across CLE subtypes

Substantial heterogeneity exists in the clinical presentation of CLE, as the numerous subtypes of CLE have distinct morphological characteristics. For clinical trials, it is essential to utilize an instrument that can perform consistently across multiple CLE subtypes, given that individual patients might have unknown or multiple CLE subtype diagnoses[44]. Several publications support the use of CLASI in a wide variety of CLE subtypes, including acute CLE, subacute CLE, discoid lupus, chilblain lupus and tumid lupus[6,10,11,45,46]. Many of these studies have utilized CLASI to demonstrate therapeutic efficacy in various CLE subtypes, including belimumab in patents with acute CLE, anifrolumab in multiple CLE subtypes (including chilblain lupus) and litifilimab in acute CLE, subacute CLE and chronic CLE[6,10,47,48]. These data show the potential ability of CLASI to assess disease activity across the diverse clinical presentations of CLE, especially given that discoid and subacute CLE are the predominant subtypes being studied in clinical trials.

CLASI-50 captures clinically meaningful improvement in disease activity

Given the widespread usage of CLASI in existing clinical trials, the question of whether CLASI can capture clinically meaningful improvement in disease activity has been of particular interest. To date, CLASI-A score improvement of at least 50% (CLASI-50) and 70% (CLASI-70) have both been included as primary or secondary end points in numerous SLE and CLE clinical trials[7,11,13,47,49,50]. Several studies have supported the use of CLASI-50, as it has been associated with clinically meaningful improvement in patient quality of life as measured via SKINDEX-29 emotion and function domains[19,43]. CLASI-50 responders also reported a greater improvement in disease activity over 6 months than non-responders[37]. As such, CLASI-50 could be a viable end point of disease improvement that is both clinically meaningful to patients and widely used in existing clinical trials. However, the optimal clinically meaningful improvement threshold of CLASI is not yet known, and the CLASI working group seeks to answer this important question with clinical trial and real-world data in a future project.

Progress and recommendations of the Lupus ABC CLASI working group

After identifying and addressing the potential limitations of CLASI as a primary end point in CLE clinical trials, the Lupus ABC CLASI working group compiled and summarized the aforementioned data in an informational packet that was shared with the FDA in June 2024. A pivotal virtual meeting between members of the FDA and CLASI working group took place in August 2024 to explain the working group data and provide opportunities for the FDA to provide feedback. The Lupus ABC CLASI working group concluded in November 2024 that CLASI is a viable clinician-rated instrument that can be utilized as an outcome measure for therapeutic efficacy in clinical trials for CLE patients (Table 1 and Fig. 2). This decision clears the path for clinical drug development with the ability for clinical trials in CLE to utilize the CLASI to provide relevant clinical evidence. The working group recognized the need for additional information to assess what degree of change in CLASI-A score captures clinically meaningful improvement, which will help to define the threshold of therapeutic efficacy specific to CLE. Other important upcoming studies that the working group will undertake include characterizing low disease activity and defining minimal skin activity levels for inclusion in CLE clinical trials. CLASI-50 and CLASI-70 are already widely used as end points in existing CLE and SLE clinical trials, and determining clinically meaningful improvement in disease activity with CLASI will be critical for defining inclusion criteria and therapeutic response moving forward. In addition, the potential application of CLASI to the measurement of mucocutaneous treatment responses in general SLE trial end points, such as the planned Treatment Response Measure for SLE (TRM-SLE)[51], should be evaluated.

Conclusions

The collaborative nature of the Lupus ABC CLASI working group with multi-stakeholder involvement has provided important momentum for drug development in CLE by reaching consensus on the CLASI as a suitable outcome measure within a short period. Furthermore, the aggregate data affirm the potential for CLASI to evaluate clinically relevant aspects of disease and lesion morphology, assess disease

activity across patients with different skin pigmentations and CLE subtypes, and demonstrate clinically meaningful CLE improvement, giving the green light for clinical trials to use CLASI as an outcome measure to evaluate therapeutic efficacy in CLE. This has important implications for CLE drug development, as the use of an established outcome measure of disease activity in clinical trials will provide a standardized approach to assessing therapeutic response.

Published online: 26 January 2026

References

1. Vasquez, R. et al. A multicentre, cross-sectional study on quality of life in patients with cutaneous lupus erythematosus. *Br. J. Dermatol.* **168**, 145–153 (2013).
2. Xie, L., Lopes Almeida Gomes, L., Stone, C. J., Faden, D. F. & Werth, V. P. An update on clinical trials for cutaneous lupus erythematosus. *J. Dermatol.* **51**, 885–894 (2024).
3. Arnaud, L., Parodis, I., Devilliers, H. & Chasset, F. Clinical trial outcomes for SLE: what we have and what we need. *Lupus Sci. Med.* **11**, e001114 (2024).
4. Cepica, T. B., Gupta, R., Werth, V. P. & Chong, B. F. Severity scores for cutaneous lupus erythematosus. *J. Invest. Dermatol.* **144**, 2354–2363 (2024).
5. Gaffney, R. G., Werth, V. P. & Merola, J. F. Cutaneous lupus erythematosus disease assessment: highlighting CLE outcome measures. *Front. Med.* **9**, 968469 (2022).
6. Carter, L. M., Wigston, Z., Laws, P. & Vital, E. M. Rapid efficacy of anifrolumab across multiple subtypes of recalcitrant cutaneous lupus erythematosus parallels changes in discrete subsets of blood transcriptomic and cellular biomarkers. *Br. J. Dermatol.* **189**, 210–218 (2023).
7. Furie, R. et al. Anifrolumab, an anti-interferon-α receptor monoclonal antibody, in moderate-to-severe systemic lupus erythematosus. *Arthritis Rheumatol.* **69**, 376–386 (2017).
8. Furie, R. et al. A phase III, randomized, placebo-controlled study of belimumab, a monoclonal antibody that inhibits B lymphocyte stimulator, in patients with systemic lupus erythematosus. *Arthritis Rheum.* **63**, 3918–3930 (2011).
9. Furie, R. et al. Monoclonal antibody targeting BDCA2 ameliorates skin lesions in systemic lupus erythematosus. *J. Clin. Invest.* **129**, 1359–1371 (2019).
10. Iaccarino, L. et al. Effects of belimumab on flare rate and expected damage progression in patients with active systemic lupus erythematosus. *Arthritis Care Res.* **69**, 115–123 (2017).
11. Merrill, J. T. et al. Phase 2 trial of iberdomide in systemic lupus erythematosus. *N. Engl. J. Med.* **386**, 1034–1045 (2022).
12. Ker, K. J., Teske, N. M., Feng, R., Chong, B. F. & Werth, V. P. Natural history of disease activity and damage in patients with cutaneous lupus erythematosus. *J. Am. Acad. Dermatol.* **79**, 1053–1060 e1053 (2018).
13. Bender, A. M., Laageide, L., Kaur, J., Babkowski, N. & Richardson, C. T. Ruxolitinib cream for discoid lupus erythematosus: An open-label pilot study of 10 subjects. *J. Am. Acad. Dermatol.* **92**, 655–657 (2025).
14. Albrecht, J. et al. The CLASI (Cutaneous Lupus Erythematosus Disease Area and Severity Index): an outcome instrument for cutaneous lupus erythematosus. *J. Invest. Dermatol.* **125**, 889–894 (2005).
15. Chakka, S. et al. The CLASI, a validated tool for the evaluation of skin disease in lupus erythematosus: a narrative review. *Ann. Transl. Med.* **9**, 431 (2021).
16. Krathen, M. S. et al. The Cutaneous Lupus Erythematosus Disease Activity and Severity Index: expansion for rheumatology and dermatology. *Arthritis Rheum.* **59**, 338–344 (2008).
17. Klein, R. et al. Development of the CLASI as a tool to measure disease severity and responsiveness to therapy in cutaneous lupus erythematosus. *Arch. Dermatol.* **147**, 203–208 (2011).
18. Arevalo-Bermudez, M. P., Pita-Fernandez, S., Paradela, S. & Fonseca, E. Cutaneous lupus erythematosus: quality of life and related factors in a cohort of 260 patients from A Coruna, Spain. *Br. J. Dermatol.* **178**, e117–e118 (2018).
19. Chakka, S. et al. Evaluating change in disease activity needed to reflect meaningful improvement in quality of life for clinical trials in cutaneous lupus erythematosus. *J. Am. Acad. Dermatol.* **84**, 1562–1567 (2021).
20. Chang, A. Y., Ghazi, E., Okawa, J. & Werth, V. P. Quality of life differences between responders and nonresponders in the treatment of cutaneous lupus erythematosus. *JAMA Dermatol.* **149**, 104–106 (2013).
21. Gaines, E. et al. Quality of life and disease severity in a cutaneous lupus erythematosus pilot study. *Arch. Dermatol.* **144**, 1061–1062 (2008).
22. Ishiguro, M., Hashizume, H., Ikeda, T., Yamamoto, Y. & Furukawa, F. Evaluation of the quality of life of lupus erythematosus patients with cutaneous lesions in Japan. *Lupus* **23**, 93–101 (2014).
23. Mallbris, M. J., Jia, B., Zhao, Y., Kahlenberg, J. M. & Gudjonsson, J. E. Concomitant moderate to severe cutaneous lesions have marked impact on quality of life in patients with active systemic lupus erythematosus: a cross-sectional insight from two phase 3 randomised clinical trials in adults. *Br. J. Dermatol.* **191**, 458–460 (2024).
24. Yan, D. et al. Cutaneous lupus concerns from the patient perspective: a qualitative study. *Lupus Sci. Med.* **8**, e000444 (2021).
25. Nguyen, H. & Staeva, T. P. Lupus ABC spearheading a new era of collaboration to advance lupus drug development. *Nat. Rev. Rheumatol.* **21**, 253–254 (2025).
26. Symmons, D. P. et al. Development and assessment of a computerized index of clinical disease activity in systemic lupus erythematosus. Members of the British Isles Lupus Assessment Group (BILAG). *Q. J. Med.* **69**, 927–937 (1988).
27. Bombardier, C., Gladman, D. D., Urowitz, M. B., Caron, D. & Chang, C. H. Derivation of the SLEDAI. A disease activity index for lupus patients. The Committee on Prognosis Studies in SLE. *Arthritis Rheum.* **35**, 630–640 (1992).
28. Gladman, D. D., Ibanez, D. & Urowitz, M. B. Systemic lupus erythematosus disease activity index 2000. *J. Rheumatol.* **29**, 288–291 (2002).
29. Petri, M. et al. Combined oral contraceptives in women with systemic lupus erythematosus. *N. Engl. J. Med.* **353**, 2550–2558 (2005).
30. Guo, L. N. et al. Development of a working core outcome set for cutaneous lupus erythematosus: a practical approach to an urgent unmet need. *Lupus Sci. Med.* **8**, e000529 (2021).
31. Kuhn, A. et al. Revised Cutaneous Lupus Erythematosus Disease Area and Severity Index (RCLASI): a modified outcome instrument for cutaneous lupus erythematosus. *Br. J. Dermatol.* **163**, 898–899 (2010).
32. Werth, V. P. et al. Development of a conceptual model of the patient experience of disease activity in cutaneous lupus erythematosus. *Qual. Life Res.* **33**, S227–S227 (2024).
33. Ogunsanya, M. E., Cho, S. K., Hudson, A. & Chong, B. F. Validation and reliability of a disease-specific quality-of-life measure in patients with cutaneous lupus erythematosus. *Br. J. Dermatol.* **180**, 1430–1437 (2019).
34. Finlay, A. Y. & Khan, G. K. Dermatology life quality index (DLQI) — a simple practical measure for routine clinical use. *Clin. Exp. Dermatol.* **19**, 210–216 (1994).
35. Erickson, S. & Kim, B. S. Research techniques made simple: itch measurement in clinical trials. *J. Invest. Dermatol.* **139**, 264–269.e1 (2019).
36. Lu, G. et al. Erythema and scale in cutaneous lupus erythematosus significantly impacts patient quality of life and disease course impression. *Br. J. Dermatol.* **93**, 558–560 (2025).
37. Cepica, T. B. et al. Smoking status is a negative predictor of six-month cutaneous lupus activity trends: a prospective cohort study. *J. Am. Acad. Dermatol.* **92**, 912–914 (2024).
38. Werth, V. et al. Improvement of individual mucocutaneous manifestations in patients with systemic lupus erythematosus treated with anifrolumab. *Ann. Rheum. Dis.* **81**, 436–437 (2022).
39. Werth, V., Merola, J. F., Li, Q. Y., Yang, W. H. & Barbey, C. Effect of litifilimab on cutaneous lupus erythematosus disease area and severity index-activity (CLASI-A) Subcomponents and Physician Global Assessment-Skin (PGA-Skin) in patients with cutaneous lupus erythematosus (CLE) in a phase 2 study. *Arthritis Rheumatol.* **76**, 1387–1390 (2024).
40. Stull, C., Sprow, G. & Werth, V. P. Cutaneous involvement in systemic lupus erythematosus: a review for the rheumatologist. *J. Rheumatol.* **50**, 27–35 (2023).
41. Kushner, C. J. et al. Evaluation of the reliability and validity of the Cutaneous Lupus Erythematosus Disease Area and Severity Index (CLASI) in paediatric cutaneous lupus among paediatric dermatologists and rheumatologists. *Br. J. Dermatol.* **180**, 165–171 (2019).
42. Xie, L. et al. Subtype and racial erythema variation for cutaneous lupus trials. *JAMA Dermatol.* **161**, 67–74 (2025).
43. Kleitsch, J. et al. Change in disease activity needed for meaningful change in cutaneous lupus by patient characteristic: a retrospective analysis of a longitudinal database. *J. Am. Acad. Dermatol.* **90**, 406–408 (2024).
44. Lu, G., Brown, L. S. & Chong, B. F. Systemic lupus erythematosus is a risk factor for having multiple subtypes of cutaneous lupus erythematosus. *Lupus* **34**, 181–186 (2025).
45. Bein, D. et al. Evaluation of disease activity and damage in different subtypes of cutaneous lupus erythematosus using the CLASI. *J. Eur. Acad. Dermatol. Venereol.* **25**, 652–659 (2011).
46. Kreuter, A. et al. Lupus erythematosus tumidus: response to antimalarial treatment in 36 patients with emphasis on smoking. *Arch. Dermatol.* **145**, 244–248 (2009).
47. Werth, V. P. et al. Trial of anti-BDCA2 antibody litifilimab for cutaneous lupus erythematosus. *N. Engl. J. Med.* **387**, 321–331 (2022).
48. Furie, R. A. et al. Trial of Anti-BDCA2 antibody litifilimab for systemic lupus erythematosus. *N. Engl. J. Med.* **387**, 894–904 (2022).
49. Morand, E. et al. Deucravacitinib, a tyrosine kinase 2 inhibitor, in systemic lupus erythematosus: a phase ii, randomized, double-blind, placebo-controlled trial. *Arthritis Rheumatol.* **75**, 242–252 (2023).
50. van Vollenhoven, R. F. et al. Efficacy and safety of ustekinumab, an IL-12 and IL-23 inhibitor, in patients with active systemic lupus erythematosus: results of a multicentre, double-blind, phase 2, randomised, controlled study. *Lancet* **392**, 1330–1339 (2018).
51. Connelly, K. et al. Towards a novel clinical outcome assessment for systemic lupus erythematosus: first outcomes of an international taskforce. *Nat. Rev. Rheumatol.* **19**, 592–602 (2023).
52. Merrill, J. T. et al. The efficacy and safety of abatacept in patients with non-life-threatening manifestations of systemic lupus erythematosus results of a twelve-month, multicenter, exploratory, phase IIb, randomized, double-blind, placebo-controlled trial. *Arthritis Rheum.* **62**, 3077–3087 (2010).
53. US National Library of Medicine. *ClinicalTrials.gov* https://clinicaltrials.gov/study/NCT04877691 (2025).
54. Gordon, C. et al. Effects of atacicept on disease activity in patients with moderate to severe systemic lupus erythematosus: APRIL-SLE randomized trial. *Ann. Rheum. Dis.* **73**, 77–77 (2014).
55. US National Library of Medicine. *ClinicalTrials.gov* https://clinicaltrials.gov/study/NCT01702740 (2012).

56. Furie, R. A. et al. Phase 2, randomized, placebo-controlled trial of dapirolizumab pegol in patients with moderate-to-severe active systemic lupus erythematosus. *Rheumatology* **60**, 5397–5407 (2021).
57. US National Library of Medicine. *ClinicalTrials.gov* https://clinicaltrials.gov/study/NCT02656082 (2018).
58. US National Library of Medicine. *ClinicalTrials.gov* https://clinicaltrials.gov/study/NCT02847598 (2023).
59. US National Library of Medicine. *ClinicalTrials.gov* https://clinicaltrials.gov/study/NCT05162586 (2025).
60. US National Library of Medicine. *ClinicalTrials.gov* https://clinicaltrials.gov/study/NCT01845740 (2021).
61. Merrill, J. T. et al. Efficacy and safety of rituximab in moderately-to-severely active systemic lupus erythematosus: the randomized, double-blind, phase II/III systemic lupus erythematosus evaluation of rituximab trial. *Arthritis Rheum.* **62**, 222–233 (2010).
62. US National Library of Medicine. *ClinicalTrials.gov* https://clinicaltrials.gov/study/NCT03288324 (2024).
63. US National Library of Medicine. *ClinicalTrials.gov* https://clinicaltrials.gov/study/NCT01294774 (2017).
64. US National Library of Medicine. *ClinicalTrials.gov* https://clinicaltrials.gov/study/NCT05531565 (2023).
65. McDonnell, S. R. P. et al. Mezagitamab in systemic lupus erythematosus: clinical and mechanistic findings of CD38 inhibition in an autoimmune disease. *Lupus Sci. Med.* **11**, e001112 (2024).
66. US National Library of Medicine. *ClinicalTrials.gov* https://clinicaltrials.gov/study/NCT06015737 (2025).
67. Wallace, D. J., Furie, R. A. & Tanaka, Y. Baricitinib for systemic lupus erythematosus: a double-blind, randomised, placebo-controlled, phase 2 trial. *Lancet* **392**, 476–476 (2018).
68. US National Library of Medicine. *ClinicalTrials.gov* https://clinicaltrials.gov/study/NCT04186871 (2024).
69. US National Library of Medicine. *ClinicalTrials.gov* https://clinicaltrials.gov/study/NCT05591222 (2025).
70. US National Library of Medicine. *ClinicalTrials.gov* https://clinicaltrials.gov/study/NCT05629208 (2025).
71. US National Library of Medicine. *ClinicalTrials.gov* https://clinicaltrials.gov/study/NCT03134222 (2020).
72. Burge, D. J., Werth, V. P., Boackle, S. A. & Posada, J. Evaluation of RNase therapy in systemic lupus erythematosus: a randomised phase 2a clinical trial of RSLV-132. *Lupus Sci. Med.* **11**, e001113 (2024).
73. US National Library of Medicine. *ClinicalTrials.gov* https://clinicaltrials.gov/study/NCT04781816 (2025).
74. US National Library of Medicine. *ClinicalTrials.gov* https://clinicaltrials.gov/study/NCT03817424 (2024).
75. US National Library of Medicine. *ClinicalTrials.gov* https://clinicaltrials.gov/study/NCT01352988 (2014).
76. US National Library of Medicine. *ClinicalTrials.gov* https://clinicaltrials.gov/study/NCT02927457 (2021).

Acknowledgements
The authors thank N. Cooper for her support on this project. This manuscript reflects the views of the authors and should not be construed to represent the views or policies of the FDA.

Author contributions
B.F.C., G.L. and T.C. researched data for the article and wrote the article. All authors contributed substantially to discussion of the content and reviewed and/or edited the manuscript before submission.

Competing interests
B.F.C. is an investigator for Biogen Incorporated and EMD Serono; has consulted for Amgen Incorporated, AstraZeneca, Biogen Incorporated, Bristol Meyers Squibb, EMD Serono and Lupus Research Alliance; receives royalties from MAPI Research Trust; served as a chairperson for a seminar sponsored by Amgen Incorporated; and was a speaker for Cesas Medical. V.P.W. has received grants from Amgen, Argenx, AstraZeneca, Biogen, BMS, Celgene, Corbus Pharmaceuticals, CSL Behring, Genentech, Gilead, Horizon, Janssen, Pfizer, Q32 Bio, Regeneron, Syntimmune, Ventus and Viela; and has consulted for AbbVie, Akari, Amgen, Argenx, AstraZeneca, Bayer, Beacon Bioscience, Biogen, BMS, Calyx, Cabaletta Bio, Celgene, Corcept, Crisalis, CSL Behring, Cugene, EMD Sorona, Genentech, Gilead, GSK, Incyte, Horizon, Janssen, Kezar, Kwoya Kirin, Lilly, Medscape, Merck, Nektar, Octapharma, Pfizer, Principia, Regeneron, Rome Pharmaceuticals, Sanofi, UCB, Viela Bio; and receives royalties from MAPI Research Trust. A.P.F. has received research support and is an investigator for Alexion, AstraZeneca, Castle Biosciences, Mallinckrodt, Pfizer and Priovant; he is a consultant for AbbVie, Biogen and Mallinckrodt; and is a speaker for AbbVie, Amgen, BMS and Mallinckrodt. C.B. is a former employee of Biogen and may hold stock in Biogen. The University of Pennsylvania owns the copyright for the CLASI. The other authors declare no competing interests.

Additional information
Supplementary information The online version contains supplementary material available at https://doi.org/10.1038/s41584-025-01351-5.

Peer review information *Nature Reviews Rheumatology* thanks Francois Chasset and Andrew Franks for their contribution to the peer review of this work.

[1]Department of Dermatology, University of Texas Southwestern Medical Center, Dallas, TX, USA. [2]Biogen, Baar, Switzerland. [3]AstraZeneca, Durham, NC, USA. [4]EMD Serono, Boston, MA, USA. [5]Departments of Dermatology and Pathology, Cleveland Clinic, Cleveland, OH, USA. [6]Bristol Meyers Squibb, Princeton, NJ, USA. [7]Division of Dermatology and Dentistry, Center for Drug Evaluation and Research, US Food and Drug Administration, Silver Spring, MD, USA. [8]Office of Immunology and Inflammation, Center for Drug Evaluation and Research, US Food and Drug Administration, Silver Spring, MD, USA. [9]Lupus Research Alliance, New York, NY, USA. [10]Department of Dermatology, University of Rochester Medical Center, Rochester, NY, USA. [11]Department of Dermatology, University of Pennsylvania, Philadelphia, PA, USA. [12]Corporal Michael J. Crescenz Veterans Affairs Medical Center Philadelphia, Philadelphia, PA, USA.

The Lupus Accelerating Breakthroughs Consortium CLASI Working Group

Catherine Barbey[2], Ilimbek Beketaev[3], Denesh Chitkara[4], Anthony P. Fernandez[5], Shimon Korish[6], Joseph F. Merola[1], Jill A. Lindstrom[7], Hoang Nguyen[9], Christopher T. Richardson[10], Teodora P. Staeva[9], Victoria P. Werth[11,12] & Benjamin F. Chong[1]

A full list of members and their affiliations appears in the Supplementary Information.